Mpemba effect in granular and Langevin systems

By

Apurba Biswas

PHYS10201804003

The Institute of Mathematical Sciences, Chennai

A thesis submitted to the

Board of Studies in Physical Sciences

In partial fulfillment of requirements

for the Degree of

DOCTOR OF PHILOSOPHY

of

HOMI BHABHA NATIONAL INSTITUTE

13/07/2023

Homi Bhabha National Institute

Recommendations of the Viva Voce Committee

As members of the Viva Voce Committee, we certify that we have read the dissertation prepared by Apurba Biswas entitled " Mpemba effect in granular and Langevin systems" and recommend that it may be accepted as fulfilling the thesis requirement for the award of Degree of Doctor of Philosophy.

Chairman - Satyavani Vemparala Date: 13/07/2023

Guide/Convenor - R. Rajesh Date: 13/07/2023

Prasad Perlekar

Examiner - Prasad Perlekar Date: 13/07/2023

Member 1 - Pinaki Chaudhuri Date: 13/07/2023

Member 2 - Sitabhra Sinha Date: 13/07/2023

Manjari Bagchi

Member 3 - Manjari Bagchi Date: 13/07/2023

Dibyendu Das

Member 4 - Dibyendu Das Date: 13/07/2023

Final approval and acceptance of this thesis is contingent upon the candidate's submission of the final copies of the thesis to HBNI.

I hereby certify that I have read this thesis prepared under my direction and recommend that it may be accepted as fulfilling the thesis requirement.

Date: 13/07/2023

Place: Chennai

Guide

STATEMENT BY AUTHOR

This dissertation has been submitted in partial fulfillment of requirements for an advanced degree at Homi Bhabha National Institute (HBNI) and is deposited in the Library to be made available to borrowers under rules of the HBNI.

Brief quotations from this dissertation are allowable without special permission, provided that accurate acknowledgement of source is made. Requests for permission for extended quotation from or reproduction of this manuscript in whole or in part may be granted by the Competent Authority of HBNI when in his or her judgement the proposed use of the material is in the interests of scholarship. In all other instances, however, permission must be obtained from the author.

Biswas

Apurba Biswas

DECLARATION

I hereby declare that the investigation presented in the thesis has been carried out by me. The work is original and has not been submitted earlier as a whole or in part for a degree / diploma at this or any other Institution / University.

ABiswas

Apurba Biswas

List of publications arising from the thesis

- **Published**

  1. Mpemba effect in driven granular Maxwell gases

     Apurba Biswas, V. V. Prasad, Oren Raz and R. Rajesh, Phys. Rev. E **102**, 012906 (2020)

  2. Mpemba effect in an anisotropically driven granular gas

     Apurba Biswas, V. V. Prasad and R. Rajesh, Euro. Phys. Letters, **136**, 46001 (2021)

  3. Mpemba effect in anisotropically driven inelastic Maxwell gases

     Apurba Biswas, V. V. Prasad and R. Rajesh, Journal of Statistical Physics **186**, 45 (2022)

  4. Mpemba effect in driven granular gases: Role of distance measures

     Apurba Biswas, V. V. Prasad and R. Rajesh, Arxiv:2303.10900 (2023)

  5. Mpemba effect in a Langevin system: population statistics, metastability and other exact results

     Apurba Biswas, R. Rajesh, Arnab Pal, Arxiv:2304.06420 (2023), Accepted (Journal of Chemical Physics)

Biswas

Apurba Biswas

List of publications not arising from the thesis

- **Published**

  1. Asymptotic velocity distribution of a driven one dimensional binary granular Maxwell gas
     Apurba Biswas, V. V. Prasad and R. Rajesh, J. Stat. Mech. 013202 (2020)
  2. Lattice models for ballistic aggregation: cluster-shape dependent exponents
     P. Fahad, Apurba Biswas, V. V. Prasad and R. Rajesh, Arxiv:2301.11250 (2023)
  3. Mpemba effect for a Brownian particle trapped in a single well potential
     Apurba Biswas and R. Rajesh, Arxiv:2305.06613 (2023)

Biswas

Apurba Biswas

List of presentations and participations at conferences

• Contributed presentations

1. Presented poster on *Asymptotic velocity distribution of driven binary granular Maxwell gas* at StatPhys-Kolkata X, Presidency University, India
2. Presented poster on *Asymptotic velocity distribution of driven binary granular Maxwell gas* at Recent Topics in Statistical Mechanics, NISER, India
3. Presented poster on *Asymptotic velocity distribution of driven binary granular Maxwell gas* at 7^{th} Indian Statistical Physics Community Meeting, ICTS, India
4. Presented poster on *Anomalous relaxation phenomena in driven granular gases* at StatPhys-Kolkata XI, IISER Kolkata, India
5. Presented poster on *Anomalous relaxation phenomena in driven granular gases* at Non-Markovian Dynamics Far from Equilibrium, ICTP, Italy
6. Presented poster on *Anomalous relaxation phenomena in stochastic systems* at Fluctuations in small complex systems VI, Venice, Italy
7. Gave a talk on *Mpemba effect in non-equilibrium systems* for Frontiers in Non-equilibrium Physics at IMSc, India (2023)

• Conferences attended

1. StatPhys-Kolkata X at Presidency University, India (2019)

2. Recent Topics in Statistical Mechanics at NISER, India (2019)
3. 7^{th} Indian Statistical Physics Community Meeting at ICTS, India (2020)
4. Current Trends in Non-Equilibrium Physics held *online* by JNU, India (2021)
5. StatPhys-Kolkata XI held *online* by IISER Kolkata, India (2022)
6. Non-Markovian Dynamics Far from Equilibrium held *online* by ICTP, Italy (2022)
7. Fluctuations in small complex systems VI at Venice, Italy (2022)
8. Frontiers in Non-equilibrium Physics at IMSc, India (2023)

Research visits and seminars

• Research visits

1. Visited group of Hartmut Lowen at Heinrich Heinne Universitat, Dusselsorf, Germany (2022)
2. Visited Edgar Roldan and Christian Maes at ICTP, Trieste, Italy (2022)

• Seminars

1. Seminar on *Asymptotic velocity distribution of driven inelastic binary Maxwell gases* at IMSc, India (2019)
2. Seminar on *Mpemba effect in driven granular gases* for Institute Seminar Day at IMSc, India (2021)

3. Seminar on *Mpemba effect in non-equilibrium systems* at ICTP, Italy (2022)

Dedicated to

Maa, Baba and Bhai

ACKNOWLEDGEMENTS

This thesis represents not only the culmination of my academic efforts over the past few years but is also associated with the fond memories and experiences I had at Matscience that contributed to its creation. I take immense pride in being affiliated with Matscience and conducting my doctoral research in such an excellent environment. As I reflect on my thesis, I cherish the opportunity to revisit the fond memories of the people listed in here.

I am deeply grateful to my supervisor, Prof. R. Rajesh, for his invaluable guidance, support, and encouragement throughout my research journey. His expertise of the subject matter, and insightful ideas have been instrumental in shaping the direction and quality of this thesis. I am grateful to him for providing the space and independence to explore the research problems, and providing the opportunity to work on several different topics. I feel fortunate to have had him as my advisor and mentor, and I will always be grateful for his contribution to building my confidence and academic growth.

I also want to express my gratitude to the members of my doctoral committee, Prof. Satyavani Vemparala, Prof. Pinaki Chaudhuri, Prof. Dibyendu Das, Prof. Manjari Bagchi and Prof. Sitabhra Sinha, for their valuable feedback and suggestions. Particularly, I am grateful to Prof. Satyavani, Prof. Pinaki, and Prof. Dibyendu for their valuable contributions in the form of critical questions during my doctoral committee meetings, which aided in refining my research presentations.

This thesis would not have this outcome without Dr. V. V. Prasad who also played a significant role in this thesis, and I am grateful to him for his collaborative efforts in the research work. I express my gratitude to him for his approachability, especially during the pandemic, and for patiently addressing my doubts. I am also grateful to have had the chance to work with Dr. Arnab Pal (*Arnab da*) on a topic pertaining to my thesis, and I am thankful for that as it also provided me with an opportunity to acquire new techniques. Furthermore, he has assisted me greatly in crafting research statements and preparing

presentations for my postdoctoral applications. I am grateful for his academic support and the discussions with him. I also thank Fahad, my friend and collaborator, who has helped me greatly with numerical tools on several occasions and also got to work with him on a topic different from my thesis. I would also like to thank Dr. Oren Raz for a wonderful collaboration. I am thankful to my colleagues Amit, Subashri and Amir for the various discussions we had regarding our respective work, which also facilitated our learning process. I am grateful for the computation infrastructure provided by Matscience. I sincerely thank Vasan for help related to computing needs. I appreciate the help received from R. Indra, P. Prema and other administrative members of the institute on several occasions.

The years spent at Matscience would not have been as memorable as they were without the presence of the wonderful friends that I made during that time. I would like to take this opportunity to express my gratitude to many of them: Sushovan (*Susho*), Jyotijwal (*JJ*), Tanmay (*Saha*), Manas (*Mansa*), Tanmoy (*Bera*), Ankur Sarkar, Sidhu, Vinod, Anupam da, Tanmoy Sengupta, Hitesh, Sabiar da, Sujoy da, Pranendu da, Soumya da, Rupam da, Pritam da, Sahil da, Satish, Sunil, Akhil, Toshali, Prateek, Subashri, Himangshu, Prabhat, Gopal, Nishant, Pavan, Debabrata da, Mrinal da, Arpan da, Sumit Shaw, Aritra, Sourav, Arup, Vishwajeet, Sashikanta, Pavitra, Piyasa, Sadhana, and many others whom I might have missed to mention it over here. I thank my friends for the wonderful time spent in gossips, cooking on Sundays, institute trips and at the badminton court. The enjoyable moments at the tea shop every evening accompanied by a large group of us would be missed. My sincere thanks to my classmates of 2018 Physics batch: Tanmay, Jyotijwal, Sushovan, Amit, Vinod, Gopal, Prateek, Toshali, Subashri, Pavan, Prabhat, Akhil, Nishant, Himangshu and Mahaveer for their friendly nature and help in completing the assignments on several occasions. The time spent at RSA-04 would be special. Many thanks and gratitude to Dipanjan da, Sagnik da and Sanjoy da for their insightful advice for someone beginning his PhD journey. Later the office was shared by four of us: JJ, Susho, Saha and myself, and I enjoyed the laughter and fun times amidst our research work cracking jokes, playing music and pointless conversations.

Outside of the institute, I am thankful to my friends from my M. Sc. days: Deborjyoti, Tufaan, Debopriyo, Tarik, Alokesh, Kiran, Bibhoo, Anupama, Nihar, Maneesha, Vijayshankar with whom I have shared some memorable experiences at the university. I sincerely thank all the teachers whom I have come across in my academics for their motivations and appreciations especially from Prof. E. Harikumar and Prof. Shyamal Biswas at the University of Hyderabad.

I am ever indebted to *maa*, *baba*, *bhai* and Asit dada for their constant support because of which I could pursue my doctoral studies. Their patience and frequent inquiries about my research progress were instrumental in keeping me motivated throughout the journey. They have consistently encouraged me to believe in myself and have helped me develop the confidence. They have always provided me with moral support and a positive outlook in life whenever I required it. This thesis is a dedication to their sacrifice, love, and support, and their invaluable contributions are reflected in its content.

Contents

Synopsis **1**

List of Figures **10**

List of Tables **29**

1 Introduction **30**

1.1 Mpemba effect 30

1.2 Driven granular gas 34

1.3 Single particle Langevin system 38

1.4 Overview of the thesis 42

2 Mpemba effect in driven granular Maxwell gases **44**

2.1 Introduction 44

2.2 Model 47

2.3 Calculation of the two point correlations 50

2.3.1 Mono-dispersed Maxwell gas 50

2.3.2 Bi-dispersed Maxwell gas 52

2.4 The Mpemba effect in Mono-dispersed Maxwell gas 56

2.5 Mpemba effect in bi-dispersed Maxwell gas 59

2.5.1 One component is driven 60

2.5.2 Both components are driven 67

2.5.3 The Inverse Mpemba Effect 69

2.5.4 The Strong Mpemba Effect 72

2.6 Conclusion 75

3 Mpemba effect in an anisotropically driven granular gas 78

3.1 Introduction 78

3.2 Model 79

3.3 Mpemba effect 84

3.4 Comparison with simulations 93

3.5 Conclusion 96

4 Mpemba effect in anisotropically driven inelastic Maxwell gases 97

4.1 Introduction 97

4.2 The Model 99

4.3 Two point correlations 102

4.4 The Mpemba effect in an anisotropically driven gas 106

4.4.1 The inverse Mpemba effect 110

4.4.2 The strong Mpemba effect 112
4.5 Special case when the driving is only in one direction 113
4.6 Summary and discussion 117
5 Mpemba effect and role of distance measures in driven granular gases 121
5.1 Introduction 121
5.2 Model 124
5.3 Characterising the steady states 124
5.3.1 Inelastic Maxwell model 125
5.3.2 Hard disc granular gas model 127
5.4 Mpemba effect and distance measures in phase space 129
5.4.1 Total energy 130
5.4.2 Euclidean Distance 133
5.4.3 Manhattan Distance 136
5.4.4 KL Divergence 137
5.5 Comparison between various measures 140
5.6 Conclusion 145
6 Mpemba effect in a Langevin system: Exact results and other properties 148
6.1 Introduction 148
6.2 Model system and general formalism 150
6.2.1 Eigenspectrum decomposition 151

6.2.2 Shape of the potential 153

6.2.3 Jump conditions 155

6.2.4 Eigenspectrum analysis 156

6.3 Distance function and the Mpemba effect 161

6.4 Modulation of the potential and population – connection to the experiments 163

6.5 Mpemba effect in double well potential 166

6.5.1 Asymmetry is not a sufficient criterion 167

6.5.2 Equal domain widths 169

6.5.3 Unequal domain widths 171

6.6 Mpemba effect without a metastable minimum 174

6.7 Illustration of the Mpemba effect in terms of distance measures 176

6.8 Conclusion 178

7 Conclusions 181

A Derivation of the Boltzmann equation 184

B Motivations for the choice of driving 189

C Velocity distribution of driven granular gases 191

Bibliography 194

Synopsis

In physics, relaxation refers to the process by which a system in an excited state returns to equilibrium. This can occur through various mechanisms, such as the emission of thermal radiation or the dissipation of energy into other degrees of freedom. Relaxation phenomena is ubiquitous in nature and is studied in different setups depending on the system of interest. Some examples in the context are relaxation of a heated liquid to the equilibrium condition of its environment, relaxation of a charged capacitor as it discharges, relaxation of a magnetised material as the magnetisation decreases, relaxation of an over compressed gas, relaxation of a strained solid as it is unstrained and numerous other phenomena. In order to come to the context of this thesis, we consider the case of hot water relaxing when suddenly cooled to a lower temperature. Does an initially hotter sample of water equilibrate faster than an equal volume of cold water? The well-known Newton's cooling law, which assumes quasi static relaxation, states that the rate of change of temperature of an object is proportional to the difference between the temperature of the object and the temperature of its surroundings. The law predicts that the relaxation time increases logarithmically with the increase in the initial temperature difference of the system with respect to its surrounding. Thus, the hotter sample should take longer time to cool, consistent with intuition.

In contrast, E. Mpemba in 1960s showed that water that is initially hotter can indeed freeze faster than an equal volume of cold water [1]. Clearly, it violates Newton's cooling law and such anomalous cooling has been referred to as Mpemba effect. Numerous experiments that have since been done confirm the existence of the anomalous behaviour. While multiple reasons have been put forward, there is no concensus for the explanation of Mpemba effect in water. Mpemba effect is not restricted to water and has been observed experimentally in many different physical systems. Examples include magnetic alloys [2], polylactides [3], colloidal systems [4], etc. More recently, the Mpemba effect behaviour has been observed in idealised theoretical models such as spin systems [5, 6, 7, 8, 9, 10],

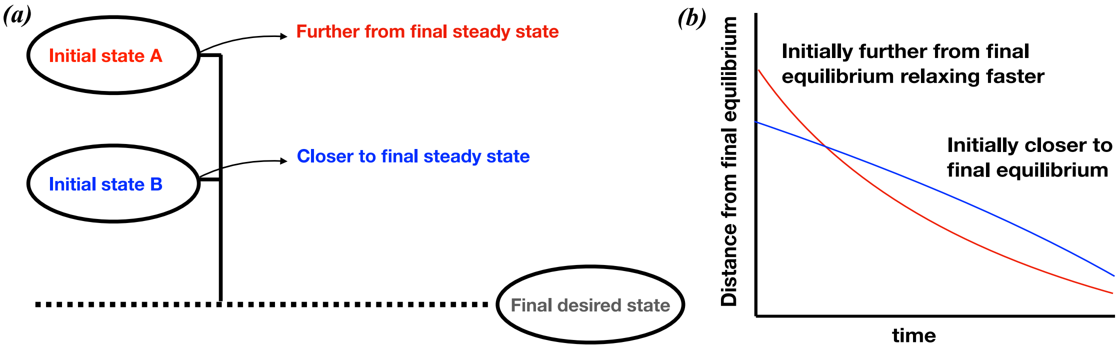
(a)
Initial state A
Further from final steady state
Initial state B
Closer to final steady state
Final desired state
(b)
Distance from final equilibrium
Initially further from final equilibrium relaxing faster
Initially closer to final equilibrium
time

Figure 1: Schematic diagram describing the general scenario of the Mpemba effect: (a) state A is initially farther in the phase space than state B from the final desired state, (b) state A which is initially farther in the phase space equilibrates faster illustrating the Mpemba effect.

discrete state Markovian system [11, 12], particles diffusing in a potential [13, 14, 15], active systems [16], spin glasses [17], molecular gases in contact with a thermal reservoir [18, 19, 20, 21], granular systems [22, 23, 24, 25, 26, 27] and quantum systems [28]. The analysis in terms of these model systems are more tractable and hence provides better understanding of the Mpemba effect.

The general protocol to study the Mpemba effect is to consider two different initial states in the phase space of a given physical system. The initial states can be either equilibrium state or non-equilibrium steady states. Both the initial states are then quenched to a common final state as shown in Fig. 1(a). As a result of the quench, the system is driven out of equilibrium till it reaches the final steady or equilibrium state. The question that is asked in this context is whether the initial state which is initially farther in the phase space from a given final state can undergo faster relaxation compared to another initially prepared state of the same system but placed closer to the final state in phase space [see Fig. 1(b)].

In this thesis, we investigate the anomalous behaviour in the relaxation dynamics of both single particle systems as well as multi-particle systems. The choice of the single particle Langevin system for the study of the Mpemba effect is directly motivated from experiments on colloidal particles. Granular systems is a prototypical example of a system far from equilibrium. Most of the studies on Mpemba effect focus on relation to equilibrium. By studying granular systems, we are able to explore Mpemba effect in nonequilibrium context. Also, granular systems is an area where a strong interplay between experiments and analytical calculations is possible, promoting a deeper understanding on the Mpemba effect. In the following, we summarise our results for Mpemba effect obtained for Langevin and granular systems.

Mpemba effect in driven granular gases

The system of driven granular gas consists of a dilute collection of particles that undergo momentum conserving inelastic collisions. The inelastic interaction among the particles results in the dissipation of kinetic energies of the particles. However, in addition, the particles are also driven at a constant rate which drives the system to a time invariant non-equilibrium steady state. In this setup, the relaxation dynamics of the system is studied as it is quenched from a non-equilibrium steady state to another. In this setup, the Mpemba effect is identified by measuring the time evolution of the total kinetic energy of the system as the system relaxes from an initial to a final state. The previous approaches for the study of the Mpemba effect in both smooth (only translational degrees of freedom are considered) and rough granular gases (both translational and rotational degrees of freedom are considered) looked at the existence of the such anomalous relaxations for non-stationary initial states of the system. But the final state of the system is a non-equilibrium steady state. In the analysis for both the rough and smooth granular gas, the velocity distribution at all times is approximated by a Gaussian or Gaussian and first order corrections, respectively, making the calculations perturbative in nature.

Nature of the initial condition: We try to understand the nature of the initial conditions required for the existence of the Mpemba effect in the system of driven granular gases through an exact analysis. We consider the inelastic Maxwell model for granular gas where the equations for the two point correlations close among themselves resulting in a coupled set of linear equations allowing for an exact solution. This linearity happens to be natural to the model and thus does not require any approximations that have been employed in models where the collision rates are velocity dependent. To demonstrate the existence of the Mpemba effect, we determine the conditions under which a hotter system relaxes faster than a cooler system when quenched to a temperature lower than both. We investigate the existence of the Mpemba effect for both mono-dispersed and bi-dispersed Maxwell gases. For the case of mono-dispersed Maxwell gas, which consist of only one type of particles, we show that the Mpemba effect is possible only if the initial states do not correspond to steady states. On the other hand, for bi-dispersed Maxwell gas, consisting of two types of particles, there is a range of parameters for which the Mpemba effect exists, even when the states from which the quench is done are restricted to valid steady states. In a similar framework, we also demonstrate the existence of the inverse Mpemba effect where a system is heated instead of cooled, i.e., a system at a lower initial temperature relaxes to a high temperature state faster than another system with an intermediate initial temperature. We also demonstrate the existence of a strong Mpemba effect in the binary Maxwell gas which refers to the phenomenon wherein the system at higher temperature relaxes to a final steady state exponentially faster, namely with a larger exponential rate compared to other initial conditions.

Anisotropically driven granular gas: The existence of the Mpemba effect for the case of isotropically driven granular gases is far from experimental realisation as the initial states from where the quench is done involves a non-stationary state. But we demonstrate the existence of the Mpemba effect starting from steady state initial conditions by considering anisotropically driven granular gases. We present analysis for the Mpemba effect in such systems for two different cases. First we present a kinetic theory analysis for the Mpemba effect in a system of two-dimensional granular gas composed of identical, smooth, inelastic hard particles. The particles evolve through momentum conserving inelastic binary collisions. The rate of collison between two particles is proportional to the relative velocities of the particles. In addition, the particles are anisotropically driven at a constant rate such that at long times, the system reaches a stationary state. Here, we derive the time evolutions for mean kinetic energies of the particles based on the Enskog-Boltzmann equation for granular gases with the simplifying assumption that the velocity distribution of the particles is a gaussian. We linearise the time evolution equations by considering initial states close to the final stationary state to derive the condition for the existence of the Mpemba effect. The results for the spatially homogeneous system is also verified with the results of molecular dynamics simulations of hard discs in two dimensions. The good agreement between the two results show that the results continue to hold even for spatially extended systems. Using the same analysis, we also demonstrate the existence of the inverse Mpemba effect where the system is heated instead of being cooled and also the existence of the strong Mpemba effect where the initially hotter system cools at an exponentially faster rate leading to smaller equilibration time. The analysis shows that the ansiotropic driving is the key to demonstrate the Mpemba effect from steady state initial conditions. Such a set up should allow for an experimental realisation of the Mpemba effect in granular systems as anisotropic driving can be achieved by different amplitudes and frequency of shaking in the two directions.

We also do an exact analysis of the system of monodispersed inelastic gas with anisotropic driving based on the inelastic Maxwell model in two dimensions. In the Maxwell gas, the rate of collision is independent of the relative velocities of the particles. The Maxwell gas allows for a rigorous analysis and at the same time retaining the qualitative features of that of a more realistic collision model. The equations for the time evolution of the relevant two point velocity correlations for the Maxwell gas form a closed set of equations. We analyse these equations to determine the condition and the parameter regime for the existence of the Mpemba effect. We demonstrate the existence of the Mpemba effect and its inverse for steady state initial conditions. In this analysis, we also demonstrate the existence of the strong Mpemba effect where for certain specific initial steady states, the equilibration rate is exponentially faster compared to any other initial steady states. The exact analysis for the anisotropically driven Maxwell gas puts the kinetic theory results for the Mpemba effect, which depended on many simplifying assumptions, on a more sound footing.

Different measures to study the Mpemba effect: In driven granular gases, granular temperature or the mean kinetic energy of the system is used to track the evolution of the system [22, 24, 23, 25, 26, 27] as it relaxes from an initial state to a final state. The system with higher granular temperature is considered further away from the final steady state and is referred to as the hot system whereas the system with lower granular temperature is referred to as the colder system. Here, the Mpemba effect occurs if the system which is further from final steady state relaxes faster than an identical system which is initially closer to the final state when both the systems are quenched to the common steady state, having granular temperature lower than both the initial temperatures.

However, the measure of mean kinetic energy seems ad-hoc and there is an ambiguity in the present definition. It is because the time evolution of the system is being projected onto only one of the variables which is the total granular temperature. In that way, the demonstration of the time evolution of the system do not provide the complete picture and it is not known a priori whether mean kinetic energy correctly predicts the distance of the initial states from the final steady states. It is also not clear whether one observes the Mpemba effect if the evolution of the system is described in the phase space of all the relevant variables instead of projecting the evolution in one of the variables.

In order to address the issues related to the use of a certain measure, we introduce several other measures such as Manhattan measure ($\mathcal{L}_1$), Euclidean measure ($\mathcal{L}_2$) and Kullback-Leibler (KL) divergence which can describe the evolution of the system in the complete phase space of all the relevant variables. We do the analysis in the setup of anisotropically driven granular gas [26, 27] as such a model shows the Mpemba effect for initial steady states. We derive the criteria for the existence of the Mpemba effect with the various measures and show the non-universality of the various definitions in predicting the existence of the Mpemba effect. The non-universality in the description of the Mpemba effect using the various measures is in contrast to the systems obeying Markovian dynamics where all the measures show qualitatively similar behaviour. It is because the distance functions satisfy the following properties [11]: (1) as the system relaxes toward thermal equilibrium, the distance function is monotonically non-increasing with time, (2) for three temperatures $T_h > T_c > T_b$, where T_b is the temperature of bath, the distance from T_b is larger for T_h compared to T_c, and (3) the distance function is a continuous, convex probability distribution function. As a result, there is an one to one correspondence between the distance from the final steady state and the initial temperature difference of the systems from that of the final steady state irrespective of the choice of the various measures. Because of the above features, the identification of the Mpemba effect is indifferent to the choice of the distance function. However, granular systems have certain differences compared to the systems studied in Refs. [11, 14]. It is a system far from equilibrium. Also, it is an athermal system with no natural definition of temperature. As a result, the distance measures defined for the study of the Mpemba effect in the case of granular systems do not satisfy the above features and hence there is lack of universality among the various measures.

Mpemba effect in Langevin system

The system of a single particle Langevin system consists of a Brownian particle immersed in a heat bath and diffusing in a potential landscape. Here, the initial state of the system is an equilibrium state corresponding to the bath temperature. The relaxation dynamics of such a system is studied in the overdamped limit as the bath temperature is quenched to some lower temperature. In order to probe the existence of the Mpemba effect, we compare the relaxations of two such out-of-equilibrium systems. The two systems are initially prepared at the equilibrium of the two different temperatures, T_h and T_c corresponding to a comparatively hot and a cold temperature of a bath respectively. Both the systems are

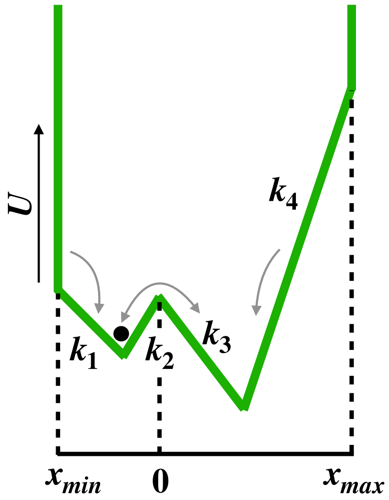

Figure 2: Schematic diagram of the potential landscape

then quenched to an even colder bath temperature and their relaxation is studied. In this study, the Mpemba effect is evaluated by defining certain measures for the distance of the systems from their final equilibrium state in the space of probability densities. To this end, the probability densities of the initially hot and the comparatively cooler system is known in terms of their equilibrium (Boltzmann) densities of the hot and the cold temperature. As both the systems are then quenched into an environment with a colder temperature, the probability densities of the systems evolve in time toward the equilibrium of the final temperature. By tracking the distance in the space of probability densities, the Mpemba effect can be identified.

We analyse the various key configurations of the external potential as shown in Fig. 2 that lead to the Mpemba effect. The choice of the double well piece-wise linear potential allows for an exact analysis of the problem. We show that the presence of a larger potential barrier between its two wells leads to the Mpemba effect. The explanation is given in terms of the concentration of the population of the Brownian particle as a result of modulation of the external potential. The larger barrier leads to a significant amount of population concentration for the initially colder system in the intermediate energy well or the metastable state as compared to the initially hotter system. The population concentration of the initially hotter system is effectively flat across the domain of the potential and does not experience the metastable state. As a result, the colder system takes effectively more time to relax to the equilibrium configuration as compared to the hotter system which leads to the Mpemba effect.

List of Figures

1 Schematic diagram describing the general scenario of the Mpemba effect: (a) state A is initially farther in the phase space than state B from the final desired state, (b) state A which is initially farther in the phase space equilibrates faster illustrating the Mpemba effect. 2

2 Schematic diagram of the potential landscape 8

1.1 Schematic diagram describing the general scenario of the Mpemba effect 33

1.2 Schematic diagram of a driven granular setup. The discs represents the granular particles in two dimensions. The arrows of different lengths represent the different velocities of the particles. The particles are driven at a constant rate with the driving strength ξ_0. 35

1.3 Schematic diagram for a double well potential. Here, ΔE is the difference of energy between the two wells of the potential. 39

1.4 Schematic diagram for the population distribution of the Brownian particle in the potential landscape at two different temperatures. The curves shown in black solid line denote the potential landscape whereas the population distribution of the Brownian particle across the potential landscape is shown by red and blue solid lines corresponding to the initially hot and cold particles respectively. Two configurations of the potential landscape is shown corresponding to a slightly (a) deeper and (b) shallow well. 41

2.1 The time evolution of the mean kinetic energy, E of the mono-dispersed Maxwell gas for two systems P and Q with initial conditions $E^P(0) = 4$, $E^Q(0) = 2$, $C^P(0) = 3$ and $C^Q(0) = 23$, which satisfy the conditions for the Mpemba effect as described in Eq. (2.39). The choice of the other parameters defining the system are $r = 0.5$, $r_w = 0.5$ and $\sigma = 1$. P relaxes to the steady state faster than Q, though its initial energy is larger. The time at which the trajectories cross each other is $\tau = 0.1334$, as given by Eq. (2.36). 58

2.2 The $\Delta E/\Delta C$–r phase diagram showing regions where the Mpemba effect is observed for mono-dispersed Maxwell gas (see Sec. 2.4), where r is the coefficient of restitution. All other parameters are kept constant. The region below the critical line show the Mpemba effect. 59

2.3 The time evolution of the total energy, $E_{tot}(t)$ for two systems P and Q of the bi-dispersed Maxwell gas where only one component is driven with initial conditions: $E^P_{tot}(0) = 22$, $E^Q_{tot}(0) = 14$, $E^P_{diff}(0) = 18$ and $E^Q_{diff}(0) = 4$ such that $E^P_{tot}(0) > E^Q_{tot}(0)$, which satisfies the condition for the Mpemba effect as described in Eq. (4.36). The choice of the other parameters defining the system are $m_B = 2m_A$, $r_{AA} = r_{AB} = r_{BB} = r_w = 0.5$, $\nu_A = 0.2$, $\nu_B = 0.8$ and $\sigma = 1$. P relaxes to the steady state faster than Q, though its initial energy is larger. The time at which the trajectories cross each other is τ=0.807 as given by Eq. (5.11). 64

2.4 The $\Delta E_{tot}/\Delta E_{diff}$–$r_{AB}$ phase diagram showing regions where the Mpemba effect is observed for the bi-dispersed Maxwell gas, where only one component of the gas is driven (see Sec. 2.5.1) and r_{AB} is the coefficient of restitution. All other parameters are kept constant. The choice of the other parameters defining the system are $m_A = 2m_B$, $\nu_A = \nu_B = 0.5$ and $r_{AA} = r_{BB} = r_w = 0.5$. The region below the critical line shows the Mpemba effect whereas the region on the other side of the critical line does not show the Mpemba effect. 65

2.5 The time evolution of the total energy, $E_{tot}(t)$ for two systems P and Q of a bi-dispersed Maxwell gas where both components are driven with initial steady state conditions: $E^P_{tot}(0) = 150.4$, $E^Q_{tot}(0) = 132$, $E^P_{diff}(0) = 75.2$ and $E^Q_{diff}(0) = 30.5$ such that $E^P_{tot}(0) > E^Q_{tot}(0)$, which satisfies the condition for the Mpemba effect as described in Eq. (4.36). The choice of the other parameters defining the system are $m_B = 10m_A$, $r_{AA} = r_{BB} = r_w = 0.5$, $r_{AB} = 0.6$, $\nu_A = 0.2$, $\nu_B = 0.8$, $\sigma_A = 2$ and $\sigma_B = 1$. P relaxes to the steady state faster than Q, though its initial energy is larger. The time at which the trajectories cross each other is τ=0.39 as given by Eq. (5.11). 68

2.6 The $\Delta E_{tot}/\Delta E_{diff}$–$r_{AB}$ phase diagram showing regions where the Mpemba effect is observed for the bi-dispersed Maxwell gas, where both components of the gas are driven (see Sec 2.5.2) and r_{AB} is the coefficient of restitution. All other parameters are kept constant. The choice of the other parameters defining the system are $m_B = 2m_A$, $\nu_A = 0.2$, $\nu_B = 0.8$, $r_w = 0.6$ and $r_{AA} = r_{BB} = 0.5$. The region below the critical line gives the set of initial steady states that show the Mpemba effect whereas the region on the other side of the critical line correspond to initial states that do not show the Mpemba effect. 70

2.7 The time evolution of the total energy, $E_{tot}(t)$ for two systems P and Q of bi-dispersed Maxwell gas where both components are driven with initial steady state conditions: $E^P_{tot}(0) = 150.4$, $E^Q_{tot}(0) = 132$, $E^P_{diff}(0) = 75.2$ and $E^Q_{diff}(0) = 30.5$ such that $E^P_{tot}(0) > E^Q_{tot}(0)$, which satisfies the condition for the inverse Mpemba effect as described in Eq. (4.36). The choice of the other parameters defining the system are $m_B = 10m_A$, $r_{AA} = r_{BB} = r_w = 0.5$, $r_{AB} = 0.6$, $\nu_A = 0.2$, $\nu_B = 0.8$, $\sigma_A = 8$ and $\sigma_B = 8$. P relaxes to the steady state slower than Q, though its initial energy is larger. The time at which the trajectories cross each other is τ=0.39 as given by Eq. (5.11). 71

2.8 The time evolution of the total energy, $E_{tot}(t)$ for two systems P and Q of bi-dispersed Maxwell gas, both components are initially in steady states, with $E^P_{tot}(0) = 47.8$, $E^Q_{tot}(0) = 43.8$, $E^P_{diff}(0) = 45.6$ and $E^Q_{diff}(0) = 39$ such that $E^P_{tot}(0) > E^Q_{tot}(0)$. These initial values satisfy both the conditions for the Mpemba effect as described in Eq. (4.36) as well as those for the strong Mpemba effect (for system P) as described in Eq. (4.40). The choice of the other parameters defining the system are $m_B = 10m_A$, $r_{AA} = 0.5$, $r_{BB} = 0.4$, $r_w = 0.6$, $r_{AB} = 0.35$, $\nu_A = 0.2$, $\nu_B = 0.8$, $\sigma_A = 2$ and $\sigma_B = 1$. P equilibrates to the final state at an exponentially faster rate compared to Q. Inset: The trajectories for P and Q cross at a time $\tau = 0.73$, as given by Eq. (5.11). 74

3.1 Variation of $\tilde{T}^{st}_{tot}(r,\mu)$ and $\tilde{T}^{st}_{dif}(r,\mu)$ with μ for two different cases of (a) $r = 0.01$ and (b) $r = 0.65$. $\tilde{T}^{st}_{dif}(r,\mu)$ goes to zero in the limit of isotropic driving, $\mu \to 1$ and its value decreases with the increase in r for any given value of the ratio of driving strengths, μ. 84

3.2 (a) The time evolution of $T_{tot}(t^*)$ with time t^* for two systems P and Q, with initial conditions $T^P_{tot}(0)/T^{st}_{tot}$=1.005, $T^P_{dif}(0)/T^{st}_{tot}$=0.28 ($\xi^2_{oy}/\xi^2_{ox} = 6 \times 10^{-3}$), $T^Q_{tot}(0)/T^{st}_{tot}$=1.004 and $T^Q_{dif}(0)/T^{st}_{tot}$=0.2 ($\xi^2_{oy}/\xi^2_{ox} = 0.168$), show the Mpemba effect when quenched to the final stationary state values of T^{st}_{tot}=1.00 and $T^{st}_{dif}/T^{st}_{tot}$=0.28 ($\xi^2_{oy}/\xi^2_{ox} = 1.54 \times 10^{-4}$). (b) The initial conditions $T^P_{tot}(0)/T^{st}_{tot}$=0.997, $T^P_{dif}(0)/T^{st}_{tot}$=0.277 ($\xi^2_{oy}/\xi^2_{ox} = 7.34 \times 10^{-2}$), $T^Q_{tot}(0)/T^{st}_{tot}$=0.996 and $T^Q_{dif}(0)/T^{st}_{tot}$=0.198 ($\xi^2_{oy}/\xi^2_{ox}$=0.169) show the inverse Mpemba effect when heated to the final stationary state values of T^{st}_{tot}=1.0 and $T^{st}_{dif}/T^{st}_{tot}$=0.28 ($\xi^2_{oy}/\xi^2_{ox} = 1.54 \times 10^{-4}$). The solid lines represent the exact time evolution of T_{tot} and the dashed lines represent its time evolution after linearisation. The other parameters used for the systems are m=1, $n\sigma^2$=0.02 and r=0.65. 90

3.3 The $\Delta T_{tot}/\Delta T_{dif}$–$r$ phase diagram showing regions where the Mpemba effect is observed and r is the coefficient of restitution. All other parameters are kept constant. Here, both the systems are quenched to the final stationary state given by $T^{st}_{tot} = 1.0$ and $T^{st}_{dif}/T^{st}_{tot} = 0.15$. The region below the critical line show the Mpemba effect whereas the region on the other side of the critical line does not show the Mpemba effect. 91

3.4 Time evolution of $T_{tot}(t^*)$ with t^* for two identical systems P and Q with initial conditions $T^P_{tot}(0)/T^{st}_{tot}$=1.026, $T^P_{dif}(0)/T^{st}_{tot}$=0.456 ($\xi^2_{oy}/\xi^2_{ox}$=0.08), $T^Q_{tot}(0)/T^{st}_{tot}$=1.014 and $T^Q_{dif}(0)/T^{st}_{tot}$=0.2 ($\xi^2_{oy}/\xi^2_{ox}$=0.438) which are chosen close to the final stationary state values of T^{st}_{tot}=1.0 and $T^{st}_{dif}/T^{st}_{tot}$=0.1 ($\xi^2_{oy}/\xi^2_{ox}$=0.667). P cools exponentially faster than Q though it has higher initial temperature and thus exhibits the strong Mpemba effect. The other parameters used for the systems are m=1, $n\sigma^2$=0.02 and r=0.2. 92

3.5 (a) The time evolution of $T_{tot}(t^*)$ with time t^* for two systems P and Q, with initial conditions $T^P_{tot}(0)/T^{st}_{tot}$=1.051, $T^P_{dif}(0)/T^{st}_{tot}$=0.294 ($\xi^2_{oy}/\xi^2_{ox}$=3.64×10^{-3}), $T^Q_{tot}(0)/T^{st}_{tot}$=1.046 and $T^Q_{dif}(0)/T^{st}_{tot}$=−0.172 ($\xi^2_{oy}/\xi^2_{ox}$=3.87), show the Mpemba effect when quenched to the final stationary state values of T^{st}_{tot}=1.0 and $T^{st}_{dif}/T^{st}_{tot}$=0.279 ($\xi^2_{oy}/\xi^2_{ox}$=3.89×10^{-3}). (b) The initial conditions $T^P_{tot}(0)/T^{st}_{tot}$=0.953, $T^P_{dif}(0)/T^{st}_{tot}$=0.267 ($\xi^2_{oy}/\xi^2_{ox}$=3.59×10^{-3}), $T^Q_{tot}(0)/T^{st}_{tot}$=0.948 and $T^Q_{dif}(0)/T^{st}_{tot}$=−0.156 ($\xi^2_{oy}/\xi^2_{ox}$=3.89) show the inverse Mpemba effect when heated to the final stationary state values of T^{st}_{tot}=1.0 and $T^{st}_{dif}/T^{st}_{tot}$=0.279 ($\xi^2_{oy}/\xi^2_{ox}$=3.89×10^{-3}). The solid lines represent the exact time evolution of T_{tot} and the points represent the results from simulation. The other parameters used for the systems are m=1, $n\sigma^2$=0.02 and r=0.65. 94

3.6 Time evolution of $T_{tot}(t^*)$ with t^* for two identical systems P and Q with initial conditions $T^P_{tot}(0)/T^{st}_{tot}$=2.1, $T^P_{dif}(0)/T^{st}_{tot}$=1.26 ($\xi^2_{oy}/\xi^2_{ox}$=5.89$\times$10^{-5}), $T^Q_{tot}(0)/T^{st}_{tot}$=2.0 and $T^Q_{dif}(0)/T^{st}_{tot}$=$-$1.2 ($\xi^2_{oy}/\xi^2_{ox}$=1.697$\times$10^4) show the Mpemba effect when quenched to the final stationary state values of T^{st}_{tot}=1.0 and $T^{st}_{dif}/T^{st}_{tot}$=0.6 ($\xi^2_{oy}/\xi^2_{ox}$=5.893$\times$10^{-5}). The other parameters used for the system are $r = 0.05$, $m = 1$ and $n\sigma^2 = 0.02$. The solid lines represent the exact time evolution of T_{tot} and the points represent the results from simulation. . . 95

4.1 (a) The time evolution of the total energy, $E_{tot}(t)$ for anisotropically driven systems P and Q of a two dimensional inelastic Maxwell gas, driven along both the directions of the plane, with initial conditions $E^P_{tot}(0)$=20.27, $E^Q_{tot}(0)$=17.32, $E^P_{dif}(0)$=-7.93 and $E^Q_{dif}(0)$=6.26 such that $E^P_{tot}(0) > E^Q_{tot}(0)$, which satisfies the condition for the Mpemba effect as described in Eq. (4.36). The other parameters decribing the systems are chosen to be r=0.3, $r_{wx} = 0.88$ and $r_{wy} = 0.39$. P relaxes to the steady state faster than Q, though its initial energy is larger. The time at which the trajectories cross each other is $\tau = 0.73$ as given by Eq. (5.11). (b) $\Delta E_{tot}/\Delta E_{dif}$–$A$ phase diagram showing regions where the Mpemba effect is observed and A [given by Eq. (4.37)] is a function of the parameters of the system. The region below the line given by Eq. (4.36) denotes the set of steady state initial conditions that show the Mpemba effect whereas the region on the other side of the line corresponds to initial states that do not show the Mpemba effect. 109

4.2 The time evolution of the total energy, $E_{tot}(t)$ for anisotropically driven systems P and Q of a two dimensional inelastic Maxwell gas, driven along both the directions of the plane, with initial conditions $E^P_{tot}(0)$=20.27, $E^Q_{tot}(0)$=17.32, $E^P_{dif}(0)$=-7.93 and $E^Q_{dif}(0)$=6.26 such that $E^P_{tot}(0) > E^Q_{tot}(0)$, which satisfies the condition for the inverse Mpemba effect as described in Eq. (4.36). The other parameters decribing the systems are chosen to be r=0.3, $r_{wx} = 0.88$ and $r_{wy} = 0.39$. P relaxes to the steady state slower than Q, though its initial energy is larger. The time at which the trajectories cross each other is $\tau = 0.73$ as given by Eq. (5.11). 111

4.3 (a)The time evolution of the total energy, $E_{tot}(t)$ for anisotropically driven systems P and Q of a two dimensional inelastic Maxwell gas, driven along both the directions of the plane, with $E^P_{tot}(0) = 95.89$, $E^Q_{tot}(0) = 61.57$, $E^P_{diff}(0) = -59.82$ and $E^Q_{diff}(0) = -4.26$ such that $E^P_{tot}(0) > E^Q_{tot}(0)$. These initial values satisfy both the conditions for the Mpemba effect as described in Eq. (4.36) as well as those for the strong Mpemba effect (for system P) as described in Eq. (4.40). The other parameters defining the system are chosen to be $r = 0.2$, $r_{wx} = 0.88$ and $r_{wy} = 0.49$. P equilibrates to the final state at an exponentially faster rate compared to Q and the time at which the trajectories cross each other is $\tau = 4.14$ as given by Eq. (5.11). (b) $E^P_{tot}(0)$–$E^P_{dif}(0)$ phase diagram showing regions of initial conditions where the system P shows the Mpemba effect as well as the strong Mpemba effect. The initial conditions for system Q and all the other parameters describing the two systems are similar to (a). Both the systems are quenched to the final steady state condition $E_{tot} = 35.92$ and $E_{dif} = 23.66$. The region below the solid line given by Eq. (4.36) denotes the set of steady state initial conditions that show the Mpemba effect and the dashed line denotes the set of initial conditions of system P for which it shows the strong Mpemba effect. 114

4.4 (a) The time evolution of the total energy, $E_{tot}(t)$ for anisotropically driven systems P and Q of a two dimensional inelastic Maxwell gas driven along a single direction with initial conditions $E^P_{tot}(0)$=28, $E^Q_{tot}(0)$=22, $E^P_{dif}(0)$=26 and $E^Q_{dif}(0)$=5 such that $E^P_{tot}(0) > E^Q_{tot}(0)$, which satisfies the condition for the Mpemba effect as described in Eq. (4.36). The other parameters decribing the systems are chosen to be r=0.5 and $r_{wx} = 0.6$. P relaxes to the steady state faster than Q, though its initial energy is larger. The time at which the trajectories cross each other is $\tau = 1.07$ as given by Eq. (5.11). (b) $\Delta E_{tot}/\Delta E_{dif}$–$A$ phase diagram showing regions where the Mpemba effect is observed and A [given by Eq. (4.45)] is a function of the parameters of the system. The region below the line given by Eq. (4.36) shows the Mpemba effect whereas the region on the other side of the line does not show the Mpemba effect. 117

5.1 The time evolution of anisotropically driven (a) inelastic Maxwell and (b) hard disc granular gas is illustrated in terms of the mean kinetic energy, E_{tot} for two systems P and Q. The initial conditions for the inelastic Maxwell gas in (a) are $E_{tot}^{P}(0) = 1.148$, $E_{tot}^{Q}(0) = 0.92$, $E_{dif}^{P}(0) = -0.595$ and $E_{dif}^{Q}(0) = 0.455$, corresponding to the choice of the driving strengths $\sigma_x^P = 0.25$, $\sigma_y^P = 1.0$, $\sigma_x^Q = 0.6$ and $\sigma_y^Q = 0.45$. The choice of the other parameters defining the system are $r = 0.3$, $r_{wx} = 0.88$, $r_{wy} = 0.39$, $\sigma_x = 0.1$ and $\sigma_y = 0.05$. The initial conditions for the hard disc granular gas in (b) are $E_{tot}^{P}(0) = 10.05$, $E_{tot}^{Q}(0) = 10.04$, $E_{dif}^{P}(0) = 2.797$ and $E_{dif}^{Q}(0) = 1.979$, corresponding to the choice of the driving strengths $\sigma_x^P = 0.476$ and $\sigma_y^P = 0.003$ and $\sigma_x^Q = 0.405$, $\sigma_y^Q = 0.070$. The final steady state is characterized by $E_{tot}^{st} = 10.0$ and $E_{dif}^{st} = 2.82$ corresponding to the driving strengths $\sigma_x = 0.476$ and $\sigma_y = 7.351 \times 10^{-5}$. The choice of the other parameters defining the system are $r = 0.65$, $m = 1$, $n = 0.02$. P relaxes to the steady state faster than Q, though it is initially at a larger distance compared to the final steady state. 132

5.2 The time evolution of the anisotropically driven inelastic Maxwell gas in terms of the Euclidean measure, $\mathcal{L}_2(t)$ for two systems P and Q with initial conditions $\mathcal{L}_2^P(0) = 6.34$ and $\mathcal{L}_2^Q(0) = 6.15$, shows two crossings as illustrated in (a) and (b) for the different times. The multiple crossing times are obtained using Eq. (5.16). The choice of the other parameters defining the system are $r = 0.1$, $r_{wx} = 0.95$, $r_{wy} = 0.39$, $\sigma_x = 1.6$ and $\sigma_y = 1.1$. 135

5.3 The time evolution of anisotropically driven (a) inelastic Maxwell and (b) hard disc granular gas is illustrated in terms of Euclidean measure, $\mathcal{L}_2(t)$ for two systems P and Q. The initial conditions for the inelastic Maxwell gas in (a) are $\mathcal{L}_2^P(0) = 3.13$ and $\mathcal{L}_2^Q(0) = 2.79$, corresponding to the choice of the driving strengths $\sigma_x^P = 1.9$, $\sigma_y^P = 1.2$, $\sigma_x^Q = 1.55$ and $\sigma_y^Q = 2.0$. The driving strengths corresponding to final steady state are $\sigma_x = 1.6$ and $\sigma_y = 1.1$ whereas the choice of the other parameters defining the system are $r = 0.3$, $r_{wx} = 0.95$, $r_{wy} = 0.39$. The initial conditions for the hard disc granular gas in (b) are $\mathcal{L}_2^P(0) = 0.432$ and $\mathcal{L}_2^Q(0) = 0.208$, corresponding to the choice of the driving strengths $\sigma_x^P = 0.491$ and $\sigma_y^P = 7.572 \times 10^{-5}$ and $\sigma_x^Q = 0.444$, $\sigma_y^Q = 0.037$. The driving strengths corresponding to final steady state are $\sigma_x = 0.476$ and $\sigma_y = 7.351 \times 10^{-5}$ whereas the choice of the other parameters defining the system are $r = 0.65$, $m = 1$ and $n = 0.02$. P relaxes to the steady state faster than Q, though its initial Euclidean distance from the final steady state is larger. 135

5.4 The time evolution of anisotropically driven (a) inelastic Maxwell and (b) hard disc granular gas is illustrated in terms of Manhattan measure, $\mathcal{L}_1(t)$ for two systems P and Q. The initial conditions for the inelastic Maxwell gas in (a) are $\mathcal{L}_1^P(0) = 7.54$ and $\mathcal{L}_1^Q(0) = 7.06$, corresponding to the choice of the driving strengths $\sigma_x^P = 2.2$, $\sigma_y^P = 1.2$, $\sigma_x^Q = 0.1$ and $\sigma_y^Q = 1.2$. The driving strengths corresponding to final steady state are $\sigma_x = 1.6$ and $\sigma_y = 1.1$ whereas the choice of the other parameters defining the system are $r = 0.9$, $r_{wx} = 0.88$ and $r_{wy} = 0.3$. The initial conditions for the hard disc granular gas in (b) are $\mathcal{L}_1^P(0) = 0.52$ and $\mathcal{L}_1^Q(0) = 0.42$, corresponding to the choice of the driving strengths $\sigma_x^P = 0.466$ and $\sigma_y^P = 0.023$ and $\sigma_x^Q = 0.444$, $\sigma_y^Q = 0.037$. The driving strengths corresponding to final steady state are $\sigma_x = 0.476$ and $\sigma_y = 7.351 \times 10^{-5}$ whereas the choice of the other parameters defining the system are $r = 0.65$, $m = 1$ and $n = 0.02$. P relaxes to the steady state faster than Q, though its initial Manhattan distance from the final steady state is larger. 138

5.5 The time evolution of anisotropically driven (a) inelastic Maxwell and (b) hard disc granular gas is illustrated in terms of KL divergence measure, $D_{KL}(t)$ for two systems P and Q. The initial conditions for the inelastic Maxwell gas in (a) are $D^P_{KL}(0) = 0.82$ and $D^Q_{KL}(0) = 0.64$, corresponding to the choice of the driving strengths $\sigma^P_x = 1.4$, $\sigma^P_y = 4.0$, $\sigma^Q_x = 2.45$ and $\sigma^Q_y = 2.3$. The driving strengths corresponding to final steady state are $\sigma_x = 1.5$ and $\sigma_y = 0.9$ whereas the choice of the other parameters defining the system are $r = 0.3$, $r_{wx} = 0.88$ and $r_{wy} = 0.39$. The initial conditions for the hard disc granular gas in (b) are $D^P_{KL}(0) = 0.01$ and $D^Q_{KL}(0) = 0.0078$, corresponding to the choice of the driving strengths $\sigma^P_x = 7.148$, $\sigma^P_y = 0.026$, $\sigma^Q_x = 1.144$ and $\sigma^Q_y = 5.609$. The driving strengths corresponding to the final steady state are $\sigma_x = 6.62$ and $\sigma_y = 0.026$, whereas the choice of the other parameters defining the system are $r = 0.65, m = 1, n = 0.02$. P relaxes to the steady state faster than Q, though its initial KL divergence with respect to the final steady state is larger. 140

5.6 The time evolution of the two systems P and Q for an anisotropically driven inelastic Maxwell gas is illustrated for the following measures: (a) total energy, (b) Euclidean measure, (c) Manhattan measure and for (d) KL divergence. The initial conditions for the various measures are identical and are given in terms of the driving strengths for systems P and Q as $(\sigma^P_x = 1.9, \sigma^P_y = 1.2)$ and $(\sigma^Q_x = 1.55, \sigma^Q_y = 2.0)$. The choice of the other parameters defining the system are $r = 0.3$, $r_{wx} = 0.95$, $r_{wy} = 0.39$, $\sigma_x = 1.6$ and $\sigma_y = 1.1$. The existence of the Mpemba effect and the notion of “hot“ and “cold” system in terms of distance from the final steady state for a given pair of initial conditions is not unique among the various measures. 142

5.7 The phase diagram in the $(\delta E^{Q}_{dif}/\delta E^{P}_{tot})$-$(\delta E^{Q}_{tot}/\delta E^{P}_{tot})$ plane shows the existence of the Mpemba effect in the driven inelastic Maxwell gas for the use of different distance measures: (a) total energy, (b) Manhattan, (c) Euclidean, and (d) KL-divergence. The red (green) region corresponds to absence (presence) of the Mpemba effect, while the regions outside the triangular shape are not valid steady states. The white regions inside the triangle in (d) is due to discrete sampling of phase space. The choice of the parameters defining the system are $r = 0.4$, $r_{wx} = 0.44$, $r_{wy} = 0.95$, $\delta E^{P}_{tot} = 1.00$ and $\delta E^{P}_{dif}/\delta E^{P}_{tot} = 0.53$, which are kept constant across all the various measures. 143

5.8 The phase diagram in the $(\delta E^{Q}_{dif}/\delta E^{P}_{tot})$-$(\delta E^{Q}_{tot}/\delta E^{P}_{tot})$ plane shows the existence of the Mpemba effect in the driven hard disc granular gas for the use of different distance measures: (a) total energy, (b) Manhattan, and (c) Euclidean. The red (green) region corresponds to absence (presence) of Mpemba effect, while the white regions are not accessible. The choice of the parameters defining the system are $n = 0.02$, $\sigma = 1$, $m = 1$, $r = 0.1$, $\delta E^{P}_{tot} = 1.00$ and $\delta E^{P}_{dif}/\delta E^{P}_{tot} = 0.11$, which are kept constant across all the various measures. 144

6.1 Schematic diagram of the piecewise linear double well potential. The boundaries of the potential are situated at $-x_{min}$ and x_{max}. The two minima of the double well potential are located at $-\alpha x_{min}$ and βx_{max}, where $\alpha, \beta \in (0,1)$. The parameters k_1, k_2, k_3 and k_4 refer to the various slopes. ΔU depicts the difference in the depths of the two wells. 154

6.2 Modulation of the potential and its effect on the population distribution of the Brownian particle in the two wells. Panel (a) and (c) corresponds to different configurations of the potential well. The parameters of the potential in (a) are chosen to be $\alpha = 0.3$, $\beta = 0.3$, $x_{min} = \pi$, $x_{max} = \pi$, $k_1 = 2$, $k_2 = 5$, $k_3 = 6$ and $k_4 = 7$ and in (c) $\alpha = 0.5$, $\beta = 0.3$, $|x_{min}| = \pi$, $x_{max} = \pi$, $k_1 = 0.1$, $k_2 = 0.1$, $k_3 = 0.1$ and $k_4 = 0.9$. Panels (b) and (d) depict the population distribution corresponding to the external potentials in (a) and (c) respectively for the initial temperatures T_h (red), T_c (blue) and final temperature T_b (black) with $T_h > T_c > T_b$. 164

6.3 Illustration of the absence of the Mpemba effect in an asymmetric double well potential indicating that *asymmetry is not sufficient*. (a) Asymmetric shape of the potential with different depths for the left and right wells while keeping all the other parameters of the potential symmetric about the origin. The potential heights at its left, center and right edges are equal and so are the positions of the two wells about the origin. The shape of the potential corresponds to the choice of the parameters $x_{max} = x_{min} = \pi$, $\alpha = \beta = 0.5$, $k_1 = k_2 = 0.32$ and $k_3 = k_4 = 0.57$. (b) Monotonic evolution of $|a_2(T)|$ with T showing the absence of the Mpemba effect. Inset: Initial population distribution of the confined Brownian particle for the chosen temperatures $T_h = 50$ (red) and $T_c = 10$ (blue) showing almost similarly distributed populations across the potential landscape. The final equilibrium distribution (black) corresponds to bath temperature $T_b = 1$. . . 168

6.4 Illustration of the Mpemba effect in a confined double well potential with equal domain widths. (a) Shape of the potential with equal domain widths (3 units) about the origin. The asymmetry in the potential configuration is introduced through the choice of different slopes in separate domains. The configuration of the potential is determined by the choice of the parameters: $x_{max} = x_{min} = \pi$, $\alpha = \beta = 0.1$, $k_1 = 2$, $k_2 = 5$, $k_3 = 6$ and $k_4 = 7$. Inset: Initial population distribution of the confined Brownian particle for the chosen temperatures $T_h = 1000$ (red) and $T_c = 7$ (blue) such that $|a_2^h| < |a_2^c|$. This shows a significant population distribution for T_c around the metastable state compared to that (which is almost flat) of T_h. The final equilibrium distribution (black) corresponds to bath temperature $T_b = 1$. (b) Non-monotonic evolution of $|a_2(T)|$ with T clearly indicates the presence of the Mpemba effect in this set-up. 170

6.5 ΔU-T_h phase diagram illustrating the region of the Mpemba effect in the case of double well potential with equal domain widths. The phase diagram is obtained by varying the depth of the right well of the potential while keeping the depth of its left well fixed and by changing the temperature ratio. The phase space is partitioned into two domains: one where the Mpemba effect is present corresponding to the criteria $|a_2^h| < |a_2^c|$, and other complementary region. The phase diagrams correspond to different choices of the position of the potential wells which are symmetric about the origin and are determined by: (a) $\alpha = \beta = 0.1$, (b) $\alpha = \beta = 0.5$. . . . 171

6.6 Illustration of the Mpemba effect in a confined double well potential with unequal domain widths while keeping every other parameters symmetric about the origin. (a) Shape of the potential with unequal domain widths ($x_{max} \neq x_{min}$) about the origin. The various slopes of the potential are kept equal. The configuration of the potential is determined by the choice of the parameters: $x_{min} = \pi$, $x_{max} = 1.5\pi$, $\alpha = \beta = 0.1$ and $k_1 = k_2 = k_3 = k_4 = 7$. Inset: Initial population distribution of the confined Brownian particle for the chosen temperatures $T_h = 50$ (red) and $T_c = 10$ (blue) such that $|a_2^h| < |a_2^c|$. This shows a significant population distribution around the metastable state for T_c compared to the same for T_h. The final equilibrium distribution (black) corresponds to the bath temperature $T_b = 1$. (b) Non-monotonic evolution of $|a_2(T)|$ with T confirms the presence of the Mpemba effect in this set-up. 173

6.7 ΔU-T_h phase diagram illustrating the region of the Mpemba effect for the case of double well potential with unequal domain widths. The phase diagram is constructed in the similar manner as in Fig. (6.5). The phase diagrams in the left- and right- panel correspond to different choices of the widths for the right domain of the potential : (a) $x_{max} = 1.2\pi$, (b) $x_{max} = 1.5\pi$ keeping the width of its left domain fixed at $x_{min} = \pi$. The position of the two wells are determined by the parameters $\alpha = \beta = 0.1$ for both the cases. 174

6.8 Illustration of the Mpemba effect in a confined single well potential with no metastable state. (a) Shape of the single well potential is determined by the choice of the parameters: $x_{max} = x_{min} = \pi$, $\alpha = \beta = 0.5$, $k_2 = k_3 = 0$, $k_1 = 3.18$ and $k_4 = 5.73$. (b) Non-monotonic evolution of $|a_2(T)|$ with T showing the presence of the Mpemba effect. (c) Initial population distribution of the confined Brownian particle for the chosen temperatures $T_h = 48$ (red) and $T_c = 6$ (blue). Here, $|a_2^h| < |a_2^c|$ which shows a significant difference in the population density at the minimum of the potential well. The final equilibrium distribution (black) corresponds to bath temperature $T_b = 1$. The Mpemba effect disappears for the above configuration of the potential if the depth of the potential well is decreased as shown in (d). The modified potential configuration corresponds to a change in the slopes to $k_1 = 0.38$ and $k_4 = 2.93$ while keeping the other parameters same as in the earlier case. (e) Monotonic evolution of $|a_2(T)|$ with T shows the absence of the Mpemba effect for the modified configuration. (f) Initial population distribution of the confined Brownian particle for the same pair of temperatures $T_h = 48$ (red) and $T_c = 6$ (blue) show nearly similar population distribution at the minimum of the potential well. 177

6.9 ΔU-T_h phase diagram illustrating the region of the Mpemba effect for the case of a single well potential. The phase diagram is obtained as before by varying the depth of the potential minimum & the temperature ratio. Here, there are two distinct regions and the criterion $|a_2^h| < |a_2^c|$ marks the one where the Mpemba is observed. Here, $T_c = 4$ as before and the other parameters determining the configuration of the potential are: $\alpha = \beta = 0.5$. 178

6.10 Illustration of the Mpemba effect in terms of the distance measures: the norm measure (L_1) in left panel (a) and Kullback-Leibler (KL) divergence measure in right panel (b). The configuration of the potential is the same as in Fig. 6.4 where it is determined by the choice of the parameters: $x_{max} = x_{min} = \pi$, $\alpha = \beta = 0.1$, $k_1 = 2$, $k_2 = 5$, $k_3 = 6$ and $k_4 = 7$. The temperatures of the initially hot and the cold systems are $T_h = 100$ and $T_c = 8$ respectively. Both the plots confirm the existence of the Mpemba effect. 179

A.1 Schematic diagram for the collision between two hard discs. 185

List of Tables

1.1 Different setups of the driven granular system. 38

Chapter 1

Introduction

1.1 Mpemba effect

Does a hotter system indeed cool faster? We will be addressing this counter-intuitive question in this thesis.

Consider the simple experiment: Let us put two equal volume of water that are initially heated to two different temperatures and they are placed in a freezer at the same time. Now let us ask the question whether the initially hotter sample can freeze faster. But common sense suggests that the initially colder sample should freeze faster as it is closer to the freezing temperature. A similar kind of phenomena is observed by plumbers reporting the damage of hot water pipes in winter as they burst in subzero temperature whereas the cold water pipes remain in good shape.

Such anomalous phenomena is an apparent paradox that finds its description in the science literature from the time of Aristotle, Rene Descartes and Sir Francis Bacon. However, the modern terminology for the anomalous behaviour in the relaxation dynamics is called the Mpemba effect as it finds its name after Erasto Mpemba who was a Tanzanian school student when he did the first scientific study of the anomalous relaxation phenomenon for the case of water, along with the physicist Denis Osborne who was at University College in Dar es Salaam, in the 1960s. The scientific study about the Mpemba effect finds its description in the 1969 paper [1] and it has an interesting story behind the discovery which goes as:

"*My name is Erasto B. Mpemba, and I am going to tell you about my discovery, which was due to misusing a refrigerator.*"

Mpemba and his friends used to make ice-creams in school. However, space was limited in the school's freezer. As a result, Mpemba prefers to skip waiting for the mixture of boiled milk and sugar to cool down before putting it in the freezer as is usually followed by his other friends in order to keep the freezer in order. After certain time has passed by, Mpemba finds that his mixture of milk and sugar has turned into ice whereas others' mixture is still in a thick liquid state. Later Mpemba and Osborne found evidence for the anomalous behaviour in a proper scientific study with the freezing of water. However, Osborne had concluded that the tests were crude and more sophisticated experiments would be required to know the exact cause of the effect.

In proper terms, the Mpemba effect refers to the counter-intuitive relaxation phenomenon wherein a system initiated at a hot temperature equilibrates faster than the one prepared at a lower temperature when both are quenched to a cold temperature bath. Clearly, it contradicts Newton's law of cooling which states that the relaxation time of a system increases logarithmically with the increase in the initial temperature with respect to its surrounding. However, in Newton's law of cooling, it is inherently assumed that the cooling process is quasi-static and in that case, the initially hot system always lags behind the initially cold system as they relax towards a common state. Here, the cooling process involves quenching which is completely different from quasi-static cooling and is rather a far-from-equilibrium relaxation process.

The case of water is still debated and there is no clear consensus as of today about the cause of the effect in water. The numerous possible causes that are cited for the case of water involve supercooling, convection, presence of impurities, hydrogen bonding, etc. One such study for the case of water also casts doubt about the presence of the Mpemba effect [29]. The Mpemba effect, as described in the case of water, involves a phase transition where the final phase is ice and the initial phase is water or steam, the Mpemba like effect has been observed in other physical systems that does not involve a phase transition. The measurement of freezing time in the study of the Mpemba effect brings ambiguity in the analysis as water may exhibit supercooling where its temperature goes below the freezing time without undergoing the freezing. Moreover, as the water equilibrates, the temperature varies throughout the volume as it is out-of-equilibrium. As a result, the particles at the boundary layer of the volume of the water experiences the freezing environment while those that are present in the bulk are still warm. Hence, variables like temperature are not well defined in this scenario and brings ambiguity in the measurement.

The other physical systems where this effect has been demonstrated experimentally that does not involve a phase transition and does not involve the measurement of temperature that brings ambiguity in the out-of-equilibrium scenario includes magnetic alloys [2] and polylactides [3]. For example, in the case of magnetic alloys, two identical systems are prepared but with different initial magnetisations. Both the systems are quenched to a same magnetisation state which is lower than the initial magnetisations of the two systems. As both the systems relax towards the final equilibrium state, magnetisation of the systems is measured as a function of time. It is observed that the system with the initial equilibrium state having magnetisation further away from that of the final state relaxes faster compared to the system which is initially equilibrated to a state having magnetisation closer to the final state, thus exhibiting a Mpemba like behaviour.

On the theoretical front, the Mpemba effect has been studied in various model systems that provides more rigorous understanding of the effect. Such systems includes spin systems [5, 6, 7, 8, 9, 10], discrete state Markovian system [11, 12], particle diffusing in a po-

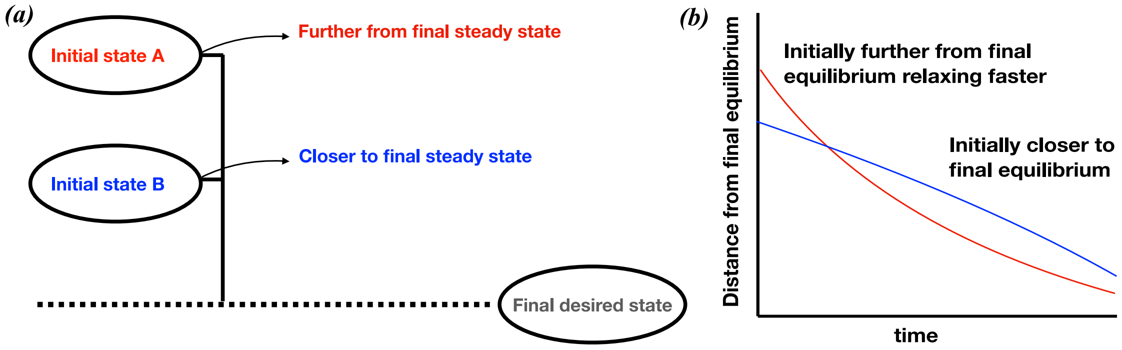
(a)
Initial state A
Further from final steady state
Initial state B
Closer to final steady state
Final desired state
(b)
Distance from final equilibrium
Initially further from final equilibrium relaxing faster
Initially closer to final equilibrium
time

Figure 1.1: Schematic diagram describing the general scenario of the Mpemba effect

tential [13, 14, 15, 30], active systems [16], systems with phase transitions [31, 8, 32, 33], spin glasses [17], molecular gases in contact with a thermal reservoir [18, 19, 20, 21], granular systems [22, 23, 24, 25, 26, 27, 34] and quantum systems [28, 35]. We will learn about the various models and their framework in slightly more details in the later chapters.

All the studies indicate to the fact that the Mpemba effect is more general and can be studied as a general relaxation phenomena in the physical systems for both thermal as well as athermal systems (where temperature is not even the physical observable that can be tracked to study the relaxation). Figure 1.1 shows the general protocol of studying the Mpemba effect in any out-of-equilibrium system. It consists of two different initial states of a given system. The states can be equilibrium or the non-equilibrium steady states. Both the initial states are quenched to a common final state following some mechanism which is system dependent. The relevant question of interest is whether the system that starts from an initially further distance in phase space from the final desired state actually relaxes faster compared to the state which is initially closer to the final state, thus showing a Mpemba like behaviour in the relaxation dynamics of out-of-equilibrium systems.

In this thesis, we study the Mpemba effect in the two class of stochastic systems namely the interacting many particle driven granular gases and the model of single particle Langevin system. The Mpemba effect is highly counter-intuitive and it is required to study the phenomena in terms of simple models that have experimental relevance in order to underpin the cause of the effect. The motivation for the choice of the system of driven granular gas is that it is a prototypical far from equilibrium system which provides a strong interplay between theoretical studies and the experiments at the same time. On the other hand, our study of the Mpemba effect in the model of single particle Langevin system is motivated from an experimental setup [4]. Unlike the case of driven granular gas where the initial and final states are steady sates here, the states are in equilibrium and described by the Boltzmann distribution. Our studies of the Mpemba effect in both the systems consist of analytically tractable models and the results are also verified using numerical simulations.

Now we briefly discuss the systems of many particle driven granular gas and single particle Langevin system.

1.2 Driven granular gas

The system of driven granular gas is a dilute collection of identical point particles, hard discs or spheres in one, two and three dimensions respectively. In this thesis, we will be constrained to one and two dimensions for the purpose of analytical tractability. The particles undergo inelastic collisions which are momentum conserving. The change in velocities of two particles undergoing collision and having velocities $\boldsymbol{v}_1$ and $\boldsymbol{v}_2$ in two dimensions is given by

$$\begin{aligned} \boldsymbol{v}_i' &= \boldsymbol{v}_i - \frac{1+r}{2}[(\boldsymbol{v}_i - \boldsymbol{v}_j).\hat{e}]\hat{e}, \\ \boldsymbol{v}_j' &= \boldsymbol{v}_j + \frac{1+r}{2}[(\boldsymbol{v}_i - \boldsymbol{v}_j).\hat{e}]\hat{e}, \end{aligned} \tag{1.1}$$

where r is the co-efficient of restitution and $\hat{e}$ is the unit vector along the line joining the centres of the particles at contact. Note that the case of $r = 0$ corresponds to completely inelastic collisions where two particles stick together after collision whereas $r = 1$ corresponds to elastic collisions. The collision between any pair of particles having velocities $\boldsymbol{v}_1$ and $\boldsymbol{v}_2$ is proportional to the absolute of their relative velocities, $|\boldsymbol{v}_1 - \boldsymbol{v}_2|$.

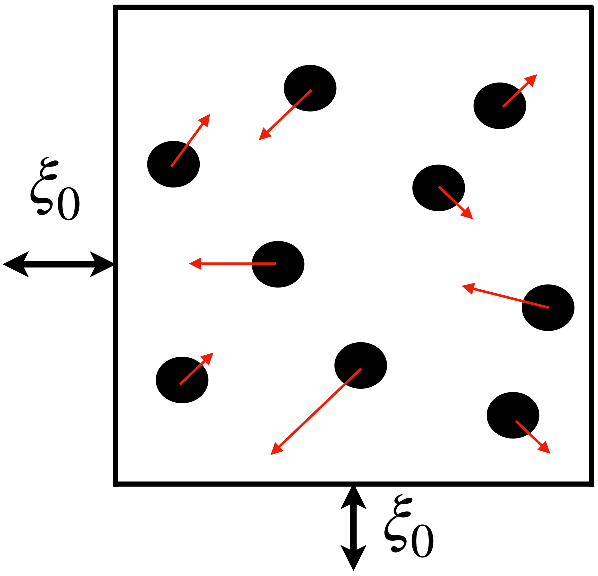

Figure 1.2: Schematic diagram of a driven granular setup. The discs represents the granular particles in two dimensions. The arrows of different lengths represent the different velocities of the particles. The particles are driven at a constant rate with the driving strength ξ_0.

In the absence of any external supply of mechanical energy, the mean kinetic energy of the particles decreases with time. In order to compensate for the loss of kinetic energies during the collision, the particles are driven at a constant rate λ_d. The stochastic driving is modelled as

$$\boldsymbol{v}' = -r_w \boldsymbol{v} + \boldsymbol{\eta}, \tag{1.2}$$

where r_w is a parameter that reduces the velocity and $\boldsymbol{\eta}$ is a noise taken from a fixed distribution $\phi(\boldsymbol{\eta})$. The form of the driving ensures that the system reaches a steady state in a long time. The motivations for the chosen form of driving will be discussed in the later part of this section. The scenario of the driven granular system in two dimensions is depicted in Fig. 1.2 where the particles are discs and are moving with different velocities resulting in collisions and at the same time, the particles are driven with driving strength ξ_0.

On the theoretical front, the evolution of the system in the presence of dissipation and driving is studied using the Enskog-Boltzmann's description of the kinetic theory of gases. Enskog-Boltzmann equation describes the particle collision rules in terms of the velocity distribution function $f(\boldsymbol{x},\boldsymbol{v},t)$ which is defined as the probability to find a particle at position $\boldsymbol{x}$ with velocity $\boldsymbol{v}$ at time t. The integral of the velocity distribution function $f(\boldsymbol{x},\boldsymbol{v},t)$ over the phase space gives the total number of particles, N present in the system

$$\int f(\boldsymbol{x},\boldsymbol{v},t) d\boldsymbol{x} d\boldsymbol{v} = N. \tag{1.3}$$

We will consider the case of homogeneous systems where the distribution function is independent of the position $\boldsymbol{x}$ of the particles and in that case,

$$\int f(\boldsymbol{v},t) d\boldsymbol{v} = n, \tag{1.4}$$

where n is the number density of the particles. The description of the system in terms of Enskog-Boltzmann equation involves setting up a master equation for the single particle velocity distribution function $f(\boldsymbol{v},t)$ at any time t. The master equation takes into account the gain and loss terms from the collision and driving events and is given by

$$\begin{aligned}\frac{\partial}{\partial t} f(v_1,t) &= \chi(\sigma)\sigma \int dv_2 \int d\theta \Theta(-v_{12}.e)|v_{12}.e| \left[\tfrac{1}{r^2} f(\boldsymbol{v}_1^{''},t) f(\boldsymbol{v}_2^{''},t) - f(v_1,t) f(v_2,t)\right] \\ &\quad -\lambda_d f(\boldsymbol{v}_1,t) + \lambda_d \int\int d\boldsymbol{\eta} d\boldsymbol{v}_1' \phi(\boldsymbol{\eta}) f(\boldsymbol{v}_1',t) \delta[-r_w \boldsymbol{v}_1' + \boldsymbol{\eta} - \boldsymbol{v}_1]. \end{aligned} \tag{1.5}$$

The details of the derivation for the Enskog-Boltzmann equation and the various terms are explained in the Appendix A. The contribution from the driving terms in the Enskog-Boltzmann equation is of particular interest for the system of driven granular gases as there are certain motivations for the chosen form of driving [see Eq. (1.2)]. The motivations for the choice of driving scheme are detailed in the Appendix B.

The system of driven granular gas is of particular interest as it provides a strong interplay with experiments. There exists vast literature on the experimental studies regarding various aspects of driven granular systems. Experimental setups of the driven granular systems in two dimensions generally consists of a collection of millimetre sized particles (such as steel balls or active disks resting on circularly aligned tilted elastic legs) resting on a two dimensional surface. The surface is vibrated along the vertical direction of the plane by external means to provide the input of kinetic energies to the particles [36, 37, 38, 39, 40, 41, 42, 43, 44].

The characterisation of the steady state velocity distribution $f(\boldsymbol{v})$ of driven granular systems is one such aspect and is one of the central problem in the kinetic theory of driven granular gases. We briefly discuss about the nature of velocity distribution of driven granular gases in Appendix C.

Inelastic Maxwell gas

As discussed earlier, the system of granular gas is modelled as collection of agitated hard discs or spheres in two and three dimensions respectively. However, the fact that the rate of collision in the model of hard discs or spheres is proportional to the relative velocities of the colliding particles hampers the analytical tractability of the model. In that case, the collision moments cannot be expressed in terms of finite number of velocity moments. Thus, in order to overcome the drawbacks of hard disc or hard sphere model of granular gas, a simplified model is introduced where the rate of collision among the particles is independent of their relative velocities. The collision between the particles take place with an associated constant rate. Such a simplification in the collision dynamics captures the major features of the granular gas while allowing for an exact analysis.

Table 1.1: Different setups of the driven granular system.

Model	Collision rate	Driving
Mono-dispersed Maxwell gas (1D) (one type of particle)	Constant	Isotropic drive
Bi-dispersed Maxwell gas (1D) (two species of particles: A & B)	Constant	Isotropic drive (different strengths for A & B)
Mono-dispersed hard disc granular gas (2D)	Velocity dependent	Anisotropic drive (different strengths along x & y)
Mono-dispersed Maxwell gas (2D)	Constant	Anisotropic drive (different strengths along x & y)

The Enskog-Boltzmann equation for the inelastic Maxwell gas simplifies to

$$\begin{aligned} \frac{\partial}{\partial t} f(v_{\mathbf{1}},t) \quad &= \chi(\sigma)\sigma \int dv_2 \int d\theta \left[\tfrac{1}{r^2} f(\boldsymbol{v}_1'',t) f(\boldsymbol{v}_2'',t) - f(v_1,t) f(v_2,t) \right] \\ &-\lambda_d f(\boldsymbol{v}_1,t) + \lambda_d \int \int d\boldsymbol{\eta} d\boldsymbol{v}_1' \phi(\boldsymbol{\eta}) f(\boldsymbol{v}_1',t) \delta[-r_w \boldsymbol{v}_1' + \boldsymbol{\eta} - \boldsymbol{v}_1]. \end{aligned} \tag{1.6}$$

We will be studying the Mpemba effect in driven granular gases with both the models of hard disc granular gas as well as the inelastic Maxwell model. Although the analysis based on the model of hard disc granular gas requires certain approximations, we provide numerical evidence about the validity of such approximations in the analysis. On the other hand, we derive exact results for the case of inelastic Maxwell model.

Various variants of the driven granular setups

In this thesis, we will study the Mpemba effect in several setups of the granular system. Here, we briefly outline the various setups in Table 1.1.

1.3 Single particle Langevin system

Unlike the case of driven granular gases which is an interacting many-particle system, here we will discuss about a single particle Langevin system. The system consists of

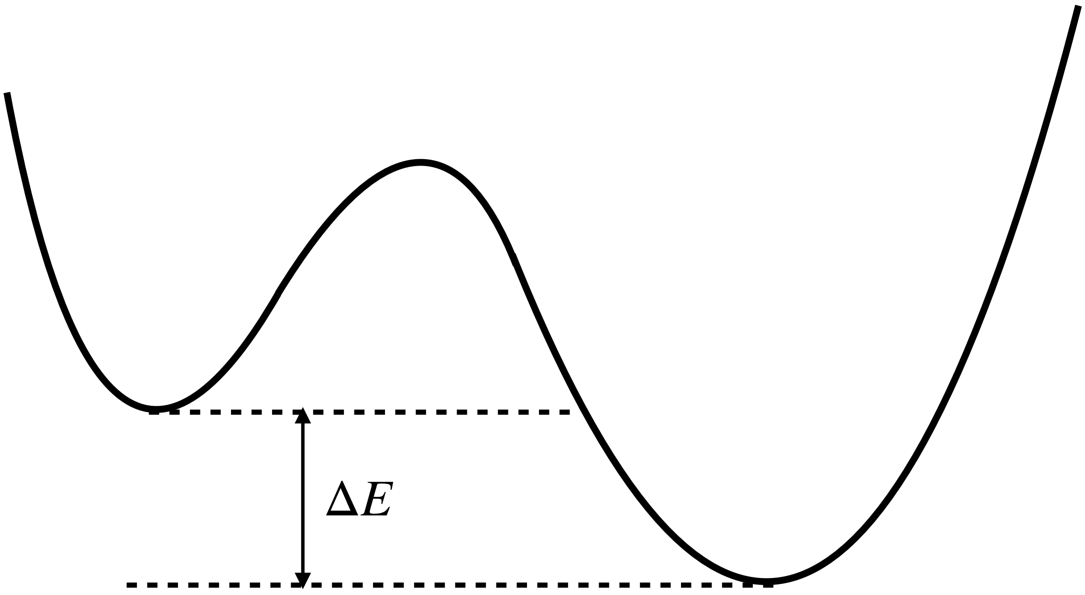

Figure 1.3: Schematic diagram for a double well potential. Here, ΔE is the difference of energy between the two wells of the potential.

a colloidal particle undergoing diffusion while immersed in water. The water having a temperature T_b acts as heat bath to the colloidal particle. The colloidal particle exhibits Brownian motion due to the impact of the water molecules. The equation of motion or the Langevin equation of the particle having mass m, position coordinate x at time t is given by

$$m\frac{d^2x(t)}{dt^2} = -\gamma\frac{dx(t)}{dt} + \Gamma(t), \tag{1.7}$$

where γ represents the damping or the drag experienced by the colloidal particle due to water molecules. Γ is uncorrelated white noise whose mean and variance satisfies

$$\langle\Gamma(t)\rangle = 0, \quad \langle\Gamma(t)\Gamma(t')\rangle = 2\gamma k_B T_b \delta(t-t'), \tag{1.8}$$

where k_B is the Boltzmann's constant.

Many interesting problems are studied when the particle diffuses in addition of an external potential. A schematic diagram of the potential landscape is shown in Fig. 1.3. Here, it's a quartic shaped potential with ΔE being the difference in energy between the two wells of the potential landscape. In experiments, the external potentials are realised using optical traps. One particular problem of interest in this setup being the famous Kramer's escape problem where the rate at which the Brownian particle can escape from one well to the other is determined. In the presence of an external potential $U(x)$, Langevin equation is given by

$$m\frac{d^2x(t)}{dt^2} = -\frac{dU(x)}{dx} - \gamma\frac{dx(t)}{dt} + \Gamma(t). \tag{1.9}$$

For simplification, we consider the overdamped limit where we neglect the second order time derivative and the Langevin Eq. (1.9) reduces to

$$\frac{dx(t)}{dt} = -\frac{1}{\gamma}\frac{dU(x)}{dx} + \frac{1}{\gamma}\Gamma(t). \tag{1.10}$$

The corresponding Fokker-Planck equation for the evolution of the probability density of the particle of being at position x and time t is given by

$$\frac{\partial p(x,t)}{\partial t} = \frac{\partial}{\partial x}\Big[\frac{1}{\gamma}\frac{dU}{dx}p(x,t)\Big] + \frac{k_B T_b}{\gamma}\frac{\partial^2 p(x,t)}{\partial x^2}. \tag{1.11}$$

The stationary solution of Eq. (1.11) is the equilibrium Boltzmann distribution given by

$$p(x,T_b) = \frac{e^{-U(x)/k_B T_b}}{\mathscr{Z}(T_b)}, \tag{1.12}$$

where $\mathscr{Z}(T_b) = \int dx e^{-U(x)/k_B T_b}$ is the normalization constant of the Boltzmann distribution at temperature T_b. We would be analysing in details about the solution of the Fokker-Planck equation in Chapter 6 for analytically tractable models of the external potentials.

For the analysis of the Mpemba effect in the setup of the single particle Langevin system, we will study in details about the role of the external potential in inducing Mpemba like

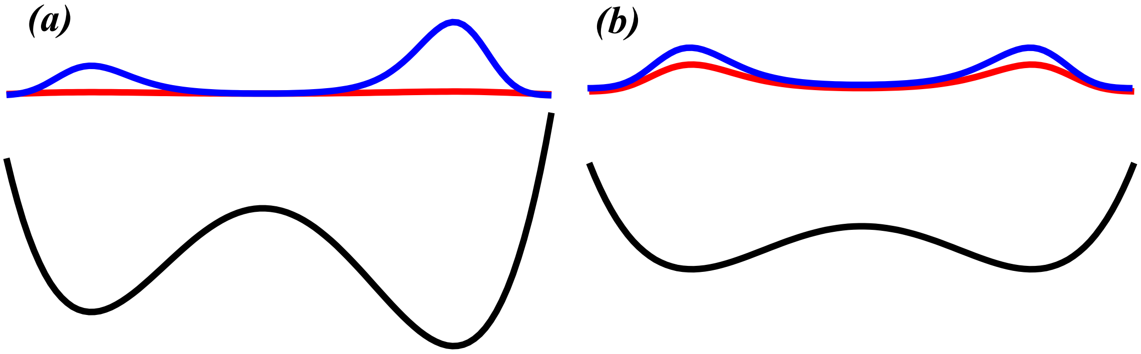

Figure 1.4: Schematic diagram for the population distribution of the Brownian particle in the potential landscape at two different temperatures. The curves shown in black solid line denote the potential landscape whereas the population distribution of the Brownian particle across the potential landscape is shown by red and blue solid lines corresponding to the initially hot and cold particles respectively. Two configurations of the potential landscape is shown corresponding to a slightly (a) deeper and (b) shallow well.

anomalous behaviour in the relaxation dynamics. In addition, we will also study the role of population distribution or the probability density of the Brownian particle as a function of the modulation of the shape of the external potential and the temperature in order to understand the Mpemba effect. As an example to illustrate the effect of the external potential in the population distribution of the Brownian particle, we consider two different configurations of the external potential as shown in Fig. 1.4.

In the potential landscape where there is a significant height of the barrier between the two wells of the potential [see Fig. 1.4(a)], the hotter particle has a flat population distribution (shown by red curve) compared to the initially colder particle which has a localised population distribution (shown by blue curve) across the potential landscape. On the other hand, Fig. 1.4(b) shows the potential landscape which has a relatively flat barrier between the two wells of the potential. In this case, both the hotter and the colder particles have relatively similar population distribution (shown by red and blue curves respectively). Thus, the presence of a barrier of significant height between the two wells of the potential affect the population distribution of the Brownian particle. We will study the role of such difference in the population distribution of the Brownian particle for different configurations of the potential in inducing the Mpemba effect.

1.4 Overview of the thesis

The thesis is organised as follows:

In Chapter 2, we consider the inelastic driven Maxwell gas, a simplified model for a granular gas, where the rate of collision is assumed to be independent of the relative velocity. Through an exact analysis, we determine the conditions under which the Mpemba effect is present in this model. For mono-dispersed gases, we show that the Mpemba effect is present only when the initial states are allowed to be non-stationary, while for bi-dispersed gases, it is present for some steady state initial states. We also demonstrate the existence of the strong Mpemba effect for bi-dispersed Maxwell gas wherein the system at higher temperature relaxes to a final steady state at an exponentially faster rate leading to smaller equilibration time.

In Chapter 3, we demonstrate the existence of Mpemba effect in anisotropically driven granular gases, even when quenched from initial states that are stationary. Our theoretical predictions, based on kinetic theory, for the regular, inverse and strong Mpemba effects agree well with results of event-driven molecular dynamics simulations of hard discs.

In Chapter 4, we do an exact analysis for the existence of the Mpemba effect in an anisotropically driven inelastic Maxwell gas, a simplified model for granular gases, in two dimensions. We demonstrate the existence of the Mpemba effect in anisotropically driven granular gases even when the initial states are non-equilibrium steady states. The precise conditions for the Mpemba effect, its inverse, and the stronger version, where the hotter system cools exponentially faster are derived.

In Chapter 5, we define several measures for the choice of distance function from the final steady state for the study of the Mpemba effect. We derive the criteria for the existence of the Mpemba effect based on the different measures. In this chapter, by studying four different distance measures based on the mean kinetic energies as well as velocity distribution, we show that the Mpemba effect depends on the definition of the measures. The non-universality among the various measures of the Mpemba effect in driven granular systems in terms of the phase space initial conditions is illustrated and the possible cause of it is discussed.

In Chapter 6, we present an exact analysis of the Mpemba effect in a single particle Langevin system by considering an exactly solvable model for the external potential. We consider different configurations of the external potential in order to understand its role in inducing the Mpemba effect. We discuss the role of metastable states in the energy landscape as well as the initial population distribution of the Brownian particle in its confined domain as the possible cause of the Mpemba effect in the presence of external potential with a local minima. However, we find that presence of metastable state is not the necessary criteria as we show that the Mpemba effect exists even in the presence of external potential without metastable states.

In Chapter 7, we summarize the findings of this thesis and give future outlook.

Chapter 2

Mpemba effect in driven granular Maxwell gases

2.1 Introduction

Mpemba effect has been observed experimentally in a wide range of physical systems ranging from water [45, 46, 47, 48, 49, 29], magnetic alloys [2], and clathrate hydrates [50] to polylactides [3]. In addition to experiments, various numerical tools and model systems were used to shed light on such anomalous relaxations. To better understand the effect in water, detailed molecular dynamic simulations were performed [51, 48, 52]. In these simulations, the system is made of up to several thousand molecules, with pairwise interactions that model the interactions between the water molecules. The initial configuration of the system is commonly sampled from the Boltzmann distribution of the hot or warm temperature, and the dynamic follows a standard molecular dynamic protocol that corresponds to the cold temperature. A different numerical approach was applied on spin systems, for both ordered [5] as well as glassy [17] models. Using a Monte Carlo simulation, the value of some order parameters were tracked during the relaxation process of systems that were sampled from the equilibrium distribution of a hot and a warm temperature, and evolved under Markovian dynamics that corresponds to a cold temperature. If, during the relaxation process the corresponding order parameters of the hot and cold systems intersect, then the Mpemba effect exists in the system.

On the analytic front, two different approaches were used to address the Mpemba effect so far. In Refs. [11, 6, 7], the Mpemba effect was defined and evaluated through the distance between probability distributions during the relaxation process. To this end, the probability distribution describing the system is initiated at the equilibrium (Boltzmann) distribution of the hot or warm temperature. The system is then quenched into an environment with a cold temperature, and thus the probability distribution of the system evolves in time towards the equilibrium of the cold temperature. By tracking the distance, in probability space, between the time dependent probability and the final equilibrium, the Mpemba effect can be identified, and the exact conditions for its existence were derived. Moreover, this framework naturally suggest a rich class of related phenomena, including the inverse Mpemba effect [11] where a cold system heats up faster than a warmer system; the strong Mpemba effect [6] where a specific initial temperature results in a jump in the relaxation rate; and non-monotonic optimal heating protocols [5] where the optimal heating protocol has a pre-cooling stage.

A different theoretical framework was used in the context of driven granular gases [22, 23, 24]. A granular gas is a dilute composition of particles that move ballistically and interact through momentum conserving binary inelastic collisions. These dissipative systems approach a steady state when externally driven to compensate for the kinetic energy which is lost in the inter-particle collisions. For the driven granular system with smooth mono-dispersed particles (only translational velocity is considered and rotational degrees of freedom are ignored) which interact via binary collisions with a rate proportional to the magnitude of the relative velocities of the colliding particles, it was shown that the total energy of a system with a higher initial energy attains the final low energy state before a similar system with an intermediate initial energy [22]. The effect was achieved by independently varying the deviation of the velocity distribution from a Gaussian, characterized by the coefficient of the second Sonine polynomial a_2. In this approach, the system was initiated in a non-stationary distribution, and relaxed towards the corresponding steady state (which is not an equilibrium distribution) associated with the parameters of the system. The Mpemba effect then exists in the system if a non-equilibrium system which is further away from equilibrium, namely has more energy in its initial state, equilibrates faster than an initial condition which is closer to the equilibrium state. The Mpemba effect was also demonstrated for a rough granular gas (both translational and rotational velocities are considered and they couple with each other), where a much larger range of initial energies result in anomalous relaxations [23] red as well as for a gas of viscoelastic particles [24]. In both the rough and smooth granular gas, the velocity distribution at all times was approximated by a Gaussian or Gaussian and first order corrections respectively, making the calculations perturbative in nature.

Do the results in the various frameworks for different systems correspond to the same effect? This is a key question, for which the answers is yet unknown. In this chapter, we partially address a specific difference that plays an important role in both the numerical and analytical results developed so far – the initial condition of the system. In the Markovian framework, the initial condition of the hot and warm systems is an equilibrium distribution corresponding to the initial temperature [11, 6, 7]. In contrast, in the granular gas approach the initial distributions are not a steady state of the system for any (effective) temperature, but are rather transient distributions with different amount of total energy. These distributions relax towards the steady-state distribution by energy exchange between the particles as well as with some bath [22, 23]. A similar difference in the initial conditions exists between the various molecular dynamic simulations calculated for water molecules: in [52] the system was initially sampled from a hot or warm temperature and then quenched to a cold environment, whereas in [51] the initial condition is not the equilibrium distribution of any temperature, but rather an altered distribution of the final temperature.

To address this specific difference between the two approaches, we consider the inelastic Maxwell model for granular gas in which the collision rates are assumed to be independent of the relative velocity [53, 54]. The model thus presents a simpler system of granular gas keeping the essential physics intact, while allowing for exact calculation. We investigate the existence of the Mpemba effect for both mono-dispersed and bi-dispersed systems. In Maxwell gases, the equations for the relevant two-point correlations is known to form a closed set of equations [55, 56, 57]. By analyzing these equations in detail, we determine the parameter regime in which the Mpemba effect can be seen in these systems. In particular, we show that while transient initial conditions are required for the effect to be present in mono-dispersed gas, the bi-dispersed system shows the Mpemba effect for steady state initial conditions. This allows us to use the Markovian approach for the Mpemba effect in driven granular gas, and therefore identify the existence of the strong effect in this system, where for a specific initial steady state the relaxation rate is smaller than from any other initial steady state. The content of this chapter is published in Ref. [25].

2.2 Model

In this chapter, we analyze both mono-dispersed as well as bi-dispersed driven inelastic Maxwell gases. We first define the bi-dispersed gas, and then indicate the limits when it reduces to a mono-dispersed gas. Consider N_A particles of type A, each of mass m_A, and N_B particles of type B, each of mass m_B. Let $N_A + N_B = N$. Each particle has a scalar velocity $v_{i,k}$, where $i = 1, \ldots, N$ and $k \in \{A, B\}$. These velocities evolve in time through binary collisions and external driving. A pair of particles of type k and l, where $k, l \in \{A, B\}$, collide with rate λ_{kl}/N. The factor $1/N$ in the collision rates ensures that the total rate of collisions between $N_k[N_k - 1]/2$ pairs of similar type of particles and that between $N_A N_B$ pairs of different type of particles are proportional to the system size N. During a collision, momentum is conserved, but energy is dissipated. Let $v_{i,k}$ and $v_{j,l}$

denote the pre-collision velocities and $v'_{i,k}$, $v'_{j,l}$ denote the post-collision velocities. Then

$$
\begin{aligned}
v'_{i,k} &= v_{i,k} - (1+r_{kl})\frac{m_l}{m_k+m_l}(v_{i,k}-v_{j,l}), \\
v'_{j,l} &= v_{j,l} + (1+r_{kl})\frac{m_k}{m_k+m_l}(v_{i,k}-v_{j,l}),
\end{aligned} \tag{2.1}
$$

where $k,l = A,B$, $r_{kl} \in [0,1]$ is the coefficient of restitution for the collision, and m_k and m_l are the masses. There are three coefficients of restitution: r_{AA}, r_{BB}, and r_{AB} depending on whether the pair of colliding particles are of type AA, BB, or AB. It is convenient to define

$$\alpha_{kl} = \frac{1+r_{kl}}{2}, \quad k,l = A,B, \tag{2.2}$$

where $1/2 \leq \alpha_{kl} \leq 1$.

In addition to collisions, the system evolves through external driving. We implement a driving scheme that drives the system to a steady state, and has been used in earlier studies [55, 56, 58]. Each particle is driven at a rate λ_d. During such an event, the velocity of the driven particle is modified according to

$$v'_{i,k} = -r_w v_{i,k} + \eta_k, \quad -1 < r_w \leq 1, \quad k = A,B, \tag{2.3}$$

where $r_w \in (-1,1]$ is a parameter and η_k is noise drawn from a fixed distribution $\phi_k(\eta_k)$. There is no compelling reason for $\phi_k(\eta_k)$ to be Gaussian. However, we restrict ourselves to distributions with zero mean and finite second moment σ_k^2 given by

$$\sigma_k^2 = \int_{-\infty}^{\infty} d\eta \; \eta^2 \phi_k(\eta), \quad k = A,B. \tag{2.4}$$

The physical motivations for the form of driving may be found in Refs. [59, 60]. Without loss of generality, in all the plots, we set the driving rate $\lambda_d = 1$, so that time is measured in units of λ_d^{-1}.

In the model, the spatial degrees of freedom have been neglected. This corresponds to the well-mixed limit where the spatial correlations between particles are ignored. In addition, we have assumed that the collision rates are independent of the relative velocity of the colliding particles. This corresponds to the so-called Maxwell limit.

Let $P_k(v,t)$, where $k = A,B$, denote the probability that a randomly chosen particle of type k has velocity v at time t. Its time evolution is given by:

$$\begin{aligned}\frac{d}{dt}P_k(v,t) =& \frac{\lambda_{kk}(N_k-1)}{N}\int\int dv_1 dv_2 P_k(v_1,t)P_k(v_2,t)\delta[(1-\alpha_{kk})v_1+\alpha_{kk}v_2-v]\\ &+\frac{\lambda_{k\bar{k}}N_{\bar{k}}}{N}\int\int dv_1 dv_2 P_k(v_1,t)P_{\bar{k}}(v_2,t)\delta[(1-X_{\bar{k}})v_1+X_{\bar{k}}v_2-v]\\ &-\frac{\lambda_{kk}(N_k-1)}{N}P_k(v,t)-\frac{\lambda_{k\bar{k}}N_{\bar{k}}}{N}P_k(v,t)\\ &+\lambda_d\left[-P_k(v,t)+\int\int d\eta_k dv_1 \phi_k(\eta_k)P_k(v_1,t)\delta[-r_w v_1+\eta_k-v]\right], \end{aligned} \tag{2.5}$$

where

$$\bar{k} = \begin{cases} B, & \text{if} \quad k = A,\\ A, & \text{if} \quad k = B, \end{cases} \tag{2.6}$$

and

$$X_k = \alpha_{AB}\mu_k \text{ where } \mu_k = \frac{2m_k}{m_A+m_B}, \; k = A,B, \tag{2.7}$$

with $\mu_k \in (0,2)$ and α_{AB} is defined in Eq. (2.2).

The mono-dispersed Maxwell gas is obtained by taking the limit $N_A = N$ with $(N_A - 1)/N \to 1$, $N_B = 0$, $r_{AA} = r$ and setting all other coefficients of restitution to zero. The rate of inter-particle collisions is denoted by λ and the rate of driving for the particles by λ_d. If $P(v,t)$ denote the probability that a randomly chosen particle has velocity v at time

t then its time evolution, for a mono-dispersed gas is given by:

$$\begin{aligned}\frac{d}{dt}P(v,t) =& -\lambda P(v,t) - \lambda_d P(v,t)\\ &+\lambda \int\int dv_1 dv_2 P(v_1,t)P(v_2,t)\delta[(1-\alpha)v_1+\alpha v_2 - v]\\ &+\lambda_d \int\int d\eta dv_1 \phi(\eta)P(v_1,t)\delta[-r_w v_1+\eta-v],\end{aligned} \tag{2.8}$$

where

$$\alpha = \frac{1+r}{2}. \tag{2.9}$$

2.3 Calculation of the two point correlations

In this section, we define the relevant two point correlation functions for both mono-dispersed and bi-dispersed gases. The evolution equations for these correlation functions were derived in Refs. [55, 57]. We summarize these derivations and then develop a solution that will be useful for demonstrating the Mpemba effect. Sections 2.3.1 and 2.3.2 contain the derivation for mono-dispersed and bi-dispersed gases respectively.

2.3.1 Mono-dispersed Maxwell gas

We first discuss the case of mono-dispersed Maxwell gas. Consider the following two point correlation functions:

$$\begin{aligned}E(t) &= \frac{1}{N}\sum_{i=1}^{N}\langle v_i^2(t)\rangle,\\ C(t) &= \frac{1}{N(N-1)}\sum_{i=1}^{N}\sum_{j=1,j\neq i}^{N}\langle v_i(t)v_j(t)\rangle,\end{aligned} \tag{2.10}$$

where $E(t)$ is the mean kinetic energy of a particle, and $C(t)$ is the equal time velocity-velocity correlation between a pair of particles. In the steady state, the inter-particle two point correlation function is known to be zero [56]. However, for the purpose of demonstrating the Mpemba effect, we consider non-zero correlations, which correspond to non-stationary states. The time evolution of these correlation functions can be obtained in a straightforward manner from Eq. (2.8) and can be compactly represented in matrix form as [55]

$$\frac{d\Sigma(t)}{dt} = -\boldsymbol{R}\Sigma(t) + \boldsymbol{D}, \tag{2.11}$$

where $\Sigma(t) = [E(t), C(t)]^T$, $\boldsymbol{D} = [\lambda_d \sigma^2, 0]^T$, and $\boldsymbol{R}$ is given by

$$\boldsymbol{R} = \begin{bmatrix} \lambda_c(1-r^2)+\lambda_d(1-r_w^2) & -\lambda_c(1-r^2) \\ -\frac{\lambda_c(1-r^2)}{N-1} & \frac{\lambda_c(1-r^2)}{N-1}+\lambda_d(1+r_w) \end{bmatrix}. \tag{2.12}$$

Note that while R_{11} and R_{22} are positive, R_{12} and R_{21} are negative.

Equation (2.11) for the correlation functions forms a closed set of linear equations and does not involve higher order correlation functions. This allows for a complete solution. Equation (2.11) can be solved exactly by linear decomposition using the eigenvalues $\lambda_\pm$ of $\boldsymbol{R}$:

$$\lambda_\pm = \frac{R_{11}+R_{22} \pm \sqrt{(R_{11}-R_{22})^2 + 4R_{21}R_{12}}}{2}. \tag{2.13}$$

Here, the eigenvalues $\lambda_\pm > 0$ with $\lambda_+ > \lambda_-$. The solution for $E(t)$ and $C(t)$ can then be obtained as:

$$\begin{aligned} E(t) &= K_+ e^{-\lambda_+ t} + K_- e^{-\lambda_- t} + K_0, \\ C(t) &= L_+ e^{-\lambda_+ t} + L_- e^{-\lambda_- t} + L_0, \end{aligned} \tag{2.14}$$

where the coefficients K_+, K_-, K_0, L_+, L_- and L_0 are given by

$$
\begin{aligned}
K_+ &= \frac{1}{\gamma}\left[(\lambda_- - R_{11})\Sigma_1(0) - R_{12}\Sigma_2(0) - \frac{(\lambda_- - R_{11})}{\lambda_+}\lambda_d\sigma^2\right],\\
K_- &= \frac{1}{\gamma}\left[-(\lambda_+ - R_{11})\Sigma_1(0) + R_{12}\Sigma_2(0) + \frac{(\lambda_+ - R_{11})}{\lambda_-}\lambda_d\sigma^2\right],\\
K_0 &= \frac{1}{\gamma}\left[\frac{\lambda_- - R_{11}}{\lambda_+} - \frac{\lambda_+ - R_{11}}{\lambda_-}\right]\lambda_d\sigma^2,\\
L_0 &= \frac{1}{\gamma}\left[\frac{(\lambda_+ - R_{11})(\lambda_- - R_{11})}{R_{12}\lambda_+} - \frac{(\lambda_+ - R_{11})(\lambda_- - R_{11})}{R_{12}\lambda_-}\right]\lambda_d\sigma^2,\\
L_+ &= \frac{1}{\gamma}\left[\frac{(\lambda_+ - R_{11})(\lambda_- - R_{11})}{R_{12}}\Sigma_1(0) - (\lambda_+ - R_{11})\Sigma_2(0) - \frac{(\lambda_+ - R_{11})(\lambda_- - R_{11})}{R_{12}\lambda_+}\lambda_d\sigma^2\right],\\
L_- &= \frac{1}{\gamma}\left[\frac{-(\lambda_+ - R_{11})(\lambda_- - R_{11})}{R_{12}}\Sigma_1(0) + (\lambda_- - R_{11})\Sigma_2(0) + \frac{(\lambda_+ - R_{11})(\lambda_- - R_{11})}{R_{12}\lambda_-}\lambda_d\sigma^2\right],\\
\gamma &= \lambda_+ - \lambda_-.
\end{aligned}
\tag{2.15}
$$

2.3.2 Bi-dispersed Maxwell gas

For the case of bi-dispersed Maxwell gas, we can define two point correlation functions, E_A and E_B for the mean kinetic energies of type A and B particles, and three two point velocity-velocity correlation functions C_{ij}, where $i, j \in (A, B)$:

$$
\begin{aligned}
E_A(t) &= \frac{1}{N_A}\sum_{i=1}^{N_A}\langle v_{i,A}^2(t)\rangle,\\
E_B(t) &= \frac{1}{N_B}\sum_{i=1}^{N_B}\langle v_{i,B}^2(t)\rangle,\\
C_{AB}(t) &= \frac{1}{N_A N_B}\sum_{i=1}^{N_A}\sum_{j=1}^{N_B}\langle v_{i,A}(t)v_{j,B}(t)\rangle,\\
C_{AA}(t) &= \frac{1}{N_A(N_A-1)}\sum_{i=1}^{N_A}\sum_{\substack{j=1\\ j\neq i}}^{N_A}\langle v_{i,A}(t)v_{j,A}(t)\rangle,\\
C_{BB}(t) &= \frac{1}{N_B(N_B-1)}\sum_{i=1}^{N_B}\sum_{\substack{j=1\\ j\neq i}}^{N_B}\langle v_{i,B}(t)v_{j,B}(t)\rangle.
\end{aligned}
\tag{2.16}
$$

The time evolution for these correlation function can be obtained from Eq. (2.5), as derived in Ref. [57] when only one type of particle is driven. We generalize these calculations to the case where both types of particles are driven. The time evolution equations are linear and form a closed set of equations as

$$\frac{d\Sigma(t)}{dt} = \boldsymbol{R}\Sigma(t) + \boldsymbol{D}, \tag{2.17}$$

where

$$\Sigma(t) = \Big[E_A(t), \quad E_B(t), \quad C_{AB}(t), \quad C_{AA}(t), \quad C_{BB}(t) \Big]^T, \tag{2.18}$$

$$\boldsymbol{D} = \Big[\lambda_d \sigma_A^2, \quad \lambda_d \sigma_B^2, \quad 0, \quad 0, \quad 0 \Big]^T, \tag{2.19}$$

where k=A,B and the matrix $\boldsymbol{R}$ is given by

$$\boldsymbol{R} =$$

$$\begin{bmatrix} R_{2B}-R_{1A}-R_{3B}-R_d & R_{2B} & -2R_{2B}+R_{3B} & 2R_{1A} & 0 \\ R_{2A} & R_{2A}-R_{1B}-R_{3A} & -2R_{2A}+R_{3A} & 0 & -R_{1B} \\ \frac{R_{3A}}{2N_A}-R_4 & \frac{R_{3B}}{2N_B}-R_4 & \frac{4R_4+R_{3B}-R_{3A}}{2} & -\frac{R_{3A}}{2N_A}+\frac{R_{3A}}{2} & -\frac{R_{3B}}{2N_B}+\frac{R_{3B}}{2} \\ \frac{R_{1A}}{N_A-1} & 0 & R_{3B} & \frac{R_{1A}}{1-N_A}-R_{3B}-\frac{R_d}{1-r_w} & 0 \\ 0 & \frac{R_{1B}}{N_B-1} & R_{3B} & 0 & \frac{2R_{1B}}{N_B-1}-R_{3B} \end{bmatrix}. \tag{2.20}$$

The constants $R_{1k}, R_{2k}, R_{3k}, R_4, R_d$ are given by:

$$\begin{aligned} R_{1k} &= \frac{\lambda_{kk}\alpha_{kk}(1-\alpha_{kk})(N_k-1)}{N}, \\ R_{2k} &= \frac{\lambda_{AB}N_kX_k^2}{N}, \\ R_{3k} &= \frac{2R_{2k}}{X_k}, \\ R_4 &= \frac{\lambda_{AB}X_AX_B}{N}, \\ R_d &= \lambda_d(1-r_w^2). \end{aligned} \tag{2.21}$$

In the steady state, in the thermodynamic limit, the inter-particle two point correlation functions C_{ij}, where $i, j \in (A,B)$ are zero, as shown in Ref. [57]. If in the initial state, these correlations are zero, then it remains zero for all times. We will be only considering such initial states. In that case, we can ignore these correlations, and write for the time evolution of mean kinetic energies E_A and E_B as

$$\begin{aligned}\frac{dE_A(t)}{dt} =& E_A(t)\Big(\lambda_{AB}\nu_B X_B^2 - \lambda_{AA}\alpha_{AA}(1-\alpha_{AA})\nu_A - 2\lambda_{AB}\nu_B X_B - \lambda_d(1-r_w^2)\Big)\\ &+E_B(t)\Big(\lambda_{AB}\nu_B X_B^2\Big) + \lambda_d\sigma_A^2,\\ \frac{dE_B(t)}{dt} =& E_B(t)\Big(\lambda_{AB}\nu_A X_A^2 - \lambda_{BB}\alpha_{BB}(1-\alpha_{BB})\nu_B - 2\lambda_{AB}\nu_A X_A - \lambda_d(1-r_w^2)\Big)\\ & E_A(t)\Big(\lambda_{AB}\nu_A X_A^2\Big) + \lambda_d\sigma_B^2.\end{aligned} \tag{2.22}$$

We can write the time evolution of mean kinetic energies of A and B type particles, i.e., E_A and E_B respectively in a compact form as

$$\frac{d\boldsymbol{\Sigma}(t)}{dt} = \boldsymbol{R}\boldsymbol{\Sigma}(t) + \boldsymbol{D}, \tag{2.23}$$

where

$$\boldsymbol{\Sigma}(t) = \Big[E_A(t), \quad E_B(t)\Big]^T, \tag{2.24}$$

$$\boldsymbol{D} = \Big[\lambda_d\sigma_A^2, \quad \lambda_d\sigma_B^2\Big]^T, \tag{2.25}$$

and $\boldsymbol{R}$ is a 2×2 matrix, whose entries are given by

$$\begin{aligned} R_{11} =& \lambda_{AB}\nu_B X_B^2 - \lambda_{AA}\alpha_{AA}(1-\alpha_{AA})\nu_A - 2\lambda_{AB}\nu_B X_B - \lambda_d(1-r_w^2),\\ R_{12} =& \lambda_{AB}\nu_B X_B^2,\\ R_{21} =& \lambda_{AB}\nu_A X_A^2,\\ R_{22} =& \lambda_{AB}\nu_A X_A^2 - \lambda_{BB}\alpha_{BB}(1-\alpha_{BB})\nu_B - 2\lambda_{AB}\nu_A X_A - \lambda_d(1-r_w^2),\end{aligned} \tag{2.26}$$

where ν_A and ν_B are the fraction of A and B type particles, respectively. In order to obtain the steady state values, we set the time derivative of Eq. (2.22) to zero. The steady state values for E_A and E_B are given by

$$E_A = \frac{\begin{array}{l} -\lambda_d \sigma_A^2 \Big(-\lambda_d (1-r_w^2) - 2\lambda_{AB} \nu_A X_A + \lambda_{AB} \nu_A X_A^2 - \lambda_{BB} \nu_B (1-\alpha_{BB}) \alpha_{BB} \Big) \\ + \lambda_{AB} \lambda_d \nu_B X_B^2 \sigma_B^2 \end{array}}{\mathscr{F}}, \tag{2.27}$$

$$E_B = \frac{\begin{array}{l} -\lambda_d \sigma_B^2 \Big(-\lambda_d (1-r_w^2) - 2\lambda_{AB} \nu_B X_B + \lambda_{AB} \nu_B X_B^2 - \lambda_{AA} \nu_A (1-\alpha_{AA}) \alpha_{AA} \Big) \\ + \lambda_{AB} \lambda_d \nu_A X_A^2 \sigma_A^2 \end{array}}{\mathscr{F}}, \tag{2.28}$$

where

$$\begin{aligned} \mathscr{F} = & -\lambda_{AB}^2 \nu_A \nu_B X_A^2 X_B^2 \\ & + \Big(-\lambda_d (1-r_w^2) - 2\lambda_{AB} \nu_B X_B + \lambda_{AB} \nu_B X_B^2 - \lambda_{AA} \nu_A (1-\alpha_{AA}) \alpha_{AA} \Big) \\ & \quad \Big(-\lambda_d (1-r_w^2) - 2\lambda_{AB} \nu_A X_A + \lambda_{AB} \nu_A X_A^2 - \lambda_{BB} \nu_B (1-\alpha_{BB}) \alpha_{BB} \Big). \end{aligned} \tag{2.29}$$

One can do similar calculations to solve for the steady state mean kinetic energies, for the case where only one component (say A) is driven with driving strength (σ) and at a rate (λ_d). In that case, the mean kinetic energies of the components are given by

$$E_A = \frac{\lambda_d \sigma^2}{\lambda_d (1-r_w^2) + 2\nu_A \lambda_{AA} \alpha_{AA} (1-\alpha_{AA}) + \lambda_{AB} \nu_B X_B (2-X_B) - X_A^2 X_B^2 \nu_A \nu_B \lambda_{AB}^2 \mathscr{Q}}, \tag{2.30}$$

$$E_B = E_A \lambda_{AB} \nu_A X_A^2 \mathscr{Q}, \tag{2.31}$$

where

$$\mathscr{Q} = \frac{1}{(2-X_A) X_A \nu_A \lambda_{AB} + 2\alpha_{BB} \lambda_{BB} \nu_B (1-\alpha_{BB})}. \tag{2.32}$$

We note that the linearity in the evolution equations [Eqs. (2.11) and (4.19)] for the energy arises naturally for Maxwell gases (both mono-dispersed and bi-dispersed) when compared to the granular gas models studied earlier [22, 23], wherein the non-linear evolution equation limits analytical treatment unless linearized using perturbative methods [22]. Similar exact linear evolution equation has been analyzed in the case of Markovian Mpemba effect [11] where the vector denoting the probabilities of various states evolves according to an equation similar to Eqs. (2.11) and (4.19).

2.4 The Mpemba effect in Mono-dispersed Maxwell gas

In this section, we derive the conditions for the Mpemba effect to be present in the mono-dispersed driven Maxwell gas, based on an analysis of Eq. (2.14) for the solution of $E(t)$ and $C(t)$. More precisely, we define the Mpemba effect as follows. Consider two systems with two different granular temperatures, or kinetic energies [the terms “granular temperature“ and “kinetic energies” are used interchangeably]. We let these systems evolve to a steady state at the same final temperature, that is lower than the initial temperatures. If the hotter system cools faster (the energy-time plots show a crossing), then we say that the system shows the Mpemba effect.

We now proceed to find out the criteria for the Mpemba effect to be present in the mono-dispersed Maxwell gas. Consider two systems labeled as P and Q. Let their initial conditions be denoted by $(E^P(0), C^P(0))$ and $(E^Q(0), C^Q(0))$ with $E^P(0) > E^Q(0)$. Both systems are then driven to a common steady state. This is achieved when the systems P and Q are driven with the same driving strength (σ) which is chosen such that the mean kinetic energy of the common steady state is lower than the initial mean kinetic energies of P and Q, while keeping all the other parameters of both the systems constant.

If this system shows a Mpemba effect, then the trajectories $E^P(t)$ and $E^Q(t)$ must cross each other, such that there is a time $t = \tau$ at which

$$E^P(\tau) = E^Q(\tau). \tag{2.33}$$

Substituting into Eq. (2.14), we obtain relation:

$$K_+^P e^{-\lambda_+\tau} + K_-^P e^{-\lambda_-\tau} = K_+^Q e^{-\lambda_+\tau} + K_-^Q e^{-\lambda_-\tau}, \tag{2.34}$$

whose solution is

$$\tau = \frac{1}{\lambda_+ - \lambda_-} \ln \left[\frac{K_+^P - K_+^Q}{K_-^P - K_-^Q} \right], \tag{2.35}$$

which in terms of the initial conditions reduce to

$$\tau = \frac{1}{\lambda_+ - \lambda_-} \ln \left[\frac{R_{12}\Delta C - (\lambda_- - R_{11})\Delta E}{R_{12}\Delta C - (\lambda_+ - R_{11})\Delta E} \right], \tag{2.36}$$

where

$$\Delta E = E^P(0) - E^Q(0), \tag{2.37}$$

$$\Delta C = C^P(0) - C^Q(0). \tag{2.38}$$

For the Mpemba effect to be present, we require that $\tau > 0$. Since $\lambda_+ > \lambda_-$, the argument of logarithm in Eq. (2.36) should be greater than one. We immediately obtain the criterion

$$(\lambda_+ - R_{11})\Delta E < R_{12}\Delta C. \tag{2.39}$$

Note that $R_{12} < 0$, and $\lambda_+ > R_{11}$ [see Eq. (2.12)]. Since $\Delta E > 0$ by definition, we conclude that Eq. (2.39) can be satisfied only if $\Delta C < 0$, i.e., the two point velocity-velocity correlation of the hotter initial system $C^P(0)$ is sufficiently smaller than that of the cooler counterpart $C^Q(0)$. Note that if the two systems P and Q were initially in a steady state,

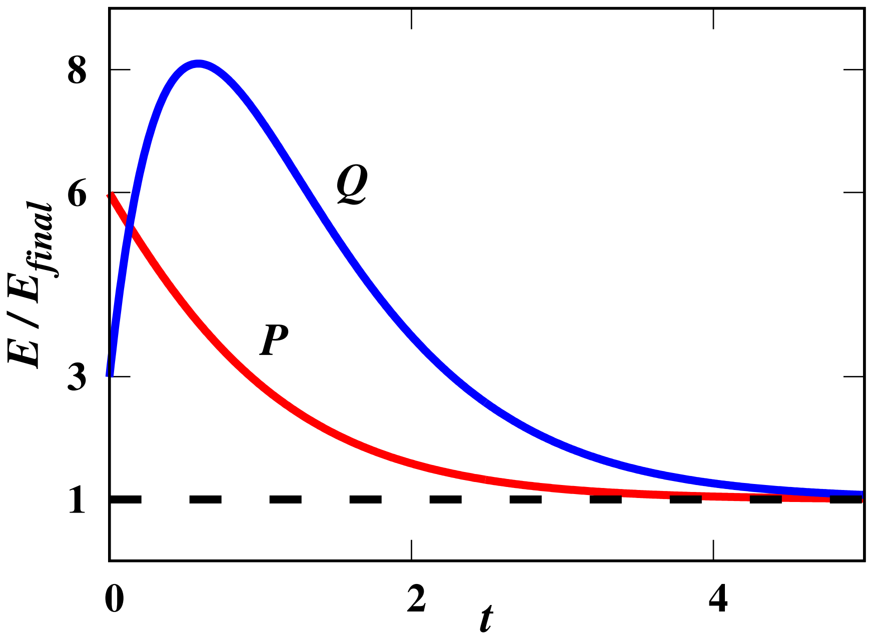

Figure 2.1: The time evolution of the mean kinetic energy, E of the mono-dispersed Maxwell gas for two systems P and Q with initial conditions $E^P(0) = 4$, $E^Q(0) = 2$, $C^P(0) = 3$ and $C^Q(0) = 23$, which satisfy the conditions for the Mpemba effect as described in Eq. (2.39). The choice of the other parameters defining the system are $r = 0.5$, $r_w = 0.5$ and $\sigma = 1$. P relaxes to the steady state faster than Q, though its initial energy is larger. The time at which the trajectories cross each other is $\tau = 0.1334$, as given by Eq. (2.36).

then in the thermodynamic limit the correlations vanish, i.e., $\Delta C = \mathscr{O}(1/N)$, and the inequality in Eq. (2.39) cannot be satisfied. Thus, for the Mpemba effect to be present in the mono-dispersed gas, the initial condition of the cooler component cannot be a steady state of the system.

In Fig. 2.1, we demonstrate the time evolution of the energies of two systems with initial conditions that satisfy Eq. (2.39). Though the initial energy of P is larger, it relaxes to the steady state faster than Q. As predicted by Eq. (2.36), the two relaxation trajectories cross at some finite time.

Keeping all other parameters fixed, and allowing only the coefficient of restitution to vary, we can identify the region of phase space (initial condition) where the Mpemba effect is observable, based on Eq. (2.39). This is shown in Fig. 2.2. Clearly, as r decreases to zero,

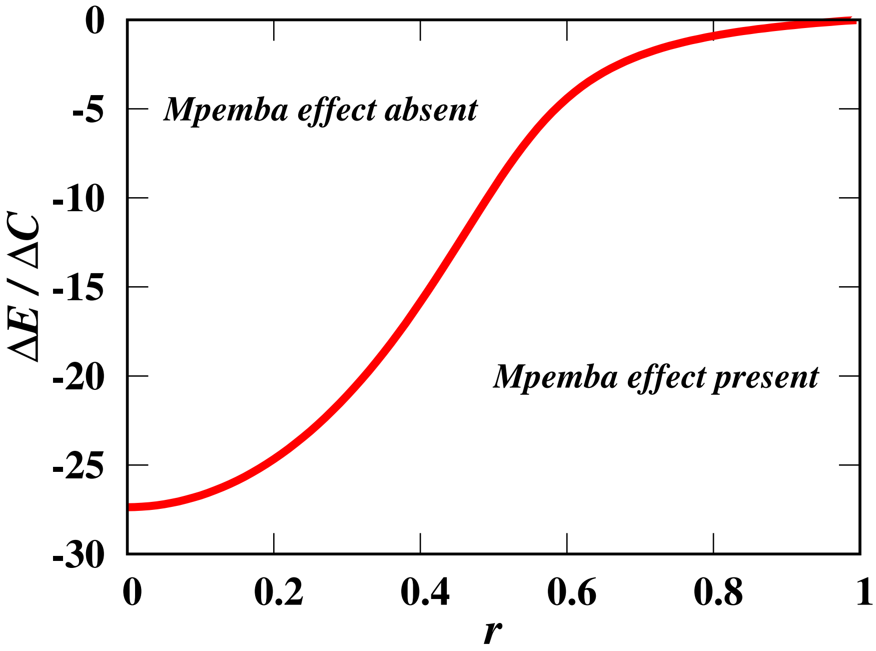

Figure 2.2: The $\Delta E/\Delta C$–r phase diagram showing regions where the Mpemba effect is observed for mono-dispersed Maxwell gas (see Sec. 2.4), where r is the coefficient of restitution. All other parameters are kept constant. The region below the critical line show the Mpemba effect.

the correlations need to be large for the Mpemba effect to be present. On the other hand, that in the near elastic limit $r \to 1$, it is much easier to observe the Mpemba effect, as the only requirement is that ΔC and ΔE are anti-correlated. However, we note that even in this case, non-zero correlations imply that the system is not in a steady state.

2.5 Mpemba effect in bi-dispersed Maxwell gas

In Sec. 2.4, we discussed the possibility of the Mpemba effect in mono-dispersed gas. The Mpemba effect was only present when the initial states were different from the steady states at that corresponding temperature. We now generalize the analysis to bi-dispersed gases, based on an analysis of Eq. (4.19), and show the presence of the Mpemba effect even when the initial states are restricted to steady states.

In a bi-dispersed gas, the temperatures of the two components are generally different [see

Eqs. 2.28 and 2.29]. We denote them by E_A and E_B. We denote the total kinetic energy of the system by E_{tot}, where

$$E_{tot} = E_A + E_B, \tag{2.40}$$

and the difference in energies by E_{diff}:

$$E_{diff} = E_A - E_B. \tag{2.41}$$

We define the Mpemba effect in bi-dispersed gases similarly to the definition in the mono-dispersed gases. To this end, we consider two systems P and Q where E_{tot} of P is larger. Both P and Q are initially in their steady states. We then quench both systems to a lower temperature. The Mpemba effect is present in this case when the E_{tot} trajectories of the two systems cross each other.

We next consider separately the cases of one or both components driven. The reason for this separation is that in some experiments only one component is driven [61, 62, 63, 64, 65, 66], whereas in others both components are driven [67, 68, 69, 70, 71, 72]. The respective analysis may be found in Secs. 2.5.1 and 2.5.2.

2.5.1 One component is driven

Consider a bi-dispersed driven Maxwell gas where only component A is driven with driving strength σ. The time evolution equation [see Eq. (4.19)] for the correlation functions can be expressed in terms of E_{tot} and E_{diff} as

$$\frac{d\boldsymbol{E}(t)}{dt} = -\chi\boldsymbol{E}(t) + \boldsymbol{D}, \tag{2.42}$$

where

$$\boldsymbol{E}(t) = \Big[E_{tot}(t), \quad E_{diff}(t)\Big]^T, \tag{2.43}$$

$$\boldsymbol{D} = \Big[\lambda_d \sigma^2, \quad \lambda_d \sigma^2\Big]^T, \tag{2.44}$$

and χ is a 2×2 matrix with components χ_{11}, χ_{12}, χ_{21} and χ_{22} given by

$$\begin{aligned}
\chi_{11} &= -\frac{R_{11}+R_{12}+R_{21}+R_{22}}{2}, \\
\chi_{12} &= -\frac{R_{11}-R_{12}+R_{21}-R_{22}}{2}, \\
\chi_{21} &= -\frac{R_{11}+R_{12}-R_{21}-R_{22}}{2}, \\
\chi_{22} &= -\frac{R_{11}-R_{12}-R_{21}+R_{22}}{2}.
\end{aligned} \tag{2.45}$$

Equation (4.25) can be solved exactly by linear decomposition using the eigenvalues $\lambda_\pm$ of χ:

$$\lambda_\pm = \frac{1}{2}\Big[(\chi_{11}+\chi_{22}) \pm \sqrt{(\chi_{11}-\chi_{22})^2 + 4\chi_{12}\chi_{21}}\Big]. \tag{2.46}$$

It is straightforward to show that $\lambda_\pm > 0$ with $\lambda_+ > \lambda_-$. The solution for $E_{tot}(t)$ and $E_{diff}(t)$ is

$$\begin{aligned}
E_{tot}(t) &= K_+ e^{-\lambda_+ t} + K_- e^{-\lambda_- t} + K_0, \\
E_{diff}(t) &= L_+ e^{-\lambda_+ t} + L_- e^{-\lambda_- t} + L_0,
\end{aligned} \tag{2.47}$$

where the coefficients K_+, K_-, K_0, L_+, L_- and L_0 are by

$$\begin{aligned}
K_+ &= \frac{1}{\gamma}\Big[(-\lambda_- + \chi_{11})E_{tot}(0) + \chi_{12}E_{diff}(0) - \frac{\chi_{12} - \lambda_- + \chi_{11})}{\lambda_+}\lambda_d\sigma^2\Big],\\
K_- &= \frac{1}{\gamma}\Big[(\lambda_+ - \chi_{11})E_{tot}(0) - \chi_{12}E_{diff}(0) + \frac{\chi_{12} - \lambda_+ + \chi_{11})}{\lambda_-}\lambda_d\sigma^2\Big],\\
K_0 &= \frac{1}{\gamma}\Big[\frac{\chi_{12} - (\lambda_- - \chi_{11})}{\lambda_+} - \frac{\chi_{12} - (\lambda_+ - \chi_{11})}{\lambda_-}\Big]\lambda_d\sigma^2,\\
L_0 &= \frac{1}{\gamma}\Big[\frac{(\lambda_+ - \chi_{11})(\lambda_- - \chi_{11})}{\chi_{12}\lambda_+} - \frac{(\lambda_+ - \chi_{11})(\lambda_- - \chi_{11})}{\chi_{12}\lambda_-}\Big]\lambda_d\sigma^2,\\
L_+ &= \frac{1}{\gamma}\Big[-\frac{(\lambda_+ - \chi_{11})(\lambda_- - \chi_{11})}{\chi_{12}}E_{tot}(0) + (\lambda_+ - \chi_{11})E_{diff}(0) - \frac{(\lambda_+ - \chi_{11})(\lambda_- - \chi_{11})}{\chi_{12}\lambda_+}\lambda_d\sigma^2\Big],\\
L_- &= \frac{1}{\gamma}\Big[\frac{(\lambda_+ - \chi_{11})(\lambda_- - \chi_{11})}{\chi_{12}}E_{tot}(0) - (\lambda_- - \chi_{11})E_{diff}(0) + \frac{(\lambda_+ - \chi_{11})(\lambda_- - \chi_{11})}{\chi_{12}\lambda_-}\lambda_d\sigma^2\Big],\\
\gamma &= \lambda_+ - \lambda_-.
\end{aligned} \tag{2.48}$$

We now consider two systems labeled as P and Q with different initial conditions $(E^P_{tot}(0), E^P_{diff}(0))$ and $(E^Q_{tot}(0), E^Q_{diff}(0))$ where $E^P_{tot}(0) > E^Q_{tot}(0)$. Both the systems are quenched to a common steady state whose total energy is smaller than the initial total energies of P and Q. This is achieved when the systems P and Q are now driven with the same driving strength (σ) for the component A, while keeping all the other parameters same for both the systems.

The Mpemba effect is present when the trajectories $E^P_{tot}(t)$ and $E^Q_{tot}(t)$ cross each other at some finite time $t = \tau$ at which

$$E^P_{tot}(\tau) = E^Q_{tot}(\tau). \tag{2.49}$$

Substituting into Eq. (5.4), we obtain

$$K^P_+ e^{-\lambda_+\tau} + K^P_- e^{-\lambda_-\tau} = K^Q_+ e^{-\lambda_+\tau} + K^Q_- e^{-\lambda_-\tau}, \tag{2.50}$$

whose solution is

$$\tau = \frac{1}{\lambda_+ - \lambda_-} \ln \left[\frac{K_+^P - K_+^Q}{K_-^Q - K_-^P} \right], \tag{2.51}$$

which in terms of the initial conditions reduce to

$$\tau = \frac{1}{\lambda_+ - \lambda_-} \ln \left[\frac{\chi_{12} \Delta E_{diff} - (\lambda_- - \chi_{11}) \Delta E_{tot}}{\chi_{12} \Delta E_{diff} - (\lambda_+ - \chi_{11}) \Delta E_{tot}} \right], \tag{2.52}$$

where

$$\begin{aligned} \Delta E_{tot} &= E_{tot}^P(0) - E_{tot}^Q(0), \\ \Delta E_{diff} &= E_{diff}^P(0) - E_{diff}^Q(0). \end{aligned} \tag{2.53}$$

Following the same argument as for the case of mono-dispersed Maxwell gas in Sec. 2.4, Eq. (5.11) leads to the criterion for the crossing of the two trajectories as

$$\chi_{12} \Delta E_{diff} > (\lambda_+ - \chi_{11}) \Delta E_{tot}. \tag{2.54}$$

In Fig. 2.3, we consider such a situation where Eq. (4.36) is satisfied. The trajectories cross at the point as predicted by Eq. (5.11). It is clear that though P has larger initial energy, it relaxes faster.

In Fig. 4.2, we identify the region of phase space (initial condition) where the Mpemba effect is observable, based on Eq. (4.36). In the figure, the variation with r_{AB} is shown. The region below the line in the phase diagram shows the Mpemba effect whereas the other region does not show the effect.

In the above analysis, the systems P and Q have the same parameters once the quench is done. However, in the initial states, the parameters – reaction rates, coefficients of restitution, driving strength – could be different for P and Q. These parameters, though not explicitly mentioned, enter through the initial values E_{tot} and E_{diff}. As a result, one can tune the parameters appropriately to obtain initial steady states that satisfy the

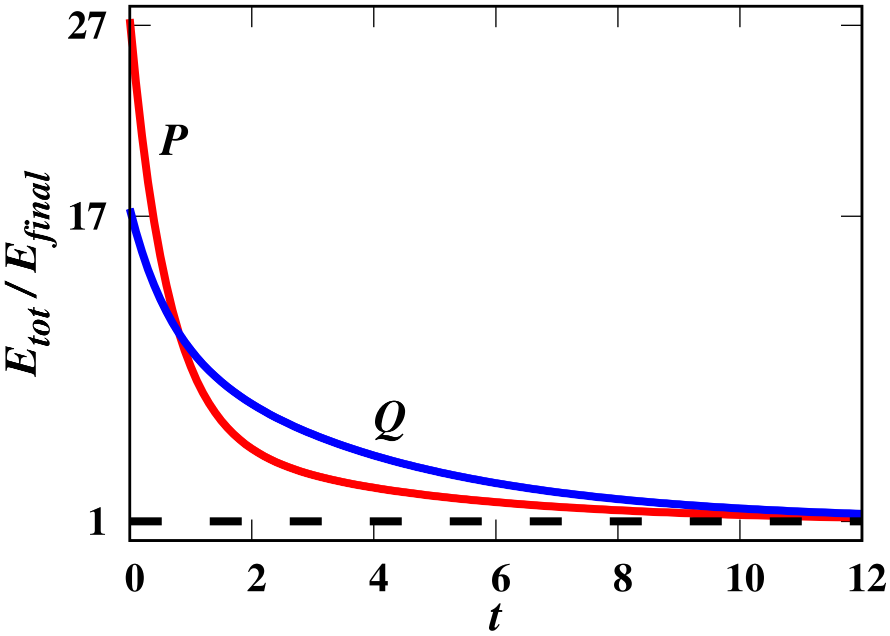

Figure 2.3: The time evolution of the total energy, $E_{tot}(t)$ for two systems P and Q of the bi-dispersed Maxwell gas where only one component is driven with initial conditions: $E^P_{tot}(0) = 22$, $E^Q_{tot}(0) = 14$, $E^P_{diff}(0) = 18$ and $E^Q_{diff}(0) = 4$ such that $E^P_{tot}(0) > E^Q_{tot}(0)$, which satisfies the condition for the Mpemba effect as described in Eq. (4.36). The choice of the other parameters defining the system are $m_B = 2m_A$, $r_{AA} = r_{AB} = r_{BB} = r_w = 0.5$, $\nu_A = 0.2$, $\nu_B = 0.8$ and $\sigma = 1$. P relaxes to the steady state faster than Q, though its initial energy is larger. The time at which the trajectories cross each other is τ=0.807 as given by Eq. (5.11).

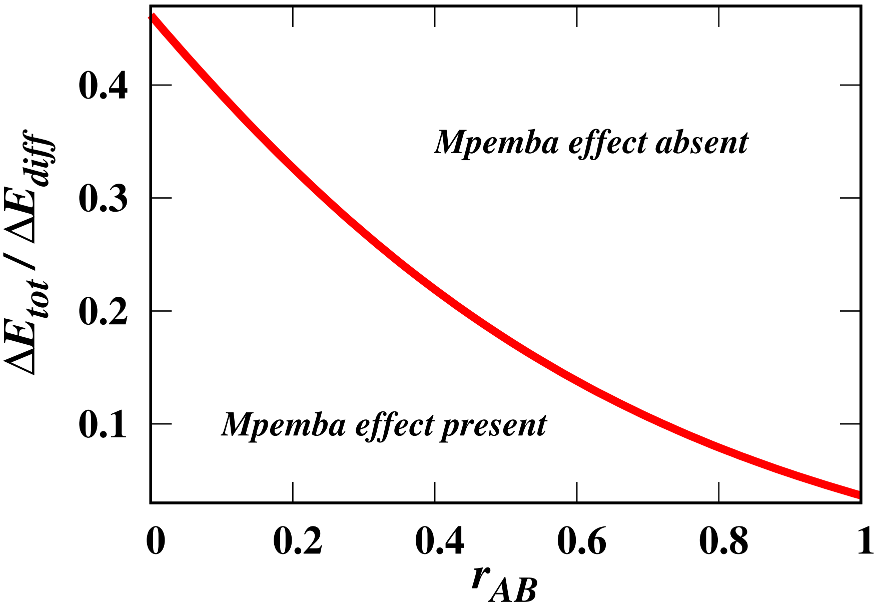

Figure 2.4: The $\Delta E_{tot}/\Delta E_{diff}$–$r_{AB}$ phase diagram showing regions where the Mpemba effect is observed for the bi-dispersed Maxwell gas, where only one component of the gas is driven (see Sec. 2.5.1) and r_{AB} is the coefficient of restitution. All other parameters are kept constant. The choice of the other parameters defining the system are $m_A = 2m_B$, $\nu_A = \nu_B = 0.5$ and $r_{AA} = r_{BB} = r_w = 0.5$. The region below the critical line shows the Mpemba effect whereas the region on the other side of the critical line does not show the Mpemba effect.

condition given by Eq. (4.36) and hence show the Mpemba effect.

We now ask a more refined question. Let us suppose that the systems P and Q have the same parameters throughout (both initially, as well as after the quench) except for the driving strength, which is different initially and the same after the quench. Can the Mpemba effect be present in this case, when only component A is driven? The condition for the Mpemba effect to be present is the same as that derived for the more general case [see Eq. (4.36)]. However, when all parameters other than driving strength are kept identical, the ratio $\Delta E_{tot}/\Delta E_{diff}$ in the initial steady states has a simple form:

$$\frac{\Delta E_{tot}}{\Delta E_{diff}} = \frac{1+\lambda_{AB}\nu_A X_A^2 \mathscr{Q}}{1-\lambda_{AB}\nu_A X_A^2 \mathscr{Q}} > 1, \tag{2.55}$$

where $\mathscr{Q}$ is defined in equation (2.32). Note that $\mathscr{Q} > 0$ and hence the ratio in Eq. (4.46) is always larger than one. On the other hand, the ratio $\Delta E_{tot}/\Delta E_{diff}$ should always be less than $\chi_{12}/(\lambda_+ - \chi_{11})$ for one to observe the Mpemba effect and it can be shown that the maximum value of the quantity is one. Thus, Eq. (4.46) does not satisfy the required condition for the existence of a Mpemba effect.

So far we have discussed the possibility of having the Mpemba effect in a bi-dispersed Maxwell gas where only one component is driven. We showed that, as compared to the mono-dispersed gas, for initial states that correspond to steady states, the bi-dispersed gas shows a Mpemba effect for a wide range of parameters. However, when the two systems P and Q are identical except for the driving strength, the Mpemba effect is not possible for steady state initial conditions. We now generalize the calculations to a bi-dispersed gas where both components are driven, and show that even for systems that differ only by the driving strength, the Mpemba effect can be observed.

2.5.2 Both components are driven

Next we consider a bi-dispersed Maxwell gas where both the components of the gas are driven. Here, type A and B particles of the bi-dispersed Maxwell gas are driven at the same rate λ_d but with different driving strengths σ_A and σ_B, respectively. The time evolution of the quantities E_{tot} and E_{diff} are given by Eq. (4.25) with the column matrix $\boldsymbol{D}$ of the form

$$\boldsymbol{D} = \Big[\lambda_d(\sigma_A^2+\sigma_B^2), \quad \lambda_d(\sigma_A^2-\sigma_B^2)\Big]^T. \tag{2.56}$$

The solutions for $E_{tot}(t)$ and $E_{diff}(t)$ are obtained in a similar way as in Eq. (5.4), but the coefficients K_+, K_-, K_0, L_+, L_- and L_0 are now given by

$$\begin{aligned}
K_+ &= \frac{1}{\gamma}\Big[-(\lambda_- - \chi_{11})E_{tot}(0) + \chi_{12}E_{diff}(0) - \frac{\lambda_d}{\lambda_+}\big[\big(\chi_{12}-(\lambda_- - \chi_{11})\big)\sigma_A^2 - \big(\chi_{12}+(\lambda_- - \chi_{11})\big)\sigma_B^2\big]\Big],\\
K_- &= \frac{1}{\gamma}\Big[(\lambda_+ - \chi_{11})E_{tot}(0) - \chi_{12}E_{diff}(0) + \frac{\lambda_d}{\lambda_-}\big[\big(\chi_{12}-(\lambda_+ - \chi_{11})\big)\sigma_A^2 - \big(\chi_{12}+(\lambda_+ - \chi_{11})\big)\sigma_B^2\big]\Big],\\
K_0 &= \frac{\lambda_d}{\gamma}\Big[\frac{\big(\chi_{12}-(\lambda_- - \chi_{11})\big)\sigma_A^2 - \big(\chi_{12}+(\lambda_- - \chi_{11})\big)\sigma_B^2}{\lambda_+} - \frac{\big(\chi_{12}-(\lambda_+ - \chi_{11})\big)\sigma_A^2 - \big(\chi_{12}+(\lambda_+ - \chi_{11})\big)\sigma_B^2}{\lambda_-}\Big],\\
L_+ &= \frac{1}{\gamma}\Big[-\frac{(\lambda_+ - \chi_{11})(\lambda_- - \chi_{11})}{\chi_{12}}E_{tot}(0) + (\lambda_+ - \chi_{11})E_{diff}(0) - \frac{\lambda_d}{\lambda_+\chi_{12}}\big[(\lambda_+ - \chi_{11})(\lambda_- - \chi_{11})(\sigma_A^2-\sigma_B^2)\big]\Big],\\
L_- &= \frac{1}{\gamma}\Big[\frac{(\lambda_+ - \chi_{11})(\lambda_- - \chi_{11})}{\chi_{12}}E_{tot}(0) - (\lambda_+ - \chi_{11})E_{diff}(0) + \frac{\lambda_d}{\lambda_-\chi_{12}}\big[(\lambda_+ - \chi_{11})(\lambda_- - \chi_{11})(\sigma_A^2-\sigma_B^2)\big]\Big],\\
L_0 &= \frac{\lambda_d}{\chi_{12}\gamma}\Big[(\lambda_+ - \chi_{11})(\lambda_- - \chi_{11})(\sigma_A^2-\sigma_B^2)\big(\frac{1}{\lambda_+} - \frac{1}{\lambda_-}\big)\Big],\\
\gamma &= \lambda_+ - \lambda_-.
\end{aligned} \tag{2.57}$$

Our main aim is to look for the existence of a Mpemba effect by considering two systems with identical parameters, except for the driving strengths. To this end, we consider two such similar systems, P and Q, driven with different noise strengths, thus attaining different initial steady states with different initial total energies.

Let system P have higher initial total energy compared to Q. Both systems are then driven to a common steady state with a lower energy compared to the initial steady state

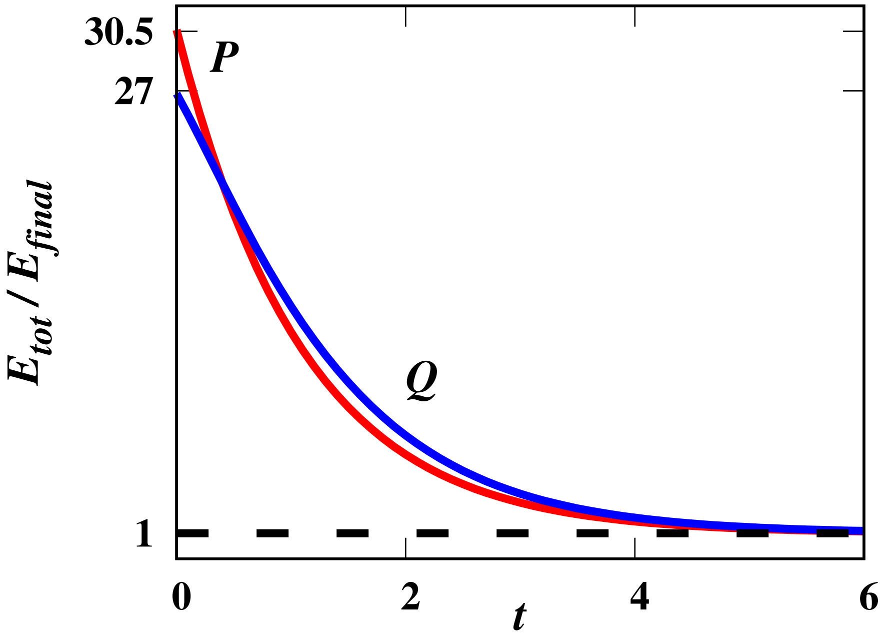

Figure 2.5: The time evolution of the total energy, $E_{tot}(t)$ for two systems P and Q of a bi-dispersed Maxwell gas where both components are driven with initial steady state conditions: $E^P_{tot}(0) = 150.4$, $E^Q_{tot}(0) = 132$, $E^P_{diff}(0) = 75.2$ and $E^Q_{diff}(0) = 30.5$ such that $E^P_{tot}(0) > E^Q_{tot}(0)$, which satisfies the condition for the Mpemba effect as described in Eq. (4.36). The choice of the other parameters defining the system are $m_B = 10m_A$, $r_{AA} = r_{BB} = r_w = 0.5$, $r_{AB} = 0.6$, $\nu_A = 0.2$, $\nu_B = 0.8$, $\sigma_A = 2$ and $\sigma_B = 1$. P relaxes to the steady state faster than Q, though its initial energy is larger. The time at which the trajectories cross each other is τ=0.39 as given by Eq. (5.11).

of systems P and Q. This is achieved when P and Q are driven with the same driving strengths (σ_A and σ_B) for the components A and B . The cross-over time τ for the crossing of the trajectories of $E^P_{tot}(t)$ and $E^Q_{tot}(t)$ is obtained using Eq. (5.11), and the criterion for the occurrence of the Mpemba effect is given by Eq. (4.36). An example of such a crossing is shown in Fig. 4.4.

In Fig. 2.6, based on Eq. (4.36), we identify the region of phase space (initial condition) where the Mpemba effect is observable. In the figure, the variation with r_{AB} is shown. If the ratio $\Delta E_{tot}/\Delta E_{diff}$ falls in the region below (above) the line in the phase diagram [see Fig. 2.6], then the system exhibits (does not exhibit) the Mpemba effect. For steady state initial conditions, the ratio $\Delta E_{tot}/\Delta E_{diff}$ is given by

$$\frac{\Delta E_{tot}}{\Delta E_{diff}} = \frac{\begin{aligned}&\lambda_{AB}\lambda_d\Big[\nu_B X_B^2((\sigma_B^P)^2-(\sigma_B^Q)^2))+\nu_A X_A^2((\sigma_A^P)^2-(\sigma_A^Q)^2)\Big]\\&-\lambda_d\Big[-\lambda_d(1-r_w^2)-2\lambda_{AB}\nu_A X_A+\lambda_{AB}\nu_A X_A^2-\lambda_{BB}\nu_B\alpha_{BB}(1-\alpha_{BB})\Big]((\sigma_A^P)^2-(\sigma_A^Q)^2)\\&-\lambda_d\Big[-\lambda_d(1-r_w^2)-2\lambda_{AB}\nu_B X_B+\lambda_{AB}\nu_B X_B^2-\lambda_{AA}\nu_A\alpha_{AA}(1-\alpha_{AA})\Big]((\sigma_B^P)^2-(\sigma_B^Q)^2)\end{aligned}}{\begin{aligned}&\lambda_{AB}\lambda_d\Big[\nu_B X_B^2((\sigma_B^P)^2-(\sigma_B^Q)^2))-\nu_A X_A^2((\sigma_A^P)^2-(\sigma_A^Q)^2)\Big]\\&-\lambda_d\Big[-\lambda_d(1-r_w^2)-2\lambda_{AB}\nu_A X_A+\lambda_{AB}\nu_A X_A^2-\lambda_{BB}\nu_B\alpha_{BB}(1-\alpha_{BB})\Big]((\sigma_A^P)^2-(\sigma_A^Q)^2)\\&+\lambda_d\Big[-\lambda_d(1-r_w^2)-2\lambda_{AB}\nu_B X_B+\lambda_{AB}\nu_B X_B^2-\lambda_{AA}\nu_A\alpha_{AA}(1-\alpha_{AA})\Big]((\sigma_B^P)^2-(\sigma_B^Q)^2)\end{aligned}}. \tag{2.58}$$

Note that the ratio $\Delta E_{tot}/\Delta E_{diff}$ is also a function of the driving strengths, σ_A and σ_B [see Eq. (2.58)]. It turns out that the driving strengths can be appropriately tuned to access the entire region of phase space (initial condition) in which the Mpemba effect is observable.

2.5.3 The Inverse Mpemba Effect

The inverse Mpemba effect refers to the phenomenon that, when quenched to a high temperature, an initially colder system heats faster than a system at intermediate temperature. The analysis for showing the Mpemba effect in Sec. 2.5.2 can be generalized to show the inverse Mpemba effect in the driven binary gas when both components are driven. We prepare two systems P and Q in steady states such that the total energy of P is larger than that of Q. Both systems are then quenched, using suitable driving strengths for the individual components of the bi-dispersed gas, to a common steady state having a higher energy compared to the initial energies of both P and Q. The cross-over time τ for the crossing of the trajectories of $E_{tot}^P(t)$ and $E_{tot}^Q(t)$ is obtained using Eq. (5.11) and the criterion for the occurrence of the inverse Mpemba effect is given by Eq. (4.36). An example of such a crossing is shown in Fig. 2.7.

The accessible steady states of the system that satisfy the condition for the inverse

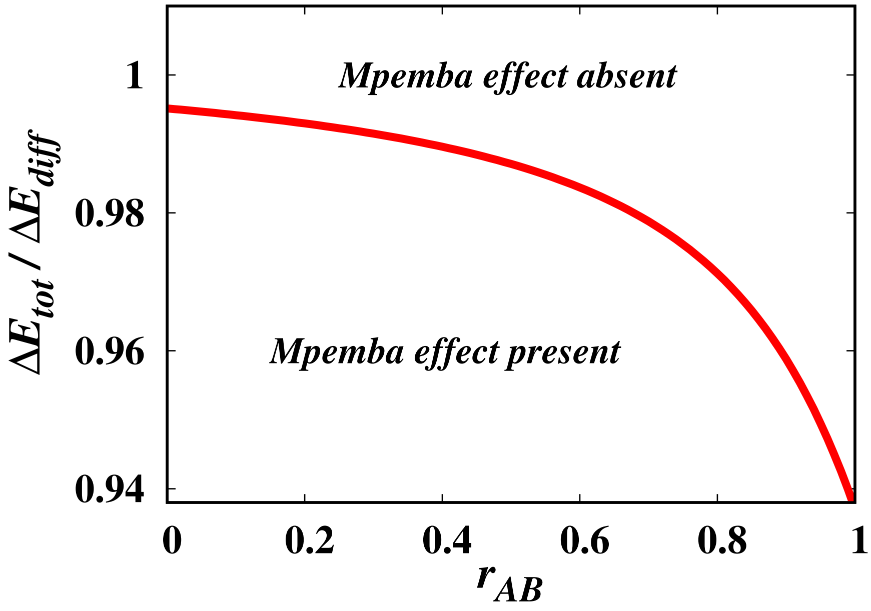

Figure 2.6: The $\Delta E_{tot}/\Delta E_{diff}$–$r_{AB}$ phase diagram showing regions where the Mpemba effect is observed for the bi-dispersed Maxwell gas, where both components of the gas are driven (see Sec 2.5.2) and r_{AB} is the coefficient of restitution. All other parameters are kept constant. The choice of the other parameters defining the system are $m_B = 2m_A$, $\nu_A = 0.2$, $\nu_B = 0.8$, $r_w = 0.6$ and $r_{AA} = r_{BB} = 0.5$. The region below the critical line gives the set of initial steady states that show the Mpemba effect whereas the region on the other side of the critical line correspond to initial states that do not show the Mpemba effect.

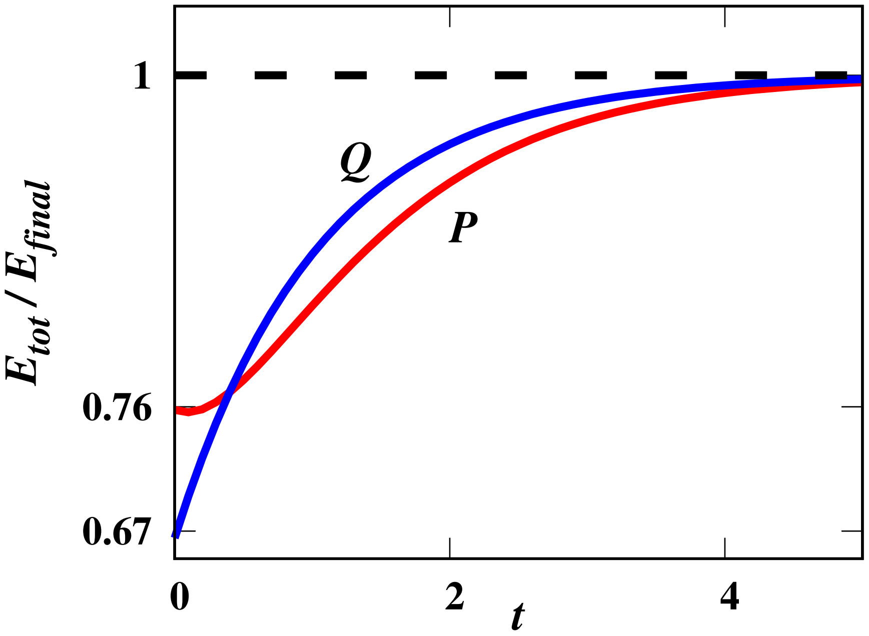

Figure 2.7: The time evolution of the total energy, $E_{tot}(t)$ for two systems P and Q of bi-dispersed Maxwell gas where both components are driven with initial steady state conditions: $E^P_{tot}(0) = 150.4$, $E^Q_{tot}(0) = 132$, $E^P_{diff}(0) = 75.2$ and $E^Q_{diff}(0) = 30.5$ such that $E^P_{tot}(0) > E^Q_{tot}(0)$, which satisfies the condition for the inverse Mpemba effect as described in Eq. (4.36). The choice of the other parameters defining the system are $m_B = 10m_A$, $r_{AA} = r_{BB} = r_w = 0.5$, $r_{AB} = 0.6$, $\nu_A = 0.2$, $\nu_B = 0.8$, $\sigma_A = 8$ and $\sigma_B = 8$. P relaxes to the steady state slower than Q, though its initial energy is larger. The time at which the trajectories cross each other is τ=0.39 as given by Eq. (5.11).

Mpemba effect turns out to be the same as that for the direct Mpemba effect and can be obtained using Eq. (2.58). Thus Fig. 2.6 also illustrates that the valid steady states of the system given by Eq. (2.58) belongs to the region of phase space (initial condition) given by Eq. (4.36) where the inverse Mpemba effect is observable.

2.5.4 The Strong Mpemba Effect

We now explore the possibility of a strong Mpemba effect in the binary Maxwell gas. The strong Mpemba effect refers to the phenomenon wherein the system at higher temperature relaxes to a final steady state exponentially faster, namely with a larger exponential rate compared to other initial conditions. Up to now, we had only considered the case where the trajectories cross, which in general does not imply that the decay rate at large times is different. The linear evolution equation in Eq (4.19) allows certain set of initial conditions to relax to the final steady state exponentially faster compared to other initial states. The effect may be realized when the coefficient (K_-) associated with the slower relaxation rate in the time evolution of total kinetic energy, $E_{tot}(t)$ [see Eq. 5.4] vanishes. In what follows, we would like to probe the system of bi-dispersed gas with both type of particles driven to look for the presence of the strong Mpemba effect.

Setting the coefficient K_- [given by Eq. (2.57)] to zero, we obtain

$$E_{tot}(0) = \frac{\chi_{12}}{\lambda_+ - \chi_{11}} E_{diff}(0) - c, \tag{2.59}$$

where

$$c = \frac{\lambda_d \left[(\chi_{12} - \lambda_+ + \chi_{11}) \sigma_A^2 - (\chi_{12} + \lambda_+ - \chi_{11}) \sigma_B^2 \right]}{\lambda_- (\lambda_+ - \chi_{11})}. \tag{2.60}$$

For a system with all other parameters kept fixed, solution of Eq. (4.40) in terms of $E_{tot}(0)$ and $E_{diff}(0)$ provides the set of initial states whose relaxation is exponentially faster than the set of generic states. Note that the set of initial states that satisfy Eq. (4.40) lie on a straight line.

Among these initial states one would like to determine the ones which are steady states. Remember that the steady state ratio of $E_{tot}(0)/E_{diff}(0)$ for a system is given by

$$\frac{E_{tot}(0)}{E_{diff}(0)} = f(\sigma_A, \sigma_B), \tag{2.61}$$

where $f(\sigma_A, \sigma_B)$ is given by

$$f(\sigma_A,\sigma_B) = \frac{\begin{aligned}&\lambda_{AB}\lambda_d\Big[\nu_B X_B^2(\sigma_B^P)^2 + \nu_A X_A^2(\sigma_A^P)^2\Big]\\ &-\lambda_d\Big[-\lambda_d(1-r_w^2) - 2\lambda_{AB}\nu_A X_A + \lambda_{AB}\nu_A X_A^2 - \lambda_{BB}\nu_B\alpha_{BB}(1-\alpha_{BB})\Big](\sigma_A^P)^2\\ &-\lambda_d\Big[-\lambda_d(1-r_w^2) - 2\lambda_{AB}\nu_B X_B + \lambda_{AB}\nu_B X_B^2 - \lambda_{AA}\nu_A\alpha_{AA}(1-\alpha_{AA})\Big](\sigma_B^P)^2\end{aligned}}{\begin{aligned}&\lambda_{AB}\lambda_d\Big[\nu_B X_B^2(\sigma_B^P)^2 - \nu_A X_A^2(\sigma_A^P)^2\Big]\\ &-\lambda_d\Big[-\lambda_d(1-r_w^2) - 2\lambda_{AB}\nu_A X_A + \lambda_{AB}\nu_A X_A^2 - \lambda_{BB}\nu_B\alpha_{BB}(1-\alpha_{BB})\Big](\sigma_A^P)^2\\ &+\lambda_d\Big[-\lambda_d(1-r_w^2) - 2\lambda_{AB}\nu_B X_B + \lambda_{AB}\nu_B X_B^2 - \lambda_{AA}\nu_A\alpha_{AA}(1-\alpha_{AA})\Big](\sigma_B^P)^2\end{aligned}}, \tag{2.62}$$

and is only a function of driving strengths (σ_A and σ_B) as all other parameters are kept constant. One observes that valid steady states with initial energies, $E_{tot}(0)$ and $E_{diff}(0)$ that satisfy the condition for the strong Mpemba effect [see Eq. (4.40)] can be obtained by appropriately tuning the driving strengths σ_A and σ_B.

Thus for a system of bi-dispersed Maxwell gas where both components are driven, there exists steady state initial conditions which satisfy the condition given by Eq. (4.40) and hence approach the final steady state exponentially faster compared to any other similar system whose initial energies lie slightly below or above the line. An example of the strong Mpemba effect is shown in Fig. 2.8. The figure shows the evolution of the total energy E_{tot} as a function of time t for two bi-dispersed systems P and Q that have identical parameters except for the initial driving strength after being quenched to a lower

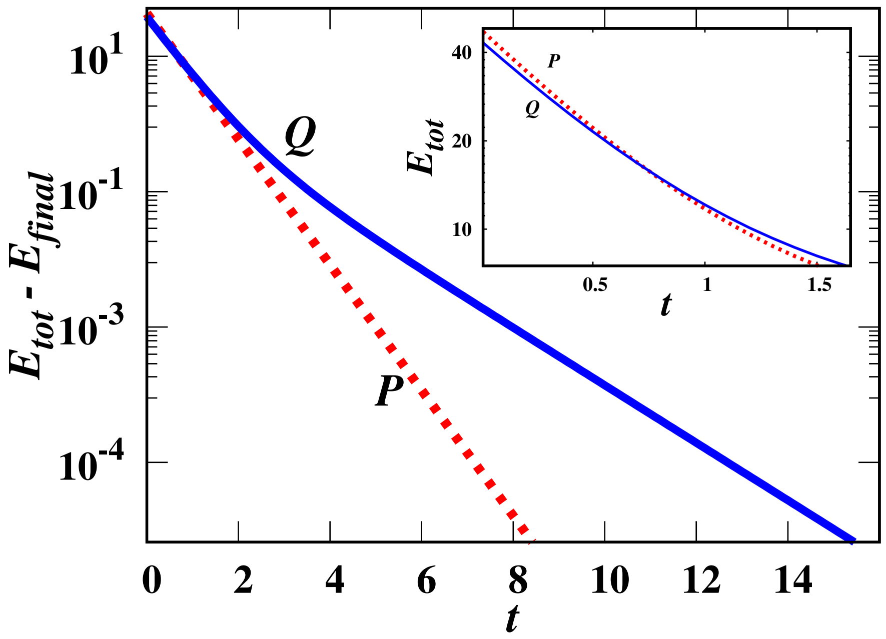

Figure 2.8: The time evolution of the total energy, $E_{tot}(t)$ for two systems P and Q of bi-dispersed Maxwell gas, both components are initially in steady states, with $E_{tot}^{P}(0) = 47.8$, $E_{tot}^{Q}(0) = 43.8$, $E_{diff}^{P}(0) = 45.6$ and $E_{diff}^{Q}(0) = 39$ such that $E_{tot}^{P}(0) > E_{tot}^{Q}(0)$. These initial values satisfy both the conditions for the Mpemba effect as described in Eq. (4.36) as well as those for the strong Mpemba effect (for system P) as described in Eq. (4.40). The choice of the other parameters defining the system are $m_B = 10m_A$, $r_{AA} = 0.5$, $r_{BB} = 0.4$, $r_w = 0.6$, $r_{AB} = 0.35$, $\nu_A = 0.2$, $\nu_B = 0.8$, $\sigma_A = 2$ and $\sigma_B = 1$. P equilibrates to the final state at an exponentially faster rate compared to Q. Inset: The trajectories for P and Q cross at a time $\tau = 0.73$, as given by Eq. (5.11).

temperature by changing the driving strength to a common lower value. The initial state of the system P is chosen in such a way that $[E_{tot}(0), E_{diff}(0)]$ satisfies the condition for the strong Mpemba effect [Eq. (4.40)], and hence evolves to the final state with a single faster relaxation rate. On the other hand, in system Q, the initial state does not satisfy the strong Mpemba effect condition, thus it relaxes differently, and asymptotically evolves with the slower rate. Further, as the initial condition of the two systems P and Q happen to satisfy the relation for the existence of the Mpemba effect [Eq. (4.36)], the trajectory of the system P with higher initial energy crosses that of Q with lower initial energy. The crossing time τ could be obtained using Eq. (5.11) which is captured in the inset of the figure.

2.6 Conclusion

In summary, through an exact analysis of the driven mono-dispersed and bi-dispersed Maxwell gases, we derived the conditions under which the Mpemba effect, the inverse Mpemba and the strong Mpemba effect can be observed. In Maxwell gas, the rate of collision between particles is independent of the relative velocity. In addition, the well-mixed limit is assumed such that spatial correlations are ignored. The equations for the two point correlations close among themselves resulting in a coupled set of linear equations allowing for an exact solution. This linearity happens to be natural to the model and thus does not require any approximations that have been employed in models where the collision rates are velocity dependent. To demonstrate the existence of the Mpemba effect, we determine the conditions under which a hotter system relaxes faster than a cooler system when quenched to a temperature lower than both. For the case of mono-dispersed Maxwell gas, we showed that the Mpemba effect is possible only if the initial states do not correspond to steady states. On the other hand, for bi-dispersed Maxwell gas, there is a range of parameters for which the Mpemba effect exists, even when the states from which the quench is done are restricted to valid steady states. In a similar framework, we also demonstrated the existence of the inverse Mpemba effect where a system is heated instead of cooled, i.e., a system at a lower initial temperature relaxes to a high temperature state faster than another system with an intermediate initial temperature. We also showed the existence of a stronger version of the Mpemba effect, where a system equilibrates to a final steady state at an exponentially faster rate.

The exact analysis allows us to identify the reason behind the Mpemba effect in these systems. First, we note that, though the system evolves stochastically, the evolution of the history-averaged correlation functions is deterministic. The evolution equations are first order differential equations, therefore two trajectories in the correlation functions-time phase space cannot intersect. However, for the mono-dispersed gas, the state of the system is defined by two quantities: energy and inter-particle correlation function. In this three dimensional space (third dimension being time), two trajectories cannot cross. Nevertheless, when projected onto the lower dimensional energy-time plane, trajectories may cross, leading to the Mpemba effect. If the initial states correspond to steady states, then the inter-particle correlations are exactly zero and remain zero during time evolution, constraining the correlation function-time plane to be two dimensional. Thus, a necessary condition for the Mpemba effect to be observed is a non-zero inter-particle correlations, or alternatively non-stationary initial states. On the other hand, for bi-dispersed gases, there are two kinetic energies and three inter-particle correlation functions. Since the energy-time dimensions are themselves three dimensional, it is possible to observe the Mpemba effect when the correlations are set to zero, as in a true steady state. Note that for the present study, we have chosen intersection of total energy as an indicator of the Mpemba effect. This is a natural choice, as this is the quantity that is easiest to track in an experiment. It is possible to characterise the state of the system by more macroscopic quantities. For example, by temperature T and second Sonine coefficient, a_2 in the expansion of velocity distribution function around Gaussian, as studied for the case of granular systems of hard sphere particles [22].

Our results are analogous to those found in the perturbative treatment of the most realistic granular systems [22, 23]. In these calculations, the Mpemba effect can be seen in mono-dispersed systems when the initial conditions do not correspond to any steady state, but rather to some transient states that are close to the final steady state. This is achieved by choosing appropriate initial velocity distribution functions for the two systems. For the case of rough granular gas, calculations were carried out by considering states with Gaussian velocity distribution at all times which may not hold good for non-equilibrium systems. In contrast, the analysis in the present work does not make any assumption regarding the nature of velocity distribution in the steady state of the granular system. Therefore, extending the calculations of Refs. [22, 23] to smooth bi-dispersed gas would be a promising area for future study. One can also search for exponentially faster relaxation protocols in these systems as studied in Refs. [5, 6]. In addition, the results in this chapter, particularly the case of bi-dispersed Maxwell gas where both components are driven, suggest that driven binary gases are a good candidate for observation of the Mpemba effect in granular experiments.

Further, in the aim of demonstrating the existence of the Mpemba effect in Maxwell gases, we have assumed that energies evolve monotonically, by not explicitly accounting for the possibility that when a hot system is quenched to a lower temperature, the temperature could drop below the final temperature. In order to include scenarios with non-monotonic evolution of energy into the present framework, one may have to look at the behavior of the absolute values of the coefficients K_- [11]. This extended case may be addressed in future, to the present and other models of granular gases. One may also look at the relation between the existence of such non monotonic relaxation and the strong Mpemba effect, as the presence of non-monotonicity indicate a change in sign of the coefficient K_-.

Chapter 3

Mpemba effect in an anisotropically driven granular gas

3.1 Introduction

In the previous chapter, we investigated the role of initial conditions for the existence of the Mpemba effect in driven granular gases. The Mpemba effect has been demonstrated for homogeneous and isotropically driven smooth as well as rough gases, which requires the initial states to be non-stationary [22, 23, 24, 25]. The results from an exact analysis of the driven, inelastic Maxwell gas where the rate of collision is taken to be independent of the relative velocity of the colliding particles, is consistent with the above results for the mono-dispersed gas [25]. However, the lack of stationarity of the initial conditions makes it difficult for experimental realisation because while stationary states are easy to achieve due to them being attractive, non-stationary states require careful preparation of the initial state.

On the other hand, we demonstrate the existence of the Mpemba effect in driven bi-dispersed granular gas, starting from steady state initial conditions. However, we find that the criteria for the steady state initial conditions is fulfilled only when the two species of particles of the bi-dispersed gas are driven differently. Such a criterion makes the model more abstract and one does not know how to drive two species of particles differently in experiments. Moreover, the model brings in too many system parameters making to difficult to analyse the minimal criteria that can lead to such effect.

In this chapter, we switch to the mono-dispersed granular gas but now anisotropically driven in two dimensions, and show the existence of the Mpemba effect starting from initial conditions that are stationary. The benefit for the choice of such a model is two fold: (a) it has fewer system parameters to analyse compared to the bi-dispersed gas where both the species are driven differently and (b) such a model is experimentally realisable. In addition, we derive the conditions for the inverse and the strong Mpemba effect in this system. The analysis is exact for stationary states that are close to the final stationary state. For generic initial stationary states, we verify our theoretical predictions with detailed event-driven molecular dynamics simulations of hard discs. We propose that this set up of anisotropically driven granular gases is ideal for studying the Mpemba effect, and later for possibly more practical applications. The content of this chapter is published in Ref. [26].

3.2 Model

Consider a two-dimensional granular gas composed of identical, smooth, inelastic hard particles. The velocities of these particles change in time through momentum conserving binary collisions. When two particles i and j with velocities $\boldsymbol{v}_i$ and $\boldsymbol{v}_j$ collide, the new velocities $\boldsymbol{v}_i'$ and $\boldsymbol{v}_j'$ are given by

$$\begin{aligned} \boldsymbol{v}_i' &= \boldsymbol{v}_i - \frac{1+r}{2}[(\boldsymbol{v}_i - \boldsymbol{v}_j).\hat{e}]\hat{e}, \\ \boldsymbol{v}_j' &= \boldsymbol{v}_j + \frac{1+r}{2}[(\boldsymbol{v}_i - \boldsymbol{v}_j).\hat{e}]\hat{e}, \end{aligned} \tag{3.1}$$

where r is the coefficient of restitution and $\hat{e}$ is the unit vector along the line joining the centres of the particles at contact. The particles are anisotropically driven at a constant rate. At long times, the system goes into a stationary state.

The velocity distribution function $f(\boldsymbol{v},t)$, defined as the number density of particles having velocity $\boldsymbol{v}$ at time t, obeys the Enskog-Boltzmann equation [73]

$$\frac{\partial}{\partial t} f(v,t) = \chi I(f,f) + \Big(\frac{\xi_{0x}^2}{2}\frac{\partial^2}{\partial v_x^2} + \frac{\xi_{0y}^2}{2}\frac{\partial^2}{\partial v_y^2}\Big) f(v,t), \tag{3.2}$$

where χ [74] is the pair correlation function, $I(f,f)$ is the collision integral which accounts for the rate of collision of two particles being proportional to their relative velocity and is given by

$$I(f,f) = \sigma \int dv_2 \int de \Theta(-v_{12}.e)|v_{12}.e| \Big[\frac{1}{r^2} f(\boldsymbol{v}_1^{''},t) f(\boldsymbol{v}_2^{''},t) - f(v_1,t) f(v_2,t)\Big]. \tag{3.3}$$

Here, ξ_{0x}^2 and ξ_{0y}^2 are the variances or strengths of the white noise along the x- and y-directions respectively. Note that in Eq. (3.2), we have introduced different driving strengths along the two directions, and we will refer to such driving as anisotropic driving. The Enskog-Boltzmann equation can be used to describe a spatial system but here we consider a spatially homogeneous system such that the spatial degrees of freedom are ignored. Moreover, as usually assumed in kinetic theory for dilute gases, we apply the molecular chaos hypothesis to use product measure for the joint velocity distribution function in the collision integral $I(f,f)$.

The anisotropic driving implies that, though the system remains homogeneous with $\langle \boldsymbol{v} \rangle = 0$, the mean kinetic energies per particle (granular temperature) along the two directions are different. The granular temperatures are defined as $T_i(t) = (2/n) \int d\boldsymbol{v} \frac{1}{2} m v_i^2 f(v,t)$, where $n = \int d\boldsymbol{v} f(v,t)$ is the number density, m is the mass of the particles, and $i = x,y$.

The time evolution equations are given by

$$\frac{\partial T_x}{\partial t} = m\xi_{0x}^2 + \frac{4n\chi\sigma(1+r)\sqrt{T_y}}{15\sqrt{m}\sqrt{\pi}(T_x - T_y)} \times \Big[\Big(4(2r-3)T_x^2 + (7-3r)T_xT_y - 2(1+r)T_y^2\Big)E\Big(1 - \tfrac{T_x}{T_y}\Big) + T_x\big(2T_x(3-2r) + T_y(1+r)\big)K\Big(1 - \tfrac{T_x}{T_y}\Big)\Big], \tag{3.4}$$

and

$$\frac{\partial T_y}{\partial t} = m\xi_{0y}^2 + \tfrac{4n\chi\sigma(1+r)\sqrt{T_y}}{15\sqrt{m}\sqrt{\pi}(T_x - T_y)} \times \Big[2(1+r)(T_x^2 - T_y^2)E\Big(1 - \tfrac{T_x}{T_y}\Big) + (3r-7)\sqrt{T_xT_y}(T_x - 2T_y)E\Big(1 - \tfrac{T_y}{T_x}\Big) - (1+r)T_x(T_x - T_y)K\Big(1 - \tfrac{T_x}{T_y}\Big) + (3r-7)\sqrt{T_x}T_y^{3/2}K\Big(1 - \tfrac{T_y}{T_x}\Big)\Big], \tag{3.5}$$

We introduce two quantities T_{tot} and T_{dif} which are the total and the difference of the temperatures in the two directions:

$$\begin{aligned} T_{tot}(t) &= T_x(t) + T_y(t), \\ T_{dif}(t) &= T_x(t) - T_y(t). \end{aligned} \tag{3.6}$$

We define the dimensionless variable for time, t^* in terms of mean collision time as

$$t^* = \nu_0 t, \tag{3.7}$$

where ν_0 is the frequency of interparticle collisions given by

$$\nu_0 = \chi\sigma n\sqrt{\frac{2(T_{tot}^{st} + T_{dif}^{st})}{\pi m}}E\Big(\frac{2T_{dif}^{st}}{T_{tot}^{st} + T_{dif}^{st}}\Big). \tag{3.8}$$

Within kinetic theory, the velocity distribution of a driven granular gas, $f(v,t^*)$, is expanded about the Gaussian in terms of Sonine polynomials [73, 74]. For the sake of simplicity, we restrict ourselves to the first term in the expansion, namely a Gaussian. Adding more terms will not change the qualitative results obtained in the chapter. Thus, we write

$$f(\boldsymbol{v},t^*) = \frac{mn}{2\pi\sqrt{T_x(t^*)T_y(t^*)}} \exp\left[-\frac{mv_x^2}{2T_x(t^*)} - \frac{mv_y^2}{2T_y(t^*)}\right]. \tag{3.9}$$

Substituting Eq. (3.9) into Eq. (3.2), we find that the equations governing the temporal evolution of $T_{tot}(t^*)$ and $T_{dif}(t^*)$ form a closed set of coupled non-linear differential equations, and is given by

$$\begin{aligned} \frac{\partial}{\partial t^*} T_{tot}(t^*) &= \mathscr{F}(T_{tot}, T_{dif}), \\ \frac{\partial}{\partial t^*} T_{dif}(t^*) &= \mathscr{G}(T_{tot}, T_{dif}), \end{aligned} \tag{3.10}$$

where

$$\begin{aligned} \mathscr{F}(T_{tot}, T_{dif}) = {} & \frac{m(\xi_{0x}^2+\xi_{0y}^2)}{v_0} + \frac{n\chi\sigma(1+r)\sqrt{T_{tot}-T_{dif}}}{15v_0\sqrt{2\pi m}T_{dif}} \\ & \times\Bigg[\Big((3r-7)T_{tot}^2 + 4(7r-3)T_{tot}T_{dif} + 3(3r-7)T_{dif}^2\Big)E\Big(\tfrac{-2T_{dif}}{T_{tot}-T_{dif}}\Big) \\ & -(3r-7)(T_{tot}-3T_{dif})\sqrt{T_{tot}^2-T_{dif}^2}E\Big(\tfrac{2T_{dif}}{T_{tot}+T_{dif}}\Big) \\ & -(T_{tot}+T_{dif})\Big((3r-7)T_{tot}+(7r-3)T_{dif}\Big)K\Big(\tfrac{-2T_{dif}}{T_{tot}-T_{dif}}\Big) \\ & +(3r-7)\sqrt{T_{tot}+T_{dif}}(T_{tot}-T_{dif})^{3/2}K\Big(\tfrac{2T_{dif}}{T_{tot}+T_{dif}}\Big)\Bigg], \end{aligned} \tag{3.11}$$

and

$$\begin{aligned} \mathscr{G}(T_{tot}, T_{dif}) = {} & \frac{m(\xi_{0x}^2-\xi_{0y}^2)}{v_0} + \frac{n\chi\sigma(1+r)(3r-7)\sqrt{T_{tot}-T_{dif}}}{15v_0\sqrt{2\pi m}T_{dif}} \times \Bigg[(T_{tot}+3T_{dif})(T_{tot}+T_{dif})E\Big(\tfrac{-2T_{dif}}{T_{tot}-T_{dif}}\Big) \\ & +(T_{tot}-3T_{dif})\sqrt{T_{tot}^2-T_{dif}^2}E\Big(\tfrac{2T_{dif}}{T_{tot}+T_{dif}}\Big) \\ & -(T_{tot}+T_{dif})^2K\Big(\tfrac{-2T_{dif}}{T_{tot}-T_{dif}}\Big) \\ & -\sqrt{T_{tot}+T_{dif}}(T_{tot}-T_{dif})^{3/2}K\Big(\tfrac{2T_{dif}}{T_{tot}+T_{dif}}\Big)\Bigg]. \end{aligned} \tag{3.12}$$

We denote the parameters of the final stationary state by T_{tot}^{st} and T_{dif}^{st}. In the stationary state, the time derivatives in Eq. (3.10) can be set to zero and hence $\mathscr{F}(T_{tot}^{st}, T_{dif}^{st}) = 0$ and

$\mathscr{G}(T^{st}_{tot}, T^{st}_{dif}) = 0$. Let us study the variation of the stationary temperatures T^{st}_{tot} and T^{st}_{dif} as a function of the system parameters. We define the following scaling functions:

$$\begin{aligned} T^{st}_{tot} &= m\Big(\frac{\xi^2_{0x}}{n\chi\sigma}\Big)^{2/3}\tilde{T}^{st}_{tot}(r,\mu), \\ T^{st}_{dif} &= m\Big(\frac{\xi^2_{0x}}{n\chi\sigma}\Big)^{2/3}\tilde{T}^{st}_{dif}(r,\mu), \quad \text{where } \mu \equiv \frac{\xi^2_{0y}}{\xi^2_{0x}}. \end{aligned} \tag{3.13}$$

On using the scaling forms for T^{st}_{tot} and T^{st}_{dif} [see Eq. (3.13)] in the steady state condition of Eqs. (3.11) and (3.12), we obtain the following coupled equations in terms of $\tilde{T}^{st}_{tot}(r,\mu)$ and $\tilde{T}^{st}_{dif}(r,\mu)$:

$$\begin{aligned} 0 = \quad & (1+\mu) + \frac{(1+r)\sqrt{\tilde{T}^{st}_{tot}-\tilde{T}^{st}_{dif}}}{15\sqrt{2\pi}\tilde{T}^{st}_{dif}} \times \Big[-(3r-7)(\tilde{T}_{tot}-3\tilde{T}_{dif})\sqrt{\tilde{T}^2_{tot}-\tilde{T}^2_{dif}}E\Big(\frac{2\tilde{T}_{dif}}{\tilde{T}_{tot}+\tilde{T}_{dif}}\Big) \\ & -(\tilde{T}^{st}_{tot}+\tilde{T}^{st}_{dif})\Big((3r-7)\tilde{T}^{st}_{tot}+(7r-3)\tilde{T}^{st}_{dif}\Big)K\Big(\frac{-2\tilde{T}^{st}_{dif}}{\tilde{T}^{st}_{tot}-\tilde{T}^{st}_{dif}}\Big) \\ & +(3r-7)\sqrt{\tilde{T}^{st}_{tot}+\tilde{T}^{st}_{dif}}(\tilde{T}^{st}_{tot}-\tilde{T}^{st}_{dif})^{3/2}K\Big(\frac{2\tilde{T}^{st}_{dif}}{\tilde{T}^{st}_{tot}+\tilde{T}^{st}_{dif}}\Big) \\ & +\Big((3r-7)(\tilde{T}^{st}_{tot})^2+4(7r-3)\tilde{T}^{st}_{tot}\tilde{T}^{st}_{dif}+3(3r-7)(\tilde{T}^{st}_{dif})^2\Big)E\Big(\frac{-2\tilde{T}^{st}_{dif}}{\tilde{T}^{st}_{tot}-\tilde{T}^{st}_{dif}}\Big)\Big], \end{aligned} \tag{3.14}$$

and

$$\begin{aligned} 0 = \quad & (1-\mu) + \frac{(1+r)(3r-7)\sqrt{\tilde{T}^{st}_{tot}-\tilde{T}^{st}_{dif}}}{15\sqrt{2\pi}\tilde{T}^{st}_{dif}} \times \Big[(\tilde{T}^{st}_{tot}+3\tilde{T}^{st}_{dif})(\tilde{T}^{st}_{tot}+\tilde{T}^{st}_{dif})E\Big(\frac{-2\tilde{T}^{st}_{dif}}{\tilde{T}^{st}_{tot}-\tilde{T}^{st}_{dif}}\Big) \\ & +(\tilde{T}^{st}_{tot}-3\tilde{T}^{st}_{dif})\sqrt{(\tilde{T}^{st}_{tot})^2-(\tilde{T}^{st}_{dif})^2}E\Big(\frac{2\tilde{T}^{st}_{dif}}{\tilde{T}^{st}_{tot}+\tilde{T}^{st}_{dif}}\Big) \\ & -(\tilde{T}^{st}_{tot}+\tilde{T}^{st}_{dif})^2K\Big(\frac{-2\tilde{T}^{st}_{dif}}{\tilde{T}^{st}_{tot}-\tilde{T}^{st}_{dif}}\Big) \\ & -\sqrt{\tilde{T}^{st}_{tot}+\tilde{T}^{st}_{dif}}(\tilde{T}^{st}_{tot}-\tilde{T}^{st}_{dif})^{3/2}K\Big(\frac{2\tilde{T}^{st}_{dif}}{\tilde{T}^{st}_{tot}+\tilde{T}^{st}_{dif}}\Big)\Big]. \end{aligned} \tag{3.15}$$

Figure 3.1 shows the variation of the scaled functions, $\tilde{T}^{st}_{tot}(r,\mu)$ and $\tilde{T}^{st}_{dif}(r,\mu)$, for two different values of coefficient of restitutions, $r = 0.01$ and $r = 0.65$. It is evident from Fig. 3.1 that as the ratio of the driving strengths (μ) approaches unity, i.e., in the limit of isotropic driving, $\tilde{T}^{st}_{dif}(r,\mu)$ goes to zero irrespective of the value of r. Also, as r increases,

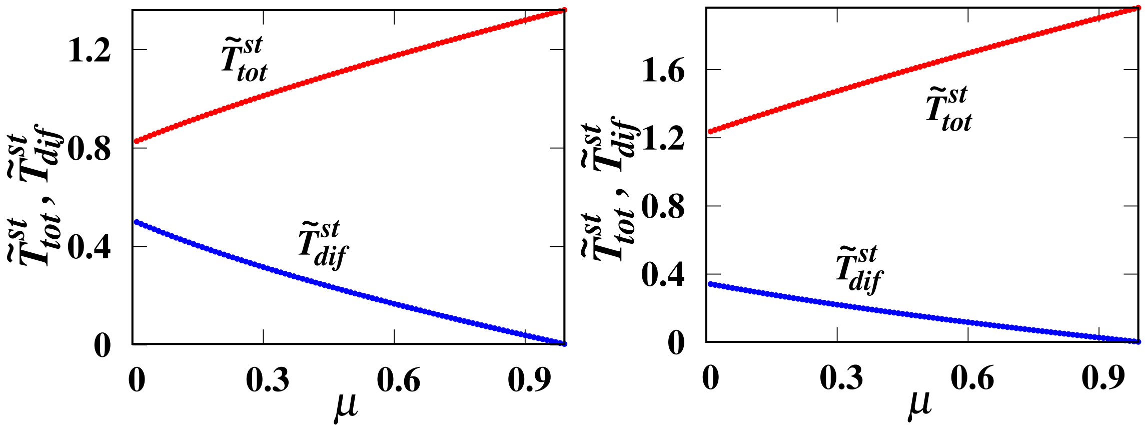

Figure 3.1: Variation of $\tilde{T}^{st}_{tot}(r,\mu)$ and $\tilde{T}^{st}_{dif}(r,\mu)$ with μ for two different cases of (a) $r = 0.01$ and (b) $r = 0.65$. $\tilde{T}^{st}_{dif}(r,\mu)$ goes to zero in the limit of isotropic driving, $\mu \to 1$ and its value decreases with the increase in r for any given value of the ratio of driving strengths, μ.

i.e., as collisions become more elastic, $\tilde{T}^{st}_{dif}(r,\mu)$ decreases to zero for any given value of μ.

3.3 Mpemba effect

We define the Mpemba effect as follows. Consider two systems with different initial T_{tot}. Both systems are quenched to the same final stationary state whose temperature is lower. If the system that is initially hotter reaches the final stationary state faster, then we say that the system shows the Mpemba effect. Likewise, if the initial systems are heated to a higher temperature and the cooler system equilibrates faster, we will say that the system shows the inverse Mpemba effect. Finally, for both effects, we will say that the system shows strong Mpemba effect, if the hotter system relaxes exponentially faster than the cooler system for the Mpemba effect and vice versa for the inverse Mpemba effect. We will demonstrate the existence of all these four features for the anisotropically driven granular gas, both analytically using a linearised theory as well as through event-driven molecular dynamics simulations.

We first analytically demonstrate the Mpemba effect by considering only those initial stationary states that are close to the final stationary state, allowing for linearisation of the system thus making it tractable. This method of linearisation closely follows that of Ref. [22]. Let $\delta T_{tot}(t^*) = T_{tot}(t^*) - T_{tot}^{st}$ and $\delta T_{dif}(t^*) = T_{dif}(t^*) - T_{dif}^{st}$ denote the time-dependent deviation from the stationary state values. For small deviations, the non-linear differential equations in Eq. (3.10) can be linearised about the stationary state values to give

$$\frac{d}{dt^*}\begin{bmatrix} \delta T_{tot}(t^*) \\ \delta T_{dif}(t^*) \end{bmatrix} = -\boldsymbol{R}\begin{bmatrix} \delta T_{tot}(t^*) \\ \delta T_{dif}(t^*) \end{bmatrix}, \tag{3.16}$$

where $\boldsymbol{R}$ is a 2×2 matrix with components R_{11}, R_{12}, R_{21} and R_{22} given by

$$\begin{aligned}
R_{11} = &-\frac{n\chi\sigma(1+r)}{30v_0\sqrt{2\pi m}T_{dif}^{st}\sqrt{T_{tot}^{st}-T_{dif}^{st}}} \\
&\times\Bigg[((3-47r)(T_{dif}^{st})^2+8(9r-1)T_{dif}^{st}T_{tot}^{st}+5(3r-7)(T_{tot}^{st})^2)E\Big(\frac{-2T_{dif}^{st}}{T_{tot}^{st}-T_{dif}^{st}}\Big) \\
&+\frac{7-3r}{\sqrt{(T_{tot}^{st})^2-(T_{dif}^{st})^2}}\Big(5(T_{dif}^{st})^3+3(T_{dif}^{st})^2T_{tot}^{st}-13T_{dif}^{st}(T_{tot}^{st})^2+5(T_{tot}^{st})^3\Big)E\Big(\frac{2T_{dif}^{st}}{T_{tot}^{st}+T_{dif}^{st}}\Big) \\
&+\frac{(7-3r)(T_{tot}^{st}-T_{dif}^{st})^{3/2}}{\sqrt{T_{tot}^{st}+T_{dif}^{st}}}\Big(T_{dif}^{st}(-4\sqrt{T_{tot}+T_{dif}}+1)-T_{tot}^{st}(2\sqrt{T_{tot}+T_{dif}}+3)\Big)K\Big(\frac{2T_{dif}^{st}}{T_{tot}^{st}+T_{dif}^{st}}\Big) \\
&+\Big((13r-17)(T_{dif}^{st})^2+2(1-9r)T_{dif}^{st}T_{tot}^{st}+5(7-3r)(T_{tot}^{st})^2\Big)K\Big(\frac{-2T_{dif}^{st}}{T_{tot}^{st}-T_{dif}^{st}}\Big) \\
&+\frac{\pi T_{dif}^{st}}{2(T_{tot}^{st}-T_{dif}^{st})}\Big(3(3r-7)(T_{dif}^{st})^2+4(7r-3)T_{dif}^{st}T_{tot}^{st}+(3r-7)(T_{tot}^{st})^2\Big){}_2F_1\Big(\frac{1}{2},\frac{3}{2};2;\frac{-2T_{dif}^{st}}{T_{tot}^{st}-T_{dif}^{st}}\Big) \\
&-\frac{\pi(3r-7)T_{dif}^{st}\sqrt{T_{tot}^{st}-T_{dif}^{st}}}{2(T_{tot}^{st}+T_{dif}^{st})^{3/2}}\Big(3(T_{dif}^{st})^2-4T_{dif}^{st}T_{tot}^{st}+(T_{tot}^{st})^2\Big){}_2F_1\Big(\frac{1}{2},\frac{3}{2};2;\frac{2T_{dif}^{st}}{T_{tot}^{st}+T_{dif}^{st}}\Big) \\
&-\frac{\pi T_{dif}^{st}(T_{tot}^{st}+T_{dif}^{st})}{2(T_{tot}^{st}-T_{dif}^{st})}\Big((7r-3)T_{dif}^{st}+(3r-7)T_{tot}^{st}\Big){}_2F_1\Big(\frac{3}{2},\frac{3}{2};2;\frac{-2T_{dif}^{st}}{T_{tot}^{st}-T_{dif}^{st}}\Big) \\
&-\frac{\pi(3r-7)T_{dif}^{st}(T_{tot}^{st}-T_{dif}^{st})^{5/2}}{2(T_{tot}^{st}+T_{dif}^{st})^{3/2}}{}_2F_1\Big(\frac{3}{2},\frac{3}{2};2;\frac{2T_{dif}^{st}}{T_{tot}^{st}+T_{dif}^{st}}\Big)\Bigg],
\end{aligned}$$

$$
\begin{aligned}
R_{12} = &-\frac{n\chi\sigma(1+r)}{30\nu_0\sqrt{2\pi m}(T_{dif}^{st})^2\sqrt{T_{tot}^{st}-T_{dif}^{st}}} \\
&\times\Bigg[\Big(9(7-3r)(T_{dif}^{st})^3-10(r+3)(T_{dif}^{st})^2T_{tot}^{st}-(7-3r)T_{dif}^{st}(T_{tot}^{st})^2+2(7-3r)(T_{tot}^{st})^3\Big)E\Big(\frac{-2T_{dif}^{st}}{T_{tot}^{st}-T_{dif}^{st}}\Big) \\
&-(7-3r)\frac{(T_{tot}^{st}-T_{dif}^{st})^{3/2}}{\sqrt{T_{tot}+T_{dif}}}\Big(15(T_{dif}^{st})^2+9T_{dif}^{st}T_{tot}^{st}-2(T_{tot}^{st})^2\Big)E\Big(\frac{2T_{dif}^{st}}{T_{tot}^{st}+T_{dif}^{st}}\Big) \\
&-\frac{(7-3r)\sqrt{T_{tot}-T_{dif}}}{\sqrt{T_{tot}+T_{dif}}}\Big(5(T_{dif}^{st})^3-4(T_{dif}^{st})^2T_{tot}^{st}-3(T_{tot}^{st})^2T_{dif}^{st}+2(T_{tot}^{st})^3\Big)K\Big(\frac{2T_{dif}^{st}}{T_{tot}^{st}+T_{dif}^{st}}\Big) \\
&+\Big(-(3-7r)(T_{dif}^{st})^3+4(1+r)(T_{dif}^{st})^2T_{tot}^{st}+5(1-5r)(T_{tot}^{st})^2T_{dif}^{st}+2(7-3r)(T_{tot}^{st})^3\Big)K\Big(\frac{-2T_{dif}^{st}}{T_{tot}^{st}-T_{dif}^{st}}\Big) \\
&-\frac{\pi T_{dif}^{st}T_{tot}^{st}}{2(T_{tot}^{st}-T_{dif}^{st})}\Big(3(7-3r)(T_{dif}^{st})^2+4(3-7r)T_{dif}^{st}T_{tot}^{st}+(7-3r)(T_{tot}^{st})^2\Big){}_2F_1\Big(\frac{1}{2},\frac{3}{2};2;\frac{-2T_{dif}^{st}}{T_{tot}^{st}-T_{dif}^{st}}\Big) \\
&-\frac{\pi(7-3r)T_{dif}^{st}T_{tot}^{st}\sqrt{T_{tot}^{st}-T_{dif}^{st}}}{2(T_{tot}^{st}+T_{dif}^{st})^{3/2}}\Big(3(T_{dif}^{st})^2-4T_{dif}^{st}T_{tot}^{st}+(T_{tot}^{st})^2\Big){}_2F_1\Big(\frac{1}{2},\frac{3}{2};2;\frac{2T_{dif}^{st}}{T_{tot}^{st}+T_{dif}^{st}}\Big) \\
&-\frac{\pi T_{dif}^{st}T_{tot}^{st}(T_{tot}^{st}+T_{dif}^{st})}{2(T_{tot}^{st}-T_{dif}^{st})}\Big((3-7r)T_{dif}^{st}+(7-3r)T_{tot}^{st}\Big){}_2F_1\Big(\frac{3}{2},\frac{3}{2};2;\frac{-2T_{dif}^{st}}{T_{tot}^{st}-T_{dif}^{st}}\Big) \\
&-\frac{\pi(7-3r)T_{dif}^{st}T_{tot}^{st}(T_{tot}^{st}-T_{dif}^{st})^{5/2}}{2(T_{tot}^{st}+T_{dif}^{st})^{3/2}}{}_2F_1\Big(\frac{3}{2},\frac{3}{2};2;\frac{2T_{dif}^{st}}{T_{tot}^{st}+T_{dif}^{st}}\Big)\Bigg],
\end{aligned}
$$

$$
\begin{aligned}
R_{21} = {} & \frac{n\chi\sigma(1+r)(7-3r)}{30\nu_0\sqrt{2\pi m}T^{st}_{dif}\sqrt{T^{st}_{tot}-T^{st}_{dif}}} \\
& \times \Bigg[\Big(-5(T^{st}_{dif})^2+8T^{st}_{dif}T^{st}_{tot}+5(T^{st}_{tot})^2\Big)E\Big(\frac{-2T^{st}_{dif}}{T^{st}_{tot}-T^{st}_{dif}}\Big) \\
& + \Big(\frac{(T^{st}_{tot}+T^{st}_{dif})^2}{2}+(3T^{st}_{tot}-T^{st}_{dif})(T^{st}_{tot}-3T^{st}_{dif})\frac{\sqrt{T^{st}_{tot}-T^{st}_{dif}}}{\sqrt{T^{st}_{tot}+T^{st}_{dif}}}\Big)E\Big(\frac{2T^{st}_{dif}}{T^{st}_{tot}+T^{st}_{dif}}\Big) \\
& - \Big(\frac{4}{\sqrt{(T^{st}_{tot})^2-(T^{st}_{dif})}}\big(4(T^{st}_{dif})^2-T^{st}_{dif}T^{st}_{tot}-(T^{st}_{tot})^2\big)\Big)E\Big(\frac{2T^{st}_{dif}}{T^{st}_{tot}+T^{st}_{dif}}\Big) \\
& - \frac{(T^{st}_{tot}-T^{st}_{dif})^{3/2}}{\sqrt{T^{st}_{tot}+T^{st}_{dif}}}\Big(3T^{st}_{dif}+5T^{st}_{tot}\Big)K\Big(\frac{2T^{st}_{dif}}{T^{st}_{tot}+T^{st}_{dif}}\Big) \\
& - \Big((5T^{st}_{tot}-3T^{st}_{dif})(T^{st}_{tot}+T^{st}_{dif})\Big)K\Big(\frac{-2T^{st}_{dif}}{T^{st}_{tot}-T^{st}_{dif}}\Big) \\
& - \frac{\pi T^{st}_{dif}(T^{st}_{tot}+3T^{st}_{dif})(T^{st}_{tot}+T^{st}_{dif})}{2(T^{st}_{tot}-T^{st}_{dif})}\,{}_2F_1\Big(\frac{1}{2},\frac{3}{2};2;\frac{-2T^{st}_{dif}}{T^{st}_{tot}-T^{st}_{dif}}\Big) \\
& - \frac{\pi T^{st}_{dif}(T^{st}_{tot}+T^{st}_{dif})^2}{2(T^{st}_{tot}-T^{st}_{dif})}\,{}_2F_1\Big(\frac{3}{2},\frac{3}{2};2;\frac{-2T^{st}_{dif}}{T^{st}_{tot}-T^{st}_{dif}}\Big) \\
& + \frac{\pi T^{st}_{dif}(T^{st}_{tot}-3T^{st}_{dif})(T^{st}_{tot}-T^{st}_{dif})^{3/2}}{2(T^{st}_{tot}+T^{st}_{dif})^{3/2}}\,{}_2F_1\Big(\frac{1}{2},\frac{3}{2};2;\frac{2T^{st}_{dif}}{T^{st}_{tot}+T^{st}_{dif}}\Big) \\
& + \frac{\pi T^{st}_{dif}(T^{st}_{tot}-T^{st}_{dif})^{5/2}}{2(T^{st}_{tot}+T^{st}_{dif})^{3/2}}\,{}_2F_1\Big(\frac{3}{2},\frac{3}{2};2;\frac{2T^{st}_{dif}}{T^{st}_{tot}+T^{st}_{dif}}\Big)\Bigg],
\end{aligned}
$$

and

$$
\begin{aligned}
R_{22} = {} & \frac{n\chi\sigma(1+r)(7-3r)}{30\nu_0\sqrt{2\pi m}(T^{st}_{dif})^2\sqrt{T^{st}_{tot}-T^{st}_{dif}}} \\
& \times \Bigg[\Big(-9(T^{st}_{dif})^3+2(T^{st}_{dif})^2T^{st}_{tot}+T^{st}_{dif}(T^{st}_{tot})^2-2(T^{st}_{tot})^3\Big)E\Big(\frac{-2T^{st}_{dif}}{T^{st}_{tot}-T^{st}_{dif}}\Big) \\
& + \frac{\sqrt{T^{st}_{tot}-T^{st}_{dif}}}{\sqrt{T_{tot}+T_{dif}}}\Big(9(T^{st}_{dif})^3+2(T^{st}_{dif})^2T^{st}_{tot}-T^{st}_{dif}(T^{st}_{tot})^2-2(T^{st}_{tot})^3\Big)E\Big(\frac{2T^{st}_{dif}}{T^{st}_{tot}+T^{st}_{dif}}\Big) \\
& + \frac{(T_{tot}-T_{dif})^{3/2}}{\sqrt{T_{tot}+T_{dif}}}\Big(3(T^{st}_{dif})^2+3T^{st}_{dif}T^{st}_{tot}+2(T^{st}_{tot})^2\Big)K\Big(\frac{2T^{st}_{dif}}{T^{st}_{tot}+T^{st}_{dif}}\Big) \\
& + \Big(3(T^{st}_{dif})^2-3T^{st}_{dif}T^{st}_{tot}+2(T^{st}_{tot})^2\Big)K\Big(\frac{-2T^{st}_{dif}}{T^{st}_{tot}-T^{st}_{dif}}\Big) \\
& + \frac{\pi T^{st}_{dif}T^{st}_{tot}(T^{st}_{tot}+T^{st}_{dif})(T^{st}_{tot}+3T^{st}_{dif})}{2(T^{st}_{tot}-T^{st}_{dif})}{}_2F_1\Big(\frac{1}{2},\frac{3}{2};2;\frac{-2T^{st}_{dif}}{T^{st}_{tot}-T^{st}_{dif}}\Big) \\
& - \frac{\pi T^{st}_{dif}T^{st}_{tot}(T^{st}_{tot}-3T^{st}_{dif})(T^{st}_{tot}-T^{st}_{dif})^{3/2}}{2(T^{st}_{tot}+T^{st}_{dif})^{3/2}}{}_2F_1\Big(\frac{1}{2},\frac{3}{2};2;\frac{2T^{st}_{dif}}{T^{st}_{tot}+T^{st}_{dif}}\Big) \\
& + \frac{\pi T^{st}_{dif}T^{st}_{tot}(T^{st}_{tot}+T^{st}_{dif})^2}{2(T^{st}_{tot}-T^{st}_{dif})}{}_2F_1\Big(\frac{3}{2},\frac{3}{2};2;\frac{-2T^{st}_{dif}}{T^{st}_{tot}-T^{st}_{dif}}\Big) \\
& - \frac{\pi T^{st}_{dif}T^{st}_{tot}(T^{st}_{tot}-T^{st}_{dif})^{5/2}}{2(T^{st}_{tot}+T^{st}_{dif})^{3/2}}{}_2F_1\Big(\frac{3}{2},\frac{3}{2};2;\frac{2T^{st}_{dif}}{T^{st}_{tot}+T^{st}_{dif}}\Big)\Bigg].
\end{aligned}
$$

$\delta T_{tot}(t^*)$ and $\delta T_{dif}(t^*)$ then relaxes in time to zero as

$$
\begin{aligned}
\delta T_{tot}(t^*) &= K_+e^{-\lambda_+t^*}+K_-e^{-\lambda_-t^*}, \\
\delta T_{dif}(t^*) &= L_+e^{-\lambda_+t^*}+L_-e^{-\lambda_-t^*},
\end{aligned}
\tag{3.17}
$$

where the coefficients K_+, K_-, L_+ and L_- are given by

$$
\begin{aligned}
K_+ &= \frac{1}{\gamma}\Big[R_{12}\delta T_{dif}(0)-(\lambda_--R_{11})\delta T_{tot}(0)\Big], \\
K_- &= \frac{1}{\gamma}\Big[-R_{12}\delta T_{dif}(0)+(\lambda_+-R_{11})\delta T_{tot}(0)\Big], \\
L_+ &= \frac{1}{\gamma}\Big[(\lambda_+-R_{11})\delta T_{dif}(0)-\frac{(\lambda_+-R_{11})(\lambda_--R_{11})}{R_{12}}\delta T_{tot}(0)\Big], \\
L_- &= \frac{1}{\gamma}\Big[-(\lambda_--R_{11})\delta T_{dif}(0)+\frac{(\lambda_+-R_{11})(\lambda_--R_{11})}{R_{12}}\delta T_{tot}(0)\Big].
\end{aligned}
\tag{3.18}
$$

Here, $\lambda_\pm$ are the eigenvalues of $\boldsymbol{R}$ and $\gamma=\lambda_+-\lambda_-$.

We now derive the condition for the Mpemba effect to be present in the linearised regime, based on the analysis of Eq. (5.6). Consider two systems P and Q whose stationary state parameters are denoted as $[T_{tot}^P, T_{dif}^P]$ and $[T_{tot}^Q, T_{dif}^Q]$ respectively. We will assume that P is hotter than Q, i.e., $T_{tot}^P > T_{tot}^Q$. On quenching to $[T_{tot}^{st}, T_{dif}^{st}]$, the Mpemba effect will be present when there exists a finite time τ such $T_{tot}^P(t^*) < T_{tot}^Q(t^*)$ for $t^* > \tau$. To characterise the difference between the two system, we introduce the quantities $\Delta T_{tot} = T_{tot}^P(0) - T_{tot}^Q(0)$ and $\Delta T_{dif} = T_{dif}^P(0) - T_{dif}^Q(0)$. From Eq. (5.6), written for both P and Q, the time τ at which the two relaxation curves cross, corresponding to $T_{tot}^P(\tau) = T_{tot}^Q(\tau)$, is given by

$$\tau = \frac{1}{\gamma} \ln \left[\frac{R_{12}\Delta T_{dif} - (\lambda_- - R_{11})\Delta T_{tot}}{R_{12}\Delta T_{dif} - (\lambda_+ - R_{11})\Delta T_{tot}} \right]. \tag{3.19}$$

For the Mpemba effect to be present, we require that $\tau > 0$, or equivalently (since $\gamma > 0$), the argument of the logarithm in Eq. (3.19) should be greater than one. We immediately obtain the criterion for the crossing of the two trajectories as

$$R_{12}\Delta T_{dif} > (\lambda_+ - R_{11})\Delta T_{tot}. \tag{3.20}$$

In Fig. 3.2(a), we choose initial conditions P and Q such that Eq. (3.20) is satisfied. The trajectories cross at the point as predicted by Eq. (3.19). For initial stationary states that are close to the final state, there is little difference between the linearised (dotted lines) and the full numerical solutions (solid lines).

In Fig. 3.3, we identify the region of phase space (initial conditions) where the Mpemba effect is observable for varying coefficient of restitution r, based on Eq. (3.20). The initial conditions in the region below the line in the phase diagram show the Mpemba effect whereas the other region does not show the effect. The phase diagram is for a generic final stationary state with parameters $T_{tot}^{st} = 1.0$ and $T_{dif}^{st} = 0.15$. As r approaches unity, the gas becomes more isotropic, and the the key feature responsible for the presence of

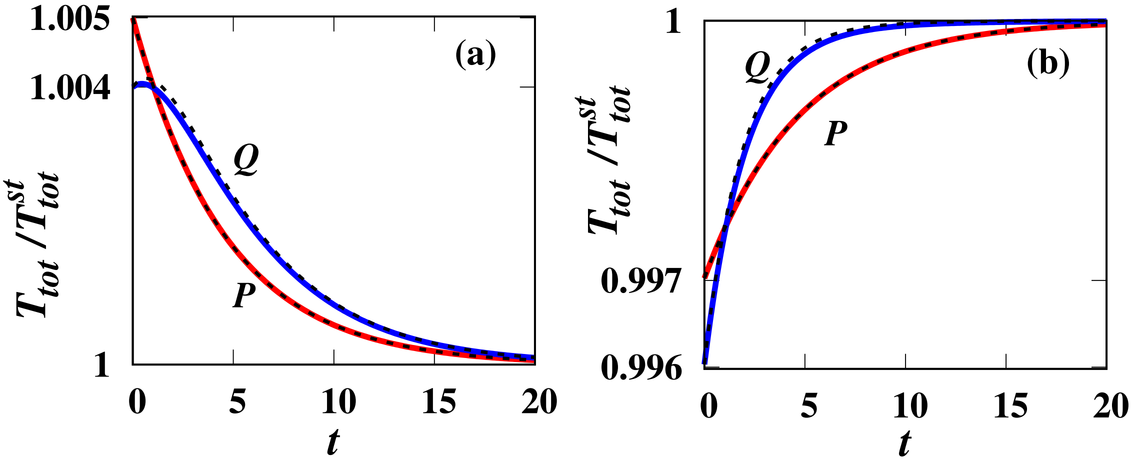

Figure 3.2: (a) The time evolution of $T_{tot}(t^*)$ with time t^* for two systems P and Q, with initial conditions $T^P_{tot}(0)/T^{st}_{tot}$=1.005, $T^P_{dif}(0)/T^{st}_{tot}$=0.28 ($\xi^2_{oy}/\xi^2_{ox} = 6\times10^{-3}$), $T^Q_{tot}(0)/T^{st}_{tot}$=1.004 and $T^Q_{dif}(0)/T^{st}_{tot}$=0.2 ($\xi^2_{oy}/\xi^2_{ox} = 0.168$), show the Mpemba effect when quenched to the final stationary state values of T^{st}_{tot}=1.00 and $T^{st}_{dif}/T^{st}_{tot}$=0.28 ($\xi^2_{oy}/\xi^2_{ox} = 1.54\times10^{-4}$). (b) The initial conditions $T^P_{tot}(0)/T^{st}_{tot}$=0.997, $T^P_{dif}(0)/T^{st}_{tot}$=0.277 ($\xi^2_{oy}/\xi^2_{ox} = 7.34\times10^{-2}$), $T^Q_{tot}(0)/T^{st}_{tot}$=0.996 and $T^Q_{dif}(0)/T^{st}_{tot}$=0.198 ($\xi^2_{oy}/\xi^2_{ox}$=0.169) show the inverse Mpemba effect when heated to the final stationary state values of T^{st}_{tot}=1.0 and $T^{st}_{dif}/T^{st}_{tot}$=0.28 ($\xi^2_{oy}/\xi^2_{ox} = 1.54\times10^{-4}$). The solid lines represent the exact time evolution of T_{tot} and the dashed lines represent its time evolution after linearisation. The other parameters used for the systems are m=1, $n\sigma^2$=0.02 and r=0.65.

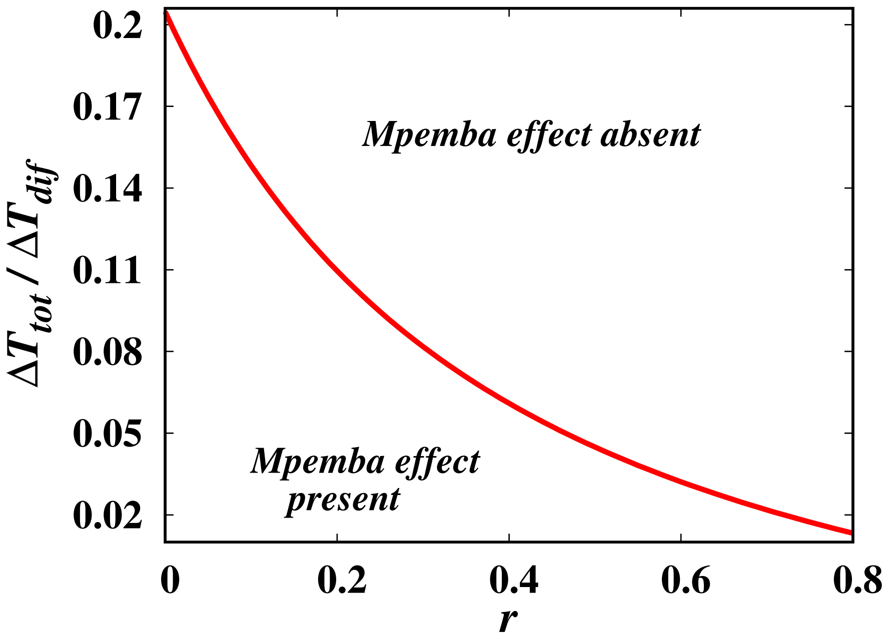

Figure 3.3: The $\Delta T_{tot}/\Delta T_{dif}$–$r$ phase diagram showing regions where the Mpemba effect is observed and r is the coefficient of restitution. All other parameters are kept constant. Here, both the systems are quenched to the final stationary state given by $T_{tot}^{st} = 1.0$ and $T_{dif}^{st}/T_{tot}^{st} = 0.15$. The region below the critical line show the Mpemba effect whereas the region on the other side of the critical line does not show the Mpemba effect.

the Mpemba effect, i.e., anisotropy of temperatures, is lost and hence the Mpemba effect is not observed.

It can be shown that an inverse Mpemba effect also exists wherein the system is heated instead of being cooled. The condition for the inverse Mpemba effect to be present turns out to be the same as in Eq. (3.20). An example is illustrated in Fig. 3.2(b). Initially Q is at a lower temperature. On being heated to a common higher temperature, it can be seen that Q equilibrates faster. Again, the difference between the exact linearised solution and the full numerical solution of the non-linear equation is negligible.

We also explore the possibility of the strong Mpemba effect in which the system at higher temperature cools exponentially faster. The linear evolution equation in Eq. (5.6) allows certain set of initial conditions to relax to the final stationary state exponentially faster compared to other initial states. The effect may be realised when the coefficient associated with the slower relaxation rate in the time evolution of total temperature, $T_{tot}(t^*)$

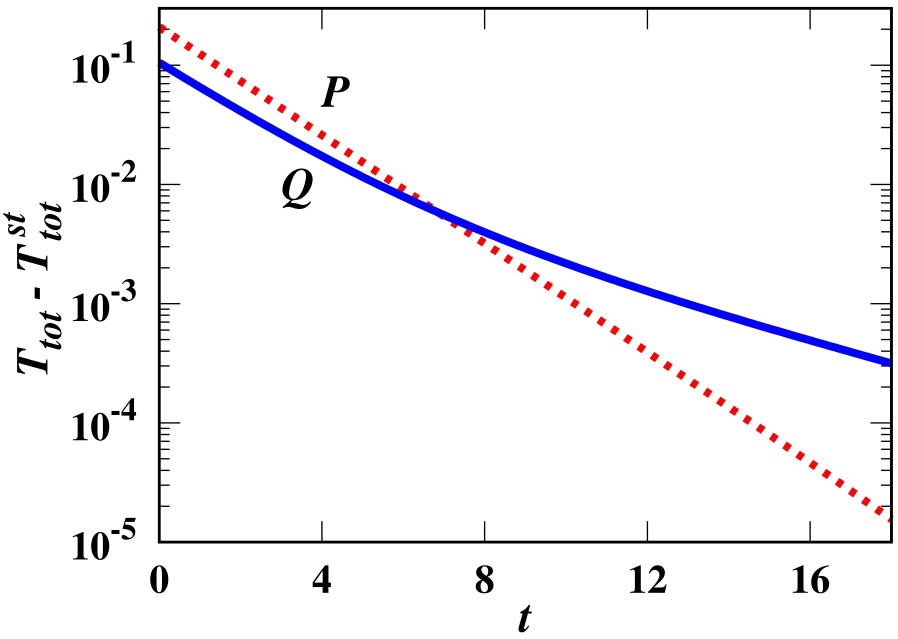

Figure 3.4: Time evolution of $T_{tot}(t^*)$ with t^* for two identical systems P and Q with initial conditions $T_{tot}^{P}(0)/T_{tot}^{st}$=1.026, $T_{dif}^{P}(0)/T_{tot}^{st}$=0.456 ($\xi_{oy}^2/\xi_{ox}^2$=0.08), $T_{tot}^{Q}(0)/T_{tot}^{st}$=1.014 and $T_{dif}^{Q}(0)/T_{tot}^{st}$=0.2 ($\xi_{oy}^2/\xi_{ox}^2$=0.438) which are chosen close to the final stationary state values of T_{tot}^{st}=1.0 and $T_{dif}^{st}/T_{tot}^{st}$=0.1 ($\xi_{oy}^2/\xi_{ox}^2$=0.667). P cools exponentially faster than Q though it has higher initial temperature and thus exhibits the strong Mpemba effect. The other parameters used for the systems are m=1, $n\sigma^2$=0.02 and r=0.2.

vanishes. Setting the coefficient (K_-) associated with the slower relaxation rate to zero [see Eq. (5.6)], we obtain the condition for the strong Mpemba effect to be

$$T_{tot}(0) = \frac{R_{12}}{\lambda_+ - R_{11}} T_{dif}(0) - c, \tag{3.21}$$

where $c = R_{12}/(\lambda_+ - R_{11})T_{dif}^{st} - T_{tot}^{st}$. For a system with all other parameters kept fixed, solution of Eq. (3.21) in terms of $T_{tot}(0)$ and $T_{dif}(0)$ provides the set of initial states whose relaxation is exponentially faster than the set of generic states. Among these initial states, we look for stationary states that can be obtained by applying suitable driving strengths ξ_{0x}^2 and ξ_{0y}^2. One such example is illustrated in Fig. (3.4). Here, P which is hotter cools exponentially faster.

3.4 Comparison with simulations

In these calculations, the spatial degrees of freedom have been ignored. To show that the results continue to hold even when spatial correlations may be present, we compare the analytical results with event-driven molecular dynamics (MD) simulations. In the MD simulations, we have analysed the systems with dimensionless number density, $n\sigma^2$ =0.02 and $r = 0.65$. During a collision, the velocities are updated according to Eq. (4.1). For driving, after a certain time step dt, a particle is chosen at random at rate λ_d and the velocity of the particle is updated according to: $v_i' = -v_i + \sqrt{\xi_{0i}^2/\lambda_d}\phi_i$, where $i = x, y$ and ϕ is drawn from a normal distribution. We prepare two systems P and Q in their stationary state initial conditions having different initial temperatures and then quenched to the same lower temperature. The driving strengths ξ_{0x}^2 and ξ_{0y}^2 corresponding to the initial and final stationary temperatures are computed using Eqs. (3.11) and (3.12).

Figure 3.5 shows the time evolution of the total temperature, T_{tot} with time, t^* when the two systems, P and Q are driven from their different stationary state initial conditions to a same final state. In order to compare between the theory and simulation results, we plot the ratio of T_{tot}/T_{tot}^{st} obtained from the respective theoretical and simulation results. The solid lines represent the theoretical predictions as obtained by solving the full non-linear Eq. (3.10) by assuming Gaussian distribution for the velocity distribution function whereas the points denote the results obtained from the MD simulations. Clearly, there is a good agreement between the theoretical predictions and the results from the MD simulations for both the Mpemba effect [see Fig. 3.5(a)] and its inverse [see Fig. 3.5(b)]. For much larger initial temperatures (twice as large), the comparison between simulation and the numerical solution of Eq. (3.10) is shown in Fig. (3.6). While there is a small quantitative difference, the qualitative features of the Mpemba effect persist.

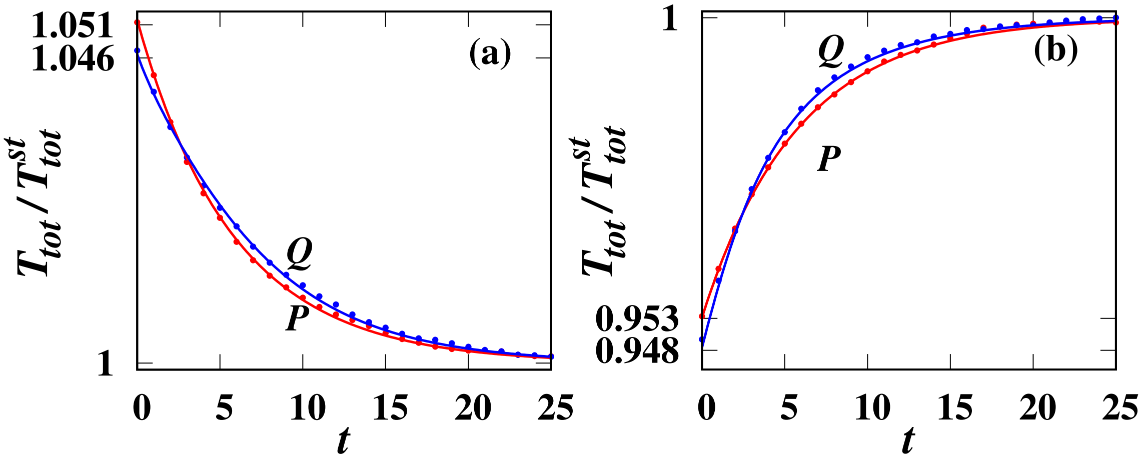

Figure 3.5: (a) The time evolution of $T_{tot}(t^*)$ with time t^* for two systems P and Q, with initial conditions $T_{tot}^P(0)/T_{tot}^{st}$=1.051, $T_{dif}^P(0)/T_{tot}^{st}$=0.294 ($\xi_{oy}^2/\xi_{ox}^2$=3.64×10^{-3}), $T_{tot}^Q(0)/T_{tot}^{st}$=1.046 and $T_{dif}^Q(0)/T_{tot}^{st}$=−0.172 ($\xi_{oy}^2/\xi_{ox}^2$=3.87), show the Mpemba effect when quenched to the final stationary state values of T_{tot}^{st}=1.0 and $T_{dif}^{st}/T_{tot}^{st}$=0.279 ($\xi_{oy}^2/\xi_{ox}^2$=3.89×10^{-3}). (b) The initial conditions $T_{tot}^P(0)/T_{tot}^{st}$=0.953, $T_{dif}^P(0)/T_{tot}^{st}$=0.267 ($\xi_{oy}^2/\xi_{ox}^2$=3.59×10^{-3}), $T_{tot}^Q(0)/T_{tot}^{st}$=0.948 and $T_{dif}^Q(0)/T_{tot}^{st}$=−0.156 ($\xi_{oy}^2/\xi_{ox}^2$=3.89) show the inverse Mpemba effect when heated to the final stationary state values of T_{tot}^{st}=1.0 and $T_{dif}^{st}/T_{tot}^{st}$=0.279 ($\xi_{oy}^2/\xi_{ox}^2$=3.89×10^{-3}). The solid lines represent the exact time evolution of T_{tot} and the points represent the results from simulation. The other parameters used for the systems are m=1, $n\sigma^2$=0.02 and r=0.65.

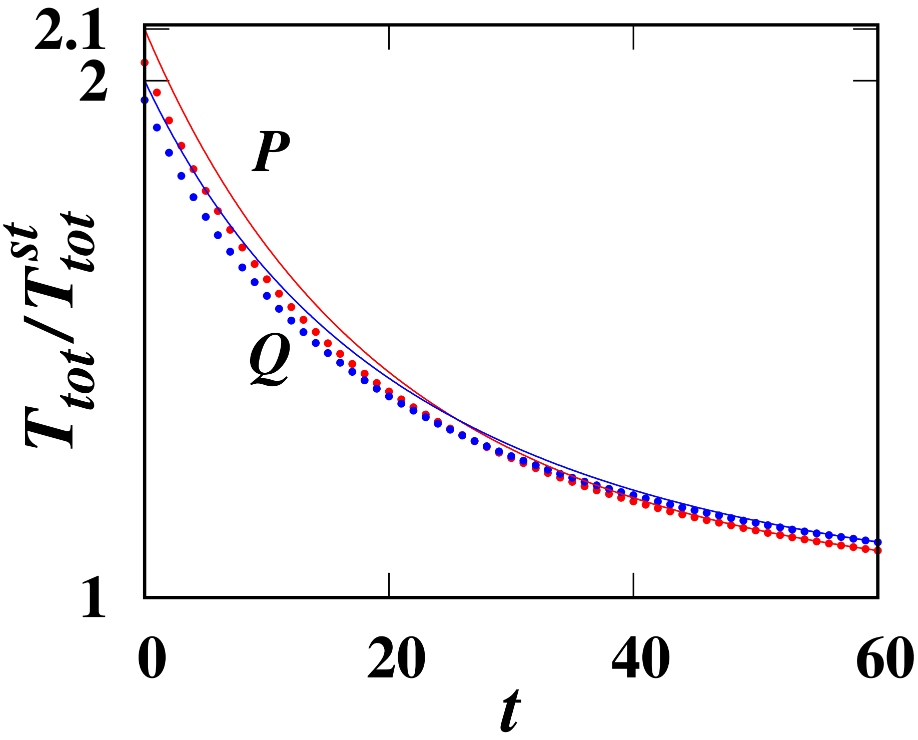

Figure 3.6: Time evolution of $T_{tot}(t^*)$ with t^* for two identical systems P and Q with initial conditions $T^P_{tot}(0)/T^{st}_{tot}$=2.1, $T^P_{dif}(0)/T^{st}_{tot}$=1.26 ($\xi^2_{oy}/\xi^2_{ox}$=5.89$\times10^{-5}$), $T^Q_{tot}(0)/T^{st}_{tot}$=2.0 and $T^Q_{dif}(0)/T^{st}_{tot}$=$-1.2$ (ξ^2_{oy}/ξ^2_{ox}=1.697$\times10^4$) show the Mpemba effect when quenched to the final stationary state values of T^{st}_{tot}=1.0 and $T^{st}_{dif}/T^{st}_{tot}$=0.6 ($\xi^2_{oy}/\xi^2_{ox}$=5.893$\times10^{-5}$). The other parameters used for the system are $r = 0.05$, $m = 1$ and $n\sigma^2 = 0.02$. The solid lines represent the exact time evolution of T_{tot} and the points represent the results from simulation.

3.5 Conclusion

To summarise, we showed the existence of the Mpemba effect, the inverse Mpemba effect and the strong Mpemba effect in an anisotropically driven granular gas. The key feature is that the initial states are stationary states unlike earlier analysis of the Mpemba effect in isotropically driven granular systems which required the initial states to be non-stationary. Our analysis also shows that anisotropy in the velocity distribution of particles is a key ingredient for the existence of such anomalous behaviour, and the Mpemba effect vanishes when the collisions become elastic. It also demonstrates that the Mpemba effect, though usually studied in detailed balanced systems, is more general and is applicable to systems far from equilibrium. The time taken to relax to the steady state could depend anomalously on the distance of the steady state from which it is quenched. Though the exact results were based on a linearised theory for a spatially homogeneous system, MD simulations of hard discs in two dimensions show that the results are true for a spatially extended system also. Achieving anisotropic driving in experiments is not difficult as the amplitude and frequency of shaking can be chosen to be different in different directions, and should therefore allow for an experimental realisation, which has been hitherto lacking, of the Mpemba effect in granular systems.

Chapter 4

Mpemba effect in anisotropically driven inelastic Maxwell gases

4.1 Introduction

To achieve the Mpemba effect in a granular system with stationary initial conditions, a couple of systems have been put forward. Through an exact analysis of a driven binary granular Maxwell gases [25], it was shown that the coupling between the mean kinetic energies of the two components of the binary gas leads to the Mpemba effect, the inverse Mpemba effect and the strong Mpemba effect starting from steady state initial conditions. Here, a mechanism of driving the two types of particles differently is required, which may be difficult to achieve in practice. For a monodispersed gas in two dimensions, it was shown in the previous chapter that it is possible to achieve the Mpemba effect, its inverse and the strong counterpart with initial stationary states provided the driving is anisotropic (different in the two directions) [26]. This was established based on an analysis of the Enskog-Boltzmann equation for driven granular gases with the simplifying assumption that the velocity distribution is a gaussian. By linearising the theory about the stationary states, it is shown that the Mpemba effect can be achieved by simply tuning the driving strengths, thus making it an effective system for experimental realisation of the effect. Results from event-driven simulations are consistent with the results from the linearised theory [26]. However, it is not very clear how much the results depend on the simplifying assumptions which are ad-hoc and not perturbative. In addition, the Enskog-Boltzmann equation for driven granular gases assumes that the driving is diffusive and hence limits the form of driving. It would thus be of importance to have a more rigorous derivation of the results.

In this chapter, we do an exact analysis of the system of monodispersed inelastic gas with anisotropic driving based on the inelastic Maxwell model in two dimensions. Compared to the system studied in Ref. [26] where the rate of collision is proportional to the relative velocity, in the Maxwell gas, the rate of collision is independent of the relative velocity. While this makes the Maxwell gas more unrealistic, it renders it more amenable to exact analysis, at the same time retaining the qualitative features. This advantageous feature has been exploited in obtaining more rigorous results in both freely cooling granular gas [75, 76, 77, 78] as well as in the velocity distributions of driven granular gases [79, 80, 81, 55, 56, 58, 57]. The equations for the time evolution of the relevant two point velocity correlations for the Maxwell gas form a closed set of equations [60]. We analyse these equations to determine the condition and the parameter regime for the existence of the Mpemba effect. Compared to the model studied in Ref. [26], the rigorous analysis in the Maxwell model allows us to explore the entire region of phase space of the system as well as to analyse every aspects of the possible anisotropy that can demonstrate the Mpemba effect. With our exact analysis of the anisotropically driven Maxwell gas, we are able to put the results of Ref. [26], which depended on many simplifying assumptions, on a more sound footing. We show that the Mpemba and the inverse Mpemba effects exist for steady state initial conditions which can be prepared by tuning the physical parameters defining the system. In this analysis, we also demonstrate the existence of the strong Mpemba effect where for certain specific initial steady states, the equilibration rate is exponentially faster compared to any other initial steady states. The content of this chapter is published in Ref. [27].

4.2 The Model

Consider a monodispersed granular gas composed of N identical particles. We label the particles by $i = 1, \ldots, N$ and denote their two dimensional velocities by $\boldsymbol{v_i} = (v_{ix}, v_{iy})$. These velocities evolve in time through momentum conserving inelastic binary collisions and external driving. A pair of particles i and j collide at a constant rate λ_c/N (*Maxwell model*). The factor $1/N$ in the collision rates ensures that the total rate of collisions between $N[N-1]/2$ pairs of particles are proportional to the system size N. The new velocities $\boldsymbol{v_i'}$ and $\boldsymbol{v_j'}$ are given by

$$\begin{aligned} \boldsymbol{v}_i' &= \boldsymbol{v}_i - \alpha[(\boldsymbol{v}_i - \boldsymbol{v}_j).\hat{e}]\hat{e}, \\ \boldsymbol{v}_j' &= \boldsymbol{v}_j + \alpha[(\boldsymbol{v}_i - \boldsymbol{v}_j).\hat{e}]\hat{e}, \end{aligned} \tag{4.1}$$

where

$$\alpha = \frac{1+r}{2}, \tag{4.2}$$

r being the co-efficient of restitution, and $\hat{e}$ is the unit vector along the line joining the centres of the particles at contact. We assume that $\hat{e}$ takes a value uniformly from $[0, 2\pi)$ for each collision. In addition to collisions, the system evolves through external driving. Each particle is driven at a rate λ_d. During a driving event, the new velocity $\boldsymbol{v_i'}$ is given by

$$\begin{aligned} v_{ix}' &= -r_{wx} v_{ix} + \eta_x, \quad -1 < r_{wx} \leq 1, \\ v_{iy}' &= -r_{wy} v_{iy} + \eta_y, \quad -1 < r_{wy} \leq 1, \end{aligned} \tag{4.3}$$

where the parameters r_{wx} and r_{wy} are scalars that are related to the driving along the x and y directions respectively and $\boldsymbol{\eta}$ is a noise taken from a fixed distribution $\Phi(\boldsymbol{\eta})$. We denote the second moment of the noise distribution by σ_x^2 and σ_y^2:

$$\sigma_k^2 = \int_{-\infty}^{\infty} d\eta_k \eta_k^2 \Phi(\boldsymbol{\eta}), \quad k = x, y. \tag{4.4}$$

Note that $\sigma_x^2 \neq \sigma_y^2$ or $r_{wx} \neq r_{wy}$ corresponds to anisotropic driving and will introduce an anisotropy in the resultant velocity distribution of the particles.

The driving scheme described above [Eq. (4.3)] takes the system to a steady state and the isotropic case has been used extensively in earlier studies [55, 56, 58]. We note that if $r_{wx} = -1$ or $r_{wy} = -1$, then the driving is equivalent to the diffusive driving, $d\boldsymbol{v}/dt = \boldsymbol{\eta}$, in which case the total energy diverges with time and therefore there is no steady state [59, 60]. This model of dissipative driving [Eq. (4.3)] can be thought of as particles colliding with a vibrating wall. In that case, the velocity of a particle $v_{x,y}$ after the collision with the wall is given by: $v'_{x,y} - V'_{wx,y} = -r_{wx,y}(v_{x,y} - V_{wx,y})$, where $r_{wx,y}$ is the coefficient of restitution between the wall and the particle and $V_{wx,y}$ being the wall velocity. Since the velocity of the wall remains unchanged during a collision, we have $V'_{wx,y} = V_{wx,y}$. Therefore, we can write $v'_{x,y} = -r_{wx,y}v_{x,y} + (1 + r_{wx,y})V_{wx,y}$. We assume that the velocity of the wall in each collision is like an uncorrelated random noise. Hence, we can write $v'_{x,y} = -r_{wx,y}v_{x,y} + \eta_{x,y}$. The physical values for $r_{wx,y}$ lie in $[0, 1]$, where zero denotes completely inelastic wall collisions and one denotes elastic wall collisions. However, as a mathematical model for driving, it is valid for the range $r_{wx,y} \in (-1, 1]$. A detailed explanation regarding the physical motivations for the form of driving in Eq. (4.3) may be found in Refs. [59, 60].

Let $P(\boldsymbol{v}, t)$ denote the probability that a randomly chosen particle has velocity $\boldsymbol{v}$ at time t.

Its time evolution is given by

$$
\begin{aligned}
\frac{d}{dt}P(\boldsymbol{v},t) = \lambda_c \int\int\int d\hat{e}d\boldsymbol{v}_1 d\boldsymbol{v}_2 P(\boldsymbol{v}_1,t)P(\boldsymbol{v}_2,t)\delta(\boldsymbol{v}_1 - \alpha[(\boldsymbol{v}_1-\boldsymbol{v}_2).\hat{e}]\hat{e} - \boldsymbol{v}) \\
+ \lambda_d \int\int d\boldsymbol{\eta} d\boldsymbol{v}_1 \Phi(\boldsymbol{\eta})P(\boldsymbol{v}_1,t)\delta[-r_{wx}v_{1x}+\eta_x - v_x]\delta[-r_{wy}v_{1y}+\eta_y-v_y] \\
-\lambda_c P(\boldsymbol{v},t) - \lambda_d P(\boldsymbol{v},t), \qquad (4.5)
\end{aligned}
$$

where the first and third terms on the right hand side describe the gain and loss terms due to collisions while the second and fourth terms describe the gain and loss terms due to driving. We now analyse the driving terms for the special case of $r_{wx} = r_{wy} = 1$ and for small $\boldsymbol{\eta}$ and show that it leads to a diffusive term. We denote the driving terms as I_D and is given by

$$
I_D = -\lambda_d P(\boldsymbol{v},t) + \lambda_d \int\int d\boldsymbol{\eta} d\boldsymbol{v}_1 \Phi(\boldsymbol{\eta})P(\boldsymbol{v}_1,t)\delta[-v_{1x}+\eta_x-v_x]\delta[-v_{1y}+\eta_y-v_y]. \quad (4.6)
$$

Integrating over $\boldsymbol{v_1}$ and using the property $P(\boldsymbol{v},t) = P(-\boldsymbol{v},t)$, we obtain

$$
I_D = -\lambda_d P(\boldsymbol{v},t) + \lambda_d \int d\boldsymbol{\eta}\Phi(\boldsymbol{\eta})P(\boldsymbol{v}-\boldsymbol{\eta},t). \qquad (4.7)
$$

Upon Taylor expanding the integrand about $|\boldsymbol{\eta}| = 0$ and then integrating over $\boldsymbol{\eta}$ gives

$$
I_D = \frac{\lambda_d\langle|\boldsymbol{\eta}|^2\rangle}{2}\nabla^2 P(\boldsymbol{v}) + \text{higher order terms}, \quad r_{wx} = r_{wy} = 1. \qquad (4.8)
$$

When the higher order terms are ignored, the driving terms in the time evolution equation for $P(\boldsymbol{v},t)$ takes the form of Fokker-Planck diffusive term, and we therefore call the case $r_{wx} = r_{wy} = 1$ as diffusive driving.

4.3 Two point correlations

We are interested in the time evolution of the following two-point correlation functions:

$$\begin{aligned} E_x(t) &= \frac{1}{N}\sum_{i=1}^{N}\langle v_{ix}^2(t)\rangle, \quad C_x(t) = \tfrac{1}{N(N-1)}\textstyle\sum_{i=1}^{N}\sum_{\substack{j=1\\ j\neq i}}^{N}\langle v_{ix}(t)v_{jx}(t)\rangle, \\ E_y(t) &= \frac{1}{N}\sum_{i=1}^{N}\langle v_{iy}^2(t)\rangle, \quad C_y(t) = \tfrac{1}{N(N-1)}\textstyle\sum_{i=1}^{N}\sum_{\substack{j=1\\ j\neq i}}^{N}\langle v_{iy}(t)v_{jy}(t)\rangle, \\ E_{xy}(t) &= \frac{1}{N}\sum_{i=1}^{N}\langle v_{ix}(t)v_{iy}(t)\rangle, \quad C_{xy}(t) = \tfrac{1}{N(N-1)}\textstyle\sum_{i=1}^{N}\sum_{\substack{j=1\\ j\neq i}}^{N}\langle v_{ix}(t)v_{jy}(t)\rangle. \end{aligned} \tag{4.9}$$

$E_x(t)$ and $E_y(t)$ denote the mean kinetic energies of the particles along x and y directions respectively. $E_{xy}(t)$ denote the correlations between v_x and v_y of the same particle whereas $C_x(t)$, $C_y(t)$ and $C_{xy}(t)$ denote the velocity-velocity correlations between pairs of particles. The time evolution for these correlation functions can be obtained starting from Eq. (4.5) [55, 56, 58, 60, 25]. These may be written compactly in a matrix form as

$$\frac{d\tilde{\Sigma}(t)}{dt} = \tilde{\boldsymbol{R}}\tilde{\Sigma}(t) + \tilde{\boldsymbol{D}}, \tag{4.10}$$

where the column vectors $\tilde{\Sigma}(t)$ and $\tilde{\boldsymbol{D}}$ are given by:

$$\tilde{\Sigma}(t) = [E_x(t), E_y(t), E_{xy}(t), C_x(t), C_y(t), C_{xy}(t)]^T, \tag{4.11}$$

$$\tilde{\boldsymbol{D}} = [\lambda_d\sigma_x^2, \lambda_d\sigma_y^2, 0, 0, 0, 0]^T. \tag{4.12}$$

While the matrix $\tilde{\boldsymbol{R}}$ can be written for any N, in the thermodynamic limit $N \to \infty$, it simplifies to

$$\tilde{\boldsymbol{R}} = \begin{bmatrix} A_1 + A_4^{xx} & A_2 & 0 & -A_1 & -A_2 & 0 \\ A_2 & A_1 + A_4^{yy} & 0 & -A_2 & -A_1 & 0 \\ 0 & 0 & -A_3 + A_4^{xy} & 0 & 0 & A_3 \\ 0 & 0 & 0 & 2A_5^x & 0 & 0 \\ 0 & 0 & 0 & 0 & 2A_5^y & 0 \\ 0 & 0 & 0 & 0 & 0 & A_5^x + A_5^y \end{bmatrix}. \tag{4.13}$$

The constants $A_1, A_2, A_3, A_4^{ij}, A_5^i$ are given by:

$$\begin{aligned} & A_1 = \frac{3}{4}\lambda_c \alpha^4 - \lambda_c \alpha, \quad A_2 = \frac{\lambda_c \alpha^4}{4}, \\ & A_3 = \lambda_c \alpha (1 - \frac{\alpha}{2}), \quad A_4^{ij} = -\lambda_d (1 - r_{wi} r_{wj}), \\ & A_5^i = -\lambda_d (1 + r_{wi}), \quad \text{where } i, j \in (x, y). \end{aligned} \tag{4.14}$$

In the steady state, the left-hand side of Eq. (4.10) equals zero. After taking the thermodynamic limit ($N \to \infty$), we obtain the steady state values of the different two point correlation functions as

$$E_x = \frac{\lambda_d \left[\left(4\lambda_d (1 - r_{wy}^2) + \lambda_c \alpha (4 - 3\alpha) \right) \sigma_x^2 + \alpha^2 \lambda_c \sigma_y^2 \right]}{\mathscr{F}}, \tag{4.15}$$

$$E_y = \frac{\lambda_d \left[\left(4\lambda_d (1 - r_{wx}^2) + \lambda_c \alpha (4 - 3\alpha) \right) \sigma_y^2 + \alpha^2 \lambda_c \sigma_x^2 \right]}{\mathscr{F}}, \tag{4.16}$$

$$E_{xy} = C_x = C_y = C_{xy} = 0, \tag{4.17}$$

where

$$\mathscr{F} = 4\lambda_d^2 (1 - r_{wx}^2)(1 - r_{wy}^2) + \alpha \lambda_c \lambda_d (4 - 3\alpha)(2 - r_{wx}^2 - r_{wy}^2) + 2\alpha^2 \lambda_c^2 (2 - 3\alpha + \alpha^2). \tag{4.18}$$

From the structure of $\tilde{\boldsymbol{R}}$ [see Eq. (4.13)], it is evident that the time evolution of velocity-velocity correlations only depend (linearly) on other velocity-velocity correlations and do not depend on the mean kinetic energies. Thus, if in the initial state, these correlations are zero, then they remain zero for all times. Since we will be considering only initial states that are stationary, the velocity-velocity correlations are initially zero [see Eq. (4.17)] and will continue to remain zero for all times.

We therefore set these velocity correlations to zero and write the time evolution for only the non-zero quantities, E_x and E_y as:

$$\frac{d\Sigma(t)}{dt} = \boldsymbol{R}\Sigma(t) + \boldsymbol{S}, \tag{4.19}$$

where

$$\Sigma(t) = \Big[E_x(t), E_y(t)\Big]^T, \tag{4.20}$$

$$\boldsymbol{S} = \Big[\lambda_d \sigma_x^2, \lambda_d \sigma_y^2\Big]^T, \tag{4.21}$$

and $\boldsymbol{R}$ is a 2×2 matrix, whose entries are given by

$$\begin{aligned} R_{11} =& \frac{3}{4}\lambda_c\alpha^2 - \lambda_c\alpha - \lambda_d(1 - r_{wx}^2), \quad R_{12} = \frac{\lambda_c}{4}\alpha^2, \\ R_{22} =& \frac{3}{4}\lambda_c\alpha^2 - \lambda_c\alpha - \lambda_d(1 - r_{wy}^2), \quad R_{21} = \frac{\lambda_c}{4}\alpha^2. \end{aligned} \tag{4.22}$$

It is convenient to work in a different set of variables than $E_x(t)$ and $E_y(t)$. We introduce the total energy, E_{tot}, and the difference in energies, E_{dif}, as:

$$E_{tot} = E_x + E_y, \tag{4.23}$$

$$E_{dif} = E_x - E_y. \tag{4.24}$$

Note that since the driving is anisotropic, $E_{dif} \neq 0$ in general.

The time evolution equations for E_{tot} and E_{dif} can be expressed, starting from Eq. (4.19), as

$$\frac{d\boldsymbol{E}(t)}{dt} = -\chi\boldsymbol{E}(t) + \boldsymbol{D}, \tag{4.25}$$

where

$$\boldsymbol{E}(t) = \Big[E_{tot}(t), E_{dif}(t)\Big]^T, \tag{4.26}$$

$$\boldsymbol{D} = \Big[\lambda_d(\sigma_x^2 + \sigma_y^2), \lambda_d(\sigma_x^2 - \sigma_y^2)\Big]^T, \tag{4.27}$$

and χ is a 2×2 matrix with the components of the matrix given by

$$\begin{aligned} \chi_{11} &= \frac{2\lambda_c\alpha(1-\alpha) + \lambda_d(2 - r_{wx}^2 - r_{wy}^2)}{2}, \quad \chi_{12} = \frac{\lambda_d(r_{wy}^2 - r_{wx}^2)}{2}, \\ \chi_{22} &= \frac{\lambda_c\alpha(2-\alpha) + \lambda_d(2 - r_{wx}^2 - r_{wy}^2)}{2}, \quad \chi_{21} = \frac{\lambda_d(r_{wy}^2 - r_{wx}^2)}{2}. \end{aligned} \tag{4.28}$$

Equation (4.25) can be solved exactly by linear decomposition using the eigenvalues $\lambda_\pm$ of χ:

$$\lambda_\pm = \frac{1}{4}\Big[2\lambda_d(2 - r_{wx}^2 - r_{wy}^2) + \alpha\lambda_c(4 - 3\alpha) \pm \sqrt{4\lambda_d^2(r_{wy}^2 - r_{wx}^2)^2 + \alpha^4\lambda_c^2}\Big]. \tag{4.29}$$

It is straightforward to show that $\lambda_\pm > 0$ with $\lambda_+ > \lambda_-$. The solution for $E_{tot}(t)$ and $E_{dif}(t)$ is

$$\begin{aligned} E_{tot}(t) - \langle E_{tot}\rangle &= K_+ e^{-\lambda_+ t} + K_- e^{-\lambda_- t}, \\ E_{dif}(t) - \langle E_{dif}\rangle &= L_+ e^{-\lambda_+ t} + L_- e^{-\lambda_- t}, \end{aligned} \tag{4.30}$$

where $\langle E_{tot}\rangle$ and $\langle E_{dif}\rangle$ are steady state values of $E_{tot}(t)$ and $E_{dif}(t)$ respectively. The coefficients K_+, K_-, L_+ and L_- along with $\langle E_{tot}\rangle$ and $\langle E_{dif}\rangle$ are given by

$$
\begin{aligned}
K_+ =&\frac{1}{\gamma}\Big[-(\lambda_- - \chi_{11})E_{tot}(0) + \chi_{12}E_{dif}(0)\\
&-\frac{\lambda_d}{\lambda_+}\left[\big(\chi_{12} - (\lambda_- - \chi_{11})\big)\sigma_x^2 - \big(\chi_{12} + (\lambda_- - \chi_{11})\big)\sigma_y^2\right]\Big],\\
K_- =&\frac{1}{\gamma}\Big[(\lambda_+ - \chi_{11})E_{tot}(0) - \chi_{12}E_{dif}(0)\\
&+\frac{\lambda_d}{\lambda_-}\left[\big(\chi_{12} - (\lambda_+ - \chi_{11})\big)\sigma_x^2 - \big(\chi_{12} + (\lambda_+ - \chi_{11})\big)\sigma_y^2\right]\Big],\\
\langle E_{tot}\rangle =&\frac{\lambda_d}{\gamma}\Big[\frac{\big(\chi_{12} - (\lambda_- - \chi_{11})\big)\sigma_x^2 - \big(\chi_{12} + (\lambda_- - \chi_{11})\big)\sigma_y^2}{\lambda_+}\\
&-\frac{\big(\chi_{12} - (\lambda_+ - \chi_{11})\big)\sigma_x^2 - \big(\chi_{12} + (\lambda_+ - \chi_{11})\big)\sigma_y^2}{\lambda_-}\Big],\\
L_+ =&\frac{1}{\gamma}\Big[-\frac{(\lambda_+ - \chi_{11})(\lambda_- - \chi_{11})}{\chi_{12}}E_{tot}(0) + (\lambda_+ - \chi_{11})E_{dif}(0)\\
&-\frac{\lambda_d}{\lambda_+\chi_{12}}\left[(\lambda_+ - \chi_{11})(\lambda_- - \chi_{11})(\sigma_x^2 - \sigma_y^2)\right]\Big],\\
L_- =&\frac{1}{\gamma}\Big[\frac{(\lambda_+ - \chi_{11})(\lambda_- - \chi_{11})}{\chi_{12}}E_{tot}(0) - (\lambda_+ - \chi_{11})E_{dif}(0)\\
&+\frac{\lambda_d}{\lambda_-\chi_{12}}\left[(\lambda_+ - \chi_{11})(\lambda_- - \chi_{11})(\sigma_x^2 - \sigma_y^2)\right]\Big],\\
\langle E_{dif}\rangle =&\frac{\lambda_d}{\chi_{12}\gamma}\Big[(\lambda_+ - \chi_{11})(\lambda_- - \chi_{11})(\sigma_x^2 - \sigma_y^2)\big(\frac{1}{\lambda_+} - \frac{1}{\lambda_-}\big)\Big],\\
\gamma =&\lambda_+ - \lambda_-.
\end{aligned}
$$

These coefficients depend only on the system parameters and initial conditions. Equation (5.4) gives the full time dependent solution for the energies, and we utilise them to demonstrate the Mpemba effect.

4.4 The Mpemba effect in an anisotropically driven gas

In this section, we show and determine the conditions for the existence of the Mpemba effect in the anisotropically driven monodispersed Maxwell gas based on the analysis of $E_{tot}(t)$ and $E_{dif}(t)$ [see Eq. (5.4)]. The Mpemba effect in granular systems has been defined as follows [22, 23, 25, 24, 26]. Consider two systems P and Q which have identical parameters except for the pair of driving strengths, σ_x^2 and σ_y^2. We will choose E_{tot} of P to be higher. Note that the systems P and Q are initially in steady states. We denote their steady state values for the energies by $[E_{tot}^P(0), E_{dif}^P(0)]$ and $[E_{tot}^Q(0), E_{dif}^Q(0)]$ respectively. Both the systems are then quenched to a common steady state having lower energy compared to the initial steady state energies of P and Q. This is achieved by changing the driving strengths of P and Q to the common driving strengths, σ_x^2 and σ_y^2 of the final steady state, keeping all the other parameters of both the systems constant.

We say that the Mpemba effect is present if the two trajectories $E_{tot}^P(t)$ and $E_{tot}^Q(t)$ cross each other at some finite time $t = \tau$ at which

$$E_{tot}^P(\tau) = E_{tot}^Q(\tau). \tag{4.31}$$

To obtain the value of τ, we equate the energies for P and Q from Eq. (5.4) to obtain

$$K_+^P e^{-\lambda_+\tau} + K_-^P e^{-\lambda_-\tau} = K_+^Q e^{-\lambda_+\tau} + K_-^Q e^{-\lambda_-\tau}, \tag{4.32}$$

whose solution is

$$\tau = \frac{1}{\lambda_+ - \lambda_-} \ln\left[\frac{K_+^P - K_+^Q}{K_-^Q - K_-^P}\right]. \tag{4.33}$$

In terms of the parameters of the initial steady states, τ reduces to

$$\tau = \frac{1}{\lambda_+ - \lambda_-} \ln\left[\frac{\chi_{12}\Delta E_{dif} - (\lambda_- - \chi_{11})\Delta E_{tot}}{\chi_{12}\Delta E_{dif} - (\lambda_+ - \chi_{11})\Delta E_{tot}}\right], \tag{4.34}$$

where

$$\begin{aligned} \Delta E_{tot} &= E_{tot}^P(0) - E_{tot}^Q(0), \\ \Delta E_{dif} &= E_{dif}^P(0) - E_{dif}^Q(0). \end{aligned} \tag{4.35}$$

For the Mpemba effect to be present, we require that $\tau > 0$. Since $\lambda_+ > \lambda_-$, the argument of logarithm in Eq. (5.11) should be greater than one. Simplifying, we obtain the criterion for the crossing of the two trajectories to be

$$\frac{\Delta E_{tot}}{\Delta E_{dif}} < \frac{A}{1+\sqrt{A^2+1}}, \tag{4.36}$$

where,

$$A(\lambda_c, \lambda_d, \alpha, r_{wx}, r_{wy}) = \frac{2\lambda_d}{\lambda_c \alpha^2}(r_{wy}^2 - r_{wx}^2). \tag{4.37}$$

The right hand side of Eq. (4.36) depends only on the intrinsic parameters of the system and it is always less than one (since $\alpha, \lambda_d, \lambda_c > 0$). On the other hand, the ratio $\Delta E_{tot}/\Delta E_{dif}$, depends on the initial steady state energies of P and Q [see Eq. (5.12)]. In the stationary state, the ratio $\Delta E_{tot}/\Delta E_{dif}$ is given by

$$\frac{\Delta E_{tot}}{\Delta E_{dif}} = \frac{\left[2\lambda_d(1-r_{wy}^2)+\alpha\lambda_c(2-\alpha)\right]\Delta\sigma_x^2 + \left[2\lambda_d(1-r_{wx}^2)+\alpha\lambda_c(2-\alpha)\right]\Delta\sigma_y^2}{2\Big[\left[\lambda_d(1-r_{wy}^2)+\alpha\lambda_c(1-\alpha)\right]\Delta\sigma_x^2 - \left[\lambda_d(1-r_{wx}^2)+\alpha\lambda_c(1-\alpha)\right]\Delta\sigma_y^2\Big]}, \tag{4.38}$$

where,

$$\Delta\sigma_i^2 = (\sigma_i^P)^2 - (\sigma_i^Q)^2, \quad i \in (x,y). \tag{4.39}$$

Equation (4.38) shows that the ratio $\Delta E_{tot}/\Delta E_{dif}$ depends on the intrinsic parameters of the system as well as the driving strengths, σ_x^2 and σ_y^2. As a result, the driving strengths can be appropriately tuned, keeping all the other intrinsic parameters identical for both P and Q, to prepare the initial conditions that satisfy Eq. (4.36). In Fig. 4.1(a), we consider such a situation where Eq. (4.36) is satisfied. Here, the systems P and Q have identical intrinsic parameters but the pair of driving strengths, σ_x^2 and σ_y^2, are different for the two systems. The trajectories cross at the point as predicted by Eq. (5.11). It is clear that

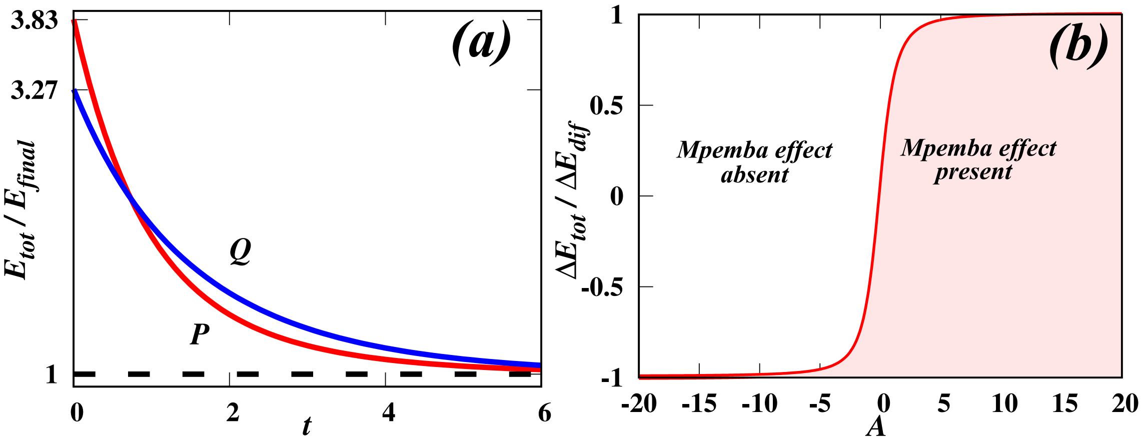

Figure 4.1: (a) The time evolution of the total energy, $E_{tot}(t)$ for anisotropically driven systems P and Q of a two dimensional inelastic Maxwell gas, driven along both the directions of the plane, with initial conditions $E^P_{tot}(0)$=20.27, $E^Q_{tot}(0)$=17.32, $E^P_{dif}(0)$=-7.93 and $E^Q_{dif}(0)$=6.26 such that $E^P_{tot}(0) > E^Q_{tot}(0)$, which satisfies the condition for the Mpemba effect as described in Eq. (4.36). The other parameters decribing the systems are chosen to be r=0.3, $r_{wx} = 0.88$ and $r_{wy} = 0.39$. P relaxes to the steady state faster than Q, though its initial energy is larger. The time at which the trajectories cross each other is $\tau = 0.73$ as given by Eq. (5.11). (b) $\Delta E_{tot}/\Delta E_{dif}$–$A$ phase diagram showing regions where the Mpemba effect is observed and A [given by Eq. (4.37)] is a function of the parameters of the system. The region below the line given by Eq. (4.36) denotes the set of steady state initial conditions that show the Mpemba effect whereas the region on the other side of the line corresponds to initial states that do not show the Mpemba effect.

though P has larger initial energy than Q, it relaxes faster compared to the latter.

Note that the time evolution of $E_{tot}(t)$ and $E_{dif}(t)$ [see Eqs. (4.28)-(5.4)] remains invariant of the sign of r_{wx} and r_{wy}. Similarly, the condition for the Mpemba effect [see Eqs. (4.36) and (4.37)] do not change irrespective of the sign of r_{wx} and r_{wy}. Hence, even if the model allows for the range $-1 < r_{wx,y} \leq 1$, we consider only the physical positive range of $r_{wx,y} \in [0,1]$ as the result is invariant irrespective of its sign.

Figure 4.1(b) illustrates the phase space (initial conditions), based on Eq. (4.36), where the Mpemba effect is observable. In the figure, the line denotes the variation of right hand side of Eq. (4.36) with A [given by Eq. (4.37)]. If the ratio $\Delta E_{tot}/\Delta E_{dif}$ which depends on the initial conditions of P and Q, falls in the region below (above) the line in the phase diagram [see Fig. 4.1(b)], then the system exhibits (does not exhibit) the Mpemba effect.

For steady state initial conditions, the ratio $\Delta E_{tot}/\Delta E_{dif}$ is given by Eq. (4.38). As the ratio $\Delta E_{tot}/\Delta E_{dif}$ is a function of the driving strengths, σ_x^2 and σ_y^2 [see Eq. (4.38)], they can be appropriately tuned, independently for the systems P and Q as well as along the x and y directions, to access the entire region of phase space where the Mpemba effect is observable.

Note that one can introduce anisotropy in the mean kinetic energies by simply considering the case $\sigma_x^2 \neq \sigma_y^2$, and keeping $r_{wx} = r_{wy}$ [see Eqs. (4.15) and (4.16)]. But in that case, the condition for the Mpemba effect reduces to $\Delta E_{tot} < 0$ [see Eq. (4.36)] which is not possible to realise as we have assumed $\Delta E_{tot} = E_{tot}^P(0) - E_{tot}^Q(0) > 0$. Therefore, to demonstrate the Mpemba effect, we restrict ourselves to the case $r_{wx} \neq r_{wy}$.

4.4.1 The inverse Mpemba effect

Consider now the case where a system is heated instead of being cooled unlike the direct Mpemba effect. Now if an initially colder system heats up faster than a system at an intermediate one then it is called the inverse Mpemba effect. We follow the same analysis as in the direct Mpemba effect. The condition for the inverse Mpemba effect is same as that for the direct Mpemba effect as given in Eq. (4.36). We prepare two systems P and Q such that P has a higher initial total energy than Q and also satisfy the condition for the inverse Mpemba effect [Eq. (4.36)]. We then quench both the systems to a common steady state having higher total energy compared to the initial total energies of both P and Q. The cross-over time τ at which the trajectories $E_{tot}^P(t)$ and $E_{tot}^Q(t)$ cross is given by Eq. (5.11). An example is illustrated in Fig. 4.2.

The phase space of the initial steady states that satisfy the condition for the inverse Mpemba effect turns out to be the same as that for the direct Mpemba effect and is given by Eq. (4.38). Thus, Fig. 4.1(b) also illustrates the valid initial steady states given by Eq. (4.38) that satisfy the condition [Eq. (4.36)] where the inverse Mpemba effect is observable.

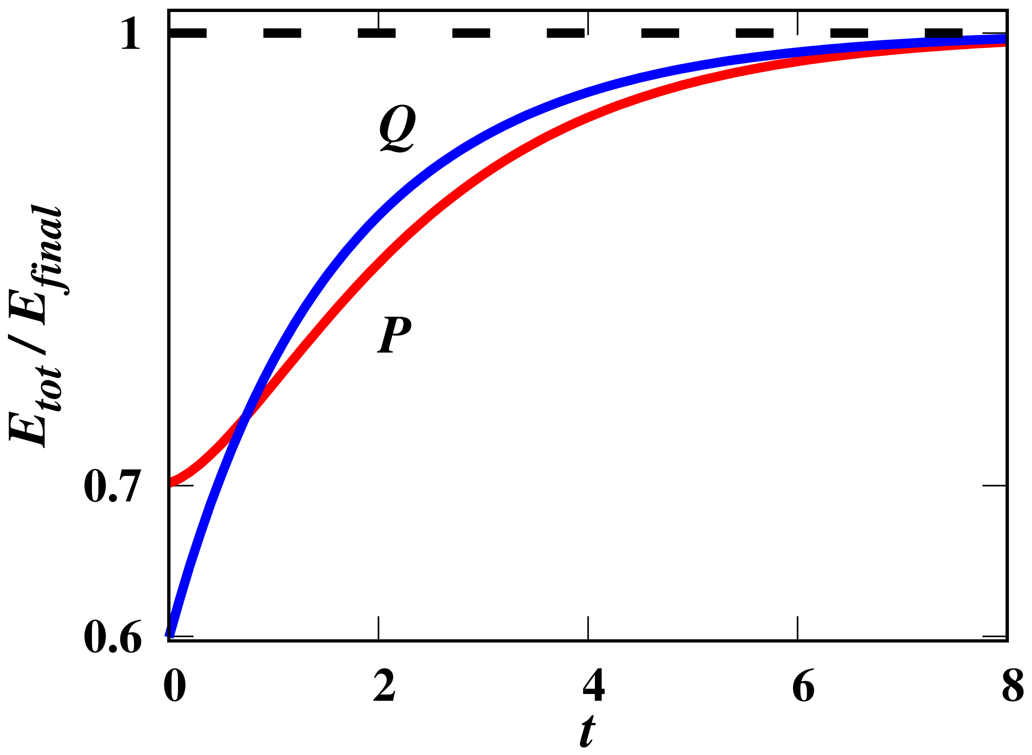

Figure 4.2: The time evolution of the total energy, $E_{tot}(t)$ for anisotropically driven systems P and Q of a two dimensional inelastic Maxwell gas, driven along both the directions of the plane, with initial conditions $E^P_{tot}(0)$=20.27, $E^Q_{tot}(0)$=17.32, $E^P_{dif}(0)$=-7.93 and $E^Q_{dif}(0)$=6.26 such that $E^P_{tot}(0) > E^Q_{tot}(0)$, which satisfies the condition for the inverse Mpemba effect as described in Eq. (4.36). The other parameters decribing the systems are chosen to be r=0.3, $r_{wx} = 0.88$ and $r_{wy} = 0.39$. P relaxes to the steady state slower than Q, though its initial energy is larger. The time at which the trajectories cross each other is $\tau = 0.73$ as given by Eq. (5.11).

4.4.2 The strong Mpemba effect

It can be shown that there exists certain initial conditions such that the system at higher temperature relaxes to a final steady state exponentially faster compared to other initial conditions. This phenomenon is called the strong Mpemba effect. The effect may be realised when the coefficient (K_-) associated with the slower relaxation rate in the time evolution of total kinetic energy, $E_{tot}(t)$ [see Eq. (5.4)] vanishes.

Setting the coefficient K_- [given by Eq. (2.57)] to zero, we obtain

$$E_{tot}(0) = \frac{A}{1+\sqrt{1+A^2}} E_{dif}(0) - c, \tag{4.40}$$

where

$$c = \frac{4\lambda_d \left[\frac{A}{1+\sqrt{1+A^2}}(\sigma_x^2 - \sigma_y^2) + (\sigma_x^2 + \sigma_y^2)\right]}{\left(2\lambda_d(-2 + r_{wx}^2 + r_{wy}^2) - 4\lambda_c\alpha + \lambda_c\alpha^2(3+\sqrt{1+A^2})\right)}, \tag{4.41}$$

and A is as given in Eq. (4.37). The solution of Eq. (4.40) in terms of $E_{tot}(0)$ and $E_{dif}(0)$ yields the set of initial states whose relaxation is exponentially faster than the set of generic states. Among these initial states one would like to determine the ones which are steady states. The steady state ratio of $E_{tot}(0)/E_{dif}(0)$ [see Eq. (2.57)] for a system is given by

$$\frac{E_{tot}(0)}{E_{dif}(0)} = \frac{\left[2\lambda_d(1 - r_{wy}^2) + \alpha\lambda_c(2-\alpha)\right]\sigma_x^2 + \left[2\lambda_d(1 - r_{wx}^2) + \alpha\lambda_c(2-\alpha)\right]\sigma_y^2}{2\Big[\left[\lambda_d(1 - r_{wy}^2) + \alpha\lambda_c(1-\alpha)\right]\sigma_x^2 - \left[\lambda_d(1 - r_{wx}^2) + \alpha\lambda_c(1-\alpha)\right]\sigma_y^2\Big]}, \tag{4.42}$$

and is a function of the driving strengths, σ_x^2 and σ_y^2, as all other parameters are kept constant. One observes that the valid steady states with initial energies, $E_{tot}(0)$ and $E_{dif}(0)$ that satisfy the condition for the strong Mpemba effect [see Eq. (4.40)] can be obtained by appropriately tuning the driving strengths.

Thus, for a system of monodispersed Maxwell gas in two dimensions, there exists steady state initial conditions that satisfy the condition given by Eq. (4.40) and hence approach the final steady state exponentially faster compared to any other similar system whose initial energies lie slightly below or above the line. An example of the strong Mpemba effect is shown in Fig. 4.3(a).

Figure 4.3(b) illustrates the phase space (initial conditions) of system P where the Mpemba effect as well as the strong Mpemba effect are observable. In the figure, the region below the solid line denotes the initial conditions where the system exhibits the Mpemba effect. In the region of the phase diagram where the Mpemba effect is observable, the dashed line denotes the set of initial states that also satisfy the condition given by Eq. (4.40) for which the system P exhibits the strong Mpemba effect.

4.5 Special case when the driving is only in one direction

In Sec. 4.4, we discussed the possibility of the Mpemba effect in the case of anisotropically driven monodispersed Maxwell gas where the particles are driven along both the directions. We now consider a similar system but the driving is restricted to one direction. We follow the same analysis as in Sec. 4.4. Here, for the case when particles are driven only along x-direction (say) with driving strengths, $\sigma_x^2 \neq 0$ and $\sigma_y^2 = 0$, the time evolution of mean kinetic energies E_x and E_y is

$$\begin{aligned} \frac{dE_x(t)}{dt} &= E_x\big[\lambda_c \alpha(\frac{3}{4}\alpha - 1) - \lambda_d(1 - r_{wx}^2)\big] + E_y\big[\frac{\lambda_c}{4}\alpha^2\big] + \lambda_d \sigma_x^2, \\ \frac{dE_y(t)}{dt} &= E_x\big[\frac{\lambda_c}{4}\alpha^2\big] + E_y\big[\lambda_c \alpha(\frac{3}{4}\alpha - 1)\big]. \end{aligned} \tag{4.43}$$

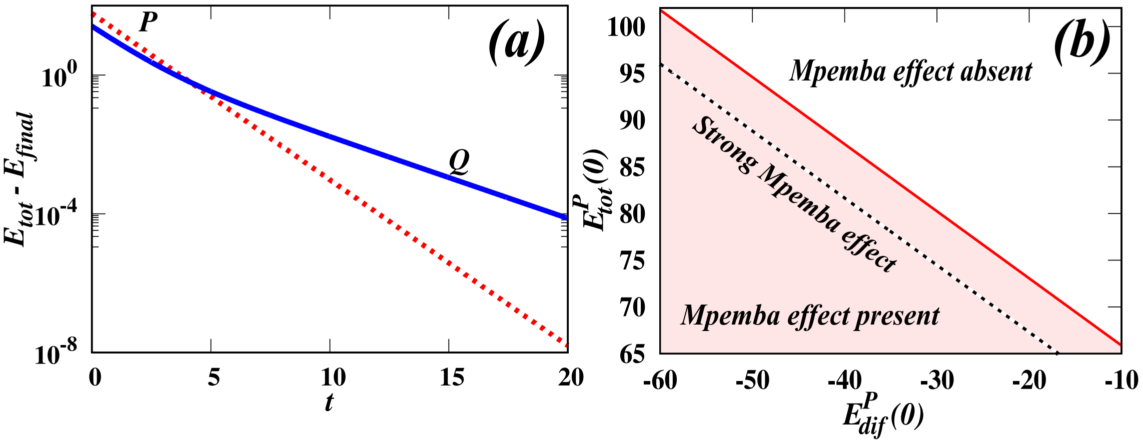

Figure 4.3: (a)The time evolution of the total energy, $E_{tot}(t)$ for anisotropically driven systems P and Q of a two dimensional inelastic Maxwell gas, driven along both the directions of the plane, with $E^P_{tot}(0) = 95.89$, $E^Q_{tot}(0) = 61.57$, $E^P_{diff}(0) = -59.82$ and $E^Q_{diff}(0) = -4.26$ such that $E^P_{tot}(0) > E^Q_{tot}(0)$. These initial values satisfy both the conditions for the Mpemba effect as described in Eq. (4.36) as well as those for the strong Mpemba effect (for system P) as described in Eq. (4.40). The other parameters defining the system are chosen to be $r = 0.2$, $r_{wx} = 0.88$ and $r_{wy} = 0.49$. P equilibrates to the final state at an exponentially faster rate compared to Q and the time at which the trajectories cross each other is $\tau = 4.14$ as given by Eq. (5.11). (b) $E^P_{tot}(0)$–$E^P_{dif}(0)$ phase diagram showing regions of initial conditions where the system P shows the Mpemba effect as well as the strong Mpemba effect. The initial conditions for system Q and all the other parameters describing the two systems are similar to (a). Both the systems are quenched to the final steady state condition $E_{tot} = 35.92$ and $E_{dif} = 23.66$. The region below the solid line given by Eq. (4.36) denotes the set of steady state initial conditions that show the Mpemba effect and the dashed line denotes the set of initial conditions of system P for which it shows the strong Mpemba effect.

The time evolution for the quantities E_{tot} and E_{dif} are given by Eq. (4.25) but now the column matrix $\boldsymbol{D}$ takes the form

$$\boldsymbol{D} = \left[\lambda_d \sigma_x^2, \lambda_d \sigma_x^2\right]^T, \tag{4.44}$$

The solutions for $E_{tot}(t)$ and $E_{dif}(t)$ are obtained in the similar way as in Eq. (5.4) with the coefficients K_+, K_-, L_+ and L_- along with the steady state energies $\langle E_{tot} \rangle$ and $\langle E_{dif} \rangle$ are now given by

$$\begin{aligned}
K_+ &= \frac{1}{\gamma}\Big[(-\lambda_- + \chi_{11})E_{tot}(0) + \chi_{12}E_{dif}(0) - \frac{\chi_{12} - \lambda_- + \chi_{11})}{\lambda_+}\lambda_d\sigma_x^2\Big],\\
K_- &= \frac{1}{\gamma}\Big[(\lambda_+ - \chi_{11})E_{tot}(0) - \chi_{12}E_{dif}(0) + \frac{\chi_{12} - \lambda_+ + \chi_{11})}{\lambda_-}\lambda_d\sigma_x^2\Big],\\
\langle E_{tot} \rangle &= \frac{1}{\gamma}\Big[\frac{\chi_{12} - (\lambda_- - \chi_{11})}{\lambda_+} - \frac{\chi_{12} - (\lambda_+ - \chi_{11})}{\lambda_-}\Big]\lambda_d\sigma_x^2,\\
\langle E_{dif} \rangle &= \frac{1}{\gamma}\Big[\frac{(\lambda_+ - \chi_{11})(\lambda_- - \chi_{11})}{\chi_{12}\lambda_+} - \frac{(\lambda_+ - \chi_{11})(\lambda_- - \chi_{11})}{\chi_{12}\lambda_-}\Big]\lambda_d\sigma_x^2,\\
L_+ &= \frac{1}{\gamma}\Big[-\frac{(\lambda_+ - \chi_{11})(\lambda_- - \chi_{11})}{\chi_{12}}E_{tot}(0) + (\lambda_+ - \chi_{11})E_{dif}(0)\\
&\quad - \frac{(\lambda_+ - \chi_{11})(\lambda_- - \chi_{11})}{\chi_{12}\lambda_+}\lambda_d\sigma_x^2\Big],\\
L_- &= \frac{1}{\gamma}\Big[\frac{(\lambda_+ - \chi_{11})(\lambda_- - \chi_{11})}{\chi_{12}}E_{tot}(0) - (\lambda_- - \chi_{11})E_{dif}(0)\\
&\quad + \frac{(\lambda_+ - \chi_{11})(\lambda_- - \chi_{11})}{\chi_{12}\lambda_-}\lambda_d\sigma_x^2\Big],\\
\gamma &= \lambda_+ - \lambda_-.
\end{aligned}$$

We now consider two systems labeled as P and Q with different initial conditions $[E^P_{tot}(0), E^P_{dif}(0)]$ and $[E^Q_{tot}(0), E^Q_{dif}(0)]$ where $E^P_{tot}(0) > E^Q_{tot}(0)$. Both the systems are quenched to a common steady state whose total energy is smaller than the initial total energies of P and Q. This is achieved by changing the driving strengths of P and Q to the common driving strengths, $\sigma_x^2 \neq 0$ and $\sigma_y^2 = 0$ of the final steady state, keeping all the other parameters constant for both the systems.

The condition for the Mpemba effect to be present is the same as that derived for the more general case [see Eq. (4.36)] but now the variable A is given by

$$A(\lambda_c, \lambda_d, \alpha, r_{wx}) = \frac{-2\lambda_d}{\lambda_c \alpha^2} r_{wx}^2. \tag{4.45}$$

In Fig. 4.4(a), we consider such a situation where Eq. (4.36) is satisfied and hence the systems P and Q show the Mpemba effect. The trajectories cross at the point as predicted by Eq. (5.11).

In Fig. 4.4(b), we identify the region of phase space (initial condition) where the Mpemba effect is observable, based on Eq. (4.36). In the figure, the line denotes the variation of right hand side of Eq. (4.36) with A [given by Eq. (4.45)]. The region below the line in the phase diagram corresponds to the initial conditions $\Delta E_{tot}/\Delta E_{dif}$ [see Fig. 4.4(b)] that show the Mpemba effect [Eq. (4.36)] whereas the other region does not show the effect.

Here, we consider that the systems P and Q have identical intrinsic parameters once the quench is done to the common steady state. However, these intrinsic parameters that characterise the initial conditions of P and Q or equivalently $\Delta E_{tot}/\Delta E_{dif}$, could be different. As a result, one can tune these intrinsic parameters differently for P and Q to obtain initial steady states that satisfy the condition given by Eq. (4.36) and hence show the Mpemba effect.

However, when the intrinsic parameters other than driving strength is kept the same (both before and after the quench), the ratio $\Delta E_{tot}/\Delta E_{dif}$ for initial steady states has a simple form:

$$\frac{\Delta E_{tot}}{\Delta E_{dif}} = \frac{(2-\alpha)}{2(1-\alpha)} \geq 1.5. \tag{4.46}$$

Note that $\alpha \in [1/2, 1]$ and hence the ratio in Eq. (4.46) is always larger than or equal to 1.5. However, we know from Eq. (4.36), with the variable A given by Eq. (4.45), that for the Mpemba effect to be present, $\Delta E_{tot}/\Delta E_{dif} < 0$. Thus, Eq. (4.46) does not satisfy the required condition for the existence of the Mpemba effect. We conclude that for initial states that correspond to steady states where P and Q have identical intrinsic parameters

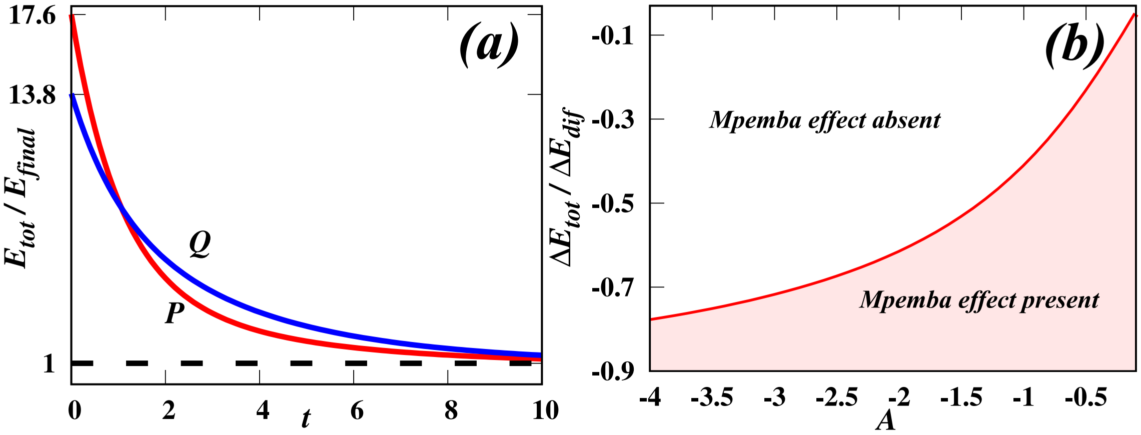

Figure 4.4: (a) The time evolution of the total energy, $E_{tot}(t)$ for anisotropically driven systems P and Q of a two dimensional inelastic Maxwell gas driven along a single direction with initial conditions $E_{tot}^P(0)$=28, $E_{tot}^Q(0)$=22, $E_{dif}^P(0)$=26 and $E_{dif}^Q(0)$=5 such that $E_{tot}^P(0) > E_{tot}^Q(0)$, which satisfies the condition for the Mpemba effect as described in Eq. (4.36). The other parameters decribing the systems are chosen to be r=0.5 and $r_{wx} = 0.6$. P relaxes to the steady state faster than Q, though its initial energy is larger. The time at which the trajectories cross each other is $\tau = 1.07$ as given by Eq. (5.11). (b) $\Delta E_{tot}/\Delta E_{dif}$–$A$ phase diagram showing regions where the Mpemba effect is observed and A [given by Eq. (4.45)] is a function of the parameters of the system. The region below the line given by Eq. (4.36) shows the Mpemba effect whereas the region on the other side of the line does not show the Mpemba effect.

except for the driving strength, the Mpemba effect is not possible when the driving is restricted to one direction.

4.6 Summary and discussion

In this chapter, we have shown an exact analysis for the existence of the Mpemba effect, the inverse Mpemba effect and the strong Mpemba effect in an anisotropically driven inelastic Maxwell gas in two dimensions. The Maxwell model for granular gases is a simplified model where the rate of collision between the granular particles is independent of their relative velocities. In addition, we assumed the well-mixed limit such that the spatial correlations were ignored. The model allows for an exact solution as the two-point velocity correlations form a coupled set of linear equations.

We show that anisotropic driving leads to the existence of the Mpemba effect starting from steady state initial conditions unlike the case of isotropic driving which required the initial conditions to be non-stationary. We considered two different cases of anisotropic driving in two dimensions: when particles are driven along one direction only and the other case where particles are driven along both the directions. In both the cases, we show that the Mpemba effect can exist for initial conditions which are valid steady states characterised by the parameters of the system. We also demonstrated the existence of the inverse Mpemba effect where a system is heated instead of being cooled. Here, an initially colder system equilibrates to a final high temperature state faster than an initially warmer system. We also derived the condition for the existence of the strong Mpemba effect where for certain initial states, a system equilibrates at an exponentially faster rate compared to any other states.

We note that in the Maxwell gas, the anisotropy can be introduced in two ways: two different driving strengths ($\sigma_x^2 \neq \sigma_y^2$) or through two different driving parameters ($r_{wx} \neq r_{wy}$). However, the analysis reveals that the necessary condition needed to observe the Mpemba effect is $r_{wx} \neq r_{wy}$ even if the driving strengths are different ($\sigma_x^2 \neq \sigma_y^2$). This is due to the lack of coupling between E_{tot} and E_{dif} when $r_{wx} = r_{wy}$. This feature is an artefact of the model, and when the rate of collision is velocity dependent as considered in Ref. [26], then it does not matter how the anisotropy is introduced. In that case, the model for driven granular gas shows the Mpemba effect for $r_{wx} = r_{wy} = 1$, and $\sigma_x^2 \neq \sigma_y^2$ [26].

The exact solution obtained for the Maxwell gas in this chapter puts on a more rigorous footing the results for the Mpemba effect that we obtained earlier for an anisotropically driven granular gas with a more realistic velocity dependent collision rate [26]. The main result of Ref. [26] was that it is possible to have the Mpemba effect in granular systems with velocity dependent collision rates when the initial states are stationary provided the driving is anisotropic. Earlier studies of the Mpemba effect in granular systems required non-stationary initial states. Since it is easier in experiments to create initial steady states that are stationary, anisotropic driving was proposed as a probe to study the Mpemba effect in granular systems. However, for analysing the case of velocity dependent collision rates in Ref. [26], we had to make several simplifying assumptions like assuming the velocity distribution to be Gaussian, linearising the equations about the steady state, restricting driving to $r_{wx} = r_{wy} = 1$ and the small noise limit [26]. In this chapter, the simplification is made in the definition of the model, in that collision rates are velocity independent. None of the other simplifying assumptions made in Ref. [26] have to be made for the Maxwell model. The solution obtained in this chapter for the Maxwell gas shows that the assumptions made for the granular gas do not affect the existence of the Mpemba effect. In addition, for the Maxwell gas, we are able to obtain an exact solution for a more realistic general form of driving. The driving could be both "dissipative" ($r_{wx,y} < 1$) or "diffusive" ($r_{wx,y} = 1$). On the other hand, for the driven granular gas [26], the analysis could be carried out for only a specific form of driving ($r_{wx} = r_{wy} = 1$) and in the limit $\eta \rightarrow 0$.

Combining the results of this chapter and Ref. [26], we conclude that anisotropic driving would allow the Mpemba effect to be observable in driven granular gases with stationary initial states, allowing for an experimental realisation, which has been hitherto lacking, of the Mpemba effect in granular systems. Stationary states are much easier to achieve in experiments than non-stationary states. In a two dimensional experimental set up, anisotropic driving can be achieved by choosing the amplitude and frequency of shaking to be different in the x- and y-directions.

Obtaining exact solution for the Maxwell model has certain other advantages. In general, for studying the Mpemba effect, it is necessary to define a distance of a state from the final steady state. When the trajectories of two different initial states cross (distance from final steady state become equal), then the Mpemba effect is said to exist. However, this choice of distance appears ad hoc. For instance, we have chosen the difference in granular temperature as the distance, like previous studies [22, 23, 24, 25, 26]. However, we could also have chosen a metric distance in the two dimensional space (E_{tot}, E_{dif}).

A third choice could be Kullback-Leibler divergence [11, 6, 5]. Is the Mpemba effect dependent on how the distance is defined? This question is important to answer, and is best answered within a solvable model. We believe that the model and the solution described in the chapter will be very useful for answering the question.

Chapter 5

Mpemba effect and role of distance measures in driven granular gases

5.1 Introduction

The protocol that is followed to test for the existence of the Mpemba effect considers two identical systems which are prepared in different initial states. Both the systems are then quenched to a common final state, and the Mpemba effect is said to be present if the system that is initially further away from the final state equilibrates faster. To quantify which initial state is further away as well as crossing of trajectories, a distance measure for points in the phase space has to be defined.

For systems relaxing to thermal equilibrium, the distance to the final equilibrium state is measured in terms of the probabilities of the different states [11]. It was argued that any distance measure satisfying the following properties should result in a unique definition of the Mpemba effect: (1) As the system relaxes toward thermal equilibrium, the distance function should decrease with time, (2) for three temperatures $T_h > T_c > T_b$, the distance from T_b is larger for T_h compared to T_c, i.e., the distance measure should be a monotonically increasing function of temperature and (3) the distance function should be a continuous, convex function of probability distribution [11]. Let π denote the equilibrium Boltzmann distribution, and $p_i(t)$ the probability of state i at time t. Then, examples of such distances are entropic distance $D_e = \sum_i (p_i(t) - \pi_i)E_i/T_b + p_i(t)\ln p_i(t) - \pi_i \ln \pi_i$ [11], total variation distance $L_1(t) = \sum_i |p_i(t) - \pi_i|$ [4] and Kullback-Leibler (KL) divergence defined as $D_{KL}(t) = \sum_i p_i(t)\ln(p_i(t)/\pi_i)$ [82].

The calculation of the above definitions of distance rely on knowing the probability distribution $p(t)$ at all times. Analytical calculation of $p(t)$ is possible only for exactly solvable problems which, in the context of the Mpemba effect, are restricted to simple single particle systems [4, 83, 84] and to systems with only a few states [11]. For interacting many-particle systems and more so in the context of out of equilibrium systems, the distance measures defined in the probability space are, however, inaccessible through direct measurements in experiments or computationally expensive to measure in simulations. The more natural choices for the distance measures that have been used in experiments are moments of the distribution which are directly observable like mean energy per spin [17, 8], magnetization [2, 8], granular temperature as used in the previous chapters and in Refs. [22, 23, 24, 25, 26, 27, 85], etc. In addition, the generalization to far from equilibrium systems, like driven granular systems is not clear. There are no conclusive studies about the correspondence or similarity between the directly observable measures and the distance measures defined in probability space. Thus, it is not evident whether the Mpemba effect that has been established using these proxy measures for distances is unique or its existence depends on the distance measure used.

To address the above issue, we study the dependence of the Mpemba effect on the choice of different measures in driven granular systems, a prototypical interacting, many-particle far from equilibrium system. The advantage of granular system is that it allows exact analysis for two-point correlation functions, at least in the linearized regime. Being an athermal system, granular temperature or the mean kinetic energy of the system has been used to track the evolution of the system with higher granular temperature being considered further away from the final steady state [22, 24, 23, 25, 26, 27]. However, it is not known a priori whether mean kinetic energy correctly predicts the distance of the initial states from the final steady states. In the following, we summarize the several results that demonstrates the existence of the Mpemba effect in granular systems. For a system of smooth monodispersed particles [22, 24, 25], the Mpemba effect is due to the coupling of the translational granular temperature with the excess kurtosis of the velocity distribution function or correlations between the velocities of the different particles. In the case of rough granular gas [23], the Mpemba effect is due to the coupling of granular temperatures defined for translational and rotational degrees of freedom. In these cases, for the Mpemba effect to exist, however the initial states need to be different from steady states. Existence of the Mpemba effect for evolution of systems from initial steady states could be realised in the context of binary inelastic gases or when inelastic gases are driven anisotropically. For the case of binary gas, Mpemba effect was traced to the energy-exchange between the energies of the smaller and bigger particles [25], while in anisotropically driven gas [26, 27], the Mpemba effect is due to the coupling between the granular temperatures along x and y directions. However, in all the above mentioned analysis, the time evolution of the system is projected onto only one of the variables which is the total granular temperature defined by the second moment of velocity distribution of the system.

In this chapter in addition to total energy, we introduce other measures such as Manhattan measure ($\mathcal{L}_1$), Euclidean measure ($\mathcal{L}_2$) and KL divergence which can describe the evolution of the system in the phase space of all the relevant variables. We perform the analysis in the setup of anisotropically driven granular gas as well as driven inelastic Maxwell gas [26, 27]. We derive the criteria for the existence of the Mpemba effect with the various measures and determine the region of phase space which shows the Mpemba effect. We show that these phase diagrams are non-universal in the sense that they depend on the measure used. The content of this chapter is published in Ref. [34].

5.2 Model

In this chapter, we analyse two models for anisotropically driven granular gas: inelastic Maxwell model and the hard disc granular gas model, both in two dimensions. The hard disc granular gas model and inelastic Maxwell gas model are discussed in Chapter 3 [see Sec. 3.2] and Chapter 4 [see Sec. 4.2] respectively.

5.3 Characterising the steady states

In this section, we define and briefly discuss the relevant two point correlation functions for both the models. The detailed description about the two point correlations, their time evolutions and their steady state values are already derived in Chapter 3 and Chapter 4 for the hard disc granular gas model and inelastic Maxwell gas model respectively.

5.3.1 Inelastic Maxwell model

We first discuss the case of inelastic Maxwell model. We are interested in the time evolution of the following two-point correlation functions:

$$
\begin{aligned}
E_x(t) &= \frac{1}{N}\sum_{i=1}^{N}\langle v_{ix}^2(t)\rangle, \\
E_y(t) &= \frac{1}{N}\sum_{i=1}^{N}\langle v_{iy}^2(t)\rangle, \\
E_{xy}(t) &= \frac{1}{N}\sum_{i=1}^{N}\langle v_{ix}(t)v_{iy}(t)\rangle, \\
C_x(t) &= \frac{1}{N(N-1)}\sum_{i=1}^{N}\sum_{\substack{j=1\\ j\neq i}}^{N}\langle v_{ix}(t)v_{jx}(t)\rangle, \\
C_y(t) &= \frac{1}{N(N-1)}\sum_{i=1}^{N}\sum_{\substack{j=1\\ j\neq i}}^{N}\langle v_{iy}(t)v_{jy}(t)\rangle, \\
C_{xy}(t) &= \frac{1}{N(N-1)}\sum_{i=1}^{N}\sum_{\substack{j=1\\ j\neq i}}^{N}\langle v_{ix}(t)v_{jy}(t)\rangle,
\end{aligned}
\tag{5.1}
$$

where $E_x(t)$ and $E_y(t)$ denote the mean kinetic energies of the particles along x and y directions respectively. $E_{xy}(t)$ denote the correlations between v_x and v_y of the same particle whereas $C_x(t)$, $C_y(t)$ and $C_{xy}(t)$ denote the velocity-velocity correlations between pairs of particles. We have already derived the time evolution of these correlation functions in Chapter 4 [see Sec. 4.3].

In the steady state, in the thermodynamic limit, the velocity-velocity correlations and the correlation between v_x and v_y of the same particle, i.e., E_{xy} vanish as shown in Chapter 4. In that case, the steady state is described by the non-zero mean kinetic energies, i.e., E_x and E_y. We will be using a different set of variables than E_x and E_y for the analysis. We define the new set of variables, namely the total kinetic energy, E_{tot}, and the difference of energies, E_{dif}, as:

$$E_{tot} = E_x + E_y, \tag{5.2}$$

$$E_{dif} = E_x - E_y. \tag{5.3}$$

The time evolution equations for E_{tot} and E_{dif} [see Eq. (4.25) in Chapter 4 for details of the calculations] is expressed as

$$\begin{aligned} E_{tot}(t) - E_{tot}^{st} &= K_+ e^{-\lambda_+ t} + K_- e^{-\lambda_- t}, \\ E_{dif}(t) - E_{dif}^{st} &= L_+ e^{-\lambda_+ t} + L_- e^{-\lambda_- t}, \end{aligned} \tag{5.4}$$

where E_{tot}^{st} and E_{dif}^{st} are steady state values of $E_{tot}(t)$ and $E_{dif}(t)$ respectively. The coefficients K_+, K_-, L_+ and L_- along with E^{st}_{tot} and E^{st}_{dif} are given by

$$\begin{aligned}
K_+ =& \frac{1}{\gamma}\Big[-(\lambda_- - \chi_{11})E_{tot}(0) + \chi_{12}E_{dif}(0) \\
& - \frac{\lambda_d}{\lambda_+}\left[\left(\chi_{12} - (\lambda_- - \chi_{11})\right)\sigma_x^2 - \left(\chi_{12} + (\lambda_- - \chi_{11})\right)\sigma_y^2\right]\Big], \\
K_- =& \frac{1}{\gamma}\Big[(\lambda_+ - \chi_{11})E_{tot}(0) - \chi_{12}E_{dif}(0) \\
& + \frac{\lambda_d}{\lambda_-}\left[\left(\chi_{12} - (\lambda_+ - \chi_{11})\right)\sigma_x^2 - \left(\chi_{12} + (\lambda_+ - \chi_{11})\right)\sigma_y^2\right]\Big], \\
E^{st}_{tot} =& \frac{\lambda_d}{\gamma}\Big[\frac{\left(\chi_{12} - (\lambda_- - \chi_{11})\right)\sigma_x^2 - \left(\chi_{12} + (\lambda_- - \chi_{11})\right)\sigma_y^2}{\lambda_+} \\
& - \frac{\left(\chi_{12} - (\lambda_+ - \chi_{11})\right)\sigma_x^2 - \left(\chi_{12} + (\lambda_+ - \chi_{11})\right)\sigma_y^2}{\lambda_-}\Big], \\
L_+ =& \frac{1}{\gamma}\Big[-\frac{(\lambda_+ - \chi_{11})(\lambda_- - \chi_{11})}{\chi_{12}}E_{tot}(0) + (\lambda_+ - \chi_{11})E_{dif}(0) \\
& - \frac{\lambda_d}{\lambda_+\chi_{12}}\left[(\lambda_+ - \chi_{11})(\lambda_- - \chi_{11})(\sigma_x^2 - \sigma_y^2)\right]\Big], \\
L_- =& \frac{1}{\gamma}\Big[\frac{(\lambda_+ - \chi_{11})(\lambda_- - \chi_{11})}{\chi_{12}}E_{tot}(0) - (\lambda_+ - \chi_{11})E_{dif}(0) \\
& + \frac{\lambda_d}{\lambda_-\chi_{12}}\left[(\lambda_+ - \chi_{11})(\lambda_- - \chi_{11})(\sigma_x^2 - \sigma_y^2)\right]\Big], \\
E^{st}_{dif} =& \frac{\lambda_d}{\chi_{12}\gamma}\Big[(\lambda_+ - \chi_{11})(\lambda_- - \chi_{11})(\sigma_x^2 - \sigma_y^2) \\
& (\frac{1}{\lambda_+} - \frac{1}{\lambda_-})\Big], \\
\gamma =& \lambda_+ - \lambda_-.
\end{aligned}$$

5.3.2 Hard disc granular gas model

For the model of anisotropically driven hard disc granular gas, the mean kinetic energies along the x and y directions are defined as

$$E_i(t) = \frac{2}{n}\int d\boldsymbol{v}\frac{1}{2}mv_i^2 f(v,t), \quad i = x, y, \tag{5.5}$$

where $n = \int d\boldsymbol{v} f(v,t)$ is the number density, m is the mass of the particles. The details of the derivation for the time evolution of the mean kinetic energies is discussed in Chapter 3.

Please note that, for convenience, we use the notation of E_i in this chapter instead of T_i (as used in Chapter 3) to denote the various mean kinetic energies for the hard disc granular gas model. Otherwise, the expressions for the time evolutions of the various mean kinetic energies remain the same. For the convenience of description, we use the variables E_{tot} and E_{dif} as defined as in Eqs. (5.2) and (5.3). However, as discussed in Chapter 3, the time evolutions of E_{tot} and E_{dif} form a non-linear set of coupled differential equations [see Eq. (3.10)]. In order to make the analysis analytically tractable, we linearize the non-linear equations by considering only the initial states that are close to the final steady state. We define $\delta E_{tot}(t) = E_{tot}(t) - E_{tot}^{st}$ and $\delta E_{dif}(t) = E_{dif}(t) - E_{dif}^{st}$ as the time-dependent deviation of the energies from the stationary state values. The linearized solutions for $\delta E_{tot}(t)$ and $\delta E_{dif}(t)$ are then given by

$$\begin{aligned} \delta E_{tot}(t) &= K_+ e^{-\lambda_+ t} + K_- e^{-\lambda_- t}, \\ \delta E_{dif}(t) &= L_+ e^{-\lambda_+ t} + L_- e^{-\lambda_- t}, \end{aligned} \tag{5.6}$$

where the coefficients K_+, K_-, L_+ and L_- are given by

$$\begin{aligned} K_+ &= \frac{1}{\gamma}\Big[\chi_{12}\delta E_{dif}(0) - (\lambda_- - \chi_{11})\delta E_{tot}(0)\Big], \\ K_- &= \frac{1}{\gamma}\Big[-\chi_{12}\delta E_{dif}(0) + (\lambda_+ - \chi_{11})\delta E_{tot}(0)\Big], \\ L_+ &= \frac{1}{\gamma}\Big[(\lambda_+ - \chi_{11})\delta E_{dif}(0) \\ &\quad - \frac{(\lambda_+ - \chi_{11})(\lambda_- - \chi_{11})}{\chi_{12}}\delta E_{tot}(0)\Big], \\ L_- &= \frac{1}{\gamma}\Big[-(\lambda_- - \chi_{11})\delta E_{dif}(0) \\ &\quad + \frac{(\lambda_+ - \chi_{11})(\lambda_- - \chi_{11})}{\chi_{12}}\delta E_{tot}(0)\Big]. \end{aligned} \tag{5.7}$$

The details of the solutions are discussed in Sec. 3.2 and 3.3 of Chapter 3. Note that for the choice of steady states which are far from the final stationary state, linearization is not enough. In that case, one needs to use the numerical solution of the complete time evolution equations.

5.4 Mpemba effect and distance measures in phase space

We first define the protocol that we will follow for illustrating the Mpemba effect. Consider two systems P and Q which have identical parameters except for the driving strengths. Both the systems, in their respective steady states, are then quenched to a common steady state. This is achieved by instantaneously changing the driving strengths of P and Q to the common driving strength of the final steady state, keeping all the other parameters of both the systems fixed. The two initial steady states P and Q differ in their initial distance (to be appropriately defined) from the final steady state. The evolution of the systems P and Q correspond to two different trajectories in phase space. Then the Mpemba effect is said to exist if the trajectory that was initially at a larger distance from the final steady state approaches the final state faster than the trajectory that was initially at a shorter distance. For granular systems, several distance measures have been used to explore the Mpemba effect. We derive the criterion for the existence of the Mpemba effect for the different measures and for each measure, we illustrate the Mpemba effect. We also ask how much the Mpemba effect depends on the distance measure being used.

The steady state of the two models for driven granular systems considered in this chapter is completely specified by the velocity distribution $P(\boldsymbol{v})$. Distance between two probability distributions may be defined in terms of an information theoretic quantity known as Kullback-Leibler (KL) divergence [86, 87, 88]. However, the velocity distribution cannot be solved exactly and therefore the KL divergence becomes unwieldy for studying Mpemba effect, though we will study this numerically. Instead, the steady state of the system has been parametrised by the moments of the velocity. Note that the equations for the two point correlation functions close among themselves for both the Maxwell gas as well as the linearized granular gas. This motivates using the second moments of velocity distribution to characterize the steady states. For the system of anisotropically driven granular gas, the mean kinetic energies, E_x and E_y along x- and y- directions respectively, are different. Thus, the total energy, $E_{tot} = E_x + E_y$ and the difference of energies,

$E_{dif} = E_x - E_y$ serve as the appropriate variable to describe a state of the system. Thus, a steady state is characterized by (E_{tot}, E_{dif}).

In this section, we introduce different measures that have been used to define the distance between two steady states of the system. When the steady state is defined through (E_{tot}, E_{dif}), the distance measures can be defined in terms of the difference of the total energy of the two states (Sec. 5.4.1), in terms of two dimensional Euclidean distance (Sec. 5.4.2) or two-dimensional Manhattan distance (Sec. 5.4.3) of the phase space variables of the two states. In terms of the velocity distribution, the convergence to the steady state can be characterized through KL divergence (Sec. 5.4.4). The different measures track the temporal evolution of the system as it evolves from an initial state to a final state, and we derive the conditions for the Mpemba effect to exist.

5.4.1 Total energy

The most common variable that is used in literature of driven granular gases to describe its state is the mean kinetic energy. The existence of the Mpemba effect in driven granular systems has been shown in Chapters 2, 3, 4 and in Refs. [25, 26, 27] in terms of these variables. In this section, we briefly discuss the condition for the existence of the Mpemba effect in an anisotropically driven granular gas in terms of the total mean kinetic energy. We consider two systems P and Q whose initial steady states are denoted by $[E^P_{tot}(0), E^P_{dif}(0)]$ and $[E^Q_{tot}(0), E^Q_{dif}(0)]$ respectively. Here, the distance of the initial states compared to the final state is measured in terms of the total energy. The initial steady states for the two systems are prepared such that $E^P_{tot}(0) > E^Q_{tot}(0)$. Both the systems are then quenched to a common steady state having the total energy lower than the initial total energies of both the systems.

The Mpemba effect is present if the two trajectories $E^P_{tot}(t)$ and $E^Q_{tot}(t)$ cross each other at some finite time $t = \tau$ at which

$$E^P_{tot}(\tau) = E^Q_{tot}(\tau). \tag{5.8}$$

To obtain the value of τ, we equate the total energies of P and Q using either Eq. (5.4) or Eq. (5.6) depending on the inelastic Maxwell gas or hard disc granular gas respectively to obtain

$$K^P_+ e^{-\lambda_+ \tau} + K^P_- e^{-\lambda_- \tau} = K^Q_+ e^{-\lambda_+ \tau} + K^Q_- e^{-\lambda_- \tau}, \tag{5.9}$$

whose solution is

$$\tau = \frac{1}{\lambda_+ - \lambda_-} \ln \left[\frac{K^P_+ - K^Q_+}{K^Q_- - K^P_-} \right]. \tag{5.10}$$

In terms of the parameters of the initial steady states, τ reduces to

$$\tau = \frac{1}{\lambda_+ - \lambda_-} \ln \left[\frac{\chi_{12} \Delta E_{dif} - (\lambda_- - \chi_{11}) \Delta E_{tot}}{\chi_{12} \Delta E_{dif} - (\lambda_+ - \chi_{11}) \Delta E_{tot}} \right], \tag{5.11}$$

where

$$\begin{aligned} \Delta E_{tot} &= E^P_{tot}(0) - E^Q_{tot}(0), \\ \Delta E_{dif} &= E^P_{dif}(0) - E^Q_{dif}(0). \end{aligned} \tag{5.12}$$

For the Mpemba effect to be present, we require that $\tau > 0$. Since $\lambda_+ > \lambda_-$, the argument of logarithm in Eq. (5.11) should be greater than one.

Figure 5.1 illustrates the existence of the Mpemba effect where the trajectories of the initial states leading to final steady state are defined in terms of the total energy and their crossing time is given by Eq. (5.11).

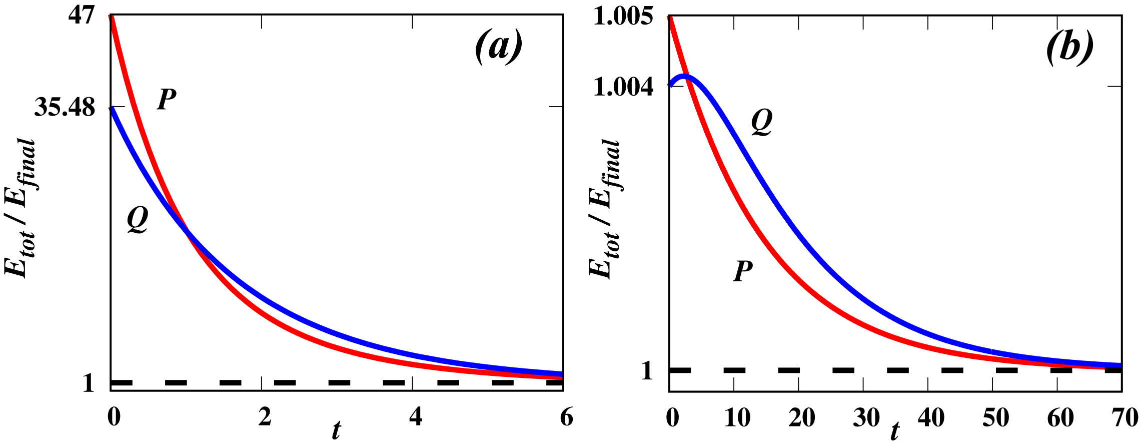

Figure 5.1: The time evolution of anisotropically driven (a) inelastic Maxwell and (b) hard disc granular gas is illustrated in terms of the mean kinetic energy, E_{tot} for two systems P and Q. The initial conditions for the inelastic Maxwell gas in (a) are $E^P_{tot}(0) = 1.148$, $E^Q_{tot}(0) = 0.92$, $E^P_{dif}(0) = -0.595$ and $E^Q_{dif}(0) = 0.455$, corresponding to the choice of the driving strengths $\sigma^P_x = 0.25$, $\sigma^P_y = 1.0$, $\sigma^Q_x = 0.6$ and $\sigma^Q_y = 0.45$. The choice of the other parameters defining the system are $r = 0.3$, $r_{wx} = 0.88$, $r_{wy} = 0.39$, $\sigma_x = 0.1$ and $\sigma_y = 0.05$. The initial conditions for the hard disc granular gas in (b) are $E^P_{tot}(0) = 10.05$, $E^Q_{tot}(0) = 10.04$, $E^P_{dif}(0) = 2.797$ and $E^Q_{dif}(0) = 1.979$, corresponding to the choice of the driving strengths $\sigma^P_x = 0.476$ and $\sigma^P_y = 0.003$ and $\sigma^Q_x = 0.405$, $\sigma^Q_y = 0.070$. The final steady state is characterized by $E^{st}_{tot} = 10.0$ and $E^{st}_{dif} = 2.82$ corresponding to the driving strengths $\sigma_x = 0.476$ and $\sigma_y = 7.351 \times 10^{-5}$. The choice of the other parameters defining the system are $r = 0.65$, $m = 1$, $n = 0.02$. P relaxes to the steady state faster than Q, though it is initially at a larger distance compared to the final steady state.

5.4.2 Euclidean Distance

Mean kinetic energy as a measure of distance has the possible issue that the trajectories may appear to cross in this one-dimensional projection, though in the two dimensional phase they do not cross. More natural definitions are to use Euclidean or Manhattan distances. As the initial and the final states are defined by the pair of variables $\{E_{tot}(t), E_{dif}(t)\}$, we can define an Euclidean measure for the trajectory connecting the two states as

$$\mathcal{L}_2(t) = \sqrt{(E_{tot}(t) - E_{tot}^{st})^2 + (E_{dif}(t) - E_{dif}^{st})^2}. \tag{5.13}$$

Here, the initially hotter system or equivalently the system which is initially farther from the final steady state has an initially larger $\mathcal{L}_2$ compared to the colder system. For this measure, we define the Mpemba effect as follows. Let us consider two systems P and Q such that P is initially at a larger distance from the final steady state compared to Q, i.e., $\mathcal{L}_2^P(0) > \mathcal{L}_2^Q(0)$. Here, the systems P and Q are identical in all respect except for the pair of driving strengths (σ_x, σ_y) that is required to prepare the systems in their initial steady states. Then both the systems are quenched to a common steady state by applying a same pair of driving strengths. In this case, the Mpemba effect is said to exist if the two trajectories for the systems P and Q quantified in terms of $\mathcal{L}_2^P(t)$ and $\mathcal{L}_2^Q(t)$ cross each other at some finite time $t = \tau$ at which

$$\mathcal{L}_2^P(\tau) = \mathcal{L}_2^Q(\tau). \tag{5.14}$$

To obtain the value of τ, we equate the Euclidean measures for the systems P and Q at

$t = \tau$ as

$$\sqrt{(E^{P}_{tot}(\tau) - E^{st}_{tot})^2 + (E^{P}_{dif}(\tau) - E^{st}_{dif})^2}$$
$$= \sqrt{(E^{Q}_{tot}(\tau) - E^{st}_{tot})^2 + (E^{Q}_{dif}(\tau) - E^{st}_{dif})^2}. \tag{5.15}$$

For the inelastic Maxwell gas, using Eq. (5.4) we obtain the crossing times as

$$\tau^{\pm} = \frac{1}{(\lambda_+ - \lambda_-)} \ln\left[\frac{2a}{d \pm \sqrt{d^2 - 4ab}}\right], \tag{5.16}$$

where,

$$\begin{aligned} a &= \left[(K^{P}_{+})^2 + (L^{P}_{+})^2 - (K^{Q}_{+})^2 - (L^{Q}_{+})^2\right], \\ b &= \left[(K^{P}_{-})^2 + (L^{P}_{-})^2 - (K^{Q}_{-})^2 - (L^{Q}_{-})^2\right], \\ d &= 2\left[K^{Q}_{+}K^{Q}_{-} + L^{Q}_{+}L^{Q}_{-} - K^{P}_{+}K^{P}_{-} - L^{P}_{+}L^{P}_{-}\right]. \end{aligned} \tag{5.17}$$

A similar expression for the crossing time [see Eq. (5.16)] is also obtained for the case of hard disc granular gas for which the constants $\lambda_{\pm}$, a, b, and d are computed using Eq. (5.7).

Note that there are two possibilities for the crossing time in Eq. (5.16). Figure 5.2 illustrates such a scenario where both the crossings are present. However, the presence of two crossings will eventually lead to no Mpemba effect. Thus, we are interested in only those cases or the initial conditions where there exists only one crossing of the trajectories of the initial states leading to the final steady state. For the Mpemba effect to be present, we require that $\tau^+ > 0$ or $\tau^- > 0$, but not both positive. Since $\lambda_+ > \lambda_-$, the argument of logarithm in Eq. (5.16) should be greater than one for $+(-)$ and less than one for $-(+)$. Figure 5.3 illustrates the existence of the Mpemba effect where the trajectories of the initial states leading to final steady state are defined in terms of the Euclidean measure and their crossing time is given by Eq. (5.16).

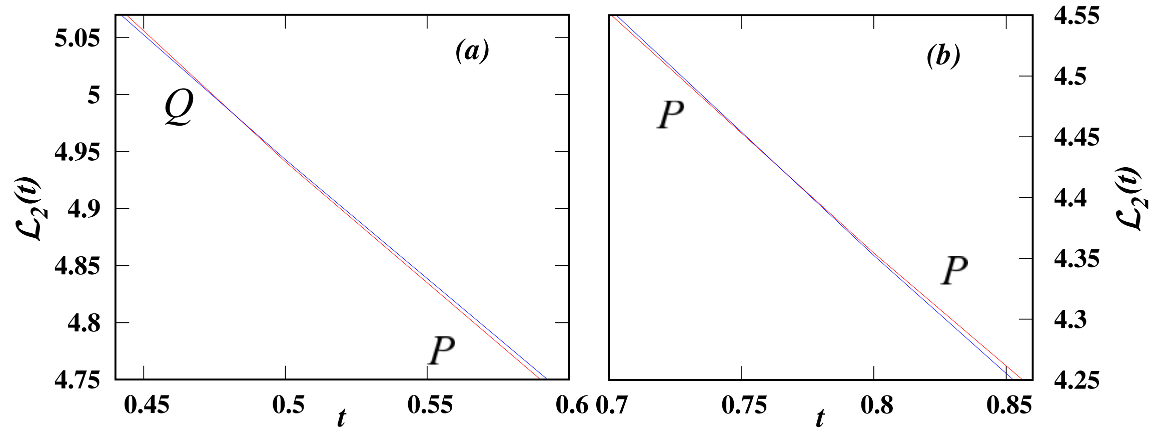

Figure 5.2: The time evolution of the anisotropically driven inelastic Maxwell gas in terms of the Euclidean measure, $\mathcal{L}_2(t)$ for two systems P and Q with initial conditions $\mathcal{L}_2^P(0) = 6.34$ and $\mathcal{L}_2^Q(0) = 6.15$, shows two crossings as illustrated in (a) and (b) for the different times. The multiple crossing times are obtained using Eq. (5.16). The choice of the other parameters defining the system are $r = 0.1$, $r_{wx} = 0.95$, $r_{wy} = 0.39$, $\sigma_x = 1.6$ and $\sigma_y = 1.1$.

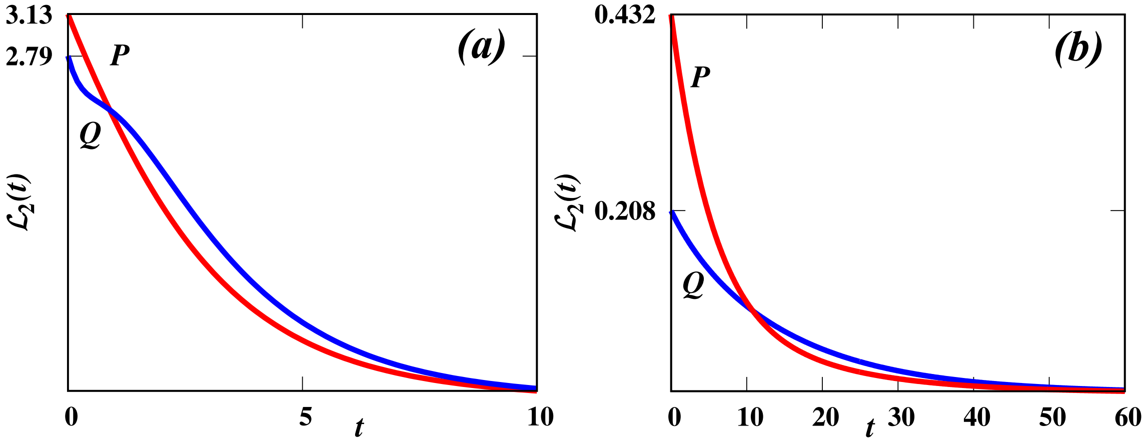

Figure 5.3: The time evolution of anisotropically driven (a) inelastic Maxwell and (b) hard disc granular gas is illustrated in terms of Euclidean measure, $\mathcal{L}_2(t)$ for two systems P and Q. The initial conditions for the inelastic Maxwell gas in (a) are $\mathcal{L}_2^P(0) = 3.13$ and $\mathcal{L}_2^Q(0) = 2.79$, corresponding to the choice of the driving strengths $\sigma_x^P = 1.9$, $\sigma_y^P = 1.2$, $\sigma_x^Q = 1.55$ and $\sigma_y^Q = 2.0$. The driving strengths corresponding to final steady state are $\sigma_x = 1.6$ and $\sigma_y = 1.1$ whereas the choice of the other parameters defining the system are $r = 0.3$, $r_{wx} = 0.95$, $r_{wy} = 0.39$. The initial conditions for the hard disc granular gas in (b) are $\mathcal{L}_2^P(0) = 0.432$ and $\mathcal{L}_2^Q(0) = 0.208$, corresponding to the choice of the driving strengths $\sigma_x^P = 0.491$ and $\sigma_y^P = 7.572 \times 10^{-5}$ and $\sigma_x^Q = 0.444$, $\sigma_y^Q = 0.037$. The driving strengths corresponding to final steady state are $\sigma_x = 0.476$ and $\sigma_y = 7.351 \times 10^{-5}$ whereas the choice of the other parameters defining the system are $r = 0.65$, $m = 1$ and $n = 0.02$. P relaxes to the steady state faster than Q, though its initial Euclidean distance from the final steady state is larger.

5.4.3 Manhattan Distance

Similar to the Euclidean measure, we can define another measure for the time evolution of the trajectory connecting the initial and the final states in terms of Manhattan distance. In the plane of $\{E_{tot}(t), E_{dif}(t)\}$, the Manhattan measure is defined as

$$\mathcal{L}_1(t) = |E_{tot}(t) - E_{tot}^{st}| + |E_{dif}(t) - E_{dif}^{st}|. \tag{5.18}$$

Here, the system having larger $\mathcal{L}_1(0)$ at time $t = 0$ is termed the “hotter“ system while compared to the initially “colder” system having a comparatively smaller $\mathcal{L}_1(0)$. For this measure, we define the Mpemba effect as follows. Let us consider two systems P and Q such that P is initially at a larger distance from the final steady state compared to Q in terms of Manhattan measure, i.e., $\mathcal{L}_1^P(0) > \mathcal{L}_1^Q(0)$. Here, the systems P and Q are identical except for the pair of driving strengths (σ_x, σ_y). Both the systems are then subjected to same pair of driving strengths. As a result, both the systems are driven to a common steady state. Then the Mpemba effect is said to exist if the two trajectories for the systems P and Q quantified in terms of $\mathcal{L}_1^P(t)$ and $\mathcal{L}_1^Q(t)$ cross each other at some finite time $t = \tau$ at which

$$\mathcal{L}_1^P(\tau) = \mathcal{L}_1^Q(\tau), \tag{5.19}$$

or equivalently,

$$\begin{aligned} &|(E_{tot}^P(\tau) - E_{tot}^{st})| + |(E_{dif}^P(\tau) - E_{dif}^{st})| \\ &= |(E_{tot}^Q(\tau) - E_{tot}^{st})| + |(E_{dif}^Q(\tau) - E_{dif}^{st})|. \end{aligned} \tag{5.20}$$

Now, using Eq. (5.4) for the case of inelastic Maxwell gas and solving Eq. (5.20), we obtain eight different solutions for the crossing time as

$$\begin{aligned}
\tau_{c,1} &= \frac{1}{\gamma}\ln\left(\frac{-K_+^P+K_+^Q+L_+^P+L_+^Q}{K_-^P-K_-^Q-L_-^P-L_-^Q}\right), \tau_{c,2} &&= \frac{1}{\gamma}\ln\left(\frac{-K_+^P-K_+^Q-L_+^P+L_+^Q}{K_-^P+K_-^Q+L_-^P-L_-^Q}\right),\\
\tau_{c,3} &= \frac{1}{\gamma}\ln\left(\frac{-K_+^P-K_+^Q+L_+^P-L_+^Q}{K_-^P+K_-^Q-L_-^P+L_-^Q}\right), \tau_{c,4} &&= \frac{1}{\gamma}\ln\left(\frac{-K_+^P+K_+^Q-L_+^P-L_+^Q}{K_-^P-K_-^Q+L_-^P+L_-^Q}\right),\\
\tau_{c,5} &= \frac{1}{\gamma}\ln\left(\frac{-K_+^P-K_+^Q+L_+^P+L_+^Q}{K_-^P+K_-^Q-L_-^P-L_-^Q}\right), \tau_{c,6} &&= \frac{1}{\gamma}\ln\left(\frac{-K_+^P+K_+^Q-L_+^P+L_+^Q}{K_-^P-K_-^Q+L_-^P-L_-^Q}\right),\\
\tau_{c,7} &= \frac{1}{\gamma}\ln\left(\frac{-K_+^P+K_+^Q+L_+^P-L_+^Q}{K_-^P-K_-^Q-L_-^P+L_-^Q}\right), \tau_{c,8} &&= \frac{1}{\gamma}\ln\left(\frac{-(K_+^P+K_+^Q+L_+^P+L_+^Q)}{K_-^P+K_-^Q+L_-^P+L_-^Q}\right).
\end{aligned} \tag{5.21}$$

For the Mpemba effect to be present, there should be odd number of crossings. Thus, we look for those initial conditions in the phase space that lead to odd number of solutions to the Eq. (5.20). Figure 5.4 illustrates the existence of the Mpemba effect where the trajectories of the initial states leading to final steady state are defined in terms of the Manhattan measure.

5.4.4 KL Divergence

In this section, we define the Mpemba effect in terms of an information theoretic quantity known as Kullback-Leibler (KL) divergence. The measure is defined as

$$D_{KL}(t) = \int d\boldsymbol{v} P(\boldsymbol{v},t)\ln\left(\frac{P(\boldsymbol{v},t)}{P^{st}(\boldsymbol{v})}\right), \tag{5.22}$$

where $P(\boldsymbol{v},t)$ is the instantaneous velocity distribution of the particles at any time t and $P^{st}(\boldsymbol{v})$ is the final steady state velocity distribution function. The above quantity is not a true measure of geometric distance as it is not symmetric between two given distribution functions. But it is a good candidate for the study of relaxation dynamics of an arbitrary initial state to a given reference steady state for the following reasons: (a) it is a monotonically non-increasing function of time as has been shown in earlier studies [86, 87, 88], (b) it provides information regarding the measure of deviation and its temporal evolution

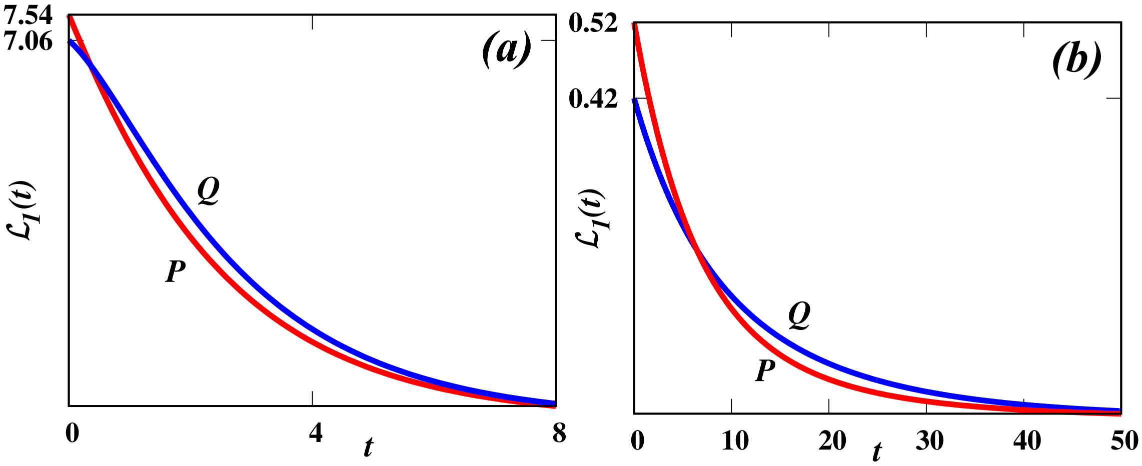

Figure 5.4: The time evolution of anisotropically driven (a) inelastic Maxwell and (b) hard disc granular gas is illustrated in terms of Manhattan measure, $\mathcal{L}_1(t)$ for two systems P and Q. The initial conditions for the inelastic Maxwell gas in (a) are $\mathcal{L}_1^P(0) = 7.54$ and $\mathcal{L}_1^Q(0) = 7.06$, corresponding to the choice of the driving strengths $\sigma_x^P = 2.2$, $\sigma_y^P = 1.2$, $\sigma_x^Q = 0.1$ and $\sigma_y^Q = 1.2$. The driving strengths corresponding to final steady state are $\sigma_x = 1.6$ and $\sigma_y = 1.1$ whereas the choice of the other parameters defining the system are $r = 0.9$, $r_{wx} = 0.88$ and $r_{wy} = 0.3$. The initial conditions for the hard disc granular gas in (b) are $\mathcal{L}_1^P(0) = 0.52$ and $\mathcal{L}_1^Q(0) = 0.42$, corresponding to the choice of the driving strengths $\sigma_x^P = 0.466$ and $\sigma_y^P = 0.023$ and $\sigma_x^Q = 0.444$, $\sigma_y^Q = 0.037$. The driving strengths corresponding to final steady state are $\sigma_x = 0.476$ and $\sigma_y = 7.351 \times 10^{-5}$ whereas the choice of the other parameters defining the system are $r = 0.65$, $m = 1$ and $n = 0.02$. P relaxes to the steady state faster than Q, though its initial Manhattan distance from the final steady state is larger.

of any two initial states from the final reference state.

Although being a good candidate for the study of relaxation dynamics, the above measure is not much fruitful in the context of granular gases. It is because Eq. (5.22) requires to have information regarding the time evolution of the velocity distribution function at any time t which is not analytically feasible in the case of granular gases. The previous theoretical studies on velocity distribution of driven granular gases attempts to find the velocity distribution of the steady state for different contexts [89, 90, 59, 60, 57]. But in all the cases, it was not possible to derive the form of instantaneous velocity distribution at an instant of time t even for the simplest model of inelastic Maxwell gas.

As a result, we use numerical methods to compute the KL divergence. We briefly discuss the procedure for the numerical computation of KL divergence for the case of inelastic Maxwell gas. Starting from a random configuration of velocities for N particles, the system is evolved to an initial steady state corresponding to an initial pair of driving strengths (σ_x, σ_y). The pair of driving strengths acting on the particles is then changed to those of the desired final steady state. The system evolves in time as follows. At each time step, either two particles collide or a particle is driven, based on the corresponding rates. At each time step we measure the time evolution of the velocity distribution, $P(\boldsymbol{v},t)$ of the N particles. The distributions are averaged over 10^4 realizations. The final steady state velocity distribution is measured separately and is averaged over 10^5 different realizations. Thus, having information about $P(\boldsymbol{v},t)$ and $P^{st}(\boldsymbol{v})$, we can then numerically determine the time evolution of KL divergence using Eq. (5.22).

We now discuss the notion of a “hotter“ and a “colder” system using the measure of KL divergence when two systems are quenched to a final steady state. The system having larger divergence at $t = 0$ is referred to as the “hotter“ system as it is farther off from the final steady state whereas the system having comparatively smaller divergence is referred to as the “colder” system. Similar to the previous definitions of the Mpemba effect for the other measures, if the hotter system equilibrates faster than the colder system to the final

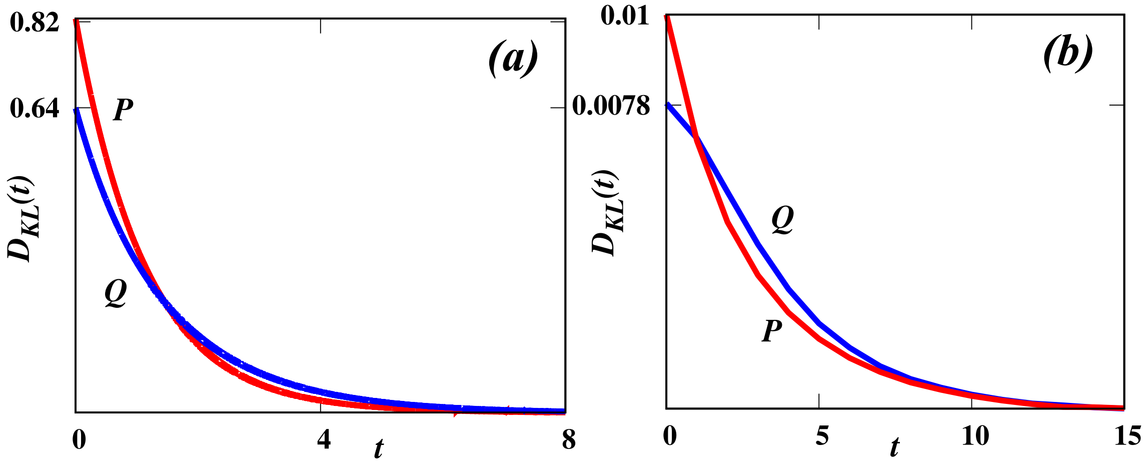

Figure 5.5: The time evolution of anisotropically driven (a) inelastic Maxwell and (b) hard disc granular gas is illustrated in terms of KL divergence measure, $D_{KL}(t)$ for two systems P and Q. The initial conditions for the inelastic Maxwell gas in (a) are $D^P_{KL}(0) = 0.82$ and $D^Q_{KL}(0) = 0.64$, corresponding to the choice of the driving strengths $\sigma^P_x = 1.4$, $\sigma^P_y = 4.0$, $\sigma^Q_x = 2.45$ and $\sigma^Q_y = 2.3$. The driving strengths corresponding to final steady state are $\sigma_x = 1.5$ and $\sigma_y = 0.9$ whereas the choice of the other parameters defining the system are $r = 0.3$, $r_{wx} = 0.88$ and $r_{wy} = 0.39$. The initial conditions for the hard disc granular gas in (b) are $D^P_{KL}(0) = 0.01$ and $D^Q_{KL}(0) = 0.0078$, corresponding to the choice of the driving strengths $\sigma^P_x = 7.148$, $\sigma^P_y = 0.026$, $\sigma^Q_x = 1.144$ and $\sigma^Q_y = 5.609$. The driving strengths corresponding to the final steady state are $\sigma_x = 6.62$ and $\sigma_y = 0.026$, whereas the choice of the other parameters defining the system are $r = 0.65$, $m = 1$, $n = 0.02$. P relaxes to the steady state faster than Q, though its initial KL divergence with respect to the final steady state is larger.

steady state, the Mpemba effect is said to exist.

Figure 5.5 illustrates the existence of the Mpemba effect where the trajectories of the initial states leading to final steady state are defined in terms of the KL divergence.

5.5 Comparison between various measures

We now compare the effect of different distance measures on the Mpemba effect. For a given initial condition in terms of intrinsic system parameters and the pair of driving strengths, we look for the existence of the Mpemba effect using the different distance measures.

We first show that for the same initial condition, different measures can give different results, as illustrated in Fig. 5.6 for the inelastic Maxwell gas. In the example shown, the Mpemba effect is absent for distance measure corresponding to the total energy distance [see Fig. 5.6(a)] which it is present for the other three measures [see Fig. 5.6(b)–(d)]. In addition to the non-uniqueness of the Mpemba effect, even the notion of “hot“ and “cold” system in terms of distance from the final steady state for a pair of initial conditions is not unique among the various definitions. What is initially hotter (shown in red) in Fig. 5.6(a)–(c) is initially colder (shown in blue) in Fig. 5.6(d)

Given that there is non-uniqueness among the definitions, we now check whether all definitions show the Mpemba effect as well as whether there is any overlap in the phase space regions that corresponds to the Mpemba effect for the different measures. The phase space is labeled by the free parameters: final steady states in terms of (E_{tot}^{st}, E_{dif}^{st}), initial steady states of P and Q, i.e., (E_{tot}^{P}, E_{dif}^{P}) and (E_{tot}^{Q}, E_{dif}^{Q}) for a fixed value of other intrinsic parameters such as r, r_{wx} and r_{wy}. However, we notice that the equations for the correlation functions [see Eqs. (5.4) and (3.16)] are linear equations in the differences in energies $\delta E_{tot} = E_{tot} - E_{tot}^{st}$, $\delta E_{dif} = E_{dif} - E_{dif}^{st}$ for both P and Q, giving four variables. We also note that the equations for the correlation function, and hence the crossing times, are invariant if all the δEs are scaled by the same factor, thus reducing the number of factors by one. To make it a two dimensional phase diagram, we fix the initial values of δE_{tot}^{P} and δE_{dif}^{P} for P, and determine the phase diagram in terms of ($\delta E_{dif}^{Q}/\delta E_{tot}^{P}$) and ($\delta E_{tot}^{Q}/\delta E_{tot}^{P}$).

The phase diagrams for the measures: total energy, Manhattan and Euclidean distance, are obtained using the exact criteria derived for the existence of the Mpemba effect, both for the inelastic Maxwell gas and hard disc granular gas (linearized analysis). However, for the case of KL divergence, the phase diagram is obtained using discrete set of points sampled from the phase space and checked individually for the existence of the Mpemba effect through the analysis of evolution of the trajectories of systems P and Q. The KL

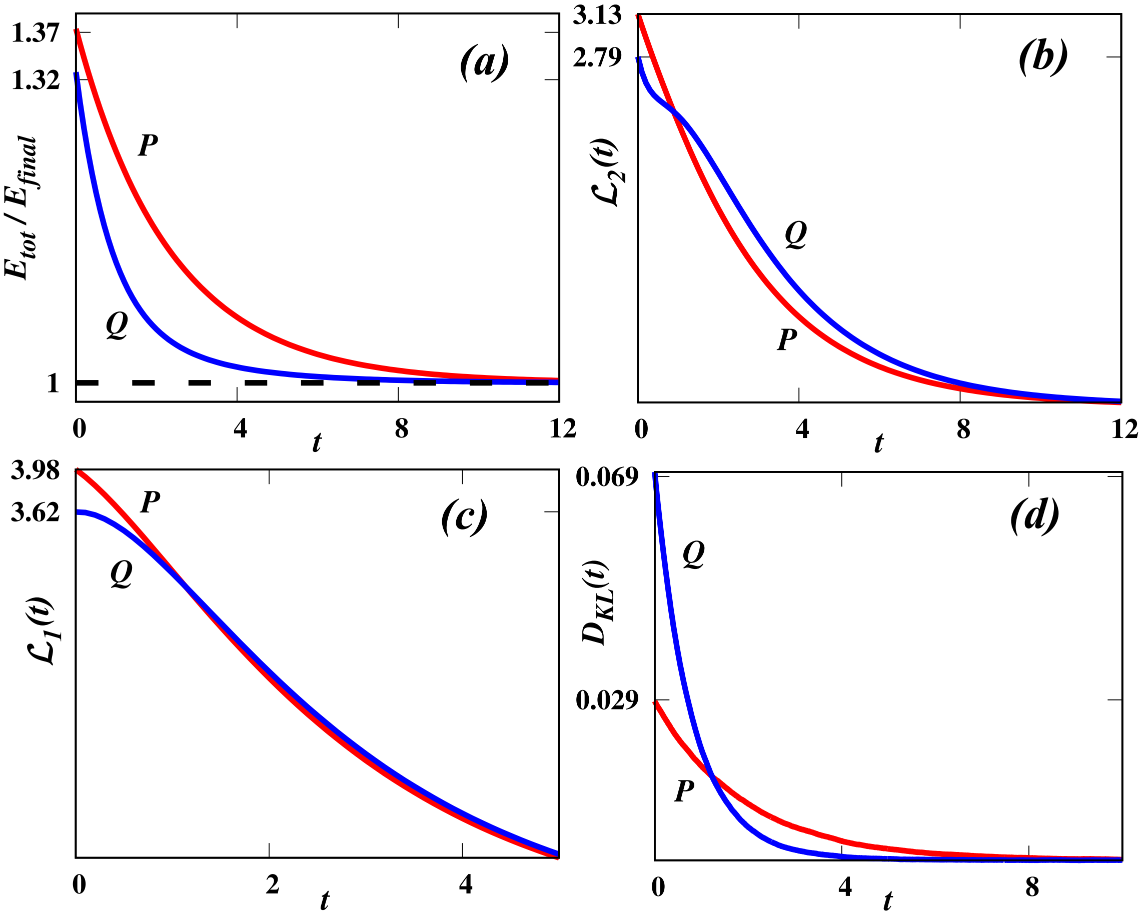

Figure 5.6: The time evolution of the two systems P and Q for an anisotropically driven inelastic Maxwell gas is illustrated for the following measures: (a) total energy, (b) Euclidean measure, (c) Manhattan measure and for (d) KL divergence. The initial conditions for the various measures are identical and are given in terms of the driving strengths for systems P and Q as $(\sigma_x^P = 1.9, \sigma_y^P = 1.2)$ and $(\sigma_x^Q = 1.55, \sigma_y^Q = 2.0)$. The choice of the other parameters defining the system are $r = 0.3$, $r_{wx} = 0.95$, $r_{wy} = 0.39$, $\sigma_x = 1.6$ and $\sigma_y = 1.1$. The existence of the Mpemba effect and the notion of “hot“ and “cold” system in terms of distance from the final steady state for a given pair of initial conditions is not unique among the various measures.

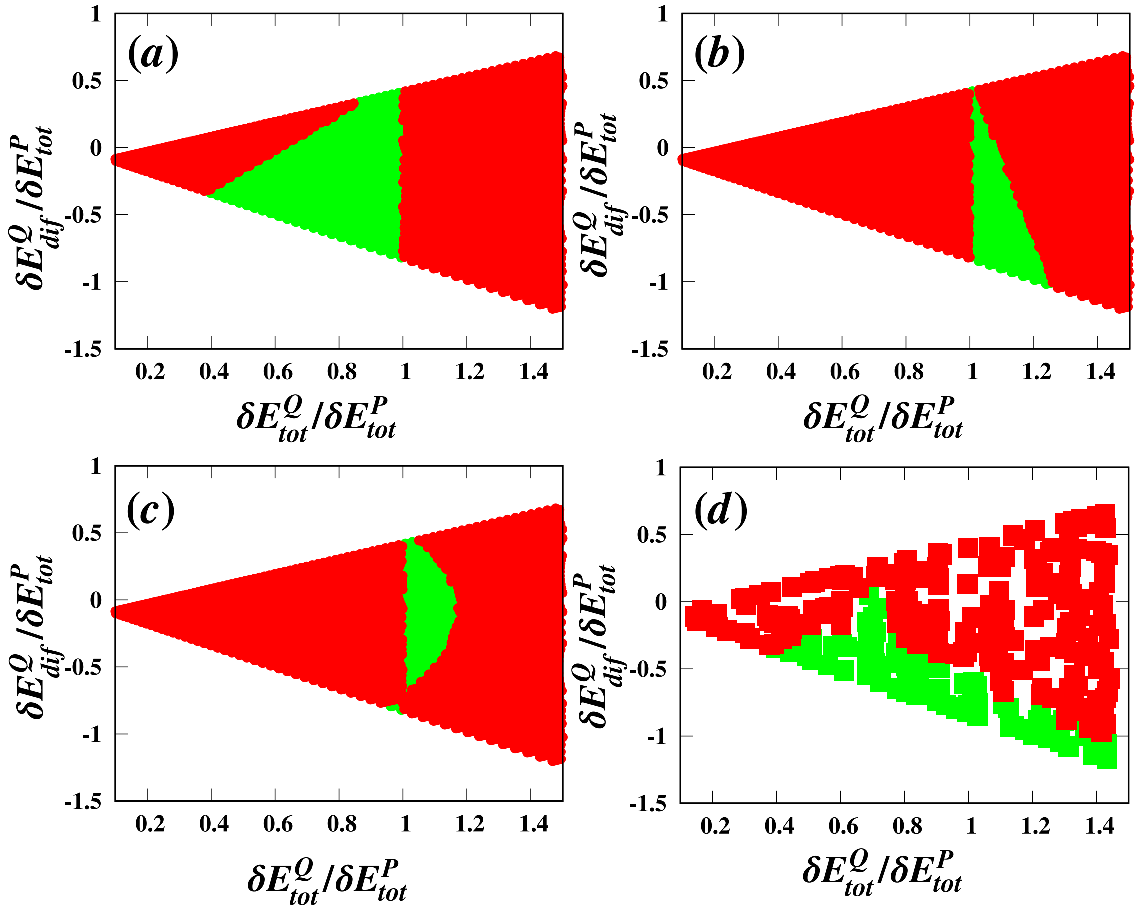

Figure 5.7: The phase diagram in the $(\delta E^{Q}_{dif}/\delta E^{P}_{tot})$-$(\delta E^{Q}_{tot}/\delta E^{P}_{tot})$ plane shows the existence of the Mpemba effect in the driven inelastic Maxwell gas for the use of different distance measures: (a) total energy, (b) Manhattan, (c) Euclidean, and (d) KL-divergence. The red (green) region corresponds to absence (presence) of the Mpemba effect, while the regions outside the triangular shape are not valid steady states. The white regions inside the triangle in (d) is due to discrete sampling of phase space. The choice of the parameters defining the system are $r = 0.4$, $r_{wx} = 0.44$, $r_{wy} = 0.95$, $\delta E^{P}_{tot} = 1.00$ and $\delta E^{P}_{dif}/\delta E^{P}_{tot} = 0.53$, which are kept constant across all the various measures.

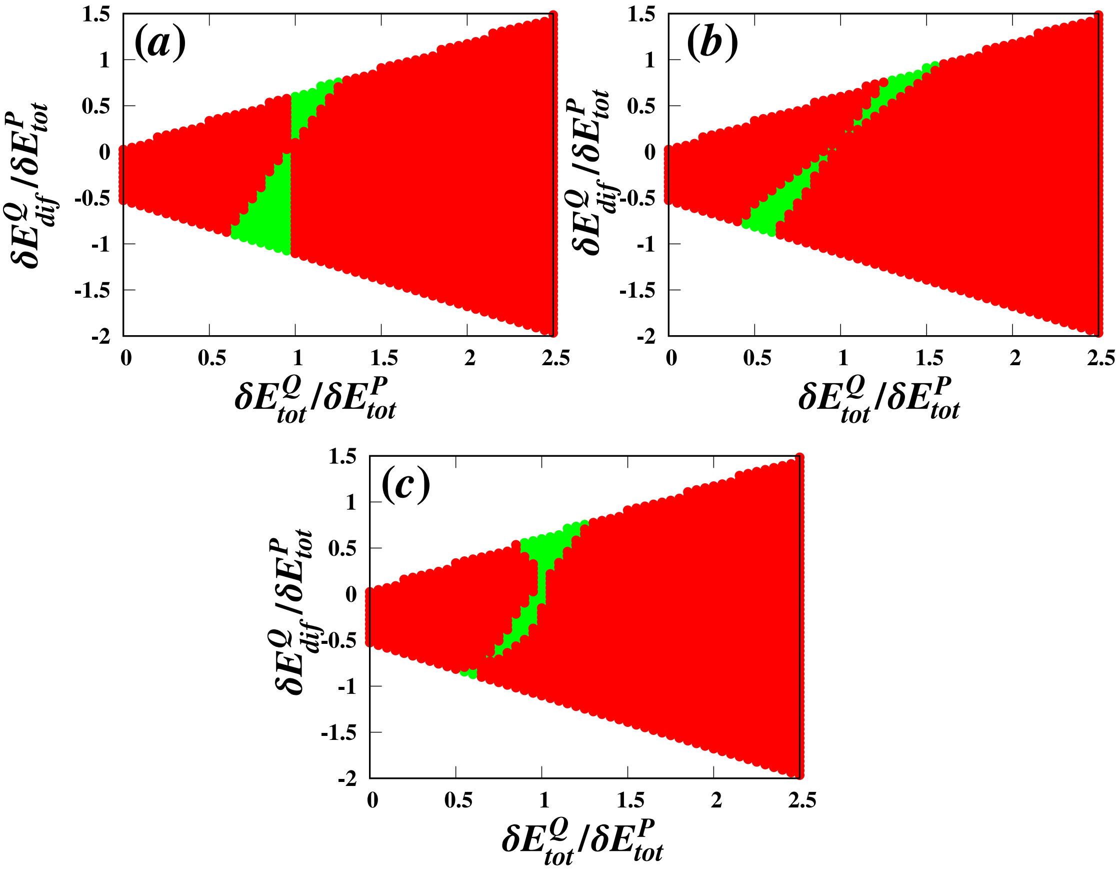

Figure 5.8: The phase diagram in the ($\delta E^{Q}_{dif}/\delta E^{P}_{tot}$)-($\delta E^{Q}_{tot}/\delta E^{P}_{tot}$) plane shows the existence of the Mpemba effect in the driven hard disc granular gas for the use of different distance measures: (a) total energy, (b) Manhattan, and (c) Euclidean. The red (green) region corresponds to absence (presence) of Mpemba effect, while the white regions are not accessible. The choice of the parameters defining the system are $n = 0.02$, $\sigma = 1$, $m = 1$, $r = 0.1$, $\delta E^{P}_{tot} = 1.00$ and $\delta E^{P}_{dif}/\delta E^{P}_{tot} = 0.11$, which are kept constant across all the various measures.

divergence is used only for the Maxwell gas as in the case of granular gas, it is not possible to make a direct comparison with the linearized theories. Figures 5.7 and 5.8 show the phase diagram of the Mpemba effect in terms of various measures for the case of inelastic Maxwell gas and hard disc granular gas respectively. The colored region corresponds to the allowed parameter space, while the green (red) regions correspond to the Mpemba effect being present (absent). It is clear that all the different distance measures show the Mpemba effect. However, the phase boundary of the initial conditions that show the Mpemba effect is very different for the various measures. We conclude that the usual measures used for driven granular gases lead to a non-universal definition of the Mpemba effect.

5.6 Conclusion

To summarize, we studied the Mpemba effect in the driven inelastic Maxwell and the driven granular gases using different definitions of distances between points in phase space. These definitions were motivated by the choices that have been used earlier in the literature for establishing the presence of the Mpemba effect in granular systems. We studied the Mpemba effect in terms of the following measures: total kinetic energy (as has been used earlier), Euclidean measure ($\mathcal{L}_2$), Manhattan measure ($\mathcal{L}_1$) and KL divergence. While the first three are based on average kinetic energy in different directions, KL divergence is based on the probability distribution of velocity. The analysis was performed for the anisotropically driven gases [26, 27].

We derived the criteria for the existence of the Mpemba effect with the various measures and showed the existence of the Mpemba effect for all the different choices of distance measures. However, the phase diagrams for the different measures are not the same with the presence or absence of the Mpemba effect for a particular phase space point depending on the measure, resulting in a non-unique definition of the Mpemba effect. Moreover, the notion of ‘hot’ and ‘cold’ initial states is different for the different choices of distance measures from the final steady state.

In a Markov process, the relaxation to the steady state at large times is dominated by the first excited state of the transition matrix, i.e., $P(C,t) = P_1(C) + a_2 \exp(-t/\tau) P_2(C) + \ldots$, where $P(C,t)$ is the probability distribution at time t, P_1 is the steady state and P_2 is the first excited state. The quantities τ, P_1 and P_2 depend only on the transition matrix, and independent of the initial states, while the pre-factor a_2 is determined by the overlap of the initial steady state with the first excited state. Given the above expansion, it is clear that the system with smaller value of $|a_2|$ will equilibrate faster [11]. The same observation will be true for the time evolution of an arbitrary observable $f(C,t)$ such as total energy, as it also follows a similar structure as $P(C,t)$. Also it has been shown that the order property of a_2 is captured by the KL-divergence [11]. Therefore, if system P approaches steady state faster according to KL-divergence, then by the above argument we should find a similar relaxation behavior when total energy is the distance measure and the phase diagrams should be identical. But this is not what we find in this chapter. This discrepancy is due to the fact that what is cold and what is hot may not be the same for the two distance measures (see Fig. 5.6(a) and 5.6(d) for an example, where the higher energy state corresponds to one with a lower distance in terms of KL divergence and vice versa), thus giving contradictory results for the Mpemba effect. Since it is difficult to come up with an observable $f(C,t)$ that has the same characteristics as KL-divergence, we generalized the total variation distance $\sum_C |P(C,t) - P_1(C)|$ (which also follows a similar structure as $P(C,t)$) to the distances $\mathcal{L}_1$ and $\mathcal{L}_2$ used in this chapter, based on the mean energies.

The ambiguity of characterising the Mpemba effect in granular systems is in contrast to the unique identification of the Mpemba effect for the case of single particle Markov systems, irrespective of the choice of distance measure. This is due to the existence of a common criteria across all the measures which is given in terms of the coefficient a_2 [11]

associated with the second eigenfunction in the eigenspectrum analysis of probability distribution function. However, it is very challenging to calculate a_2 for an interacting many particle system like the granular system considered in this chapter. The natural choices are observables like kinetic energy, rather than probability distributions, which are easier to track both in experiments and calculations. However, these choices for distance measures may not necessarily decrease monotonically with time, a requirement that was put forward in Ref. [11]. Based on the results in this chapter, the characterization of the Mpemba effect with such ad-hoc distance measures should be done with caution.

Chapter 6

Mpemba effect in a Langevin system: Exact results and other properties

6.1 Introduction

The different physical systems that have been studied reveal different causes behind the Mpemba effect. However, in the analytically tractable models with only a few states, the description of the Mpemba effect has been in terms of the ruggedness of the energy landscape [11, 4]. In particular, the presence of a metastable minimum in the free energy traps a system at lower energy more effectively than one at higher temperature, resulting in a faster relaxation of the hotter system. In this chapter, we study the role of the energy landscape in inducing the Mpemba like behaviour in the relaxation dynamics of a single particle Langevin system through an exact analysis.

Kumar and Bechhoefer [4] demonstrated experimentally the Mpemba effect for a single Brownian particle diffusing in a double well quartic potential with linear slopes near the boundaries of the domain. It was shown that the key to the observation of the Mpemba effect is the asymmetric shape of the external potential, which was realized by introducing different widths for the left and the right domains of the potential. As the asymmetry in the domain widths increases, even a stronger version of the Mpemba effect is found where the relaxation is exponentially faster for a hotter system. This was the first experimental proof of the strong Mpemba effect, which was theoretically predicted in Ref. [6]. More recently, the condition for the strong Mpemba effect was derived for the Brownian particle in the overdamped limit [91]. However, other possibilities of inducing the Mpemba effect through asymmetries in terms of different depths of the potential wells without changing the domain widths were not explored. Thus, it is not clear about what sort of asymmetry in the potential configuration is necessary or sufficient to induce the Mpemba effect. Moreover, it is not well understood whether a double well potential is necessary to realize the Mpemba effect in Langevin systems. Recently for a piecewise constant potential where the minima of the potentials have neutral equilibrium, it was shown that the Mpemba effect can be observed, questioning the need for a metastable state [13].

These issues are best addressed through an exactly solvable model. Motivated by the experiment on the Mpemba effect by Kumar and Bechhoefer [4], we consider a Brownian particle trapped in a double well potential, but in an external potential that is piece-wise linear, making it analytically tractable. In this chapter, we solve for the time evolution of the probability density using the method of eigenspectrum decomposition of the corresponding Fokker-Planck equation [92]. The potential can be made asymmetric in several different ways: (a) different widths for the left and right domains of the potential as discussed in the experiment by Kumar and Bechhoefer [4], (b) same domain widths but asymmetric placement of the potential minima, (c) different depths of the potential wells, and (d) for different heights for the left, center and right edge of the potential. We investigate the presence of the Mpemba effect for the above scenarios. In addition, we show that asymmetry of domain widths is not a necessary condition for the existence of the Mpemba effect. Also, we show that asymmetry in the potential is not a sufficient condition for the Mpemba effect. Finally, we show through an example that the presence of a metastable state is not a necessary condition for the effect. The content of this chapter is published in Ref. [93].

6.2 Model system and general formalism

We consider a particle in an asymmetric double well potential $\tilde{U}(x)$ in a thermal environment characterized by noise η and damping γ. The mean and variance of the noise are

$$\langle \eta(t) \rangle = 0 \;\text{ and }\; \langle \eta(t)\eta(t') \rangle = 2\gamma k_B T_b \delta(t-t'), \tag{6.1}$$

where T_b is the temperature of the thermal bath and k_B is the Boltzmann's constant. We consider the overdamped case where the damping γ is large compared to the mass of the particle. The motion is then described by the following overdamped Langevin equation:

$$\gamma \frac{dx}{dt} = -\frac{d\tilde{U}}{dx} + \eta(t). \tag{6.2}$$

We define the following dimensionless variables: $x = (2\pi/L)\tilde{x}$, $T = \tilde{T}/\tilde{T}_b$, $U = \tilde{U}/(k_B\tilde{T}_b)$ and $t = (4\pi^2 k_B \tilde{T}_b/\gamma L^2)\tilde{t}$. Note that L is the characteristic length of the model. For a symmetric potential domain extending from $-L/2$ to $L/2$ about the origin, the dimensionless variable $x \in (-\pi, \pi)$. The corresponding Fokker-Planck equation for the probability distribution function $p(x,t)$ in the dimensionless variables reads [92, 94]

$$\frac{\partial p}{\partial t} = \frac{\partial}{\partial x}\left[\frac{dU}{dx} p\right] + \frac{\partial^2 p}{\partial x^2}. \tag{6.3}$$

In here, we will solve $p(x,t)$ analytically for the given configuration of the potential. To this end, it will be first useful to review the formalism of eigenspectrum decomposition for solving the Fokker-Planck equation (6.3) in the presence of a generic confining potential.

6.2.1 Eigenspectrum decomposition

We follow closely the formalism described in Ref. [92]. We start by rewriting Eq. (6.3) in the form of the continuity equation

$$\frac{\partial p}{\partial t} = \frac{\partial}{\partial x}\left[\frac{dU}{dx}p\right] + \frac{\partial^2 p}{\partial x^2} = -\frac{\partial J}{\partial x}, \tag{6.4}$$

from where the probability current density is given by

$$J(x) = -\left[\frac{dU}{dx} + \frac{\partial}{\partial x}\right]p = -e^{-U(x)}\frac{d}{dx}\left[e^{U(x)}p\right], \tag{6.5}$$

corresponding to the Fokker-Planck operator

$$\mathscr{L}_{FP} = \frac{\partial}{\partial x}\left(\frac{dU}{dx}\right) + \frac{\partial^2}{\partial x^2}. \tag{6.6}$$

The stationary solution of the Fokker-Planck Eq. (6.4) for the probability density is given by the Boltzmann distribution at temperature $T_b = 1$ (in the dimensionless variable)

$$\pi(x, T_b = 1) = \frac{e^{-U(x)}}{\mathscr{Z}}, \tag{6.7}$$

where $\mathscr{Z} = \int e^{-U(x)}dx$ is the partition function. Note that the Fokker-Planck operator in Eq. (6.6) is not self-adjoint. A simple transformation leads to its self-adjoint form $\mathscr{L}$ where

$$\mathscr{L} = e^{\frac{U(x)}{2}}\mathscr{L}_{FP}e^{-\frac{U(x)}{2}} = \frac{\partial^2}{\partial x^2} - V(x), \tag{6.8}$$

and

$$V(x) = \frac{1}{4}\left(\frac{dU}{dx}\right)^2 - \frac{1}{2}\frac{d^2U}{dx^2}, \tag{6.9}$$

is now the effective potential. Thus the original problem is now reduced to analyzing the following eigenvalue problem

$$\mathscr{L}\psi_n = \lambda_n \psi_n, \tag{6.10}$$

where ψ_n are the eigenfunctions of the self-adjoint Fokker-Planck operator $\mathscr{L}$ corresponding to the eigenvalue λ_n. We denote the eigenvectors of the Fokker-Planck operator $\mathscr{L}_{FP}$ by $\phi_n(x)$ having the same eigenvalues λ_n, and are related to $\psi_n(x)$ as

$$\psi_n(x) = e^{\frac{U(x)}{2}}\phi_n(x). \tag{6.11}$$

The eigenvalues λ_n follow the order: $\lambda_1 = 0 > \lambda_2 > \lambda_3 \ldots$, where $\lambda_1 = 0$ corresponds to the stationary distribution for a bath temperature, T_b. The first eigenvector corresponding to $\lambda_1 = 0$ is given by $\psi_1(x) = e^{-U(x)/2}/\sqrt{\mathscr{Z}(T_b)}$.

Given the initial probability condition $p(x',0)$, the probability distribution function $p(x,t)$ can be obtained as

$$p(x,t) = \int W(x,t|x',0)p(x',0)dx', \tag{6.12}$$

where the transition probability or the propagator $W(x,t|x',0)$ of the Fokker-Planck equation can be written in terms of the eigenfunctions and eigenvalues (see [92, 94])

$$\begin{aligned} W(x,t|x',0) &= e^{\mathscr{L}_{FP}t}\ \delta(x-x') \\ &= e^{-\frac{U(x)}{2}+\frac{U(x')}{2}}\sum_n e^{\lambda_n t}\psi_n(x)\psi_n^*(x'). \end{aligned} \tag{6.13}$$

Substituting the transition probability into Eq. (6.12), one finds

$$p(x,t) = \int dx' e^{-\frac{U(x)}{2}+\frac{U(x')}{2}}\sum_n e^{\lambda_n t}\psi_n(x)\psi_n^*(x')p(x',0). \tag{6.14}$$

Since $\lambda_1 = 0$, we can write Eq. (6.14) for the probability density as

$$p(x,t) = \frac{e^{-U(x)}}{\mathscr{Z}(T_b = 1)} + \sum_{n \geq 2} a_n e^{\frac{-U(x)}{2}} \psi_n(x) e^{-|\lambda_n| t}, \tag{6.15}$$

where

$$a_n = \int dx p(x,0) e^{\frac{U(x)}{2}} \psi_n^*(x). \tag{6.16}$$

At large times, since $\lambda_2 > \lambda_3$, to leading order, we obtain

$$p(x,t) \simeq \frac{e^{-U(x)}}{\mathscr{Z}(T_b)} + a_2 e^{\frac{-U(x)}{2}} \psi_2(x) e^{-|\lambda_2| t},\ t \gg \frac{1}{|\lambda_3|}. \tag{6.17}$$

The equation above is central to further analysis of the relaxation properties for the particle in the potential $U(x)$.

6.2.2 Shape of the potential

The form of the potential well is crucial to the observation of the Mpemba effect as was demonstrated in the experiment [4]. In there, $U(x)$ is considered to be a double well quartic potential with linear slopes near its boundaries or domain walls. Furthermore, the potential is confined in an asymmetric domain and it was shown that the asymmetry in the widths of the left and right domains about the origin can lead to the Mpemba effect [4].

Likewise, we consider a double well potential which is piece-wise linear. In contrast to the quartic double well potential, this problem is exactly solvable as will be evident below. The boundaries of the well are situated at $(-x_{min}, x_{max})$. The potential in Fig. 6.1 can be quantified in the following way

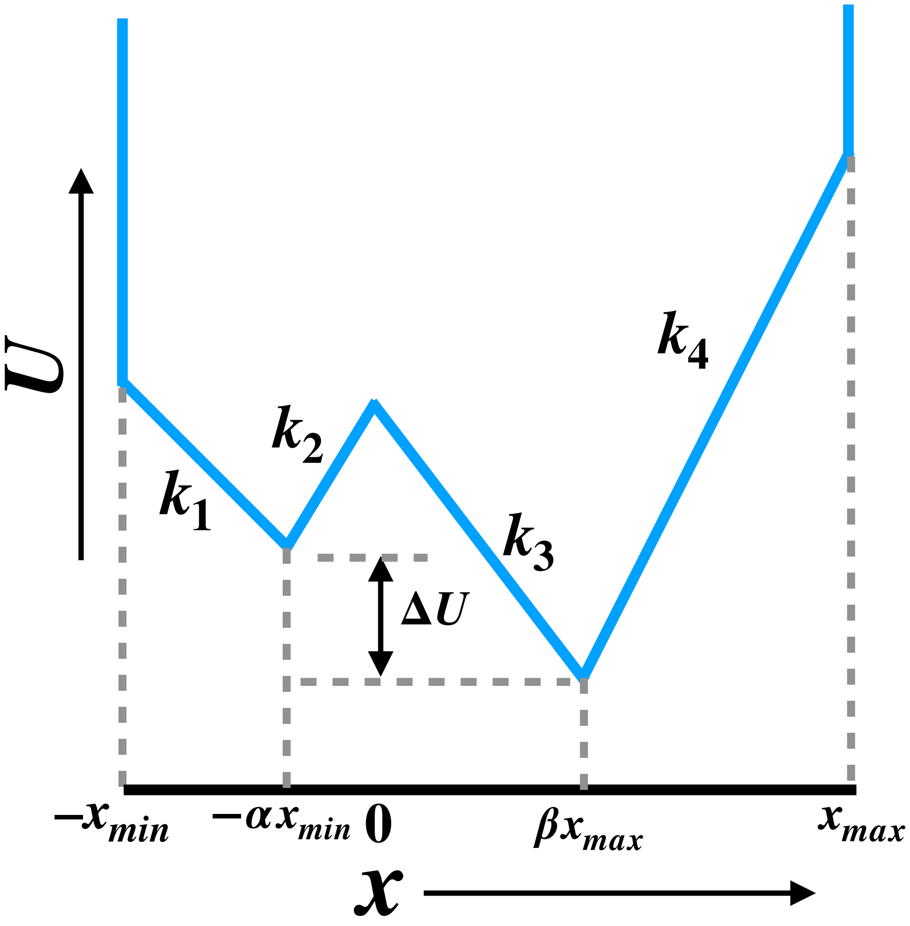

Figure 6.1: Schematic diagram of the piecewise linear double well potential. The boundaries of the potential are situated at $-x_{min}$ and x_{max}. The two minima of the double well potential are located at $-\alpha x_{min}$ and βx_{max}, where $\alpha, \beta \in (0,1)$. The parameters k_1, k_2, k_3 and k_4 refer to the various slopes. ΔU depicts the difference in the depths of the two wells.

$$U(x) = \begin{cases} -k_1 x, & -x_{min} < x < -\alpha x_{min} \\ k_2 x + \alpha(k_1 + k_2)x_{min}, & -\alpha x_{min} < x < 0 \\ -k_3 x + \alpha(k_1 + k_2)x_{min}, & 0 < x < \beta x_{max} \\ k_4 x + [\alpha(k_1 + k_2) - \beta(k_3 + k_4)]x_{max}, & \beta x_{max} < x < x_{max}, \end{cases} \tag{6.18}$$

where k_1, k_2, k_3 and k_4 are slope constants that play a crucial role in designating the potential various shapes and the two constants $\alpha, \beta \in (0,1)$.

The asymmetry in the shape of the potential can be introduced through various parameters such as different domain widths (changing x_{min} and x_{max}) about the origin, different positions of the two wells (changing α and β) about the origin or due to the different depths (ΔU) of the potential wells. Thus, out of the many parameters in the model of the potential, only the five parameters $x_{min}, x_{max}, \alpha, \beta$ and ΔU are independent. The various possibilities of asymmetry in terms of the five independent parameters will be explored in Sec. 6.5. More importantly, it turns out that the different heights of the two wells is a key factor to the observation of the Mpemba effect in contrast to the result shown in Ref. [4]. This potential set-up provides an amenable physical interpretation for underlying cause in such systems as will be discussed and illustrated in Sec. 6.4.

6.2.3 Jump conditions

The potential in Eq. (6.18) is not differentiable at $x = -\alpha x_{min}$, 0 and βx_{max}, and diverges at the boundaries $x = -x_{min}$ and $x = x_{max}$. Let x_- and x_+ denote the points just to the left and right of boundary of a linear segment. For the choice of potential $U(x_+) = U(x_-)$ while $U'(x_+) \neq U'(x_-)$. Across a boundary, both the probability currents are equal, i.e., $J(x_+,t) = J(x_-,t)$, as well as the probabilities are equal. Thus, from Eq. (6.5), we obtain

$$\begin{aligned}
&-U'(x_+)p(x_+,t) - \frac{\partial p(x_+,t)}{\partial x} = \\
&-U'(x_-)p(x_-,t) - \frac{\partial p(x_-,t)}{\partial x}. &\quad (6.19)\\
&p(x_+,t) = p(x_-,t). &\quad (6.20)
\end{aligned}$$

The jump conditions in Eqs. (6.19) and (6.20) are satisfied by each of the eigenfunctions, and hence from Eq. (6.14), we have

$$\psi_n'(x_+) + \frac{U'(x_+)\psi_n(x_+)}{2} = \psi_n'(x_-) + \frac{U'(x_-)\psi_n(x_-)}{2}, \tag{6.21}$$

$$\psi_n(x_+) = \psi_n(x_-). \tag{6.22}$$

At the boundaries, the potential diverges. This implies that the probability current must vanish and it leads to the following condition in terms of the eigenfunctions

$$\psi_n'(x) + \frac{U'(x)}{2}\psi_n(x) = 0, \text{ at } x = -x_{min},\ x_{max}. \tag{6.23}$$

The jump conditions [Eqs. (6.22), (6.21) and (6.23)] are utilized to solve the eigenspectrum of the Fokker-Planck operator $\mathscr{L}$ [see Eq. (6.10)] as discussed in the next section.

6.2.4 Eigenspectrum analysis

We need to solve the following eigenvalue problem for the Fokker-Planck operator

$$\mathscr{L}\psi_n = -|\lambda_n|\psi_n, \tag{6.24}$$

where ψ_n are the eigenfunctions of the self-adjoint Fokker-Planck operator $\mathscr{L}$ [see Eq. (6.8)] corresponding to the eigenvalue λ_n. We solve separately in each of the four domains of the potential $U(x)$, characterized by slopes k_1, k_2, k_3 and k_4. This will lead to eight constants of integration which will be determined by the jump conditions at the boundaries of the regions, leading to a transcendental equation for the eigenvalue.

(a) *Region I*: $-x_{min} < x < -\alpha x_{min}$ – Here, $U'(x) = -k_1$. Then, Eq. (6.24) takes the form:

$$\frac{d^2\psi_n^I}{dx^2} + \left(\lambda_n - \frac{k_1^2}{4}\right)\psi_n^I = 0, \tag{6.25}$$

which has the solution

$$\psi_n^I(x) = A_n \sin(m_{1n}x) + B_n \cos(m_{1n}x), \tag{6.26}$$

where A_n, B_n are constants and

$$m_{1n} = \sqrt{\lambda_n - \frac{k_1^2}{4}}. \tag{6.27}$$

The solutions for the eigenfunctions in the other regimes are similar, but with different constants. We list them below.

$(\boldsymbol{b})$ *Region II*: $-\alpha x_{min} < x < 0$ –

$$\psi_n^{II}(x) = C_n \sin(m_{2n}x) + D_n \cos(m_{2n}x), \tag{6.28}$$

where

$$m_{2n} = \sqrt{\lambda_n - \frac{k_2^2}{4}}. \tag{6.29}$$

$(\boldsymbol{c})$ *Region III*: $0 < x < \beta x_{max}$ –

$$\psi_n^{III}(x) = E_n \sin(m_{3n}x) + F_n \cos(m_{3n}x), \tag{6.30}$$

where

$$m_{3n} = \sqrt{\lambda_n - \frac{k_3^2}{4}}. \tag{6.31}$$

$(\boldsymbol{d})$ *Region IV*: $\beta x_{max} < x < x_{max}$ –

$$\psi_n^{IV}(x) = G_n \sin(m_{4n}x) + H_n \cos(m_{4n}x), \tag{6.32}$$

where

$$m_{4n} = \sqrt{\lambda_n - \frac{k_4^2}{4}}. \tag{6.33}$$

We now determine the different constants using the matching and boundary conditions.

(e) **Boundary condition at** x_{max}: Since there is an infinite jump in potential at $x = x_{max}$, the boundary condition in terms of eigenfunctions ψ_n is given by

$$\psi_n^{IV\prime}(x_{max}) + \frac{U_4'(x_{max})}{2}\psi_n^{IV}(x_{max}) = 0. \tag{6.34}$$

Substituting for ψ_n^{IV} from Eq. (6.32), we obtain

$$\begin{aligned} G_n &= -\nu_{4n}H_n, & (6.35)\\ \nu_{4n} &= \frac{\frac{k_4}{2}\cos(m_{4n}x_{max}) - m_{4n}\sin(m_{4n}x_{max})}{\frac{k_4}{2}\sin(m_{4n}x_{max}) + m_{4n}\cos(m_{4n}x_{max})}. & (6.36) \end{aligned}$$

Thus,

$$\psi_n^{IV}(x) = H_n\left[\cos(m_{4n}x) - \nu_{4n}\sin(m_{4n}x)\right]. \tag{6.37}$$

(f) **Boundary condition at** $-x_{min}$: Since there is an infinite jump in potential at $x = -x_{min}$, the boundary condition in terms of eigenfunctions ψ_n is given by

$$\psi_n^{I\prime}(-x_{min}) + \frac{U_1'(-x_{min})}{2}\psi_n^{I}(-x_{min}) = 0. \tag{6.38}$$

Substituting for ψ_n^{I} from Eq. (6.26), we obtain

$$\begin{aligned} A_n &= \nu_{1n}B_n, & (6.39)\\ \nu_{1n} &= \frac{\frac{k_1}{2}\cos(m_{1n}x_{min}) - m_{1n}\sin(m_{1n}x_{min})}{\frac{k_1}{2}\sin(m_{1n}x_{min}) + m_{1n}\cos(m_{1n}x_{min})}. & (6.40) \end{aligned}$$

Thus,

$$\psi_n^{I}(x) = B_n\left[\cos(m_{4n}x) + \nu_{1n}\sin(m_{4n}x)\right]. \tag{6.41}$$

(g) **Matching condition at** $x = -\alpha x_{min}$: Here, we use the jump conditions obtained from the continuity of the probability current[see Eqs. (6.21) and (6.22)], at $x = -\alpha x_{min}$. On simplification, we obtain

$$-C_n \sin(m_2\alpha x_{min}) + D_n \cos(m_2\alpha x_{min}) = B_n[\cos(m_1\alpha x_{min}) - \nu_{1n}\sin(m_1\alpha x_{min})]. \quad (6.42)$$

$$\begin{aligned} &C_n\Big[m_2\cos(m_2\alpha x_{min}) - \frac{k_2}{2}\sin(m_2\alpha x_{min})\Big] + D_n\Big[m_2\sin(m_2\alpha x_{min}) + \frac{k_2}{2}\cos(m_2\alpha x_{min})\Big] \\ &= B_n\Big[(m_1\nu_{1n} - \frac{k_1}{2})\cos(m_1\alpha x_{min}) + (m_1 + \frac{\nu_{1n}k_1}{2})\sin(m_1\alpha x_{min})\Big]. \end{aligned} \quad (6.43)$$

The coefficients C_n and D_n are solved using Eqs. (6.42) and (6.43) in terms of B_n and the expressions are given by

$$\begin{aligned} C_n =& \frac{B_n}{2m_2}\Big[-\Big((k_1+k_2-2m_1\nu_{1n})\cos(m_2\alpha x_{min}) + 2m_2\sin(m_2\alpha x_{min})\Big)\cos(m_1\alpha x_{min}) \\ &+ \Big(((k_1+k_2)\nu_{1n}+2m_1)\cos(m_2\alpha x_{min}) + 2m_2\nu_{1n}\sin(m_2\alpha x_{min})\Big)\sin(m_1\alpha x_{min})\Big], \end{aligned} \quad (6.44)$$

$$\begin{aligned} D_n =& \frac{B_n}{2m_2}\cos(m_2\alpha x_{min})\Big[\Big(-2m_2\nu_{1n} + (2m_1+(k_1+k_2)\nu_{1n})\tan(m_2\alpha x_{min})\Big)\sin(m_1\alpha x_{min}) \\ &+ \Big(2m_2 - (k_1+k_2-2m_1\nu_{1n})\tan(m_2\alpha x_{min})\Big)\cos(m_1\alpha x_{min})\Big]. \end{aligned} \quad (6.45)$$

(h) **Matching condition at** $x = 0$: Similar to above, using the jump conditions Eqs. (6.21) and (6.22) at $x = 0$, we obtain

$$E_n = \frac{m_2}{m_3}C_n + \frac{k_2+k_3}{2m_3}D_n, \quad (6.46)$$

$$F_n = D_n. \quad (6.47)$$

(i) **Matching condition at** $x = \beta x_{max}$: Using the jump conditions Eqs. (6.21) and (6.22) at $x = \beta x_{max}$, we obtain

$$\begin{aligned}
& C_n \frac{m_2}{m_3} \sin(m_3 \beta x_{max}) \\
& + D_n \Big(\frac{k_2 + k_3}{2m_3} \sin(m_3 \beta x_{max}) + \cos(m_3 \beta x_{max}) \Big) \\
& = H_n \Big[\cos(m_4 \beta x_{max}) - \nu_{4n} \sin(m_4 \beta x_{max}) \Big],
\end{aligned} \tag{6.48}$$

and

$$\begin{aligned}
& C_n \Big[m_2 \cos(m_3 \beta x_{max}) - \frac{k_3}{2} \frac{m_2}{m_3} \sin(m_3 \beta x_{max}) \Big] \\
& + D_n \Big[\frac{k_2}{2} \cos(m_3 \beta x_{max}) \\
& - \Big(m_3 + \frac{k_3 (k_2 + k_3)}{4m_3} \Big) \sin(m_3 \beta x_{max}) \Big] \\
& = H_n \Big[\Big(\frac{k_4}{2} - \nu_{4n} m_4 \Big) \cos(m_4 \beta x_{max}) \\
& - \Big(\frac{\nu_{4n} k_4}{2} + m_4 \Big) \sin(m_4 \beta x_{max}) \Big].
\end{aligned} \tag{6.49}$$

The coefficients C_n and D_n are solved in terms of H_n using Eqs. (6.48) and (6.49) and the expressions are given by

$$\begin{aligned}
C_n = {} & \frac{-8m_3^2 H_n}{m_2[k_2^2 - k_3^2 + 8m_3^2 + (k_3^2 - k_2^2)\cos(2m_3\beta x_{max})]} \\
& \times \Bigg[\Big[\frac{k_2}{2}\cos(m_3\beta x_{max}) - \big(m_3 + \frac{k_2(k_2+k_3)}{4m_3}\big)\sin(m_3\beta x_{max})\Big] \\
& \quad \Big[\cos(m_4\beta x_{max}) - \nu_{4n}\sin(m_4\beta x_{max})\Big] \\
& \quad - \Big[\frac{1}{2}\cos(m_3\beta x_{max}) + \frac{k_2+k_3}{4m_3}\sin(m_3\beta x_{max})\Big] \\
& \quad \Big[(k_4 - 2m_4\nu_{4n})\cos(m_4\beta x_{max}) - (2m_4 + \nu_{4n}k_4)\sin(m_4\beta x_{max})\Big]\Bigg],
\end{aligned} \tag{6.50}$$

$$\begin{aligned}
D_n = {} & \frac{4m_3 H_n}{k_2^2 - k_3^2 + 8m_3^2 + (k_3^2 - k_2^2)\cos(2m_3\beta x_{max})} \times \\
& \Bigg[2m_3\cos(m_3\beta x_{max})\Big[\cos(m_4\beta x_{max}) - \nu_{4n}\sin(m_4\beta x_{max})\Big] \\
& + \sin(m_3\beta x_{max})\Big[(2m_4 + (k_3+k_4)\nu_{4n})\sin(m_4\beta x_{max}) - (k_3 + k_4 - 2m_4\nu_{4n})\cos(m_4\beta x_{max})\Big]\Bigg].
\end{aligned} \tag{6.51}$$

Now, we consider the ratios of Eqs. (6.44), (6.45), (6.50) and (6.51) that form a transcendental equation to solve for the eigenvalues λ_n. Thus, solving for the eigenvalues λ_n in turn helps to find the constants A_n, B_n, C_n, D_n, E_n, F_n and H_n.

6.3 Distance function and the Mpemba effect

How to quantify the Mpemba effect as an anomalous relaxation phenomena? To see this, let us consider two systems: first one P, initially equilibrated at temperature T_h and second one Q, initially equilibrated at temperature T_c where $T_h > T_c$. These initial equilibrium distributions are denoted by $\pi(T_h)$ and $\pi(T_c)$ respectively. Now imagine that both P and Q are quenched at once to a common bath temperature, T_b, where $T_h > T_c > T_b$. Eventually, both of them will equilibrate to the common distribution $\pi(T_b)$ given long enough time. The Mpemba effect is said to exist if P equilibrates faster than Q during the transient/relaxation process.

To quantify this relaxation process, let us now define the *distance from equilibrium function*, $D[p(t),\pi(T_b)]$ which measures the instantaneous distance of a distribution $p(x,t)$ from the final equilibrium Boltzmann distribution, $\pi(T_b)$. It has been argued (see [11, 4]) that the Mpemba effect is independent of $D[p(t),\pi(T_b)]$ provided that the distance measure obeys the following properties: (a) If $T_h > T_c > T_b$, then the distance from equilibrium function should follow the order $D[\pi(T_h),\pi(T_b)] > D[\pi(T_c),\pi(T_b)]$, (b) $D[p(t),\pi(T_b)]$ should be a monotonically non-increasing function of time, and (c) $D[p(t),\pi(T_b)]$ should be a convex function of $p(x,t)$.

Notably, there are many well-adapted measures that exist in the literature namely the entropic distance, L_1 or norm distance and the Kullback-Leibler (KL) divergence [11, 4, 14]. Thus, as a working definition, if one has $D[\pi(T_h),\pi(T_b)] > D[\pi(T_c),\pi(T_b)]$ initially for $T_h > T_c$ followed by $D[p^h(t),\pi(T_b)] < D[p^c(t),\pi(T_b)]$ at a later time, we will state that the Mpemba effect exists.

In the rest of the chapter, we will use the L_1 or norm measure for the distance from equilibrium function. More precisely, this is defined as

$$D[p(t),\pi(T_b)] \equiv L_1(t) = \int dx |p(x,t) - \pi(x,T_b)|. \tag{6.52}$$

Now substituting the form of $p(x,t)$ from Eq. (6.17) into the above equation, we find

$$D[p(t),\pi(T_b)] = \sum_{n\geq 2} |a_n e^{\frac{-U(x)}{2}} \psi_n(x)| e^{-|\lambda_n|t}. \tag{6.53}$$

The condition for the Mpemba effect, as mentioned above, now boils down to

$$|a_2(T_c)| \equiv |a_2^c| > |a_2^h| \equiv |a_2(T_h)| \,. \tag{6.54}$$

The condition demands that $|a_2(T)|$ should have a non-monotonic behavior with the increase in temperature. Note that the coefficient a_2 is calculated using Eq. (6.16) and is a function only of the initial temperature and the bath temperature. Also, $a_2(T)$ is zero at the final temperature $T = T_b$ since the eigenvectors are orthonormal.

6.4 Modulation of the potential and population – connection to the experiments

Following the colloidal experiment by Kumar and Bechhoefer, we learnt that the asymmetry in the shape of the double well potential plays an important role to the Mpemba effect. In particular, it was shown that there is no such effect if the asymmetry in the width of the left and right domains of the potential vanishes [4]. In this section, we aim to revisit these limits from our model system by suitably changing the potential barrier.

To this end, let us turn our attention to Figs. 6.2(a) and 6.2(c) which show two different configurations for the potential barrier. The modulation of the potential barrier leads to a rearrangement in the population of the Brownian particle between the two wells for the two different temperatures as shown in Fig. 6.2(b) and 6.2(d).

In Fig. 6.2(a), we consider a configuration of a potential with a considerable potential barrier between the two minima. The corresponding population distribution of the Brownian particle for the temperatures T_h, T_c and T_b, i.e., for the hot, cold and the bath temperatures respectively is shown in Fig. 6.2(b). The initially colder system is more populated in the lowest well compared to the initially hotter system. However, there is also a considerable amount of population distributed in the metastable state for the colder system, which is not the case for the initially hotter system whose population distribution is nearly uniform i.e., it can not really 'see' the metastable state. As a result, post quenching, the population distribution of the colder system takes a significant amount of time to rearrange and

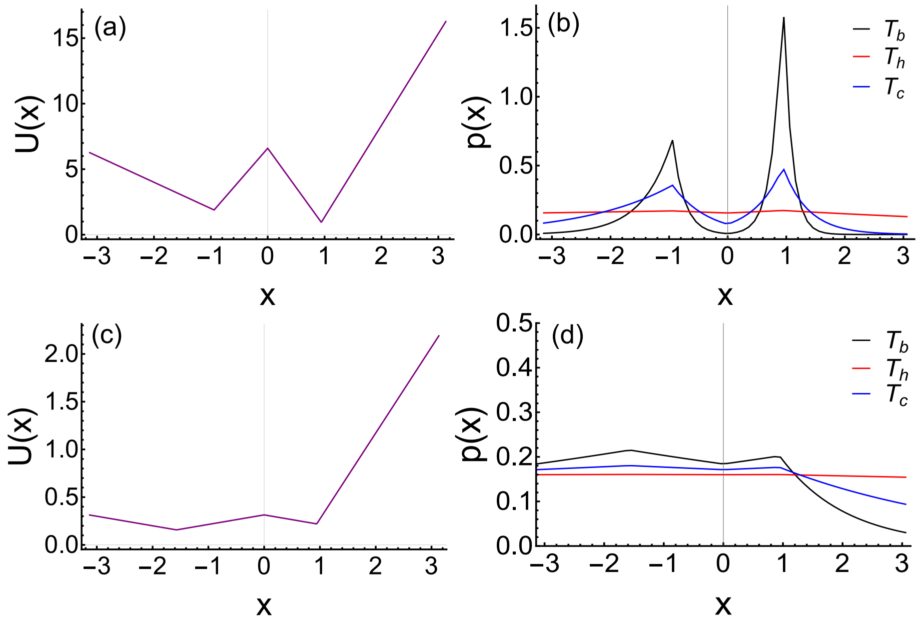

Figure 6.2: Modulation of the potential and its effect on the population distribution of the Brownian particle in the two wells. Panel (a) and (c) corresponds to different configurations of the potential well. The parameters of the potential in (a) are chosen to be $\alpha = 0.3$, $\beta = 0.3$, $x_{min} = \pi$, $x_{max} = \pi$, $k_1 = 2$, $k_2 = 5$, $k_3 = 6$ and $k_4 = 7$ and in (c) $\alpha = 0.5$, $\beta = 0.3$, $|x_{min}| = \pi$, $x_{max} = \pi$, $k_1 = 0.1$, $k_2 = 0.1$, $k_3 = 0.1$ and $k_4 = 0.9$. Panels (b) and (d) depict the population distribution corresponding to the external potentials in (a) and (c) respectively for the initial temperatures T_h (red), T_c (blue) and final temperature T_b (black) with $T_h > T_c > T_b$.

eventually relax to the lowest energy well from the metastable state. On the other hand, the initially hotter system ends with a higher population in the lowest well due to its fast relaxation. This feature grants an advantage to the initially hotter system over the colder one, and the Mpemba effect is observed.

Next, we consider the potential shown in Fig. 6.2(c), where the potential barrier between the two minima is almost diminishing thus creating a flat barrier between the wells. In this case, the population distribution at the bath temperature, T_b which corresponds to the final equilibrium state, is almost equally populated between the two wells. Moreover, not much difference can be seen in the population distribution of the initially hot and the cold system. In other words, the 'hindrance' due to the metastable state in the relaxation to the equilibrium state is absent. Owing to this, the relaxation process is similar for the both initially hot and the cold system. The initially colder system (having distribution closer to the final equilibrium state) relaxes faster compared to the initially hot system and hence, no Mpemba like effect is observed.

The above physical scenarios naturally set the stage to make the connection with the experiment [4]. In particular, the asymmetry in the widths of the left and right domains of the confined potential in the experiment plays an analogous role to a finite barrier height between the wells in our model set-up. As we have shown that this configuration leads to the Mpemba effect similar to the asymmetric domain for the left and the right well of the potential in the experiment.

On the other hand, the symmetric double well potential configuration in the experiment with equal widths for the left and right domains is analogous to our second case with almost a flat barrier between the two wells of the potential [see Figs. 6.2(c) and (d)]. It is because the symmetric potential configuration has the population of the particle almost similarly distributed between the two wells of the potential for any temperatures eliminating the effect of the presence of any metastable state. As a result, the relaxation dynamics from an initial equilibrium distribution to the final equilibrium are similar for any temperature, and the initially cold system having an initial temperature closer to the final equilibrium state relaxes faster. Hence, no Mpemba effect can be seen. These two possible configurations thus draw physical similarities between the experiment and our system.

6.5 Mpemba effect in double well potential

In this section, we showcase several key configurations of the double well potential that can lead to the Mpemba effect. These results are analyzed based on the generic criterion for the Mpemba effect as described in Sec. 6.3. The methodology we use is as follows. Given a configuration of the potential, we solve the eigenvalue Eq. (6.24) to find the eigenspectrum. Once this is known, we can immediately compute the time dependent solution for the probability distribution using Eq. (6.15). This allows us to understand the relaxation process by looking at the slowest eigenvalue. Next, we analyze the Mpemba condition namely $|a_2^c| > |a_2^h|$ (see Sec. 6.3). Specifically, this condition is scanned thoroughly to identify the set of initial temperatures for which $|a_2(T)|$ has a non-monotonic behavior with temperature T so that the above-mentioned inequality is satisfied. We provide phase diagrams spanning in the parameter space of ΔU (will be discussed in the later part) and temperature ratio to underpin the desired regimes for the Mpemba effect. We make an attempt to provide physical reasoning behind all the possible cases.

It is now understood from the discussion in Sec. 6.4 that a fully symmetric potential configuration does not lead to the Mpemba effect. In what follows, we first consider an asymmetric potential configuration. This includes equal widths for the left and right domains and equal heights at the left, center, and right edges of the potential. The only asymmetry is in the form of different depths between the two potential wells. We show in Sec. 6.5.1 that the mere presence of asymmetry in the potential configuration is *not a sufficient* condition to induce the Mpemba effect. To explore further, we take other configurations that have restricted asymmetries.

This is done by keeping different heights at the left, center, and right edge of the potential. We carefully analyze these different configurations and explore the possibility of the Mpemba effect. The following configurations are of our interest: (a) equal domain widths ($x_{max} = x_{min}$) as discussed in Sec. 6.5.2, and (b) unequal domain widths ($x_{max} \neq x_{min}$) as discussed in Sec. 6.5.3. For both cases (a) and (b), we explore the different possible configurations by varying the depths of the potential wells (ΔU) and also for different positions of the wells characterised by α and β.

6.5.1 Asymmetry is not a sufficient criterion

We start by showing that the asymmetry is not a sufficient condition for the existence of the Mpemba effect. As an example, we consider the case where the asymmetry is only in terms of different depths of the potential wells while keeping everything else symmetric, as shown in Fig. 6.3(a). The heights of the left, centre and right edges of the potential well are equal. Moreover, the potential minima are also situated symmetrically about the origin and at the centre of their respective domains. For this case, there is no Mpemba effect since $|a_2(T)|$ increases monotonically with T [see Fig. 6.3(b)]. As discussed in Sec. 6.4, the absence of the Mpemba effect can be explained based on the similar nature of the initial population distribution of the hot and the cold system for a particular choice of T_h and T_c respectively, as shown in the inset of Fig. 6.3(b), leading to similar relaxations for both the systems.

Hence, one would anticipate that additional asymmetries might be required in the potential configuration to induce the Mpemba effect. However, we find that as long as the potential heights at the left, center, and right edges are equal, there is no Mpemba effect. In what follows, further asymmetric configurations are explored by considering the cases of equal and unequal domain widths and also varying the depths between the two wells

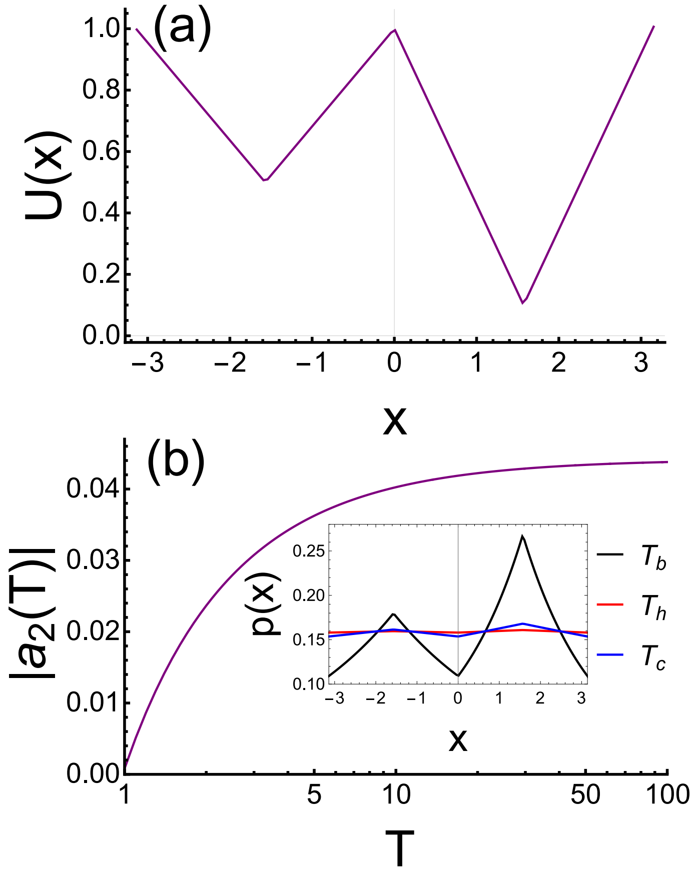

Figure 6.3: Illustration of the absence of the Mpemba effect in an asymmetric double well potential indicating that *asymmetry is not sufficient*. (a) Asymmetric shape of the potential with different depths for the left and right wells while keeping all the other parameters of the potential symmetric about the origin. The potential heights at its left, center and right edges are equal and so are the positions of the two wells about the origin. The shape of the potential corresponds to the choice of the parameters $x_{max} = x_{min} = \pi$, $\alpha = \beta = 0.5$, $k_1 = k_2 = 0.32$ and $k_3 = k_4 = 0.57$. (b) Monotonic evolution of $|a_2(T)|$ with T showing the absence of the Mpemba effect. Inset: Initial population distribution of the confined Brownian particle for the chosen temperatures $T_h = 50$ (red) and $T_c = 10$ (blue) showing almost similarly distributed populations across the potential landscape. The final equilibrium distribution (black) corresponds to bath temperature $T_b = 1$.

of the potential while satisfying the necessary condition that the heights at the left, center, and right edges of the potential are different.

6.5.2 Equal domain widths

We first examine the configurations of the potential with equal widths for the left and right domains. The boundaries of the well are situated at $x_{min} = x_{max}$ with the position of the two wells equidistant from the origin at $x = -\alpha x_{min}$ and $x = \beta x_{max}$ with $\alpha = \beta$. The various asymmetries in the configuration of the potential are introduced through the choice of the slopes k_1, k_2, k_3 and k_4 for the different domains of the confined potential. The shape of the potential with a specific choice of parameters is shown in Fig. 6.4(a).

The existence of the Mpemba effect for this particular configuration of the potential is evident from the non-monotonic behavior of the coefficient $|a_2(T)|$ with T as shown in Fig. 6.4(b). The existence of the Mpemba effect for this configuration of the potential is also qualitatively evident in terms of the population distribution of the particle as shown in the inset of Fig. 6.4(a) for $T_h = 1000$ and $T_c = 7$ which satisfy the criteria for the Mpemba effect. The population distribution of the initially cold system is localised at the intermediate potential well, thus experiencing a metastable state which leads to its slower relaxation towards the final equilibrium. On the other hand, the initially hot system has uniform distribution across the potential landscape and undergoes faster relaxation to the final equilibrium distribution.

We next explore the phase space that shows the Mpemba effect, for this form of potential configuration in terms of various asymmetries. It is done by varying the depths between the two wells of the potential landscape ΔU [see Fig. 6.4(a)] as a function of the temperature of the initially hot system T_h while keeping the temperature of the initially cold system fixed at $T_c = 4$. Changing the depths of the two wells is equivalent to making choices for different possibilities of the slopes k_1, k_2, k_3, and k_4. Figures 6.5(a) and (b)

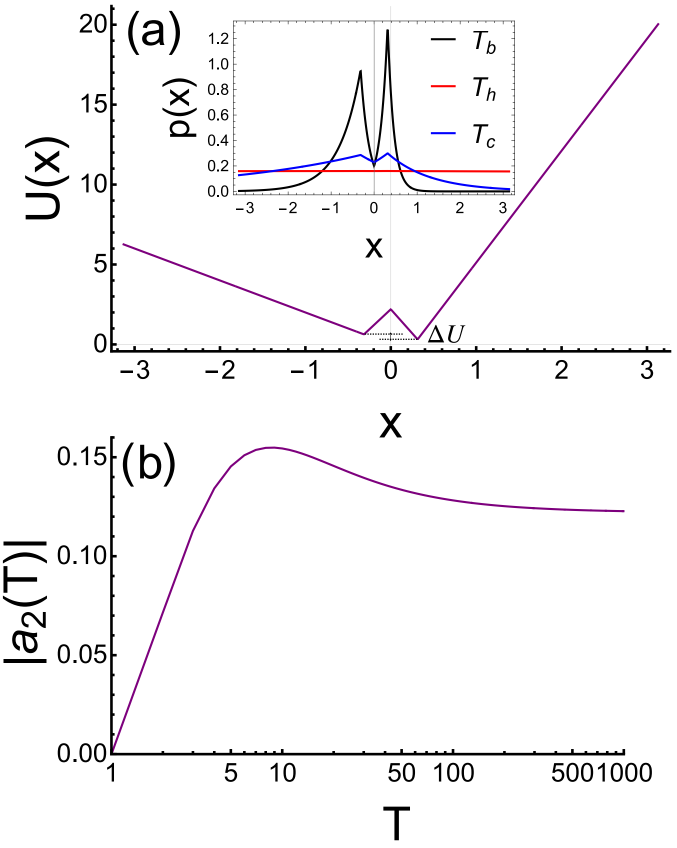

Figure 6.4: Illustration of the Mpemba effect in a confined double well potential with equal domain widths. (a) Shape of the potential with equal domain widths (3 units) about the origin. The asymmetry in the potential configuration is introduced through the choice of different slopes in separate domains. The configuration of the potential is determined by the choice of the parameters: $x_{max} = x_{min} = \pi$, $\alpha = \beta = 0.1$, $k_1 = 2$, $k_2 = 5$, $k_3 = 6$ and $k_4 = 7$. Inset: Initial population distribution of the confined Brownian particle for the chosen temperatures $T_h = 1000$ (red) and $T_c = 7$ (blue) such that $|a_2^h| < |a_2^c|$. This shows a significant population distribution for T_c around the metastable state compared to that (which is almost flat) of T_h. The final equilibrium distribution (black) corresponds to bath temperature $T_b = 1$. (b) Non-monotonic evolution of $|a_2(T)|$ with T clearly indicates the presence of the Mpemba effect in this set-up.

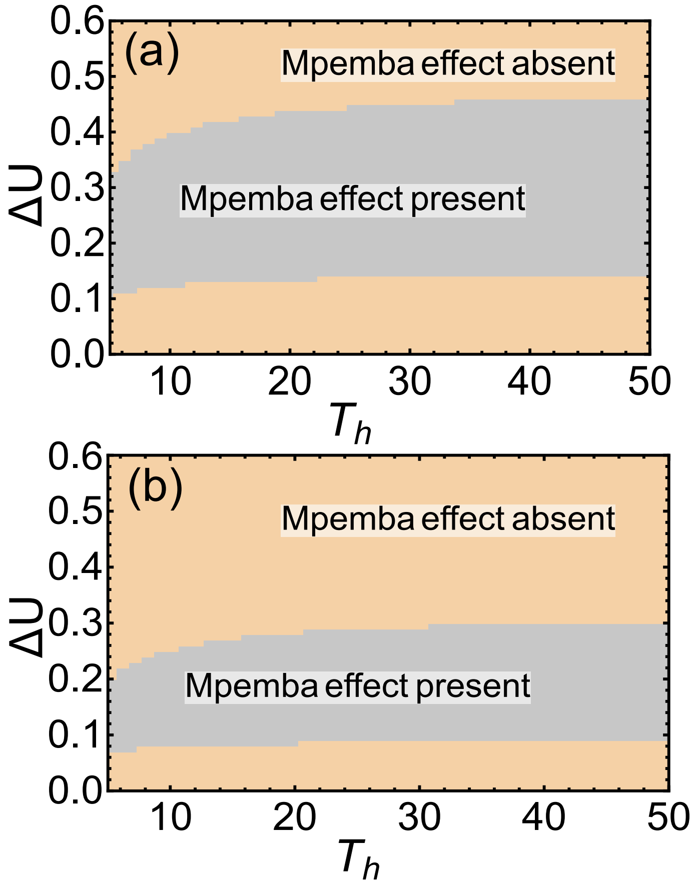

Figure 6.5: ΔU-T_h phase diagram illustrating the region of the Mpemba effect in the case of double well potential with equal domain widths. The phase diagram is obtained by varying the depth of the right well of the potential while keeping the depth of its left well fixed and by changing the temperature ratio. The phase space is partitioned into two domains: one where the Mpemba effect is present corresponding to the criteria $|a_2^h| < |a_2^c|$, and other complementary region. The phase diagrams correspond to different choices of the position of the potential wells which are symmetric about the origin and are determined by: (a) $\alpha = \beta = 0.1$, (b) $\alpha = \beta = 0.5$.

illustrate the phase diagrams of the possible asymmetries in the potential configuration leading to the Mpemba effect, in the ΔU-T_h plane for two different choices of positions for the potential minima although symmetrically placed about the origin.

6.5.3 Unequal domain widths

We now consider the potential configurations with unequal domain widths and explore the phase space of various possible asymmetries that might demonstrate the Mpemba effect. This is motivated from Ref. [4] where potential with unequal domain widths was considered in order to study the Mpemba effect.

The unequal domain widths of the potential configuration correspond to the positions of its boundaries situated at x_{min} and x_{max} respectively with the magnitudes $x_{max} \neq x_{min}$. The positions of the left and the right wells are situated at $x = -\alpha x_{min}$ and $x = \beta x_{max}$ respectively from the origin with $\alpha = \beta$. For the simplicity of our analysis, the magnitude of the slopes k_1, k_2, k_3, and k_4 are kept equal for different domains. Thus, the only asymmetry in the potential is introduced through the choice of different domain widths of the confined potential, and one such configuration with a particular choice of parameters is shown in Fig. 6.6(a).

The non-monotonic behavior of the coefficient $|a_2(T)|$ with T as shown in Fig. 6.6(b) illustrates the existence of the Mpemba effect for this configuration of the potential. We consider one such pair of temperatures $T_h = 50$ and $T_c = 10$ for the hot and cold systems respectively that satisfy the criteria $|a_2^c| > |a_2^h|$ and study the nature of the population distribution of the particle for the particular case as shown in the inset of Fig. 6.6(a). Here too, the cold system exhibits localisation of its population distribution in the local minima leading to slower relaxation towards the final equilibrium compared to the hot system.

We now explore the phase space of possible asymmetries that leads to the Mpemba effect, for this form of potential configuration. Here, the asymmetries are introduced in terms of the choices of different slopes and different widths for the left and right domains. We explore the phase space by varying the depths between the two wells of the potential landscape ΔU [see Fig 6.6(a)] as a function of the temperature of the initially hot system T_h while keeping the temperature of the initially cold system fixed at $T_c = 4$. Note that the variation of the two well depths is equivalent to making different choices for the slopes of the potential. We perform this exercise for two different choices of widths for the right domain respectively keeping the width of the left domain fixed as illustrated in Figs. 6.7 (a) and (b) respectively. As mentioned earlier, the phase diagrams allow us to provide a

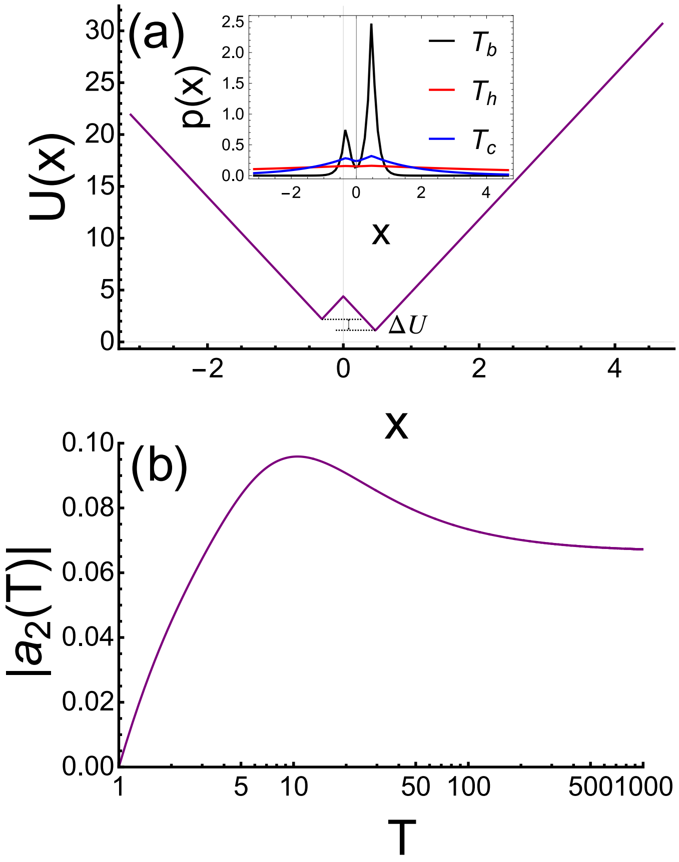

Figure 6.6: Illustration of the Mpemba effect in a confined double well potential with unequal domain widths while keeping every other parameters symmetric about the origin. (a) Shape of the potential with unequal domain widths ($x_{max} \neq x_{min}$) about the origin. The various slopes of the potential are kept equal. The configuration of the potential is determined by the choice of the parameters: $x_{min} = \pi$, $x_{max} = 1.5\pi$, $\alpha = \beta = 0.1$ and $k_1 = k_2 = k_3 = k_4 = 7$. Inset: Initial population distribution of the confined Brownian particle for the chosen temperatures $T_h = 50$ (red) and $T_c = 10$ (blue) such that $|a_2^h| < |a_2^c|$. This shows a significant population distribution around the metastable state for T_c compared to the same for T_h. The final equilibrium distribution (black) corresponds to the bath temperature $T_b = 1$. (b) Non-monotonic evolution of $|a_2(T)|$ with T confirms the presence of the Mpemba effect in this set-up.

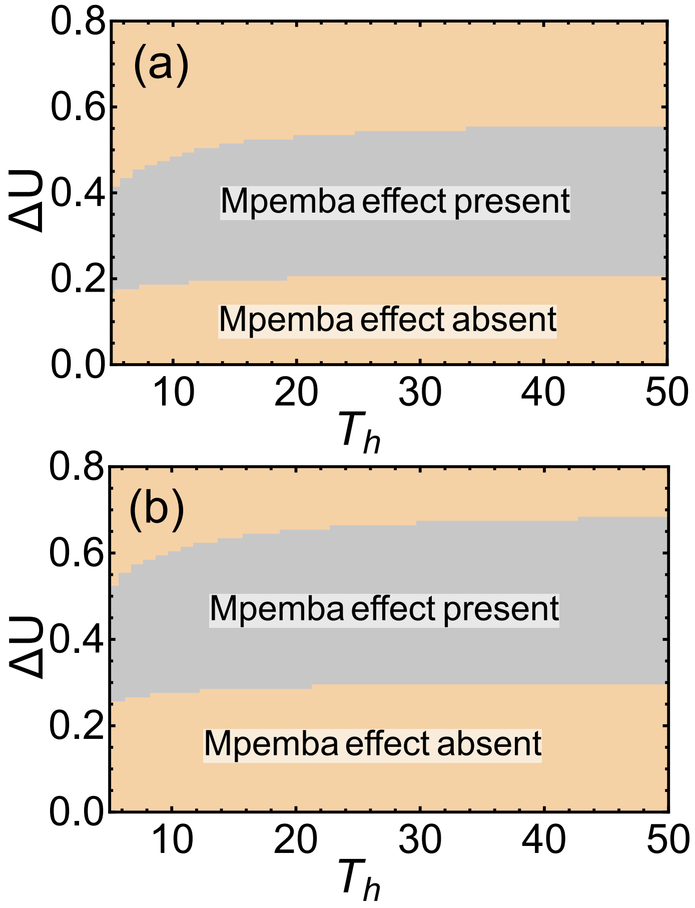

Figure 6.7: ΔU-T_h phase diagram illustrating the region of the Mpemba effect for the case of double well potential with unequal domain widths. The phase diagram is constructed in the similar manner as in Fig. (6.5). The phase diagrams in the left- and right- panel correspond to different choices of the widths for the right domain of the potential : (a) $x_{max} = 1.2\pi$, (b) $x_{max} = 1.5\pi$ keeping the width of its left domain fixed at $x_{min} = \pi$. The position of the two wells are determined by the parameters $\alpha = \beta = 0.1$ for both the cases.

comprehensive picture in terms of the parameters that are pertinent to the Mpemba effect.

6.6 Mpemba effect without a metastable minimum

In this section, we show that the presence of metastable states is not necessary for the existence of the Mpemba effect. We demonstrate this by configuring the potential with no metastable state. In a recent study, the Mpemba effect was shown for a piece-wise constant potential where the local stability of double well potential is replaced by neutral stability [13]. Likewise, we construct potential configurations with no metastable states and yet demonstrate the possibility of observing the Mpemba effect. In short, such an analysis would rationalize the claim that neither metastability nor neutral stability are necessary for the Mpemba effect.

Let us consider the single well potential with two linear slopes at the edges and with fixed magnitude in between $x = -\alpha x_{min}$ to $x = \beta x_{max}$ (see Fig. 6.8), where x_{min} and x_{max} are the boundaries where the potential goes to infinity. We find that the minimal criterion to observe the Mpemba effect in this configuration is to introduce an asymmetry in the form of different heights for the left and right edge of the potential landscape with $\alpha = \beta < 1$.

One such configuration of the potential is shown in Fig. 6.8(a). The existence of the Mpemba effect for this configuration is illustrated through the non-monotonic behavior of the coefficient $|a_2(T)|$ with temperature T – see Fig. 6.8(b). We consider one such pair of temperatures $T_h = 48$ and $T_c = 6$ for the initially hot and cold systems respectively that satisfy the criteria $|a_2^c| > |a_2^h|$ and study the nature of the population distribution of the Brownian particle for the particular case as shown in Fig. 6.8(c).

In the case of the double well potential configuration, the presence of a metastable state plays an important role in the existence of the Mpemba effect. Clearly, in this case, there is no delay in the redistribution of the populations to the final equilibrium distribution starting from two different temperatures due to the absence of any metastable state. However, the existence of the Mpemba effect for this configuration shows that there is a trade-off between the initial population density and kinetic energy of the particle in the redistribution process to the final equilibrium as evident from the population statistics near the edge of the potential landscape [see Fig. 6.8(c)].

Although the initially hot system has more population of the particles near the edge of the potential to redistribute than the same of the initially cold system, the higher kinetic energy of the hot system dominates during the relaxation process for the given configuration of the potential landscape, leading to a faster relaxation of the hot system than the cold one and hence the Mpemba effect is observed.

However, keeping the same configuration of the potential landscape and same temperatures for the initial hot and the cold system, we find that the anomalous relaxation disappears as the depth of the potential minimum is decreased as is illustrated in Fig. 6.8(d) and (e). It is evident from the monotonically increasing nature of the coefficient $|a_2(T)|$ with temperature, T [see Fig. 6.8(e)] that there is no Mpemba effect in this case. The population distribution of the particle for this configuration of the potential is shown in Fig. 6.8(f). A qualitative argument can be given based on the trade-off between the initial population density and kinetic energy of the particles present at the edges of the potential landscape. The presence of a smaller population for the initially cold system at the edges (which would eventually redistribute to the potential minimum) dominates in the relaxation process to the final equilibrium. Naturally, one would expect that the initially cold system will approach the final equilibrium faster than the initially hot system discarding the possibility of a Mpemba effect.

Finally, we explore the phase space of the single well potential landscape with the temperature ratio. We vary the minimum or the depth of the potential landscape ΔU measured with respect to the potential height at the left edge [see Figs. 6.8(a) and (d)] as a function of the temperature of the initially hot system T_h while keeping the temperature of the initially cold system fixed at $T_c = 4$. Figure 6.9 illustrates the phase diagram in the ΔU-T_h plane for a fixed choice of the heights for the left and right edge of the potential.

6.7 Illustration of the Mpemba effect in terms of distance measures

In this section, we illustrate that the existence of the Mpemba effect is indifferent to the choice of distance measures. We consider the case of the equal domain widths (see Sec. 6.5.2) with the parameters of the potential as in Fig. 6.4 where the Mpemba effect is shown to exist in terms of the criteria of $|a_2|$ for a wide range of initial temperatures.

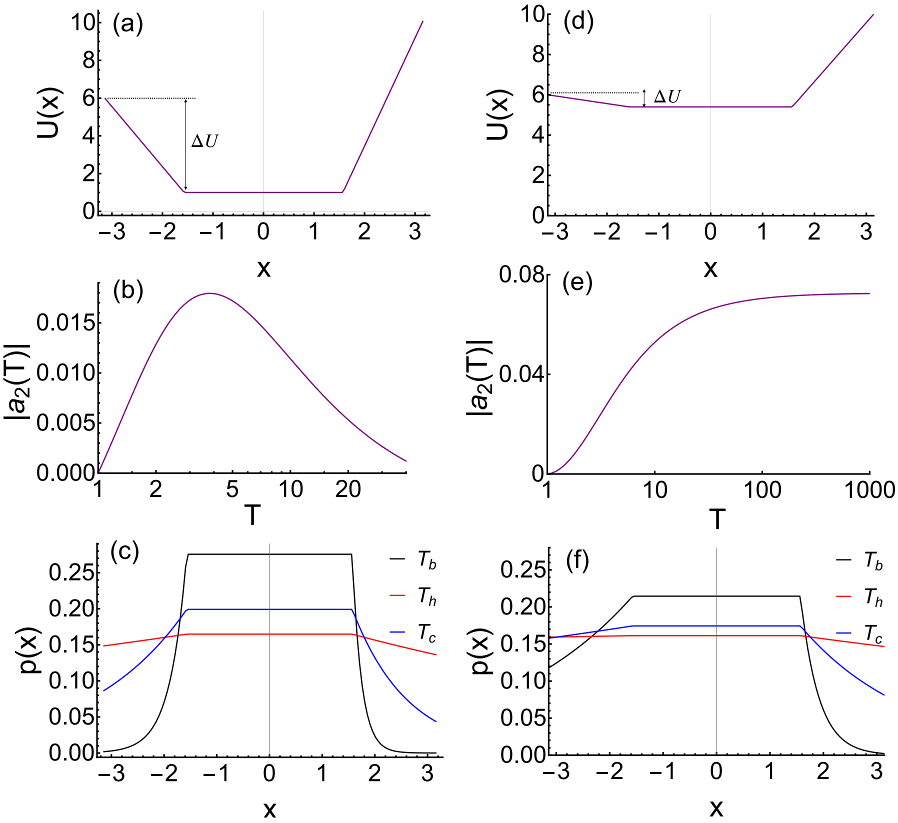

Figure 6.8: Illustration of the Mpemba effect in a confined single well potential with no metastable state. (a) Shape of the single well potential is determined by the choice of the parameters: $x_{max} = x_{min} = \pi$, $\alpha = \beta = 0.5$, $k_2 = k_3 = 0$, $k_1 = 3.18$ and $k_4 = 5.73$. (b) Non-monotonic evolution of $|a_2(T)|$ with T showing the presence of the Mpemba effect. (c) Initial population distribution of the confined Brownian particle for the chosen temperatures $T_h = 48$ (red) and $T_c = 6$ (blue). Here, $|a_2^h| < |a_2^c|$ which shows a significant difference in the population density at the minimum of the potential well. The final equilibrium distribution (black) corresponds to bath temperature $T_b = 1$. The Mpemba effect disappears for the above configuration of the potential if the depth of the potential well is decreased as shown in (d). The modified potential configuration corresponds to a change in the slopes to $k_1 = 0.38$ and $k_4 = 2.93$ while keeping the other parameters same as in the earlier case. (e) Monotonic evolution of $|a_2(T)|$ with T shows the absence of the Mpemba effect for the modified configuration. (f) Initial population distribution of the confined Brownian particle for the same pair of temperatures $T_h = 48$ (red) and $T_c = 6$ (blue) show nearly similar population distribution at the minimum of the potential well.

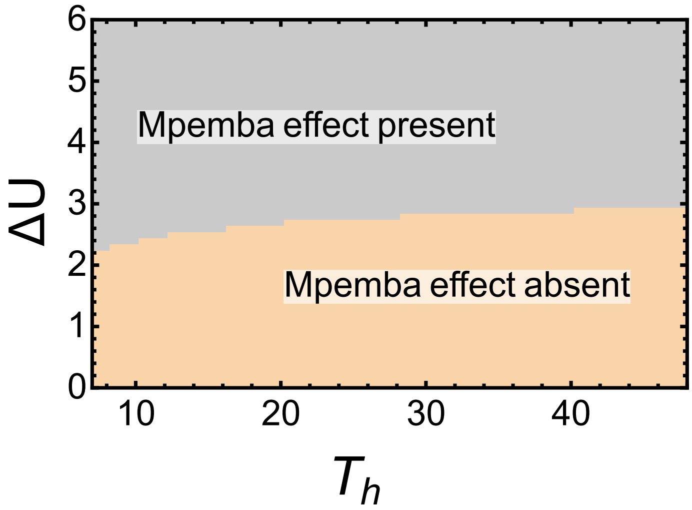

Figure 6.9: ΔU-T_h phase diagram illustrating the region of the Mpemba effect for the case of a single well potential. The phase diagram is obtained as before by varying the depth of the potential minimum & the temperature ratio. Here, there are two distinct regions and the criterion $|a_2^h| < |a_2^c|$ marks the one where the Mpemba is observed. Here, $T_c = 4$ as before and the other parameters determining the configuration of the potential are: $\alpha = \beta = 0.5$.

Here in Fig. 6.10, we illustrate the existence of the Mpemba effect in terms of two different measures, namely the norm, $L_1 = \int dx |p(x,t) - \pi(x, T_b)|$ and Kullback-Leibler divergence, $\mathrm{KL}(t) = \int dx p(x,t) \ln \left(p(x,t)/\pi(x, T_b)\right)$ for the same choice of the parameters and show that the effect is independent of the choice of the distance measures.

6.8 Conclusion

In summary, we have theoretically studied the Mpemba effect in a system of an overdamped particle trapped in an external potential motivated by a similar experimental setup [4]. The potential is generically piece-wise linear but double-welled, and moreover we can maneuver it to give various shapes. One can exactly solve this model analytically to obtain the eigenspectrum decomposition of the corresponding Fokker-Planck equation. This allows us to provide a comprehensive study of the Mpemba effect spanning a wide panorama of physical scenarios.

As noted earlier in [4] and in other works that symmetric potentials are not expected to

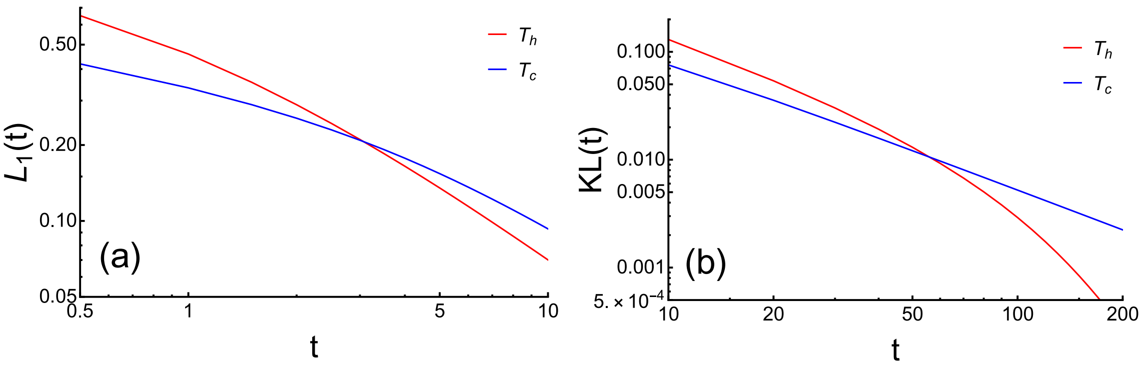

Figure 6.10: Illustration of the Mpemba effect in terms of the distance measures: the norm measure (L_1) in left panel (a) and Kullback-Leibler (KL) divergence measure in right panel (b). The configuration of the potential is the same as in Fig. 6.4 where it is determined by the choice of the parameters: $x_{max} = x_{min} = \pi$, $\alpha = \beta = 0.1$, $k_1 = 2$, $k_2 = 5$, $k_3 = 6$ and $k_4 = 7$. The temperatures of the initially hot and the cold systems are $T_h = 100$ and $T_c = 8$ respectively. Both the plots confirm the existence of the Mpemba effect.

exhibit the Mpemba effect. For symmetric potentials, a_2 is exactly zero and higher order coefficients become important. By explicit calculation, absence of the Mpemba effect was noted in piece-wise constant potential as well as the pure harmonic potential [13]. We expect the same to hold for symmetric piece-wise linear potentials. For the class of symmetric potentials that we explored, we did not find any exceptions. Asymmetry was introduced in the experiment in Ref. [4] through different domain widths for the two minima. We also demonstrate the existence of the Mpemba effect when the two widths are unequal. Through counterexamples, we also show that unequal domain widths are neither a necessary nor a sufficient condition for the Mpemba effect to be present. We also show that the Mpemba effect can be realized for equal domain widths but for other asymmetries in the potential. In particular, we find that the Mpemba effect is easily realizable when the heights of the potential at the left, center and right edges are different. This is a notable feature of our work.

Concluding, the Mpemba effect in Langevin systems is usually depicted in terms of the ruggedness in the energy landscape where the particles diffuse. The relaxation of the colder system to the lowest energy state is usually hindered by the presence of metastable states while the hotter system does not experience (i.e., can overlook) the metastable states due to its higher energy and thus can relax to the lowest energy state faster than the colder system. In this chapter, we revisit this physical picture for a variety of different cases. Generically it is understood that the larger energy barrier leads to a significant amount of population concentration at the intermediate energy well (or the metastable state) for the initially colder system as compared to the initially hotter system. This leads to the consensus that metastability might be necessary for the Mpemba effect. We benchmark this rationale within our exactly solvable model. However and in stark contrast, we also show that metastable states are not necessary for Mpemba effect by demonstrating the effect in a potential with *no metastable states*, questioning the current qualitative understanding. This result also improves on the result in Ref. [13], where for piece-wise constant potentials, metastability was replaced by neutral stability. Taken together these new observations, we believe that our work offers a significant aid to the current understanding of the Mpemba effect in Langevin systems. Finally, it is within our understanding that there is a subtle interplay between the initial population (manifesting the energy landscape) and the hopping frequency for particle rearrangement (which crucially depends on the temperature), however a rigorous quantification is yet to be made. This is a key aspect that requires further investigations. Our recent study with single well potential is an attempt in that direction where we analyse the detailed phase diagram in terms of the asymmetries of the potential configurations that show the Mpemba effect [95].

Chapter 7

Conclusions

In this thesis, we have studied an anomalous relaxation phenomenon known as the Mpemba effect wherein an initial state of a system placed at a further distance from a reference state in phase space relaxes faster compared to another similar initial state placed at a closer distance from the reference state. We have studied the existence of the Mpemba effect in both single particle and many particle systems. While the system of driven granular gases is chosen as an example for the many particle setup, a Langevin system of single Brownian particle diffusing in a potential landscape is chosen for the single particle setup.

In Chapter 2, we have studied the nature of the initial conditions required for the existence of the Mpemba effect in the system of isotropically driven granular gases through an exact analysis. We find that while non-stationary initial conditions are necessary to realise the Mpemba like anomalous behaviour in the relaxation dynamics of mono-dispersed granular gases, it can be realised for steady state initial conditions in bi-dispersed granular gases provided both the species of the bi-dispersed gas are driven with different driving strengths. However, the existence of the Mpemba effect in isotropically driven granular gases are far from experimental realisation as either the initial states from where the quench is done involves a non-stationary state or it involves a complicated way of driving the system (in bi-dispersed gases).

But in Chapters 3 and 4, we showed that the existence of the Mpemba effect is possible starting from steady state initial conditions by considering anisotropically driven granular gases. We did the analysis for both exactly solvable simple model of granular gas as well as validated our results in a more realistic model through theoretical studies and molecular dynamics simulations. We showed that anisotropy in the velocity distribution of mono-dispersed granular gases is the key to the observation of the Mpemba effect starting from initial steady states.

In the study of Mpemba effect in driven granular gases, mean kinetic energy is used as the measure to describe the distance of an initial steady state from the final reference state. However, the definition to define the closeness of an initial state from the final reference state in terms of mean kinetic energy seems ad-hoc as it is not known apriori whether it correctly predicts the distance between the states. As a result, we studied the Mpemba effect in terms of four different measures in Chapter 5. We illustrated the existence of the Mpemba effect using the various choices of the distance measures. However, it is found that the phase diagrams for the different measures are not the same with the presence or absence of the Mpemba effect for a particular phase space point depending on the measure, resulting in a non-unique definition of the Mpemba effect. Moreover, the notion of ‘hot’ and ‘cold’ initial states is different for the different choices of distance measures from the final steady state.

In Chapter 6, we studied the existence of the Mpemba effect in a Langevin system consisting of a single Brownian particle connected to a heat bath and diffusing in the presence of an external potential. Here, we studied the role of external potential in inducing the Mpemba like anomalous behaviour in the relaxation dynamics and is motivated from the experimental study in Ref. [4] where it was shown that asymmetry in the shape of the potential is the key to the observation of the Mpemba effect. We presented our results for exactly solvable models of external potential. We showed that while asymmetry in the shape of the external potential is needed to realize the Mpemba effect, it is not the sufficient condition. We have studied the existence of the Mpemba effect in the presence of both double well and single well external potential. We showed that the presence of higher barrier between the two wells of the double well potential landscape induces the Mpemba effect due to the presence of the metastable state in the local minima of the landscape. However, we found that the presence of metastable state is not the minimal criteria for inducing the Mpemba like relaxations in Langevin systems as we also showed that the effect exists even for the case of potential without metastable state. Thus, the fact that the Mpemba effect exists even in the case of single well potential landscape draws interests to look beyond the concept of metastable state and to look for the minimal criteria that induces the Mpemba effect in Langevin systems for the better understanding of the counterintuitive phenomena.

Appendix A

Derivation of the Boltzmann equation

Let us first derive the Boltzmann equation in two dimensions by considering only the collision part and then we will consider the contribution from the driving. We will follow closely the derivation as described in Ref. [74] for three dimensions. Consider the number of particles $f(\boldsymbol{x}_1, \boldsymbol{v}_1, t)$ at position $(\boldsymbol{x}_1, \boldsymbol{x}_1 + d\boldsymbol{x}_1)$ of phase space having velocity in the interval $(\boldsymbol{v}_1, \boldsymbol{v}_1 + d\boldsymbol{v}_1)$. In time interval Δt, these particles collide with another particles leading to different velocities and hence results in the loss of particles from the considered phase space region. Such events contributes to the loss term. To obtain the number of such collisions, we consider the collision or the scattering of particles having velocity $\boldsymbol{v}_1$ with particles of velocity $\boldsymbol{v}_2$. These particles move with the relative velocity $\boldsymbol{v}_{12}$ and obey the momentum conserving collision rules given by Eq. (1.1). The number of such scatterers is given by $f(\boldsymbol{v}_2, t) d\boldsymbol{v}_2 d\boldsymbol{x}_1$. In the time interval Δt, these scatterers form an area in phase space as shown in Fig. A.1. The area of the section is given by

$$dA = \sigma d\theta |\boldsymbol{v}_{12}.\boldsymbol{e}| \Delta t, \tag{A.1}$$

where σ is the radius of the disc shaped particles and θ is the angle of collision measured with respect to the normal vector $\boldsymbol{e}$. The number of particles having velocity $\boldsymbol{v}_1$ that undergoes scattering is given by $f(\boldsymbol{v}_1, t) d\boldsymbol{v}_1 dA$. Hence, the total number of collisions

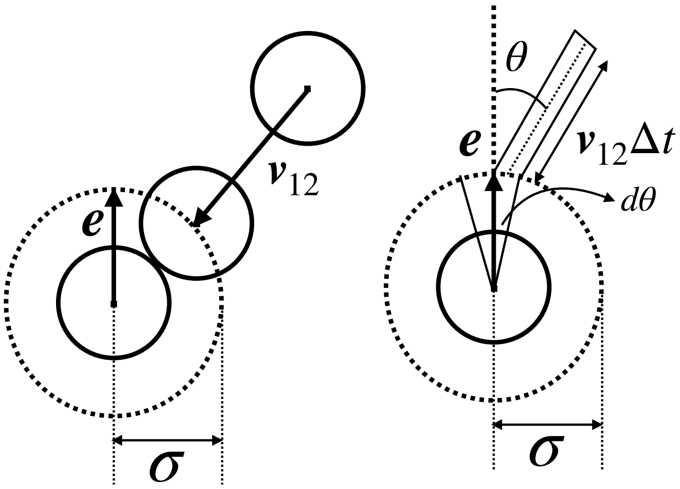

Figure A.1: Schematic diagram for the collision between two hard discs.

that occur with particles of velocity $\boldsymbol{v}_2$ in the interval Δt and leads to a loss of particles from the considered phase space region is given by

$$\begin{aligned} \mathscr{N}_- &= f(\boldsymbol{v}_1,t)d\boldsymbol{v}_1 dA f(\boldsymbol{v}_2,t)d\boldsymbol{v}_2 d\boldsymbol{x}_1, \\ &= \sigma d\theta|\boldsymbol{v}_{12}.\boldsymbol{e}|f(\boldsymbol{v}_1,t)f(\boldsymbol{v}_2,t)d\boldsymbol{v}_1 d\boldsymbol{v}_2 d\boldsymbol{x}_1\Delta t. \end{aligned} \tag{A.2}$$

On the other hand, we can have other collisions where particles having velocities $\boldsymbol{v}_1''$ and $\boldsymbol{v}_2''$ collide and results in the velocities $\boldsymbol{v}_1$ and $\boldsymbol{v}_2$. Such collisions lead to an increase in the number of particles in the previously considered phase space and hence contributes to the gain term of the Boltzmann equation. The change of velocities after the collision is given by

$$\begin{aligned} \boldsymbol{v}_1 &= \boldsymbol{v}_1'' - \frac{1+r}{2}(\boldsymbol{v}_{12}''.\hat{e})\hat{e}, \\ \boldsymbol{v}_2 &= \boldsymbol{v}_2'' + \frac{1+r}{2}(\boldsymbol{v}_{12}''.\hat{e})\hat{e}. \end{aligned} \tag{A.3}$$

It can be rewritten in the form

$$\begin{aligned} \boldsymbol{v}_1'' &= \boldsymbol{v}_1 - \frac{1+r}{2r}(\boldsymbol{v}_{12}.\hat{e})\hat{e}, \\ \boldsymbol{v}_2'' &= \boldsymbol{v}_2 + \frac{1+r}{2r}(\boldsymbol{v}_{12}.\hat{e})\hat{e}. \end{aligned} \tag{A.4}$$

From the similar argument as before, we can write for the total number of collisions in the interval Δt that leads to a gain of particles in the considered phase space region as

$$\begin{aligned}\mathscr{N}_+ &= f(\boldsymbol{v}_1'',t)d\boldsymbol{v}_1''dAf(\boldsymbol{v}_2'',t)d\boldsymbol{v}_2''d\boldsymbol{x}_1,\\ &= \sigma d\theta|\boldsymbol{v}_{12}''.\boldsymbol{e}|f(\boldsymbol{v}_1'',t)f(\boldsymbol{v}_2'',t)d\boldsymbol{v}_1''d\boldsymbol{v}_2''d\boldsymbol{x}_1\Delta t.\end{aligned} \tag{A.5}$$

For our convenience, we write the velocities $\boldsymbol{v}_1'', \boldsymbol{v}_2''$ in terms of $\boldsymbol{v}_1, \boldsymbol{v}_2$ according to Eq. (A.4) and the Jacobian of the transformation is given by

$$d\boldsymbol{v}_1''d\boldsymbol{v}_2'' = \frac{1}{r}d\boldsymbol{v}_1 d\boldsymbol{v}_2, \tag{A.6}$$

and the transformation of the normal components of the relative velocities can be obtained using Eq. (A.3) as

$$|\boldsymbol{v}_{12}''.\hat{e}| = \frac{1}{r}|\boldsymbol{v}_{12}.\hat{e}|. \tag{A.7}$$

With these transformations, we can write $\mathscr{N}_+$ as

$$\mathscr{N}_+ = \frac{1}{r^2}\sigma d\theta|\boldsymbol{v}_{12}.\boldsymbol{e}|f(\boldsymbol{v}_1'',t)f(\boldsymbol{v}_2'',t)d\boldsymbol{v}d\boldsymbol{v}_2 d\boldsymbol{x}_1\Delta t. \tag{A.8}$$

The total number of collisions that lead to the gain or the loss of particles in the considered phase space is obtained finally by integrating over all possible scatterer's velocities $\boldsymbol{v}_2$ and for all possible angle of collisions θ. Note that only those events in the integrations make an impact where $\boldsymbol{v}_{12}.\boldsymbol{e} < 0$ and $\boldsymbol{v}_{12}''.\boldsymbol{e} < 0$. Thus, the net increase in the number of particles in time Δt in the considered phase space region $d\boldsymbol{x}_1 d\boldsymbol{v}_1$ is given by

$$\Delta f d\boldsymbol{v}_1 d\boldsymbol{x}_1 = \int d\boldsymbol{v}_2 \int d\theta\Theta(-\boldsymbol{v}_{12}.\boldsymbol{e})(\mathscr{N}_+ - \mathscr{N}_-), \tag{A.9}$$

where $\Theta(y)$ is the Heaviside step function and is defined as

$$\Theta(y) = \begin{cases} 1, y \geq 0 \\ 0, y < 0. \end{cases} \tag{A.10}$$

Substituting for N_+ and N_- from Eqs. (A.8) and (A.2) and taking the limit $\Delta t \to 0$, we obtain the Boltzmann equation for the collision terms

$$\frac{\partial}{\partial t} f(v_1,t) \quad = \sigma \int dv_2 \int d\theta \Theta(-v_{12}.e)|v_{12}.e| \left[\frac{1}{r^2} f(\boldsymbol{v}_1^{''},t) f(\boldsymbol{v}_2^{''},t) - f(v_1,t) f(v_2,t)\right]. \tag{A.11}$$

Similar to the collision terms, the driving also leads to a loss and a gain in the number of particles in the considered phase space. A single particle is chosen at random and is driven at a constant rate λ_d. If the chosen particle already has the velocity $\boldsymbol{v}_1$ in the considered phase space then it contributes to the loss term in the Boltzmann equation. On the other hand, if the velocity of the chosen particle is different than $\boldsymbol{v}_1$ (say, $\boldsymbol{v}_1'$) then it can lead to $\boldsymbol{v}_1$ after driving has occurred according to Eq. (1.2). The net contribution from such term is obtained by integrating over all possible velocities $\boldsymbol{v}_1'$ and all possible noise realisations $\boldsymbol{\eta}$ that can lead to velocity $\boldsymbol{v}_1$. Hence, after incorporating the loss and the gain terms due to driving, the Boltzmann equation takes the form

$$\begin{aligned} \frac{\partial}{\partial t} f(v_1,t) \quad &= \sigma \int dv_2 \int d\theta \Theta(-v_{12}.e)|v_{12}.e| \left[\frac{1}{r^2} f(\boldsymbol{v}_1^{''},t) f(\boldsymbol{v}_2^{''},t) - f(v_1,t) f(v_2,t)\right] \\ &\quad -\lambda_d f(\boldsymbol{v}_1,t) + \lambda_d \int\int d\boldsymbol{\eta} d\boldsymbol{v}_1' \phi(\boldsymbol{\eta}) f(\boldsymbol{v}_1',t) \delta[-r_w \boldsymbol{v}_1' + \boldsymbol{\eta} - \boldsymbol{v}_1]. \end{aligned} \tag{A.12}$$

Here, the third and the fourth terms are the loss and the gain term due to driving as described above. Note that while counting the number of collisions between the scatterers and the scattered particles that lead to the gain or loss in the number of particles in the desired phase space region, we considered the individual product of their velocity distribution functions $f(\boldsymbol{v}_1,t) f(\boldsymbol{v}_2,t)$ or $f(\boldsymbol{v}_1^{''},t) f(\boldsymbol{v}_2^{''},t)$. However, the rigorous way to do the counting is by considering a joint distribution $f_2(\boldsymbol{v}_1, \boldsymbol{v}_2, t)$ for the scatterers and the scattered particles as there may be correlations between two particles. The assumption that allows us to write the joint distribution function as the product of single particle distribution function is called the molecular chaos hypothesis. The assumption is fairly valid for low densities of the particles.

Even in the spatially homogeneous case, correlations occur due to excluded volume effects when possible colliders are screened by other particles. An approximation for the finite volume effect was suggested by Enskog in the form

$$f_2(v_1, v_2) = \chi(\sigma) f(v_1) f(v_2), \tag{A.13}$$

where $\chi(\sigma)$ is the Enskog factor. For hard discs in two dimensions, $\chi(\sigma)$ is given by

$$\chi(\sigma) = \frac{1-(\frac{7}{16})\eta}{(1-\eta)^2}, \tag{A.14}$$

where η is the packing fraction of the particles given by

$$\eta(\sigma) = \frac{1}{4}\pi\sigma^2 n. \tag{A.15}$$

With the above correction for the Enskog factor, Eq. (A.12) becomes

$$\begin{aligned} \frac{\partial}{\partial t} f(v_{\mathbf{1}}, t) \quad &= \chi(\sigma)\sigma \int dv_2 \int d\theta \Theta(-v_{12}.e)|v_{12}.e| \left[\tfrac{1}{r^2} f(\boldsymbol{v}_1'', t) f(\boldsymbol{v}_2'', t) - f(v_1, t) f(v_2, t)\right] \\ &\quad -\lambda_d f(\boldsymbol{v}_1, t) + \lambda_d \int\int d\eta d\boldsymbol{v}_1' \phi(\boldsymbol{\eta}) f(\boldsymbol{v}_1', t) \delta[-r_w \boldsymbol{v}_1' + \boldsymbol{\eta} - \boldsymbol{v}_1], \end{aligned} \tag{A.16}$$

and is called as the Enskog-Boltzmann equation.

Appendix B

Motivations for the choice of driving

The contribution from the driving terms in the Enskog-Boltzmann equation is of particular interest for the system of driven granular gases. There are certain motivations for the chosen form of driving as given in Eq. (1.2). First is that the system reaches a steady state for $r_w \neq -1$. It is because if $r_w = -1$, then the driving is equivalent to the diffusive driving, $d\boldsymbol{v}/dt = \boldsymbol{\eta}$, in which case the total energy diverges with time and therefore there is no steady state [59, 60]. This model of dissipative driving [Eq. (1.2)] can be thought of as particles colliding with a vibrating wall. In that case, the velocity of a particle $\boldsymbol{v}$ after the collision with the wall is given by: $\boldsymbol{v}' - \boldsymbol{V}_w' = -r_w(\boldsymbol{v} - \boldsymbol{V}_w)$, where r_w is the coefficient of restitution between the wall and the particle and $\boldsymbol{V}_w$ being the wall velocity. Since the velocity of the wall remains unchanged during a collision, we have $\boldsymbol{V}_w' = \boldsymbol{V}_w$. Therefore, we can write $\boldsymbol{v}' = -r_w\boldsymbol{v} + (1 + r_w)\boldsymbol{V}_w$. We assume that the velocity of the wall in each collision is like an uncorrelated random noise. Hence, we can write $\boldsymbol{v}' = -r_w\boldsymbol{v} + \boldsymbol{\eta}$. The physical values for r_w lie in $[0, 1]$, where zero denotes completely inelastic wall collisions and one denotes elastic wall collisions. However, as a mathematical model for driving, it is valid for the range $r_w \in (-1, 1]$.

Moreover, the driving terms in the Enskog-Boltzmann equation can be related to the Fokker-Planck diffusive terms in the limit of small noise $\boldsymbol{\eta}$ and $r_w = 1$. In order to analyse the small noise limit, we consider the driving terms separately for $r_w = 1$ as

$$I_D = -\lambda_d f(\boldsymbol{v}_1,t) + \lambda_d \int\int d\boldsymbol{\eta} d\boldsymbol{v}_1' \phi(\boldsymbol{\eta}) f(\boldsymbol{v}_1',t)\delta[-\boldsymbol{v}_1' + \boldsymbol{\eta} - \boldsymbol{v}_1]. \tag{B.1}$$

Integrating over $\boldsymbol{v}_1'$, we obtain

$$I_D = -\lambda_d f(\boldsymbol{v}_1,t) + \lambda_d \int\int d\boldsymbol{\eta} \phi(\boldsymbol{\eta}) f(\boldsymbol{v}_1 - \boldsymbol{\eta},t). \tag{B.2}$$

For the small noise $\boldsymbol{\eta}$, we Taylor expand the integrand about $|\boldsymbol{\eta}| = 0$, and integrating over $\boldsymbol{\eta}$, we obtain

$$I_D = \frac{\lambda_d \langle |\boldsymbol{\eta}| \rangle^2}{2} \nabla^2 f(\boldsymbol{v}) + \ldots. \tag{B.3}$$

For the small noise $|\boldsymbol{\eta}|$, we can neglect its higher moments which leads to Fokker-Planck diffusive term in the Enskog-Boltzmann equation. The previous studies based on the kinetic theory [73] incorporates a phenomenological Fokker-Planck diffusive term in the Enskog-Boltzmann equation which has its origin from $\boldsymbol{v}' = \boldsymbol{v} + \boldsymbol{\eta}$. However. as discussed earlier, it does not lead to a steady state as in that case mean square velocity, $\langle v \rangle^2 \propto t$. In contrast, the present model of driving as given in Eq. (1.2) provides a microscopic model of driving and allows us to realise the diffusive driving with the system reaching the steady state.

Appendix C

Velocity distribution of driven granular gases

Here, we briefly discuss an outline and important results on the analysis of the velocity distribution function of driven granular gases. The knowledge about the form of the velocity distribution function for the system of driven granular gas will be important for the later chapters as well.

The equilibrium velocity distribution of an ideal gas where the particles undergo elastic collisions is a Maxwell distribution. However, there is a change in the energy in the system of driven granular gas due to the interplay of dissipation and gain of energy in the system. As a result, the velocity distribution function must be a function of time. The time dependence in the velocity distribution is accounted for by the time dependence in the mean energy. If we assume that the inter-particle collisions are only slightly inelastic, i.e., $r \simeq 1$ then it is fair to consider that the velocity distribution function is close to the Maxwell distribution. Hence, the analysis is done by expanding the velocity distribution function around the Maxwellian as,

$$f(\boldsymbol{v},t) = \Phi(v,t)[1 + \sum_{p=1}^{\infty} a_p S_p(v^2)], \tag{C.1}$$

where $\{S_p(v^2)\}$ are the Sonine polynomials, a_p are their corresponding coefficients and $\Phi(v,t)$ is the Maxwell distribution defined as

$$\Phi(v,t) = \frac{mn}{2\pi T(t)} \exp[-\frac{mv^2}{2T(t)}]. \tag{C.2}$$

Here, $T(t)$ is called the granular temperature and is related to the second moment of velocity distribution in two dimensions as

$$T(t) = \frac{1}{2}\int d\boldsymbol{v} m v^2 f(\boldsymbol{v},t). \tag{C.3}$$

Note that Sonine polynomials $\{S_p(v^2)\}$ form a complete set and the expansion is valid if the distribution is close to Maxwellian and the summation of higher order terms in the Sonine polynomials must converge. The orthogonality of the Sonine polynomials is given by

$$\int d\boldsymbol{v}\Phi(v)S_p(v^2)S'_p(v^2) = \frac{2(p+1/2)!}{\sqrt{\pi}p!}\delta_{pp'}, \tag{C.4}$$

where $\delta_{pp'}$ is the Kronecker delta. In order to the obtain the solution $f(\boldsymbol{v},t)$ for the Enskog-Boltzmann equation, one needs to compute the Sonine coefficients a_p. However, it needs altogether a separate discussion. The recent developments in theoretical, numerical and experimental studies can be found in the Refs. [60, 59] and the references there in. Here, we briefly discuss the known results for the velocity distribution function which might be useful for our later studies.

The classic result [73] for the form of the steady state velocity distribution function of a driven granular gas is a stretched exponential of the form

$$f(\boldsymbol{v}) \sim A\exp(-bv^{3/2}), \tag{C.5}$$

where A and b are constants. The result is based on the addition of a phenomenological

Fokker-Planck diffusive term and the perturbative expansion of the velocity distribution function about the Maxwellian. A more exact analysis [60, 59] without the consideration of perturbative expansion of the velocity distribution function and based on the calculation of higher moments while incorporating a microscopic model of driving shows two universal regimes for the tail of the distribution function

$$f(\boldsymbol{v}) \sim \exp(-b_1 v^2 (\ln v)^{\tau}), \quad \text{for } r_w < 1, \tag{C.6}$$

whereas

$$f(\boldsymbol{v}) \sim \exp(-b_2 v (\ln v)^{\frac{\gamma-1}{\gamma}}), \quad \text{for } r_w = 1. \tag{C.7}$$

Here, b_1 and b_2 are the constant pre-factors of the distribution, τ is an exponent depending on the details of the noise distribution and γ is the exponent of the noise distribution whose asymptotic form is characterised by

$$\Phi(\boldsymbol{\eta}) \sim \exp(-c|\boldsymbol{\eta}|^{\gamma}). \tag{C.8}$$

There are numerous experimental setups to investigate the tail of the velocity distribution function but with less success. If the tail of the velocity distribution function is characterised by an exponent β as $f(\boldsymbol{v}) \sim \exp(-bv^{\beta})$ then the experimental findings predict the exponent ranging from $\beta = 1$ to $\beta = 2$. Similar is the case with numerical simulations as well. The result is ambiguous due to the poor sampling of tails in experiments and simulations. However, specific numerical algorithms that can sample the tails of distributions with good accuracy can provide better information about the low probability tails. Our findings [96] implementing sophisticated algorithms to sample the rare events corresponding to the low probability tails of driven granular systems confirms the exact results about the two universal regimes of the distribution function as predicted in Refs. [60].

Bibliography

[1] E B Mpemba and D G Osborne. Cool? *Phys. Educat.*, 4(3):172–175, may 1969.

[2] P Chaddah, S Dash, Kranti Kumar, and A Banerjee. Overtaking while approaching equilibrium. *arXiv preprint arXiv:1011.3598*, 2010.

[3] Cunliang Hu, Jingqing Li, Shaoyong Huang, Hongfei Li, Chuanfu Luo, Jizhong Chen, Shichun Jiang, and Lijia An. Conformation directed mpemba effect on polylactide crystallization. *Cryst. Growth Des.*, 18(10):5757–5762, 2018.

[4] Avinash Kumar and John Bechhoefer. Exponentially faster cooling in a colloidal system. *Nature*, 584(7819):64–68, 2020.

[5] A. Gal and O. Raz. Precooling strategy allows exponentially faster heating. *Phys. Rev. Lett.*, 124:060602, Feb 2020.

[6] Israel Klich, Oren Raz, Ori Hirschberg, and Marija Vucelja. Mpemba index and anomalous relaxation. *Phys. Rev. X*, 9:021060, Jun 2019.

[7] Israel Klich and Marija Vucelja. Solution of the metropolis dynamics on a complete graph with application to the markov chain mpemba effect. *arXiv preprint arXiv:1812.11962*, 2018.

[8] Subir K Das and Nalina Vadakkayil. Should a hotter paramagnet transform quicker to a ferromagnet? monte carlo simulation results for ising model. *Phys. Chem. Chem. Phys.*, 2021.

[9] Isidoro González-Adalid Pemartín, Emanuel Mompó, Antonio Lasanta, Víctor Martín-Mayor, and Jesús Salas. Slow growth of magnetic domains helps fast evolution routes for out-of-equilibrium dynamics. *Phys. Rev. E*, 104:044114, Oct 2021.

[10] Gianluca Teza, Ran Yaacoby, and Oren Raz. Relaxation shortcuts through boundary coupling. *arXiv preprint arXiv:2112.10187*, 2021.

[11] Zhiyue Lu and Oren Raz. Nonequilibrium thermodynamics of the markovian mpemba effect and its inverse. *Proc. Natl. Acad. Sci. USA*, 114(20):5083–5088, 2017.

[12] Tan Van Vu and Yoshihiko Hasegawa. Toward relaxation asymmetry: Heating is faster than cooling. *Phys. Rev. Research*, 3:043160, Dec 2021.

[13] Matthew R Walker and Marija Vucelja. Anomalous thermal relaxation of langevin particles in a piecewise-constant potential. *Journal of Statistical Mechanics: Theory and Experiment*, 2021(11):113105, nov 2021.

[14] Daniel Maria Busiello, Deepak Gupta, and Amos Maritan. Inducing and optimizing markovian mpemba effect with stochastic reset. *New Journal of Physics*, 23(10):103012, oct 2021.

[15] Alessio Lapolla and Aljaž Godec. Faster uphill relaxation in thermodynamically equidistant temperature quenches. *Physical Review Letters*, 125(11):110602, 2020.

[16] Fabian Jan Schwarzendahl and Hartmut Löwen. Anomalous cooling and overcooling of active colloids. *Phys. Rev. Lett.*, 129:138002, Sep 2022.

[17] Marco Baity-Jesi, Enrico Calore, Andres Cruz, Luis Antonio Fernandez, José Miguel Gil-Narvión, Antonio Gordillo-Guerrero, David Iñiguez, Antonio Lasanta, Andrea Maiorano, Enzo Marinari, et al. The mpemba effect in spin glasses is a persistent memory effect. *Proc. Natl. Acad. Sci. USA*, 116(31):15350–15355, 2019.

[18] Andrés Santos and Antonio Prados. Mpemba effect in molecular gases under nonlinear drag. *Phys. Fluids*, 32(7):072010, 2020.

[19] Rubén Gómez González, Nagi Khalil, and Vicente Garzó. Mpemba-like effect in driven binary mixtures. *Physics of Fluids*, 33(5):053301, 2021.

[20] Rubén Gómez González and Vicente Garzó. Anomalous mpemba effect in binary molecular suspensions. *arXiv preprint arXiv:2011.13237*, 2020.

[21] A. Patrón, B. Sánchez-Rey, and A. Prados. Strong nonexponential relaxation and memory effects in a fluid with nonlinear drag. *Phys. Rev. E*, 104:064127, Dec 2021.

[22] Antonio Lasanta, Francisco Vega Reyes, Antonio Prados, and Andrés Santos. When the hotter cools more quickly: Mpemba effect in granular fluids. *Phys. Rev. Lett.*, 119:148001, Oct 2017.

[23] Aurora Torrente, Miguel A. López-Castaño, Antonio Lasanta, Francisco Vega Reyes, Antonio Prados, and Andrés Santos. Large mpemba-like effect in a gas of inelastic rough hard spheres. *Phys. Rev. E*, 99:060901, Jun 2019.

[24] E Mompó, MA López-Castaño, Antonio Lasanta, F Vega Reyes, and Aurora Torrente. Memory effects in a gas of viscoelastic particles. *Physics of Fluids*, 33(6):062005, 2021.

[25] Apurba Biswas, V. V. Prasad, O. Raz, and R. Rajesh. Mpemba effect in driven granular maxwell gases. *Phys. Rev. E*, 102:012906, Jul 2020.

[26] Apurba Biswas, VV Prasad, and R Rajesh. Mpemba effect in an anisotropically driven granular gas. *Europhysics Letters*, 136(4):46001, 2022.

[27] Apurba Biswas, VV Prasad, and R Rajesh. Mpemba effect in anisotropically driven inelastic maxwell gases. *Journal of Statistical Physics*, 186(3):1–21, 2022.

[28] Federico Carollo, Antonio Lasanta, and Igor Lesanovsky. Exponentially accelerated approach to stationarity in markovian open quantum systems through the mpemba effect. *Phys. Rev. Lett.*, 127:060401, Aug 2021.

[29] Henry C Burridge and Paul F Linden. Questioning the mpemba effect: hot water does not cool more quickly than cold. *Sci. Rep.*, 6:37665, 2016.

[30] Julius Degünther and Udo Seifert. Anomalous relaxation from a non-equilibrium steady state: An isothermal analog of the mpemba effect. *Europhysics Letters*, 139(4):41002, 2022.

[31] Roi Holtzman and Oren Raz. Landau theory for the mpemba effect through phase transitions. *Communications Physics*, 5(1):280, 2022.

[32] Sheng Zhang and Ji-Xuan Hou. Theoretical model for the mpemba effect through the canonical first-order phase transition. *Physical Review E*, 106(3):034131, 2022.

[33] Gianluca Teza, Ran Yaacoby, and Oren Raz. Eigenvalue crossing as a phase transition in relaxation dynamics. *Physical Review Letters*, 130(20):207103, 2023.

[34] Apurba Biswas, VV Prasad, and R. Rajesh. Mpemba effect in driven granular gases: role of distance measures. *arXiv preprint arXiv:2303.10900*, 2023.

[35] Amit Kumar Chatterjee, Satoshi Takada, and Hisao Hayakawa. Quantum mpemba effect in a quantum dot with reservoirs. *arXiv preprint arXiv:2304.02411*, 2023.

[36] W. Losert, D. G. W. Cooper, J. Delour, A. Kudrolli, and J. P. Gollub. Velocity statistics in excited granular media. *Chaos*, 9(3):682–690, 1999.

[37] Florence Rouyer and Narayanan Menon. Velocity fluctuations in a homogeneous 2d granular gas in steady state. *Phys. Rev. Lett.*, 85:3676–3679, Oct 2000.

[38] I. S. Aranson and J. S. Olafsen. Velocity fluctuations in electrostatically driven granular media. *Phys. Rev. E*, 66:061302, Dec 2002.

[39] Pedro M Reis, Rohit A Ingale, and Mark D Shattuck. Forcing independent velocity distributions in an experimental granular fluid. *Phys. Rev. E*, 75(5):051311, 2007.

[40] Hong-Qiang Wang, Klebert Feitosa, and Narayanan Menon. Particle kinematics in a dilute, three-dimensional, vibration-fluidized granular medium. *Phys. Rev. E*, 80(6):060304, 2009.

[41] Soichi Tatsumi, Yoshihiro Murayama, Hisao Hayakawa, and Masaki Sano. Experimental study on the kinetics of granular gases under microgravity. *J. Fluid Mech.*, 641:521–539, 2009.

[42] Christian Scholz and Thorsten Pöschel. Velocity distribution of a homogeneously driven two-dimensional granular gas. *Phys. Rev. Lett.*, 118(19):198003, 2017.

[43] Alexandre Vilquin, Hamid Kellay, and Jean-François Boudet. Shock waves induced by a planar obstacle in a vibrated granular gas. *J. Fluid Mech.*, 842:163–187, 2018.

[44] Yangrui Chen and Jie Zhang. High-energy velocity tails in uniformly heated granular materials. *Physical Review E*, 106(5):L052903, 2022.

[45] David Auerbach. Supercooling and the mpemba effect: When hot water freezes quicker than cold. *Am. J. Phys.*, 63(10):882–885, 1995.

[46] M. Vynnycky and S. Kimura. Can natural convection alone explain the mpemba effect? *Int. J. Heat Mass Transf.*, 80:243 – 255, 2015.

[47] Seyed Milad Mirabedin and Fatola Farhadi. Numerical investigation of solidification of single droplets with and without evaporation mechanism. *Int. J. Refrig.*, 73:219 – 225, 2017.

[48] Xi Zhang, Yongli Huang, Zengsheng Ma, Yichun Zhou, Ji Zhou, Weitao Zheng, Qing Jiang, and Chang Q. Sun. Hydrogen-bond memory and water-skin supersolidity resolving the mpemba paradox. *Phys. Chem. Chem. Phys.*, 16:22995–23002, 2014.

[49] Yunwen Tao, Wenli Zou, Junteng Jia, Wei Li, and Dieter Cremer. Different ways of hydrogen bonding in water - why does warm water freeze faster than cold water? *J. Chem. Theory Comput.*, 13(1):55–76, 2017.

[50] Yun-Ho Ahn, Hyery Kang, Dong-Yeun Koh, and Huen Lee. Experimental verifications of mpemba-like behaviors of clathrate hydrates. *Korean J. Chem. Eng.*, 33:1903–1907, 2016.

[51] A Gijón, A Lasanta, and ER Hernández. Paths towards equilibrium in molecular systems: The case of water. *Phys. Rev. E*, 100(3):032103, 2019.

[52] Jaehyeok Jin and William A Goddard III. Mechanisms underlying the mpemba effect in from molecular dynamics simulations. *J. Phys. Chem. C*, 119(5):2622–2629, 2015.

[53] E. Ben-Naim and P. L. Krapivsky. Multiscaling in inelastic collisions. *Phys. Rev. E*, 61:R5–R8, Jan 2000.

[54] A. V. Bobylev, J. A. Carrillo, and I. M. Gamba. On some properties of kinetic and hydrodynamic equations for inelastic interactions. *J. Stat. Phys.*, 98(3):743–773, Feb 2000.

[55] V. V Prasad, Sanjib Sabhapandit, and Abhishek Dhar. High-energy tail of the velocity distribution of driven inelastic maxwell gases. *Europhys. Lett.*, 104(5):54003, 2014.

[56] V. V. Prasad, Sanjib Sabhapandit, and Abhishek Dhar. Driven inelastic maxwell gases. *Phys. Rev. E*, 90:062130, Dec 2014.

[57] Apurba Biswas, V. V. Prasad, and R Rajesh. Asymptotic velocity distribution of a driven one dimensional binary granular maxwell gas. *J. Stat. Mech.: Theory Exp.*, 2020(1):013202, jan 2020.

[58] V. V. Prasad, Dibyendu Das, Sanjib Sabhapandit, and R Rajesh. Velocity distribution of a driven inelastic one-component maxwell gas. *Phys. Rev. E*, 95(3):032909, 2017.

[59] V. V. Prasad and R. Rajesh. Asymptotic behavior of the velocity distribution of driven inelastic gas with scalar velocities: Analytical results. *J. Stat. Phys.*, 176:1409–1433, Jul 2019.

[60] V. V. Prasad, Dibyendu Das, Sanjib Sabhapandit, and R Rajesh. Velocity distribution of driven granular gases. *J. Stat. Mech.: Theory Exp.*, 2019(6):063201, jun 2019.

[61] GW Baxter and JS Olafsen. Kinetics: Gaussian statistics in granular gases. *Nature*, 425(6959):680–680, 2003.

[62] GW Baxter and JS Olafsen. The temperature of a vibrated granular gas. *Granul. Matter*, 9(1-2):135–139, 2007.

[63] G. W. Baxter and J. S. Olafsen. Experimental evidence for molecular chaos in granular gases. *Phys. Rev. Lett.*, 99:028001, Jul 2007.

[64] K. Combs, J. S. Olafsen, A. Burdeau, and P. Viot. Thermostatistics of a single particle on a granular dimer lattice: Influence of defects. *Phys. Rev. E*, 78:042301, Oct 2008.

[65] Alexis Burdeau and Pascal Viot. Quasi-gaussian velocity distribution of a vibrated granular bilayer system. *Phys. Rev. E*, 79:061306, Jun 2009.

[66] C. R. K. Windows-Yule and D. J. Parker. Boltzmann statistics in a three-dimensional vibrofluidized granular bed: Idealizing the experimental system. *Phys. Rev. E*, 87:022211, Feb 2013.

[67] Klebert Feitosa and Narayanan Menon. Breakdown of energy equipartition in a 2d binary vibrated granular gas. *Phys. Rev. Lett.*, 88:198301, Apr 2002.

[68] Alain Barrat and Emmanuel Trizac. Lack of energy equipartition in homogeneous heated binary granular mixtures. *Granul. Matter*, 4(2):57–63, 2002.

[69] Riccardo Pagnani, Umberto Marini Bettolo Marconi, and Andrea Puglisi. Driven low density granular mixtures. *Phys. Rev. E*, 66:051304, Nov 2002.

[70] Hong-Qiang Wang and Narayanan Menon. Heating mechanism affects equipartition in a binary granular system. *Phys. Rev. Lett.*, 100:158001, Apr 2008.

[71] J. Javier Brey and M. J. Ruiz-Montero. Hydrodynamic character of the nonequipartition of kinetic energy in binary granular gases. *Phys. Rev. E*, 80:041306, Oct 2009.

[72] H. Uecker, W. T. Kranz, T. Aspelmeier, and A. Zippelius. Partitioning of energy in highly polydisperse granular gases. *Phys. Rev. E*, 80:041303, Oct 2009.

[73] T.P.C. van Noije and M.H. Ernst. Velocity distributions in homogeneous granular fluids: the free and the heated case. *Granul. Matter*, 1(2):57–64, 1998.

[74] Nikolai V Brilliantov and Thorsten Pöschel. *Kinetic theory of granular gases*. Oxford University Press, 2010.

[75] E. Ben-Naim and P. L. Krapivsky. Scaling, multiscaling, and nontrivial exponents in inelastic collision processes. *Phys. Rev. E*, 66:011309, Jul 2002.

[76] A Baldassarri, U. Marini Bettolo Marconi, and A Puglisi. Influence of correlations on the velocity statistics of scalar granular gases. *Europhys. Lett.*, 58(1):14–20, apr 2002.

[77] M. H Ernst and R Brito. High-energy tails for inelastic maxwell models. *Europhys. Lett.*, 58(2):182–187, apr 2002.

[78] P L Krapivsky and E Ben-Naim. Nontrivial velocity distributions in inelastic gases. *J. Phys. A*, 35(11):L147–L152, mar 2002.

[79] M. H. Ernst and R. Brito. Driven inelastic maxwell models with high energy tails. *Phys. Rev. E*, 65:040301, Mar 2002.

[80] T. Antal, Michel Droz, and Adam Lipowski. Exponential velocity tails in a driven inelastic maxwell model. *Phys. Rev. E*, 66:062301, Dec 2002.

[81] A. Santos and M. H. Ernst. Exact steady-state solution of the boltzmann equation: A driven one-dimensional inelastic maxwell gas. *Phys. Rev. E*, 68:011305, Jul 2003.

[82] Solomon Kullback and Richard A Leibler. On information and sufficiency. *The annals of mathematical statistics*, 22(1):79–86, 1951.

[83] Avinash Kumar, Raphaël Chétrite, and John Bechhoefer. Anomalous heating in a colloidal system. *Proceedings of the National Academy of Sciences*, 119(5):e2118484119, 2022.

[84] John Bechhoefer, Avinash Kumar, and Raphaël Chétrite. A fresh understanding of the mpemba effect. *Nature Reviews Physics*, pages 1–2, 2021.

[85] Alberto Megías and Andrés Santos. Mpemba-like effect protocol for granular gases of inelastic and rough hard disks. *Frontiers in Physics*, page 739, 2022.

[86] Umberto Marini Bettolo Marconi, Andrea Puglisi, and Angelo Vulpiani. About an h-theorem for systems with non-conservative interactions. *Journal of Statistical Mechanics: Theory and Experiment*, 2013(08):P08003, 2013.

[87] C. A. Plata and A. Prados. Global stability and h theorem in lattice models with nonconservative interactions. *Phys. Rev. E*, 95:052121, May 2017.

[88] Alberto Megías and Andrés Santos. Kullback–leibler divergence of a freely cooling granular gas. *Entropy*, 22(11):1308, 2020.

[89] V. V. Prasad, Sanjib Sabhapandit, Abhishek Dhar, and Onuttom Narayan. Driven inelastic maxwell gas in one dimension. *Phys. Rev. E*, 95:022115, Feb 2017.

[90] V. V. Prasad, Dibyendu Das, Sanjib Sabhapandit, and R. Rajesh. Velocity distribution of a driven inelastic one-component maxwell gas. *Phys. Rev. E*, 95:032909, Mar 2017.

[91] Matthew R Walker and Marija Vucelja. Mpemba effect in terms of mean first passage time. *arXiv preprint arXiv:2212.07496*, 2022.

[92] Hannes Risken. Fokker-planck equation. In *The Fokker-Planck Equation*, pages 63–95. Springer, 1996.

[93] Apurba Biswas, R. Rajesh, and Arnab Pal. Mpemba effect in a langevin system: population statistics, metastability and other exact results. *arXiv preprint arXiv:2304.06420*, 2023.

[94] M Mörsch, H Risken, and HD Vollmer. One-dimensional diffusion in soluble model potentials. *Zeitschrift für Physik B Condensed Matter*, 32:245–252, 1979.

[95] Apurba Biswas and R Rajesh. Mpemba effect for a brownian particle trapped in a single well potential. *arXiv preprint arXiv:2305.06613*, 2023.

[96] Apurba Biswas, V. V Prasad, and R. Rajesh. Determining the tails of the velocity distribution in driven granular gases using biased monte carlo simulations (*in preparation*).